Aus der Medizinische Klinik und Poliklinik IV

Klinikum der Ludwig-Maximilians-Universität München

Direktor: Professor Dr. med. Martin Reincke

Molecular and Cellular Mechanisms in the Pathophysiology of Primary Aldosteronism

Dissertation

zum Erwerb des Doctor of Philosophy (Ph.D.)

an der Medizinischen Fakultät der

Ludwig-Maximilians-Universität zu München

vorgelegt von

Siyuan Gong

aus

Hunan, China

Jahr 2023

Mit Genehmigung der Medizinischen Fakultät der

Ludwig-Maximilians-Universität zu München

First evaluator:	**Prof. Dr. med. Martin Reincke**
Second evaluator:	**Dr. Tracy Ann Williams**
Third evaluator:	**Prof. Dr. Heinrich Schmidt**
Fourth evaluator:	**Prof. Dr. Volker Vielhauer**

Dean: **Prof. Dr. med. Thomas Gudermann**

date of the defense:

28.08.2023

Affidavit

LMU LUDWIG-MAXIMILIANS-UNIVERSITÄT MÜNCHEN

Dekanat Medizinische Fakultät
Promotionsbüro

Affidavit

Gong, Siyuan

Surname, first name

I hereby declare, that the submitted thesis entitled

Molecular and Cellular Mechanisms in the Pathophysiology of Primary Aldosteronism

is my own work. I have only used the sources indicated and have not made unauthorised use of services of a third party. Where the work of others has been quoted or reproduced, the source is always given.

I further declare that the dissertation presented here has not been submitted in the same or similar form to any other institution for the purpose of obtaining an academic degree.

Hangzhou, China, 02.09.2023	**Siyuan Gong**
Place, Date	Signature doctoral candidate

Confirmation of congruency

LMU LUDWIG-MAXIMILIANS-UNIVERSITÄT MÜNCHEN

Dean's Office Medical Faculty
Doctoral Office

Confirmation of congruency between printed and electronic version of the doctoral thesis

Doctoral candidate: Siyuan Gong

I hereby declare that the electronic version of the submitted thesis, entitled

Molecular and Cellular Mechanisms in the Pathophysiology of Primary Aldosteronism

is congruent with the printed version both in content and format.

Hangzhou, China, 02.09.2023	**Siyuan Gong**
Place, Date	Signature doctoral candidate

Table of Contents

Affidavit **1**

Confirmation of congruency **2**

Table of Contents **3**

List of Abbreviations **4**

List of Publications **6**

1. Introduction 8

1.1 Aldosterone Biosynthesis in the Adrenal Cortex 8

1.1.1 Adrenal Zonation 8

1.1.2 Aldosterone Synthase 9

1.1.3 Physiological Regulators 10

1.2 Primary Aldosteronism 11

1.2.1 Introduction 11

1.2.2 Histopathology 11

1.2.3 Genetics and Pathophysiology 13

1.2.4 Diagnostic Investigation 23

1.3 Aims of this Thesis 27

1.4 Summary 28

1.5 Zusammenfassung 32

2. My Contribution **37**

3. Publication I **38**

4. Publication II **57**

5. Publication III **76**

6. References **114**

7. Acknowledgement **128**

List of Abbreviations

AngII	Angiotensin II
APA	aldosterone-producing adenoma
APDH	aldosterone-producing diffuse hyperplasia
APMs	aldosterone-producing micronodules
APN	aldosterone-producing nodule
ARR	aldosterone-to-renin ratio
AT1R	type-1 AngII receptor
ATF1	activating transcription factor 1
ATP1A1	alpha-1 subunit of the Na^+/K^+ ATPase
ATP2B3	plasma membrane Ca^{2+} transporting ATPase 3
AVS	adrenal vein sampling
Ca^{2+}	calcium
CACNA1D	L-type voltage-gated Ca^{2+}-channel
CACNA1H	T-type Ca^{2+} channel CaV3.2
CaMKs	calcium/calmodulin-dependent kinases
CREB	cAMP-dependent transcription factor
CT	computed tomography
CTNNB1	β-catenin
CYP11A1	cytochrome P450[scc]
CYP11B2	aldosterone synthase
DAG	diacylglycerol
FH-I	Familial hyperaldosteronism type I
FH-II	Familial hyperaldosteronism type II
FH-III	Familial hyperaldosteronism type III
FH-IV	Familial hyperaldosteronism type IV
H&E	hematoxylin-eosin staining

HISTALDO	the international histopathology consensus for unilateral primary aldosteronism
HSD3B2	3β-hydroxysteroid dehydrogenase type 2
IP3	inositol 1,4,5-trisphosphate
KCNJ5	G protein inward rectifying potassium channel Kir3.4
LC-MS/MS	liquid chromatography-tandem mass spectrometry
MALDI-MSI	matrix-assisted laser desorption/ionization mass spectrometry imaging
MAPMs	multiple aldosterone-producing micronodules
MAPNs	multiple aldosterone-producing nodules
MC2R	melanocortin receptor 2
MRA	mineralocorticoid receptor antagonist
Na^+	sodium
NNMF	non-negative matrix factorization
PA	Primary aldosteronism
PASNA	PA with seizures and neurologic abnormalities
PASO	primary aldosteronism surgical outcome
PLC	phospholipase C
RAAS	renin-angiotensin-aldosterone system
ROS	reactive oxygen species
siRNA	short interfering RNA
STAR	steroidogenic acute regulatory protein
tSNE	t-distributed stochastic neighbor embedding
TSPAN12	tetraspanin 12
zF	zona fasciculata
zG	zona glomerulosa
zR	zona reticularis

List of Publications

1. Primary Aldosteronism: Metabolic Reprogramming and the Pathogenesis of Aldosterone-Producing Adenomas

Siyuan Gong, Martina Tetti, Martin Reincke, Tracy Ann Williams

Cancers. 2021 Jul 23;13(15):3716. DOI: 10.3390/cancers13153716.

2. TSPAN12 (Tetraspanin 12) Is a Novel Negative Regulator of Aldosterone Production in Adrenal Physiology and Aldosterone-Producing Adenomas

Siyuan Gong, Martina Tetti, Elisabeth Kemter, Mirko Peitzsch, Paolo Mulatero, Martin Bidlingmaier, Graeme Eisenhofer, Eckhard Wolf, Martin Reincke, Tracy Ann Williams

Hypertension. 2023 Feb;80(2):440-450. DOI: 10.1161/HYPERTENSIONAHA.122.19783.

3. Primary aldosteronism: spatial multi-omics mapping of genotype-dependent heterogeneity and tumor expansion of aldosterone-producing adenomas

Siyuan Gong, Na Sun, Lucie S Meyer, Martina Tetti, Christina Koupourtidou, Stefan Krebs, Giacomo Masserdotti, Helmut Blum, William E. Rainey, Martin Reincke, Axel Walch, Tracy Ann Williams

Hypertension. 2023 Jul;80(7):1555-1567. DOI: 10.1161/HYPERTENSIONAHA.123.20921. Epub 2023 May 1.

Further publications during doctoral study

Original research:

Adrenal surgery for bilateral primary aldosteronism: an international retrospective cohort study

Tracy Ann Williams*, **Siyuan Gong***, Yuya Tsurutani, Yuta Tezuka, Moe Thuzar, Jacopo Burrello, Vin-Cent Wu, Yuto Yamazaki, Paolo Mulatero, Hironobu Sasano, Michael Stowasser, Tetsuo Nishikawa, Fumitoshi Satoh, Martin Reincke

Lancet Diabetes Endocrinol. 2022 Nov;10(11):769-771. DOI: 10.1016/S2213-8587(22)00253-4.

*Authors contributed equally to this work

Reviews:

1. Angiotensin II Type 1 Receptor Autoantibodies in Primary Aldosteronism

Lucie S Meyer, **Siyuan Gong**, Martin Reincke, Tracy Ann Williams

Hormone and Metabolic Research. 2020 Jun;52(6):379-385. DOI: 10.1055/a-1120-8647.

2. Primary aldosteronism: Pathophysiological mechanisms of cell death and proliferation

Martina Tetti, **Siyuan Gong**, Franco Veglio, Martin Reincke, Tracy Ann Williams

Frontiers in Endocrinology. 2022 Aug 8;13:934326. DOI: 10.3389/fendo.2022.934326.

1. Introduction

1.1 Aldosterone Biosynthesis in the Adrenal Cortex

1.1.1 Adrenal Zonation

The adrenal hormones are critical to ensure metabolic homeostasis, which is essential for the proper functioning of our daily life. The adrenal glands consist of morphologically and functionally distinct portions: an outer adrenal cortex that is responsible for the secretion of steroids and an inner adrenal medulla that synthesizes neurohormones. In the adrenal cortex, hormone biosynthesis is tightly controlled in three morphologically defined zones - the zona glomerulosa (zG), zona fasciculata (zF), and zona reticularis (zR) - which can be differentiated using hematoxylin-eosin (H&E) staining at low magnification (**Figure 1**) [1,2]. The outermost zG cells synthesize the mineralocorticoid aldosterone, which contributes to the balance between sodium reabsorption and potassium secretion. The middle zF produces the glucocorticoid cortisol, which is involved in the stress response, glucose homeostasis, and immune suppression. The innermost zR secretes androstenedione and dehydroepiandrosterone that are precursors of adrenal androgens.

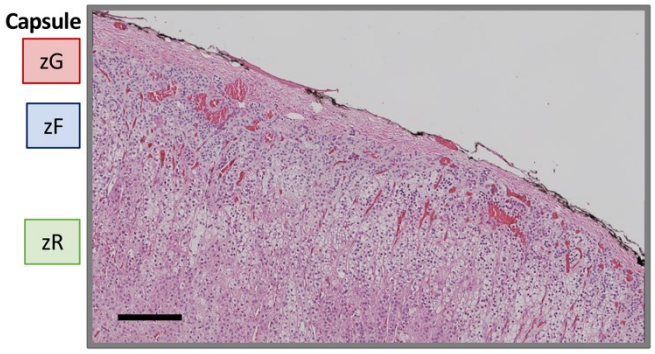

Figure 1. H&E staining shows normal zonation of the zG, zF, and zR

1.1.2 Aldosterone Synthase

Aldosterone synthase begins from the intracellular trafficking of cholesterol into the inner mitochondrial membrane through steroidogenic acute regulatory protein (encoded by *STAR*). The conversion of cholesterol to pregnenolone in mitochondria is then facilitated by cytochrome P450scc (encoded by *CYP11A1*). Once pregnenolone is formed, it diffuses into endoplasmic reticulum, an important cellular compartment for conversion of pregnenolone to progesterone by the 3β-hydroxysteroid dehydrogenase (encoded by *HSD3B2*). The 21-hydroxylase (encoded by *CYP21*) further mediates the biosynthesis of 11-deoxycorticosterone from progesterone. In the terminal step of aldosterone synthesis, 11-deoxycorticosterone is converted to aldosterone by a cytochrome p450 enzyme (encoded by *CYP11B2*) that is expressed exclusively in zG cells. The conversion comprises three reactions steps: first 11β-hydroxylation of 11-deoxycorticosterone to produce corticosterone, then 18-hydroxylation to form 18-hydroxycorticosterone and finally 18-oxidation to produce aldosterone [3]. A summary of human adrenal steroidogenesis pathways is highlighted in **Figure 2**.

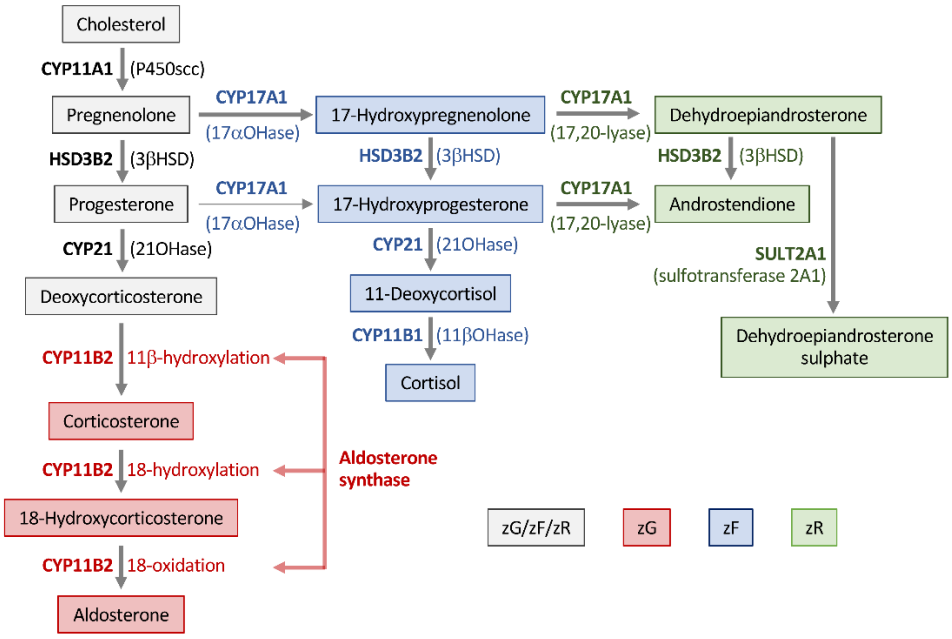

Figure 2. Overview of human adrenal steroidogenesis pathways. zG, zona glomerulosa; zF, zona fasciculata; zR, zona reticularis

1.1.3 Physiological Regulators

Under normal healthy conditions, the regulation of aldosterone production is primarily mediated by the renin-angiotensin-aldosterone system (RAAS), specifically through the action of the biologically active peptide Angiotensin II (AngII) [4,5] and its activity is dictated by salt intake and water handling. Upon blood volume and sodium load restrictions, renin secretion is activated with a consequent increased generation of AngII and its binding to the type-1 AngII receptor (AT1R) results in activation of the Gq protein family. This process generates two secondary messengers, inositol 1,4,5-trisphosphate (IP3) and diacylglycerol (DAG) via phosphoinositide-specific phospholipase C (PLC) [6]. IP3 triggers a rapid rise in cytosolic calcium (Ca^{2+}) concentration and DAG consequently activates protein kinase C, cAMP-dependent transcription factor (CREB), and activating transcription factor 1 (ATF1) [7]. Collectively, the cytosolic release of Ca^{2+} increases the transcript levels of *CYP11B2*, involved in the key rate-limiting step of aldosterone synthesis, through the consecutive activation of calcium/calmodulin-dependent kinases (CaMKs). In contrast, activating transcription ATF1/CREB plays a crucial role during the early regulatory steps, due to phosphorylation of STAR [8]. Because the expression of AT1R and CYP11B2 is specifically localized to zG cells within the adrenal gland, aldosterone production driven by CYP11B2 is restricted to these cells in the adrenocortical region.

Another important physiological stimuli of aldosterone production is extracellular potassium (K^+) [7]. Under physiological conditions, various K^+ channels, such as G protein inward rectifying potassium channel Kir3.4 (coded by *KCNJ5*), maintain the hyperpolarized membrane potential of adrenal zG cells[9-13]. Plasma membrane depolarization of zG cells is initiated by the elevated extracellular K^+ levels and voltage-dependent calcium channels are activated leading to Ca^{2+} influx, ultimately triggering aldosterone production. Adrenocorticotropic hormone (ACTH) has also modulates aldosterone synthesis via binding to transmembrane receptor melanocortin receptor 2 (MC2R) and, thus, activating AMP/PKA signaling [14,15].

1.2 Primary Aldosteronism

1.2.1 Introduction

Primary aldosteronism (PA), traditionally considered relatively rare, is now recognized as the most frequent form of endocrine hypertension. PA prevalence steadily increases according to the severity of hypertension, from 5% in hypertensive patients in a primary care setting [16,17] to over 20% in severe or treatment-resistant hypertensive patients [18-20]. Overt PA is defined as elevated aldosterone production from the adrenal gland, independent of the RAAS and non-suppressible by vasodilation and/or sodium retention. Evidence increasingly suggests that the long-term consequences of aldosterone excess are associated with a higher likelihood of developing cardiorenal associated comorbidities in PA patients. PA can be definitively diagnosed by utilizing a widely employed confirmatory test and subsequent subtyping into unilateral and bilateral forms can be achieved through adrenal computed tomography (CT) and adrenal vein sampling (AVS). Unilateral forms are typically caused by an aldosterone-producing adenoma (APA). The histology of bilateral PA is usually unknown because bilateral adrenal surgery is rarely performed for PA [21].

Aldosterone hypersecretion from most adenomas is driven by somatic mutations, with only a few pathogenic germline mutations reported in the rare familial hyperaldosteronism. In most cases, these mutations affect zG cells by lowering the threshold for depolarization and subsequently opening voltage-gated calcium channels, either spontaneously or constitutively. The resulting increase in intracellular calcium drives the activation of aldosterone synthase (CYP11B2) expression through calcium signaling. In parallel with these genetic alterations, antibodies against CYP11B2 have allowed researchers to visualize histopathological changes that may contribute to PA pathogenesis [22].

1.2.2 Histopathology

In PA patients, morphology and CYP11B2 (aldosterone synthase) immunohistochemistry are useful to trace the origins of the synthesis of aldosterone production (aldosterone-producing

areas) [23] and have provided insight into the complex histopathology[24-26]. In younger individuals, CYP11B2 is continually expressed in steroidogenic zG cells in the adrenal cortex. Histological examination of normal adrenals has shown an increased incidence of aldosterone-producing micronodules (APMs; also known as aldosterone-producing cell clusters) in elderly individuals, which may be the dominant source of increasing aldosterone concentrations with human ageing [27,28]. Another interesting possibility is that APMs might have a role in APA formation [29,30]. The cause of some bilateral forms of PA has been attributed to APMs and evidence suggests that in some cases, they can transform into APAs [31].

Table 1. The histopathologic definition of aldosterone-producing lesions in adrenal glands from unilateral PA patients, as evaluated based on the HISTALDO consensus [22].

Abbreviation	Histopathological entity	Definition
APA	Aldosterone-producing adenoma	Well circumscribed CYP11B2-positive solitary neoplasm (≥ 10 mm diameter) composed of clear or compact eosinophilic cells or both cell types.
APN	Aldosterone-producing nodule	CYP11B2-positive lesion (<10 mm diameter) morphologically visible with hematoxylin-eosin staining. An APN often displays a gradient of CYP11B2 immunostaining decreasing in intensity from the outer to the inner part of the lesion.
APM	Aldosterone-producing micronodule (formally known as aldosterone-producing cell cluster)	CYP11B2-positive lesion (<10 mm diameter) composed of zona glomerulosa cells located beneath adrenal capsule that do not differ in morphology from adjacent adrenocortical cells by hematoxylin-eosin staining. An APM often displays a gradient of CYP11B2 immunostaining decreasing in intensity from the outer to the inner part of the lesion.
MAPN or MAPM	Multiple aldosterone-producing nodules or multiple aldosterone-producing micronodules (formally known as micronodular hyperplasia)	Multiple APN or multiple APM located beneath the adrenal capsule with intermittent regions of normal zona glomerulosa. MAPN and MAPM can coexist in the same adrenal.
APDH	Aldosterone-producing diffuse hyperplasia	Relatively broad and uninterrupted strip of zona glomerulosa cells with more than half of these cells displaying CYP11B2-positive immunostaining.

The International Histopathology Consensus for Unilateral Primary Aldosteronism (HISTALDO) [22] defined the major histopathological features of surgically removed adrenal glands from PA patients (shown in **Table 1**). The HISTALDO classification system categorizes classic and non-classic histopathological forms of unilateral PA. In the classic form, a solitary APA or a dominant aldosterone-producing nodule (APN) is present [32]. In contrast, the non-classic forms include specimens that are characterized by multiple aldosterone-producing micronodules (MAPMs, formally known as nodular or micronodular hyperplasia) or multiple aldosterone-producing nodules (MAPNs) or rarely, aldosterone-producing diffuse hyperplasia (APDH) [32]. The HISTALDO classification incorporates assessment of hormonal hypersecretion with detailed morphometric evaluation and emphasizes the importance of CYP11B2 immunohistochemistry to differentiate aldosterone-producing lesions from hormonally inactivate lesions.

1.2.3 Genetics and Pathophysiology

1.2.3.1 Somatic and Germline Variants

In the past decade, major progress enabled a further understanding of genetic mechanisms underlying PA. Advances in sequencing technology, such as whole-exome sequencing, have led to the identification of somatic variants, mostly in ion channels and pumps, in sporadic PA cases and rare germline mutations in different subtypes of familial hyperaldosteronism with autosomal dominant inheritance.

1.2.3.2 Familial Hyperaldosteronism

Familial hyperaldosteronism type I (FH-I; initially referred to glucocorticoid-remediable hyperaldosteronism) is caused by a chimeric gene comprising the regulatory sequences of *CYP11B1* (promotor) and the coding region of *CYP11B2* (coding region) [33]. This chimeric *CYP11B1*/*CYP11B2* (*CYP11B1/2*) variant is controlled by ACTH, leading to ectopic expression of the aldosterone synthase gene (*CYP11B2*) in the adrenal zF cells and consequent increased concentrations of aldosterone and hybrid steroids 18-hydroxycortisol and 18-oxocortisol. Treatment with glucocorticoids is required for therapeutic management. Familial hyperaldosteronism type II (FH-II) is associated with a germline variant of *CLCN2* that encodes a

voltage-gated chloride channel [34]. This aberrant alteration causes an increased efflux of cellular chloride, membrane depolarization and Ca^{2+} influx via the activation of voltage-gated Ca^{2+} channels, which induce inappropriate aldosterone secretion. Familial hyperaldosteronism type III (FH-III) results from germline missense mutations in the inward rectifier K^+ channel, which is encoded by the *KCNJ5* gene, as a result of increased sodium (Na^+) influx into the cells and depolarization [35]. Mutations in *KCNJ5* lead to reduced selectivity for K^+ ions, an increased influx of Na^+ ions, and of Ca^{2+} ions (via voltage-gated Ca^{2+} channels), which leads to a rise in intracellular Ca^{2+} concentration and, in turn, triggers aldosterone production. Familial hyperaldosteronism type IV (FH-IV) is caused by heterozygous germline mutations in the *CACNA1H* gene (encoding the T-type Ca^{2+} channel CaV3.2), which activates Ca^{2+}-mediated signaling pathways [36]. In addition, de-novo missense gain-of-function germline mutations in Cav1.3, an L-type voltage-gated Ca^{2+}-channel (encoded by *CACNA1D* gene), are responsible for a complex neurological syndrome (PA with seizures and neurologic abnormalities [PASNA]) [37].

1.2.3.3 Somatic Variants in Primary Aldosteronism

A. Somatic Variants in APAs.

Solitary APA is the most frequent cause of sporadic forms of PA with lateralized aldosterone production, which is typically treated by unilateral adrenalectomy. Due to the availability of tumor tissues for genetic studies in APAs, somatic aldosterone-driver variants in genes encoding an ion channel (such as, *CLCN2*, *KCNJ5*, *CACNA1H*, and *CACNA1D*) that also cause familial forms of PA, ATPases (*ATP1A1* and *ATP2B3*), and β-catenin (*CTNNB1*) have been described so far that lead to upregulated aldosterone secretion. Notably, advanced genetic sequencing, together with CYP11B2 immunohistochemistry, has led to the detection of a genetic cause in 85–96% of aldosterone synthase-expressing adrenal nodules[26,32,38-40].

The first gene mutations to be identified and linked to PA were recurrent somatic mutations in the *KCNJ5* gene. Whole-exome sequencing of 22 APAs identified two variants in *KCNJ5* (causing G151R and L168R substitutions) [41]. This finding was further supported by subsequent systematic analyses of the mutations in a larger number of APAs. Of these patients, 40% were estimated to

have an identifiable *KCNJ5* variant [42,43]. These data suggest that *KCNJ5* mutations are the most recurrent mutation events in APA. One particular variant, G151R, is located within the K^+ channel's selectivity filter that conducts the outward-rectifying K^+ current to maintain the resting membrane potential, and the second variant, L168R, is located nearby. The mutations G151R and L168R lead to increased Na^+ permeation and membrane voltage depolarization, which cause the opening of voltage-gated Ca^{2+} channels and allow an inward Ca^{2+} current, thereby stimulating aldosterone secretion. Patients carrying *KCNJ5* mutations show distinct cellular compositions with clear cell dominant (60% lipid-laden [zF-like] cells versus 40% compact eosinophilic [zG-like] cells) [44]. APAs with *KCNJ5* variants are associated with a higher level of expression of the *CYP17A1* gene [45] and a greater intensity of CYP11B1 immunostaining [26]. Of note, CYP17A1 is a crucial enzyme in 11-deoxycortisol and cortisol biosynthesis as a basis for the synthesis of hybrid steroids in the presence of CYP11B2. The concomitant expression of CYP11B2 and CYP17A1 in the same cells could explain the accumulation of 18-oxocortisol and 18-hydroxycortisol, as observed in the *KCNJ5* mutated APAs. Accordingly, studies from Japanese populations in which *KCNJ5* pathogenic mutation account for most of the cases often exhibit success in the stratification of unilateral forms from bilateral forms of PA using plasma 18-oxocortisol alone [40,46]. Collectively, these data indicate the link between cellular composition and *KCNJ5* mutation status may reflect, at least in part, their characteristic steroidogenic activity [47-49].

Beyond the identification of *KCNJ5* mutations described above, numerous sequencing analyses have been undertaken in PA patient cohorts, which have together established that mutations in *CACNA1D* account for 14–42% of patients with APA[26,38,39], suggesting that *CACNA1D* mutations are the second highest mutation burden in APAs. Specifically, mutations shift the membrane potential of voltage-dependent channels to more negative values or delay the inactivation of the channels. These changes result in an increased influx of Ca^{2+} into the cells, activating Ca^{2+} signaling and increasing aldosterone production. Other less frequent mutations are *ATP1A1* (encoding alpha-1 subunit of the Na^+/K^+ ATPase) and *ATP2B3* (encoding a plasma membrane Ca^{2+} transporting ATPase 3) in approximately 3–17% and 1.5–4% of APAs, respectively [38,39,42,50,51]. In addition, activating mutations of *CTNNB1* (encoding β-catenin) are found in rare cases [37,51,52].

B. Somatic Mutations in APMs and Bilateral Primary Aldosteronism.

The terms APMs (also known as aldosterone-producing cell clusters [APCC]) refer to zG cells located beneath the adrenal capsule with immunohistochemical positivity for CYP11B2. Histological studies found APMs in the surgical resection of adrenal glands from both normotensive and hypertensive subjects [31,53,54]. Using CYP11B2 immunohistochemistry to select APMs from healthy kidney donors for mutation analysis, Nishimoto et al. found that a spectrum of somatic variants in APMs overlaps with those reported in APAs by panel sequencing candidate genes [27]. According to their study, 35% of 31 APMs harbor somatic variants, with 7 in *CACNA1D*, 3 in *ATP1A1*, and 1 in *ATP2B3*. Similar histopathological lesions are observed in specimens of tumor tissues from PA patients and no evidence of adenoma on imaging [24]. CYP11B2 immunohistochemistry-guided next-generation sequencing of adrenal glands with lateralized aldosterone production reveals 81% of APMs bearing somatic mutations in the *CACNA1D* (the most frequent genetic alteration), *KCNJ5*, *ATP1A1*, or *ATP2B3* gene, whereas none of these mutations are detected in APDH [24].

APMs might play a role in the pathophysiology of bilateral PA. A study of 15 adrenal glands from patients, with IHA without detectable masses by adrenal imaging (primarily CT scans), found APMs in all cases, while APDH was detected in only 4 adrenals [31]. APMs were also observed to be larger and more numerous in patients with IHA than those who had unilateral PA and normal adrenal glands. 99 APCCs from this cohort were sequenced, of which 58% had *CACNA1D* mutations, and 1% had *KCNJ5* mutations [31].

C. Mutations in Proliferation

Over the past decade, several mutations in genes associated with autonomous aldosterone production have been clearly identified, but their role in APA development remains debated. Much of our current understanding of APA tumorigenesis is grounded on the principle of the APM model [55] and the two-hit model [54]. According to the APM model, some zG cells accumulate the requisite somatically acquired genetic aberrations, resulting in the formation of an APM, which subsequently develops into a nodule, and ultimately an APA. Of note, transduction of

mutant *KCNJ5* causes lethality rather than proliferation in cultured HAC15 cells, likely due to massive Na^+ influx [56,57]. This observation appears to contradict in vivo evidence performed in APAs where *KCNJ5* mutated APAs tend to be larger than those without a *KCNJ5* mutation [43,58]. Furthermore, APA-associated pathogenic germline *KCNJ5* variants have been linked to massive adrenocortical hyperplasia, suggesting these mutations may trigger tumorigenesis by promoting cell proliferation or blocking transdifferentiation in vivo [56,59,60]. In line with this, adrenal hyperplasia in the adrenal gland of a patient with germline mosaicism was restricted to *KCNJ5* mutated areas [59]. These seemingly contradictory in vitro and in vivo findings can be reconciled by recent work from Yang, Y., et al showing that the role of *KCNJ5* mutation on cell proliferation depends on the expression level of the encoded mutated channel [57].

The alternative two-hit model is proposed for APA formation, with genetic or environmental factors causing abnormal cell proliferation (first hit), followed by the occurrence of a somatic mutation responsible for autonomous aldosterone production (second hit). The two-hit hypothesis is supported by a young patient who has bilateral macronodular adrenal hyperplasia due to familial adenomatous polyposis [61]. This case study showed that germline heterozygous *APC* mutation was found in all surgically resected nodules (mostly nonfunctional), whereas only the nodule that expressed aldosterone synthase carried a *KCNJ5* mutation [61], suggesting that a genetic risk (*APC* variant) provide cells with selective advantages for remodeling of the adrenal cortex (increased nodulation and decreased vascularization), and the additional risk (*KCNJ5* variant) is acquired for aldosterone hypersecretion.

D. Genotype-Phenotype Relationships

(1) Sex and Ethnicity Distribution

The frequencies of somatic aldosterone driver mutations vary between sexes and ethnicities. Female patients are more likely to carry the *KCNJ5* mutation (56–63% in females versus 22–31% in males), while male patients are more likely to carry the *CACNA1D* and *ATP1A1* mutations [42,43]. The highest prevalence of *KCNJ5* mutations occurs in Asian populations [58,62,63], followed by European [38] and African populations [39]. However, *CACNA1D* mutations outnumber *KCNJ5*

mutations in Afro-Americans [39]. The reasons for these differences in prevalence are currently unknown.

(2) AngII Responsiveness

Under physiological conditions, zG cells secrete aldosterone upon exposure to elevated levels of AngII and AngII-responsive and AngII-unresponsive forms of PA have been categorized based on the aldosterone response to AngII infusion or upright posture (which activates the RAAS). In bilateral PA patients, aldosterone secretions usually are responsive to upright posture, but such responsiveness is either absent or reversed in around 60% of unilateral PA patients [64-68]. Further, the APAs resected from AngII-unresponsive patients were characterized by predominantly adrenal zF-like cells and high urinary levels of hybrid steroids. Conversely, posture (or AngII)-responsive APAs primarily comprised adrenal zG-like or mixed cells [69-73].

A link between mutations and AngII responsiveness has been reported by Guo, Zeng, et al [47]. *CACNA1D* mutations are frequently found in posture-responsive APAs, while *KCNJ5* mutations were correlated with posture-unresponsive APAs (**Figure 3, Panel A**). In addition, posture-responsive APAs more frequently lacked *KCNJ5* mutation (**Figure 3, Panel B**). Therefore, *KCNJ5*-mutated APAs seem to represent posture-unresponsive APAs (**Figure 3, Panel C**) [74].

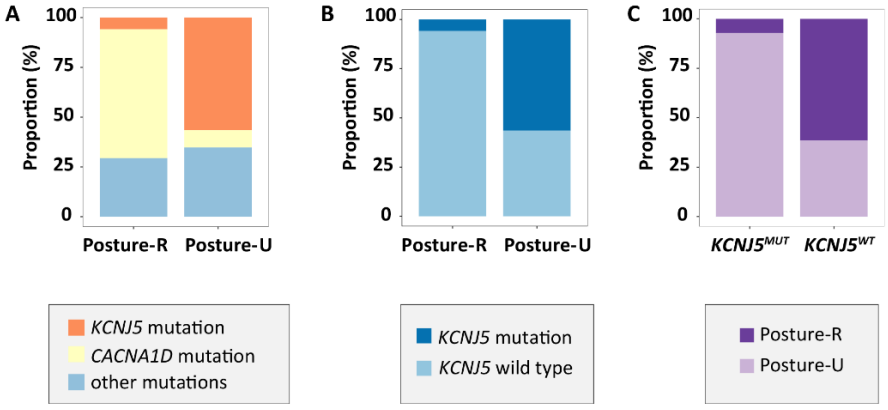

Figure 3: Data from Guo, Zeng, et al [47] show a link between mutations and AngII responsiveness. Posture-R, posture-responsive; posture-U, posture-unresponsive.

(3) Metabolic Determinants

Exploration of metabolism within adenomas and their association with aldosterone-driver mutations may unravel novel disease mechanisms. Using matrix-assisted laser desorption/ionization mass spectrometry imaging (MALDI-MSI), Murakami and colleagues found that APAs with *KCNJ5* mutations display a distinct metabolic signature from APAs with *CACNA1D* mutations [75]. Pathway analysis of metabolic signatures of *KCNJ5* mutated APAs versus *CACNA1D* mutated APAs revealed significant changes in purine synthesis and purine metabolism, suggesting that *KCNJ5* mutated APAs characterized by a larger tumor size may be energetically favored and facilitated by purine synthesis. In a separate cohort, MSI-based metabolomics analysis was carried out on 27 APMs and 6 APAs from PA patients [30]. Component analysis demonstrated that two types of APMs (APM subgroups 1 and 2) are present, in which APM subgroups 2 showed similar metabolic profiles as APAs, whereas APMs in subgroup 1 exhibited a remarkably unique metabolic property, independently of mutation status. As compared to APM subgroup 1, APAs and APM subgroup 2 showed an increase in hexose monophosphate shunt activity (the pentose phosphate pathway), which occurs primarily in the liver and adrenal gland where steroids or fats are synthesized and bypasses glycolysis for glucose metabolism [76]. Elevated activity of the pentose phosphate pathway has been shown to provide the greatest metabolic benefit for proliferating tumor cells under oxidative stress, thereby favoring the concept that a minority of APMs might evolve into APAs as a consequence [77].

1.2.3.4 Other Mechanisms

A. Transcriptional Regulation Mechanisms

Extensive efforts have been made to dissect the genetic disorders underlying aberrant aldosterone hypersecretion. Recent years have demonstrated that several transcriptional regulators, of excitatory or inhibitory nature, are involved in APA steroidogenesis and tumorigenesis, including genes coding nuclear receptor transcription factors (*NR4A2* [78-81], *NR4A1* [78-80], *NR0B1* [80,82], *NR5A1* [80,83], and *NR1B1* [84]), plasma membrane receptors (*SCARB1* [85,86]), ion channels (*KCNK1* [45,87], *KCNK5* [10,13,57], *SLC24A3* [45], *ANO4* [88], *CACNA1A* [89], *CACNA1C* [89], and *CACNA1E* [89]), Ca^{2+} signaling (*CALM2* [85], *CALR* [85], *CAMK1* [90,91], *CAMK2B* [90], *CALN1* [92], *ATP2A3* [85], *CLGN* [93], *PCP4*

[94,95], *VSNL1* [96], and *GSTA1* [97,98]), G-protein coupled receptors (*LHCGR* [99,100], *GNRHR* [100-102], *HTR4* [101,103-105], *AGTR1* [106,107], *PTGER1* [105], *GRM3* [101,105,108], *EDNRB* [85], *MC2R* [105,106,109], *AVPR1A* [101], *PTGFR* [101], and *GPER1* [110]), and genes involved in the regulation of energy (*FDX1* [111], *POR* [85,111], *CYB5* [85,94,111,112], *ATAD3C* [113], and *ACSS3* [81]), protein binding (*NEFM* [114], *NPNT* [115], *MRAP* [106], *PROM1* [113], and *SFRP2* [78]), and DNA binding/RNA polymerase (*GATA6* [80,116], *PRRX1* [113], *DACH1* [117], and *BEX1* [87,118]), as well as oncogenes and tumor suppressor genes (*COPS5* [85], *MYC* [85,119], *IGFBP2* [85,120], *CCN3* [85,121], *TDGF1* [85,122]) (**Table 2**).

More recently, from our transcriptome profiling of macro-adenomas versus micro-adenomas, a number of genes were identified with a potential function in APA pathophysiology. These genes include BEX1 which we identified as a suppressor of ferroptosis (an iron- and lipid peroxidation-driven form of cell death) in APAs [118], and *TSPAN12*, a member of the tetraspanin family [118,123]. TSPAN12 dysfunction is implicated in a wide variety of human cardiovascular diseases [124]. In addition, TSPAN12 has also been linked to cancer progression and diabetes [125,126] and was recently identified as a part of the most informative transcriptome profile for the zonal production of steroids in the adrenal gland [127]. Nevertheless, the functional role of *TSPAN12* in the physiological regulation and pathogenic mechanisms associated with autonomous aldosterone production and tumor growth was unknown.

Prior studies have shown that peripheral steroid profiles can be used to distinguish patients with APAs harboring *KCNJ5* mutations from those without *KCNJ5* mutations [49,128]. These differences in steroid production may be linked to the particular cellular phenotype and transcriptome profile in APAs with *KCNJ5* mutations [26,49,129]. Despite these observations, a comprehensive understanding of the molecular and cellular basis of the genotype-phenotype differences in APAs and their underlying mechanisms remains elusive. The emergence of spatial transcriptomics has provided a high-throughput method to investigate tumor heterogeneity in a spatial context [130-133]. Traditional next-generation sequencing approaches require dissociation of the tissue and thus lack tissue context. Spatial transcriptomics overcomes this limitation by enabling the study of gene expression patterns within the context of the APA architecture. As such, the application

of spatial transcriptomics represents a powerful tool to uncover novel insights into the pathogenic microenvironment of APAs and inform the development of targeted therapies.

Table 2: Transcriptome-identified up- or downregulated genes in APAs.

Genes	Expression		Validated biological functions
	APA[a]	zF-like APAs versus zG-like APAs[b]	
Nuclear receptors/transcription factors			
NR4A2 (NURR1)	Increase/Decrease	··	Stimulates *CYP11B2* expression
NR4A1 (NGF1B or NUR77)	Increase	··	Stimulates *CYP11B2* expression
NR0B1 (DAX1)	Increase/Decrease	··	··
NR5A1 (SF-1)	Increase	··	Suppresses *CYP11B2* expression, stimulate cell proliferation, inhibit apoptosis
NR1B1 (RARα)	Decrease	··	Maintains normal adrenal cortex structure and cell proliferation
Plasma membrane receptor			
SCARB1 (CD36 or SR-BI)	Increase	··	Involved in the HDL stimulated *CYP11B2* expression
Ion channels			
KCNK1 (TWIK-1)	··	Decrease	··
KCNK5 (TASK2)	Decrease	Decrease	Mutations of selectivity filter sequence in some human APAs and familial hyperaldosteronism III; inhibit aldosterone synthesis
SLC24A3	··	Decrease	··
ANO4	Decrease	··	Inhibits calcium-mediated aldosterone secretion and cell proliferation
CACNA1A	Increase	··	··
CACNA1C	Increase	··	··
CACNA1E	Increase	··	··
Calcium signaling			
CALM2	Increase	··	··
CALR	Increase	··	··
CAMK1	··	Increase	Stimulates *CYP11B2* expression
CAMK2B	··	Decrease	··
CALN1	Increase	··	Stimulates angiotensin II– or KCNJ5 T158A–mediated aldosterone production
ATP2A3 (SERCA3)	Increase	··	··
CLGN	Increase	··	Stimulates aldosterone production
PCP4	Increase	Increase	Stimulates angiotensin II- mediated aldosterone production
VSNL1	Increase	Increase	Stimulates basal and angiotensin II-stimulated aldosterone production, inhibit calcium-induced apoptosis
GSTA1	Decrease	Decrease	Suppresses basal and angiotensin II-stimulated aldosterone secretion

Genes	Expression		Validated biological functions
	APA[a]	zF-like APAs versus zG-like APAs[b]	
(Continued from previous page)			
G-protein coupled receptors			
LHCGR	Increase	··	Stimulates *CYP11B2* expression
GNRHR	Increase	··	Stimulates aldosterone production
HTR4	Increase	··	Stimulates aldosterone production
AGTR1 (AT1R)	Increase	Increase	Stimulates aldosterone production
PTGER1	Increase	··	··
GRM3	Increase	··	Inhibits angiotensin-II/forskolin induced aldosterone production
EDNRB	Increase	··	··
MC2R	Increase	Decrease/No change	Stimulates aldosterone secretion
AVPR1A	Decrease	··	··
PTGFR	Decrease	··	··
GPER1	Increase	··	Stimulates *CYP11B2* expression
Energy			
FDX1	Decrease	··	··
POR	Increase/No change	··	··
CYB5A (CYB5)	Increase/Decrease	··	Required for androstenedione production
ATAD3C	Increase	··	··
ACSS3	··	Increase	··
Protein binding			
NEFM	··	Decrease	Inhibits basal and dopamine D1 receptor mediated aldosterone secrection, inhibit cell proliferation
NPNT	··	Decrease	Stimulates aldosterone production, proadhesive in primary adrenal and APA cells but antiadhesive and antiapoptotic in immortalized adrenocortical cells
MRAP	Decrease	··	··
PROM1	Increase	··	··
SFRP2	Decrease	··	*Sfrp2* $^{-/-}$: increases aldosterone production and ectopic differentiation of zona glomerulosa cells
Cell growth/cell death			
COPS5 (JAB1)	Increase	··	··
MYC	Increase	··	Regulates responsiveness to paclitaxel in adrenocortical cancer cell lines
IGFBP2	Increase	··	Enhances adrenocortical tumorigenesis
CCN3 (IGFBP9 or NOV)	Increase	··	A selective proapoptotic factor for human adrenocortical cells
TDGF1	Increase	··	Stimulates aldosterone secretion, protect adrenocortical cells from staurosporine induced apoptosis
DNA binding/RNA polymerase			
GATA6	Increase	··	Required for adrenal androgen biosynthesis
PRRX1	Increase	··	··
DACH1	Decrease	··	Inhibits aldosterone production
BEX1	Increase	Decrease	Protects human adrenocortical cells from RSL3 induced-ferroptosis

[a]APAs versus normal adrenal gland or other adrenocortical tumors. [b]Alternatively, *KCNJ5* mutated APA versus *KCNJ5* wild type APAs

B. Metabolic Programming and Tumor Microenvironment

It has been increasingly recognized that metabolic programming of tumor cells in response to their elevated energy demand is required to adapt to nutritionally adverse circumstances that may restrict growth [134-138]. Hormone hypersecretion involves high metabolic activity and therefore, metabolic adaptations of hormone-hypersecreting cells have been proposed [139]. Thus, it is reasonable to hypothesize that metabolic reprogramming can contribute to tumorigenesis during the progression of APAs. Further, alterations in the utilization of nutrients under metabolic stress conditions can cause competition for metabolic substrates within the tumor microenvironment leading to an impaired anti-tumoral immune response [140-142]. Yet, the understanding of tumor microenvironment in APA remained incomplete.

1.2.4 Diagnostic Investigation

The recommended diagnosis of PA is based on a multistep process as shown in **Figure 4**.

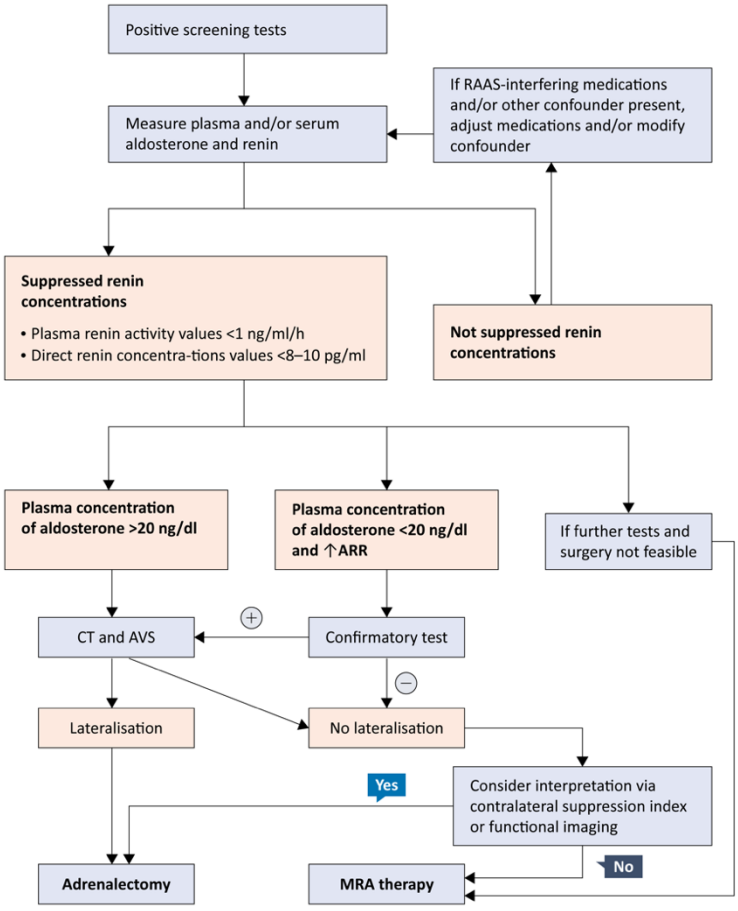

Figure 4: Proposed algorithm for diagnosing and managing PA. MRA, mineralocorticoid receptor antagonist.

1.2.4.1 Screening

As the diagnostic entry point for PA, current guidelines recommend routine aldosterone-to-renin ratio (ARR) screening across a wide population of hypertensive patients (**Table 3**) because ARR screening within high-risk subpopulations can substantially increase the proportion of individuals being diagnosed with PA, especially in patients without typical symptoms observed (such as normokalaemic).

When to Screen for Primary Aldosteronism
Patients with hypertension grade 2–3 or resistant
Patients with hypokalaemia (spontaneous or diuretic-induced)
Patients with hypertension and adrenal incidentaloma
Patients with hypertension and atrial fibrillation (without underlying cardiac structural cause)
Patients with a family history of early onset hypertension or stroke at a young age (<40 years)
all first-degree relatives with hypertension of patients with primary aldosteronism

Table 3: Recommendations for PA screening [21,143]

An increased ARR is calculated based on the plasma aldosterone concentration and plasma renin activity (or plasma renin concentration). Of note, aldosterone or renin alone varies widely [144], primarily due to posture, time of day, serum levels of potassium, dietary salt intake, and influence of antihypertensive drugs affecting the RAAS. Therefore, the interpretation of the ARR results is particularly warranted [21]. Strategies to achieve clinical benefit involve avoiding these potentially confounding effects on renin and aldosterone concentrations.

1.2.4.2 Confirmatory Testing

As a screening test with high sensitivity cannot avoid generating false-positive results, all patients with positive screening tests should then undergo one or more confirmatory tests to diagnose or exclude PA [21,143]. Available confirmatory tests include the fludrocortisone suppression test, the oral sodium loading test, the intravenous saline infusion test, and the captopril challenge test [20].

The most frequently used tests are the oral and the intravenous saline load tests [21,143]. However, there is no universally accepted gold standard test, and preferences usually depend on the availability of local resources and physician experience [145].

1.2.4.3 Subtype Differentiation

Traditionally, PA is subdivided into unilateral and bilateral forms. Subtyping of PA is driven primarily to guide treatment. In general, unilateral PA is treated by surgical removal of the dominant adrenal gland by laparoscopic unilateral adrenalectomy, whereas bilateral PA requires medical therapy. Therefore, differentiation of unilateral forms of PA is extremely important for treatment decision-making. Adrenal imaging and AVS are typically used for PA subclassification in clinical practice to identify unilateral or bilateral morphological alterations and/or aldosterone hypersecretion.

1.2.4.4 Therapy and Outcome

The current treatment strategy is centered around the prevention of cardiovascular events related to hyperaldosteronism. Additionally, the treatment goals also include normalizing the serum K^+ levels in patients with hypokalemia and the blood pressure values. According to the Endocrine Society Guidelines for PA management [21], unilateral laparoscopic adrenalectomy is the mainstay of treatment for unilateral PA; mineralocorticoid receptor blockade with spironolactone or eplerenone is recommended for patients who cannot undergo surgery or those with bilateral PA. Recent studies have demonstrated that patients may receive greater benefits from surgical adrenalectomy compared to mineralocorticoid receptor blockade. These benefits may be attributed to more effective control of blood pressure and a reduced requirement for hypertension medication, as well as the reversal of left ventricular hypertrophy[146], a lower risk of atrial fibrillation [147]or chronic kidney failure [148], and an improvement in quality of life [149].

The aim of surgical therapy for PA is to remove the source of excessive aldosterone secretion and to normalize blood pressure with the ultimate goal to reduce comorbidities associated with hyperaldosteronism, enhancing patient well-being, and reducing life-threatening events. The

standardized postoperative outcomes criteria for patients with unilateral PA undergoing laparoscopic adrenalectomy have been developed in the Primary Aldosteronism Surgical Outcome (PASO) study by a panel of 31 international experts from 28 centers [150]. The PASO criteria highlight the distinction between clinical and biochemical outcomes, each being categorized as complete, partial, or absent success (**Figure 5**).

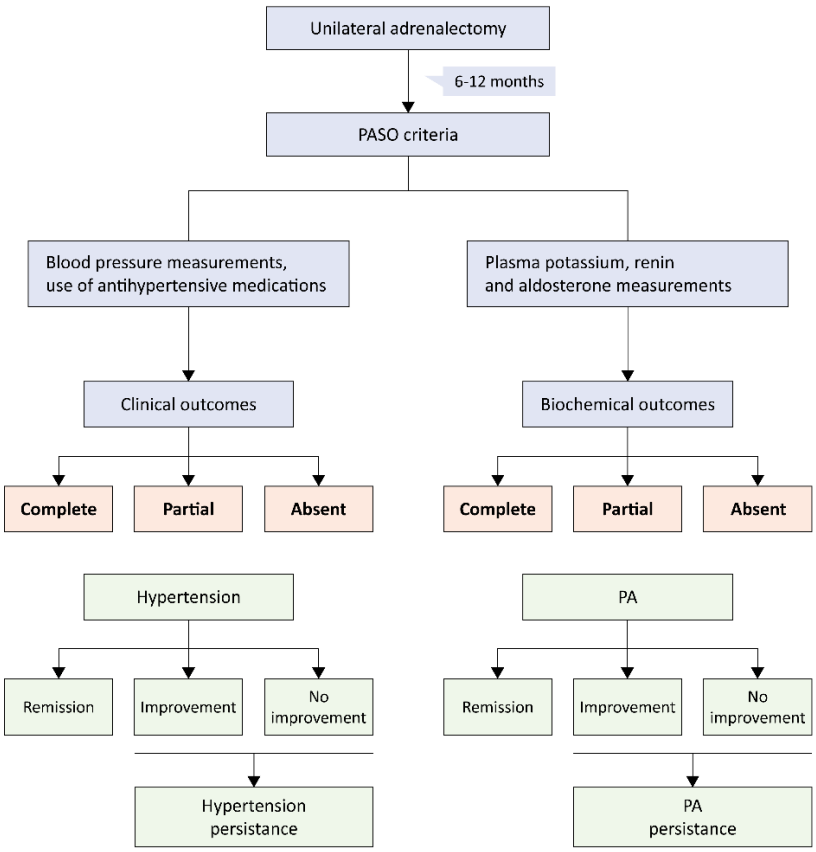

Figure 5: PASO criteria.

The results of the PASO study, which analyzed data both preoperatively and postoperatively from 705 patients with surgically treated PA, showed that 94% of the 699 patients (with a range of 83-100% between centers) achieved complete biochemical success, meaning the normalization of potassium levels and aldosterone to renin ratios. However, only 37% of the 705 patients (with a range of 17-62% between centers) achieved complete clinical success, which is defined as having

normal blood pressure without the use of antihypertensive medication. The study also found that 47% (with a range of 35-66% between centers) of patients achieved partial clinical success. These results suggest that adrenalectomy is a rewarding treatment for patients with APA, potentially reducing the future risk of adverse cardiovascular events caused by aldosterone-mediated mechanisms.

Mineralocorticoid receptor antagonists are typically prescribed for patients with bilateral PA. Of note, there is no high-quality clinical trial demonstrating that lifelong MR antagonist therapy in bilateral PA is beneficial; rather, it has been accepted as a standard practice based on logical assumptions for decades. The suitability of using laparoscopic adrenalectomy as a treatment for bilateral PA remains an open question. In the early 1970s, a study reported first data showing that unilateral adrenalectomy for bilateral PA could normalize blood pressure and aldosterone production, but eventually the condition worsened over time [151]. Some years later, Groth et al. demonstrated that five years after unilateral surgery, a significant clinical benefit was maintained in patients originally diagnosed with bilateral PA [152]. Similar observations were reported in a larger cohort of patients [153].

1.3 Aims of this Thesis

The specific aims of my dissertation included the following:

- **Aim I:** To demonstrate the metabolic diversity between APA and adjacent adrenal cortex and elucidate the characteristics of the tumor microenvironment of APA **(paper I)**
- **Aim II:** To establish a role for TSPAN12 in the pathogenesis of APA **(paper II)**
- **Aim III:** To investigate transcriptomic and metabolomic reprogramming in APA pathophysiology using spatial transcriptomics and MSI-based spatial metabolomics (**paper III**)

1.4 Summary

This dissertation applied multiple approaches to achieve the three main goals as detailed below:

In publication I [154], published in Cancers 2021, bioinformatic analyses of microarray gene expression datasets revealed the enhanced fatty acid β-oxidation and glycolysis in APA compared to paired adjacent adrenal cortex. In addition, pharmacological inhibition of fatty acid β-oxidation induced cell lethality in cultured human adrenocortical cells. Together, these data indicate that fatty acid β-oxidation might play a role in adenoma progression. Further analyses using GSEA and ESTIMATE algorithms demonstrated the downregulation of immune-related pathways and decreased stromal and immune scores in APAs when compared to paired adjacent adrenal cortex. In accordance with the transcriptomic data, staining for CD45 displayed a positive signal in adjacent adrenal cortex surrounding an APA. Distinct immune microenvironment landscapes were further determined by analyzing transcriptomic data from a cohort of 13 APAs and its adjacent matched paired zG, and zF samples using the MCP-counter algorithm. In particular, we found that the frequency of anti-immune cells was lower, and the frequency of pro-immune cells was higher in APAs than those in adjacent zG, suggesting the immunosuppressive microenvironment in APAs. Moreover, upregulated expression of a subset of inflammatory response genes in the adjacent zG were associated with oxidative stress pathways, indicating that pro-inflammatory response in the adjacent zG may be elicited by oxidative stress. In addition, anti-oxidative response pathways were enriched in APAs, concomitant with elevated aldosterone production and abnormal proliferation. Collectively, these data indicated that metabolic reprogramming and remodeling of tumor microenvironment may involve in the APA pathophysiology. Current literature suggests that active steroidogenesis, the metabolic process for producing steroid hormones, is energetically demanding and leads to elevated levels of reactive oxygen species (ROS) [155]. These elevated ROS levels cause oxidative stress, which can then lead to cellular damage and eventual cell death [118]. Future work is needed to completely elucidate the specific metabolic mechanisms that balance pathological ROS levels back to homeostatic baseline to drive aldosterone hypersecretion and adenoma formation.

In publication II [156], published in Hypertension 2023, we interrogated our RNA-seq transcriptome data from 21 APAs. The Gene Ontology analysis conducted in our study compared the *TSPAN12*^{high} and *TSPAN12*^{low} groups, distinguished based on the median of *TSPAN12* expression levels, and found that the *TSPAN12*^{high} group had increased RAAS activity, particularly in blood pressure regulation through the circulatory RAAS and hormones, indicative of a correlation between *TSPAN12* and the RAAS. In a separate cohort of 30 APA patients, *TSPAN12*^{low} group comprised a significant proportion of APAs with a *KCNJ5* mutation. TSPAN12 downregulation in APAs with a *KCNJ5* mutation compared with APAs without a *KCNJ5* mutation was further determined by immunohistochemistry, which confirmed a significant decrease in *TSPAN12* transcript levels in *KCNJ5* mutated APAs. Clinically, *TSPAN12* expression was negatively correlated with peripheral plasma concentrations of aldosterone, and with the hybrid steroids 18-oxocortisol, and 18-hydroxycortisol measured by liquid chromatography-tandem mass spectrometry (LC-MS/MS). Using a publicly available transcriptome dataset, we found the increased expression of *TSPAN12* in zG cells adjacent to pheochromocytoma (a form of high renin hypertension) compared with zG cells adjacent to APA (a form of low renin hypertension). Consistent with our transcriptomic analyses, immunostaining quantifications showed the absence of TSPAN12 expression in zG surrounding an APA. Adrenal glands from pigs with higher RAAS activities (induced by dietary sodium restrictions) exhibit a higher intensity of TSPAN12 immunostaining in the zG compared with pigs with a suppressed RAAS (induced by high dietary salt). Together, these findings indicate that TSPAN12 is a RAAS-responsive gene in zG cells. Furthermore, adrenocortical cells exposed to AngII, an active component of the RAAS, showed the marked increase of *TSPAN12* expression, and this was prevented by Ca^{2+} channel blockers, implicating that RAAS-induced TSPAN12 expression is mediated by Ca^{2+} signaling. Furthermore, knocked down *TSPAN12* using short interfering RNA (siRNA) in human adrenocortical cells established an inverse relationship between *TSPAN12* and aldosterone secretion in both unstimulated and AngII-stimulated conditions. Of note, TSPAN12 had no substantial impact on HAC15 cell proliferation, staurosporine-induced apoptosis, and RSL3-induced cell death by ferroptosis. These findings underscore TSPAN12 in regulating excess aldosterone production under physiological and pathophysiological conditions and highlight TSPAN12 as a potential

mediator in posture-responsive APA. Future efforts will be devoted to further characterization of the molecular mechanisms underlying the suppressive activities of TSPAN12 on aldosterone production and, furthermore, the potential role of chronic RAAS suppression in APA pathophysiology and TSPAN12 function in posture-responsive and posture-unresponsive APA are unclear and warrant further lines of study.

In publication III, published in Hypertension 2023, we profiled 14 adrenal samples, including APA-*KCNJ5*^{MUT} (*n* = 4) and APA-*KCNJ5*^{WT} (*n* = 3), and their paired adjacent adrenal tissues using spatial transcriptomics and MSI-based spatial metabolomic analysis. By applying a non-negative matrix factorization (NNMF) approach, we deconvolved the APA-*KCNJ5*^{MUT} samples in the spatial transcriptomics dataset individually to identify transcriptionally distinct regions within each sample. For example, NNMF analysis of the APA section from Patient 1 with a *KCNJ5* mutation revealed 3 distinct tumor related-transcriptional signatures (factor 1, 3 and 4). APA harboring *KCNJ5* mutation often show CYP11B2 heterogeneity with a diminished proportion of cells staining positive for CYP11B2. To extend this characterization to the spatial transcriptional level, we stratified tumor spatial transcriptomic spots of APA-*KCNJ5*^{MUT} samples into high and low CYP11B2 expression. Pathway analysis with PROGENy revealed increased expression of steroidogenesis-related genes (e.g, *PCP4, FDX1, MC2R*) and activation of steroidogenesis-related pathways (e.g, VEGF signaling, p53 signaling, and androgen signaling) in transcriptome populations with high expression of *CYP11B2*. We also employed NNMF analysis on APA-*KCNJ5*^{WT} samples and observed one or more tumor-related transcriptome signature in 3 patients. This overall suggested intra-tumoral transcriptional heterogeneity in APAs. To identify common transcriptional signatures (or factors) across all 7 APAs, we further performed spatially weighted correlation and hierarchical clustering analysis and identified 2 transcriptional programs in *CYP11B2*-expressing regions (refer to *CYP11B2*-type 1 and *CYP11B2*-type 2). The dominance of *CYP11B2*-type 1 in APA-*KCNJ5*^{WT} corresponded to the prevalence of compact eosinophilic cells expressing *CYP11B2* and *KCNJ5* (zG-like cells), while the dominance of *CYP11B2*-type 2 in APA-*KCNJ5*^{MUT} was linked to the higher proportion of lipid-rich clear cells expressing *CYP11B1* and *CYP17A1* (zF-like cells). The comparison of metabolic heterogeneity between APA-*KCNJ5*^{MUT} and APA-*KCNJ5*^{WT} obtained with

MSI-based spatial metabolomics showed that APA-*KCNJ5*^{WT} were enriched for polyunsaturated fatty acids (PUFAs) and phosphatidylethanolamine, while glutamine and glutamate metabolism was activated in APA-*KCNJ5*^{MUT}. Through integrative spatial transcriptomics and spatial metabolomics analysis of the APA and adjacent adrenal glands stratified by *KCNJ5* mutation status, we found genotype-dependent oxidative stress responses. Specifically, we observed a higher abundance of cell death pathways and PUFAs in the APA-*KCNJ5*^{WT}, while APA-*KCNJ5*^{MUT} exhibited upregulated activity of metabolism and steroid biosynthesis along with enriched levels of glutathione. These differential responses to oxidative stress may underlie diverse tumor expansion capacities between the two genotypic groups. Importantly, unbiased clustering analysis of APA and adjacent cortex, stratified by *KCNJ5* mutation status and utilizing t-distributed stochastic neighbor embedding (tSNE) dimensionality reduction, identified APA precursor states in the adjacent normal tissues. Our study warrants further integration of spatial omics techniques with single-cell sequencing approaches to fully understand how the tumor microenvironment influences APA development.

1.5 Zusammenfassung

Diese Dissertation wendete mehrere Ansätze an, um die drei Hauptziele zu erreichen, wie unten beschrieben:

In Publikation I [154], veröffentlicht in Cancers 2021, zeigten bioinformatische Analysen von Microarray-Genexpressionsdatensätzen die verstärkte Fettsäure-β-Oxidation und Glykolyse in APA im Vergleich zu gepaarter benachbarter Nebennierenrinde. Darüber hinaus induzierte die pharmakologische Hemmung der Fettsäure-β-Oxidation Zellletalität in kultivierten menschlichen Nebennierenrindenzellen. Zusammengenommen weisen diese Daten darauf hin, dass die β-Oxidation von Fettsäuren eine Rolle bei der Adenomprogression spielen könnte. Weitere Analysen mit GSEA- und ESTIMATE-Algorithmen zeigten die Herunterregulierung immunbezogener Signalwege und verringerte Stroma- und Immun-Scores in APAs im Vergleich zu gepaarten benachbarten Nebennierenrinden. In Übereinstimmung mit den Transkriptomdaten zeigte die Färbung für CD45 ein positives Signal in der angrenzenden Nebennierenrinde, die ein APA umgibt. Unterscheidbare Immunmikroumgebungslandschaften wurden ferner durch Analysieren von Transkriptomdaten aus einer Kohorte von 13 APAs und ihren angrenzenden gepaarten zG- und zF-Proben unter Verwendung des MCP-Counter-Algorithmus bestimmt. Insbesondere stellten wir fest, dass die Häufigkeit von Anti-Immunzellen geringer und die Häufigkeit von Pro-Immunzellen in APAs höher war als in benachbarten zG, was auf die immunsuppressive Mikroumgebung in APAs hindeutet. Darüber hinaus war die hochregulierte Expression einer Untergruppe von Entzündungsreaktionsgenen im benachbarten zG mit oxidativen Stresswegen verbunden, was darauf hindeutet, dass eine proinflammatorische Reaktion im benachbarten zG durch oxidativen Stress ausgelöst werden kann. Darüber hinaus wurden antioxidative Reaktionswege mit APAs angereichert, begleitet von erhöhter Aldosteronproduktion und abnormaler Proliferation. Zusammengenommen weisen diese Daten darauf hin, dass die metabolische Reprogrammierung und Remodellierung der Tumormikroumgebung in die APA-Pathophysiologie involviert sein können. Die aktuelle Literatur legt nahe, dass die aktive Steroidogenese, der Stoffwechselprozess zur Produktion von Steroidhormonen, energetisch anspruchsvoll ist und zu erhöhten Spiegeln reaktiver

Sauerstoffspezies (ROS) führt [155]. Diese erhöhten ROS-Spiegel verursachen oxidativen Stress, der dann zu Zellschäden und schließlich zu Zellschäden führen kann Tod 118. Zukünftige Arbeiten sind erforderlich, um die spezifischen Stoffwechselmechanismen vollständig aufzuklären, die pathologische ROS-Spiegel wieder auf den homöostatischen Ausgangswert ausgleichen, um die Aldosteron-Hypersekretion und die Bildung von Adenomen voranzutreiben.

In Publikation II [156], veröffentlicht in Hypertension 2023, haben wir unsere RNA-seq-Transkriptomdaten von 21 APAs abgefragt. Die in unserer Studie durchgeführte Gen-Ontologie-Analyse verglich die *TSPAN12*^{high}- und *TSPAN12*^{low}-Gruppen, die anhand des Medians der *TSPAN12*-Expressionsniveaus unterschieden wurden, und stellte fest, dass die *TSPAN12*^{high}-Gruppe eine erhöhte RAAS-Aktivität aufwies, insbesondere bei der Blutdruckregulierung durch das Kreislauf-RAAS und Hormone, was darauf hindeutet eine Korrelation zwischen *TSPAN12* und dem RAAS. In einer separaten Kohorte von 30 APA-Patienten umfasste die *TSPAN12*^{low}-Gruppe einen signifikanten Anteil an APAs mit einer *KCNJ5*-Mutation. Die TSPAN12-Herunterregulierung in APAs mit einer *KCNJ5*-Mutation im Vergleich zu APAs ohne *KCNJ5*-Mutation wurde weiter durch Immunhistochemie bestimmt, die eine signifikante Abnahme der *TSPAN12*-Transkriptspiegel in *KCNJ5*-mutierten APAs bestätigte. Klinisch korrelierte die *TSPAN12*-Expression negativ mit peripheren Plasmakonzentrationen von Aldosteron und mit den Hybridsteroiden 18-Oxocortisol und 18-Hydroxycortisol, gemessen durch Flüssigchromatographie-Tandem-Massenspektrometrie (LC-MS/MS). Unter Verwendung eines öffentlich zugänglichen Transkriptom-Datensatzes fanden wir die erhöhte Expression von *TSPAN12* in zG-Zellen neben Phäochromozytom (eine Form von hoher Renin-Hypertonie) im Vergleich zu zG-Zellen neben APA (eine Form von niedriger Renin-Hypertonie). In Übereinstimmung mit unseren Transkriptomanalysen zeigten Immunfärbungsquantifizierungen das Fehlen einer TSPAN12-Expression in zG, das eine APA umgibt. Nebennieren von Schweinen mit höheren RAAS-Aktivitäten (induziert durch diätetische Natriumrestriktionen) zeigen eine höhere Intensität der TSPAN12-Immunfärbung im zG im Vergleich zu Schweinen mit unterdrücktem RAAS (induziert durch hohe diätetische Salze). Zusammen weisen diese Befunde darauf hin, dass TSPAN12 ein RAAS-responsives Gen in zG-Zellen ist. Darüber hinaus zeigten

Nebennierenrindenzellen, die AngII, einer aktiven Komponente des RAAS, ausgesetzt waren, einen deutlichen Anstieg der *TSPAN12*-Expression, was durch Ca^{2+}-Kanalblocker verhindert wurde, was impliziert, dass die RAAS-induzierte TSPAN12-Expression durch Ca^{2+}-Signale vermittelt wird. Darüber hinaus stellte das Knock-down von *TSPAN12* mithilfe von Short Interfering RNA (siRNA) in menschlichen Nebennierenrindenzellen eine umgekehrte Beziehung zwischen *TSPAN12* und der Aldosteronsekretion sowohl unter nicht stimulierten als auch unter AngII-stimulierten Bedingungen her. Bemerkenswerterweise hatte TSPAN12 keinen wesentlichen Einfluss auf die HAC15-Zellproliferation, Staurosporin-induzierte Apoptose und RSL3-induzierten Zelltod durch Ferroptose. Diese Ergebnisse unterstreichen TSPAN12 bei der Regulierung einer übermäßigen Aldosteronproduktion unter physiologischen und pathophysiologischen Bedingungen und unterstreichen TSPAN12 als potenziellen Mediator bei haltungsabhängiger APA. Zukünftige Bemühungen werden der weiteren Charakterisierung der molekularen Mechanismen gewidmet, die den unterdrückenden Aktivitäten von TSPAN12 auf die Aldosteronproduktion zugrunde liegen, und darüber hinaus sind die potenzielle Rolle der chronischen RAAS-Unterdrückung in der APA-Pathophysiologie und die TSPAN12-Funktion bei haltungsabhängiger und nicht haltungsabhängiger APA unklar und weitere Studienrichtungen rechtfertigen.

In Publikation III, veröffentlicht in Hypertension 2023, haben wir 14 Nebennierenproben, darunter APA-*KCNJ5*^{MUT} (n = 4) und APA-*KCNJ5*^{WT} (n = 3), und ihre gepaarten benachbarten Nebennierengewebe mithilfe von räumlicher Transkriptomik und MSI-basierter räumlicher Metabolomanalyse profiliert . Durch Anwendung eines nicht-negativen Matrixfaktorisierungsansatzes (NNMF) haben wir die APA-*KCNJ5*^{MUT}-Proben im räumlichen Transkriptomdatensatz einzeln entfaltet, um transkriptionell unterschiedliche Regionen innerhalb jeder Probe zu identifizieren. Beispielsweise ergab die NNMF-Analyse des APA-Schnitts von Patient 1 mit einer *KCNJ5*-Mutation 3 unterschiedliche tumorbezogene transkriptionelle Signaturen (Faktor 1, 3 und 4). APA, die eine *KCNJ5*-Mutation beherbergen, zeigen häufig eine CYP11B2-Heterogenität mit einem verringerten Anteil an Zellen, die sich positiv für CYP11B2 färben. Um diese Charakterisierung auf die räumliche Transkriptionsebene auszudehnen,

stratifizierten wir räumliche Tumor-Transkriptom-Spots von APA-*KCNJ5*^{MUT}-Proben in hohe und niedrige CYP11B2-Expression. Pathway-Analysen mit PROGENy zeigten eine erhöhte Expression von Steroidogenese-bezogenen Genen (z. B. *PCP4, FDX1, MC2R*) und eine Aktivierung von Steroidogenese-bezogenen Signalwegen (z. B. VEGF-Signalweg, p53-Signalweg und Androgen-Signalweg) in Transkriptompopulationen mit hoher Expression von *CYP11B2*. Wir haben auch die NNMF-Analyse an APA-*KCNJ5*^{WT}-Proben durchgeführt und bei 3 Patienten eine oder mehrere tumorbezogene Transkriptomsignaturen beobachtet. Dies deutete insgesamt auf eine intratumorale transkriptionelle Heterogenität in APAs hin. Um gemeinsame transkriptionelle Signaturen (oder Faktoren) über alle 7 APAs hinweg zu identifizieren, führten wir ferner eine räumlich gewichtete Korrelation und hierarchische Clusteranalyse durch und identifizierten 2 transkriptionelle Programme in *CYP11B2*-exprimierenden Regionen (siehe *CYP11B2*-Typ 1 und *CYP11B2*-Typ 2). Die Dominanz von *CYP11B2*-Typ 1 in APA-*KCNJ5*^{WT} entsprach der Prävalenz kompakter eosinophiler Zellen, die *CYP11B2* und *KCNJ5* (zG-ähnliche Zellen) exprimieren, während die Dominanz von *CYP11B2*-Typ 2 in APA-*KCNJ5*^{MUT} mit dem höheren Lipidanteil verbunden war -reiche klare Zellen, die *CYP11B1* und *CYP17A1* exprimieren (zF-ähnliche Zellen). Der mit MSI-basierter räumlicher Metabolomik erhaltene Vergleich der metabolischen Heterogenität zwischen APA-*KCNJ5*^{MUT} und APA-*KCNJ5*^{WT} zeigte, dass APA-*KCNJ5*^{WT} mit mehrfach ungesättigten Fettsäuren (PUFAs) und Phosphatidylethanolamin angereichert waren, während der Glutamin- und Glutamatstoffwechsel in APA-*KCNJ5*^{MUT} aktiviert war. Durch integrative räumliche Transkriptomik- und räumliche Metabolomik-Analyse der APA und benachbarter Nebennieren, stratifiziert nach *KCNJ5*-Mutationsstatus, fanden wir genotypabhängige oxidative Stressreaktionen. Insbesondere beobachteten wir eine höhere Häufigkeit von Zelltodwegen und PUFAs in APA-*KCNJ5*^{WT}, während APA-*KCNJ5*^{MUT} eine hochregulierte Aktivität des Stoffwechsels und der Steroidbiosynthese zusammen mit angereicherten Glutathionspiegeln aufwies. Diese unterschiedlichen Reaktionen auf oxidativen Stress können unterschiedlichen Tumorexpansionskapazitäten zwischen den beiden genotypischen Gruppen zugrunde liegen. Wichtig ist, dass eine unvoreingenommene Clustering-Analyse von APA und angrenzendem Kortex, stratifiziert nach *KCNJ5*-Mutationsstatus und unter Verwendung von t-verteilter stochastischer Nachbareinbettung (tSNE)-Dimensionsreduktion, APA-Vorläuferzustände in den

angrenzenden normalen Geweben identifizierte. Unsere Studie rechtfertigt eine weitere Integration von Spatial-Omics-Techniken mit Einzelzell-Sequenzierungsansätzen, um vollständig zu verstehen, wie die Tumormikroumgebung die APA-Entwicklung beeinflusst.

2. My Contribution

For paper I, published in Cancers, I performed bioinformatic analyses of all sequencing data, in vitro cell experiments, and CD45 immunohistochemistry. All statistical analyses were conducted by myself and I prepared all figures, drafted the manuscript, and contributed to the revision.

For paper II, published in Hypertension, I performed bioinformatic analyses of all sequencing data, and did all experimental work. All statistical analyses were conducted by myself and I prepared all figures and tables, drafted the manuscript, and contributed to the revision process.

For paper III, published in Hypertension, I performed bioinformatic analyses of all sequencing and metabolomics data. All statistical analyses were conducted by myself and I prepared all figures and tables, drafted the manuscript, and contributed to the revision process.

3. Publication I

cancers

MDPI

Article

Primary Aldosteronism: Metabolic Reprogramming and the Pathogenesis of Aldosterone-Producing Adenomas

Siyuan Gong [1], Martina Tetti [1,2], Martin Reincke [1] and Tracy Ann Williams [1,2,*]

[1] Medizinische Klinik und Poliklinik IV, Klinikum der Universität München, Ludwig-Maximilians-Universität München, 80336 Munich, Germany; Siyuan.Gong@med.uni-muenchen.de (S.G.); martina.tetti@med.uni-muenchen.de (M.T.); Martin.Reincke@med.uni-muenchen.de (M.R.)

[2] Department of Medical Sciences, Division of Internal Medicine and Hypertension, University of Turin, 10126 Turin, Italy

* Correspondence: tracy.williams@med.uni-muenchen.de; Tel.: +49-089-4400-52137

Simple Summary: Primary aldosteronism is a common form of endocrine hypertension often caused by a hyper-secreting tumor of the adrenal cortex called an aldosterone-producing adenoma. Metabolic reprogramming plays a role in tumor progression and influences the tumor immune microenvironment by limiting immune-cell infiltration and suppressing its anti-tumor function. We hypothesized that the development of aldosterone-producing adenomas involves metabolic adaptations of its component tumor cells and intrinsically influences tumor pathogenesis. Herein, we use state-of-the-art computational tools for the comprehensive analysis of array-based gene expression profiles to demonstrate metabolic reprogramming and remodeling of the immune microenvironment in aldosterone-producing adenomas compared with paired adjacent adrenal cortical tissue. Our findings suggest metabolic alterations may function in the pathogenesis of aldosterone-producing adenomas by conferring survival advantages to their component tumor cells.

Abstract: Aldosterone-producing adenomas (APAs) are characterized by aldosterone hypersecretion and deregulated adrenocortical cell growth. Increased energy consumption required to maintain cellular tumorigenic properties triggers metabolic alterations that shape the tumor microenvironment to acquire necessary nutrients, yet our knowledge of this adaptation in APAs is limited. Here, we investigated adrenocortical cell-intrinsic metabolism and the tumor immune microenvironment of APAs and their potential roles in mediating aldosterone production and growth of adrenocortical cells. Using multiple advanced bioinformatics methods, we analyzed gene expression datasets to generate distinct metabolic and immune cell profiles of APAs versus paired adjacent cortex. APAs displayed activation of lipid metabolism, especially fatty acid β-oxidation regulated by PPARα, and glycolysis. We identified an immunosuppressive microenvironment in APAs, with reduced infiltration of $CD45^+$ immune cells compared with adjacent cortex, validated by CD45 immunohistochemistry (3.45-fold, $p < 0.001$). APAs also displayed an association of lipid metabolism with ferroptosis and upregulation of antioxidant systems. In conclusion, APAs exhibit metabolic reprogramming towards fatty acid β-oxidation and glycolysis. Increased lipid metabolism via PPARα may serve as a key mechanism to modulate lipid peroxidation, a hallmark of regulated cell death by ferroptosis. These findings highlight survival advantages for APA tumor cells with metabolic reprogramming properties.

Keywords: adaptive metabolism; adrenal gland; Conn adenoma; fatty acid metabolism; ferroptosis; hyperaldosteronism; metabolic reprogramming; β-oxidation; PPARα; tumor microenvironment

Citation: Gong, S.; Tetti, M.; Reincke, M.; Williams, T.A. Primary Aldosteronism: Metabolic Reprogramming and the Pathogenesis of Aldosterone-Producing Adenomas. *Cancers* **2021**, *13*, 3716. https://doi.org/10.3390/cancers13153716

Academic Editors: Adam E. Frampton

Received: 2 June 2021
Accepted: 21 July 2021
Published: 23 July 2021

Publisher's Note: MDPI stays neutral with regard to jurisdictional claims in published maps and institutional affiliations.

Copyright: © 2021 by the authors. Licensee MDPI, Basel, Switzerland. This article is an open access article distributed under the terms and conditions of the Creative Commons Attribution (CC BY) license (http://creativecommons.org/licenses/by/4.0/).

1. Introduction

Primary aldosteronism (PA) is the most frequent secondary cause of hypertension characterized by the overproduction of aldosterone relatively autonomous of the renin-angiotensin system. PA is generally classified into unilateral and bilateral forms, which determine the surgical or pharmacological treatment of the disease [1]. The surgical management of unilateral PA has made available, as a side effect, tissue sample specimens for a wide range of scientific studies. Histopathology shows that the surgically removed adrenals mainly display an aldosterone-producing adenoma (APA) with somatic mutations in a few genes that cause constitutive aldosterone production [2–5]. The variants usually occur in genes that encode ion channels or ATPases and function in the regulation of cellular ion homeostasis [6]. Of these, the KCNJ5 inwardly rectifying potassium channel (also called GIRK4) displays the highest prevalence of variants in most reported populations. Furthermore, in vivo observations and in vitro findings suggest that KCNJ5 mutations are likely to also cause cell proliferation [7–9]. The role of somatic mutations in constitutive aldosterone production is well defined, but many other mechanisms may modulate aldosterone production from APAs [10–15]. Regulated forms of cell death, including apoptosis [16] and ferroptosis [17], have also been implicated in the pathogenesis of APAs.

Metabolic reprogramming has a well-characterized role in cancer progression [18]. Increasing evidence suggests that tumor cells must modify their metabolism in response to their elevated energy requirements [19], and metabolic adaptations have been described in many types of cancers [20–22]. Of note, tumor cells undergo metabolic reprogramming that may modify the tumor microenvironment (TME) to fulfill the demands of biosynthesis and growth [23]. Tumor-infiltrating immune cells also rely on nutrients in the TME, and metabolic competition between tumor cells and infiltrating immune cells hamper or eliminate the anti-tumor immune response [23,24]. Furthermore, the high metabolic activity of tumor cells can generate metabolites (e.g., adenosine, kynurenine, and acidosis) that may accumulate to toxic concentrations, target immune suppressive cells and inhibit their function [25–27]. For instance, increased glycolysis in cancer cells (the Warburg effect) produces lactate that acidifies the TME and interferes with immune-cell effector function [28].

Because APAs are hormone-producing adenomas, an increased metabolic demand compared with adjacent tissue would be expected to sustain aldosterone hypersecretion. In this study, we investigated metabolic differences between APAs and paired adjacent cortical tissue to investigate mechanisms of the TME to support the development and progression of an APA.

2. Materials and Methods

2.1. Data Preprocessing

We analyzed microarray gene expression data from GSE64957 [29] and GSE60042 [30] from the Gene Expression Omnibus (GEO) database (https://www.ncbi.nlm.nih.gov/geo/ access date for GSE64957 and GSE60042: 01 January 2021 and 05 April 2021, respectively). GSE64957 comprised a data set from 13 APAs with corresponding paired zona glomerulosa, and zona fasciculata samples (7 APAs with a *KCNJ5* mutation and 6 APAs with no mutation detected). GSE60042 comprised 7 APAs and paired adjacent adrenal cortex tissue samples. GSE64957 Affymetrix microarray raw data were processed using the robust multichip average (RMA) algorithm with R package oligo for background adjustment, quantile normalization, log-transformation, and Combat function of R package sva (surrogate variable analysis) was used for batch correction. The expression matrix of GSE60042 was extracted from series matrix files downloaded from the GEO database using the GEOquery package, followed by standardization using the normalize Between Arrays function of the limma R package. The gene expression datasets were translated into commonly used gene symbols for further analyses.

The R package "limma" was used to clarify differentially expressed genes among paired groups; differentially expressed genes with adjust $p < 0.05$ and $\log_2$ fold change (FC) ($\log_2$FC) >1 were selected for further functional enrichments.

2.2. Patient Samples

Resected adrenal samples for histology and immunohistochemistry analyses were from patients diagnosed with unilateral primary aldosteronism following European Society of Hypertension guidelines [31,32] at the Medizinische Klinik IV, Klinikum Ludwig-Maximilians-Universität München, Munich, Germany, in accordance with local criteria for adrenal venous sampling [33]. These APAs comprised 6 with a *KCNJ5* mutation and 6 without *KCNJ5* mutations (2 *CACNA1D*, 2 *ATP1A1*, and 2 with no mutation detected). These patients gave written informed consent for use of biomaterial for medical research in accordance with the local ethics committee.

2.3. Functional Enrichments

To identify biological processes and pathway enrichment associated with differentially expressed genes, we used the gene set enrichment analysis (GSEA) method based on Gene Ontology (GO), Kyoto Encyclopedia of Genes and Genomes (KEGG), HALLMARK and Reactome gene sets from MSigDB database with the clusterProfiler package of R. The online tools of Metascape® (https://metascape.org access data: 11 April 2021) [34] and g:profiler (https://biit.cs.ut.ee/gprofiler access data: 21 April 2021) [35] were also used to identify pathway interactions, and protein–protein interaction networks, and to comprehensively understand the biology of differentially expressed genes using different independent knowledge bases (e.g., WikiPathways) to summarize the function of identified genes.

2.4. Determination of Tumor Immune Microenvironment and Immune Cell Infiltration Patterns

To assess tumor immune microenvironments, the "Estimation of Stromal and Immune cells in Malignant Tumors using Expression data" (ESTIMATE) algorithm [36] was used to quantify the infiltrating immune cell level (immune score) and stromal content (stromal score) for each sample, using gene expression signatures.

To further evaluate the immune characteristics of APA and adjacent zona glomerulosa cells, single sample GSEA (ssGSEA) [37] analysis was performed to identify the relative proportions of 28 immune cell types in the TME based on the feature gene panels for each immune cell type [38,39]. In addition, the Microenvironment Cell Populations-counter (MCP-counter) algorithm [40,41] was used to calculate stromal cell abundance, including endothelial cells and cancer-associated fibroblasts.

2.5. Identification of Ferroptosis-Related, Immune-Related, and Reactive Oxygen Species (ROS)-Related Genes

The corresponding ferroptosis-related gene list was downloaded from FerrDb [42]. In total, we identified 259 ferroptosis-related genes, including 108 drivers, 69 suppressors, and 111 markers. The immune-related gene lists were obtained from ImmPort (https://www.immport.org/resources access data: 21 December 2020). The ROS-related gene list was collected from the GeneCards database (https://www.genecards.org/ access data: 04 April 2021) using the term "reactive oxygen species", and only genes with a relevance score >7 were considered. All significantly differentially expressed genes were set at adjust p-value < 0.05 and $|\log_2 FC| > 1$.

2.6. Immunohistochemistry

Formalin fixed paraffin-embedded sections of APA tissue were incubated with anti-CD45 primary antibody (#13917; Cell Signaling Technology, Danvers, MA, USA) at 4 °C overnight. Immunohistochemistry staining was performed using ZytoChem Plus HRP

Polymer kit (Zytomed, Berlin, Germany) following the manufacturer's instructions and quantified with QuPath (v.0.2.3, University of Edinburgh, Edinburgh, UK) using the positive cell detection feature with empirical parameters.

2.7. Cell Line and Culture Conditions

Human adrenocortical (HAC15) cells (a kind gift from Professor William E. Rainey, University of Michigan, Ann Arbor, MI, USA) were cultured in Dulbecco's Modified Eagle/F12 medium with L-glutamine containing 10% (*v*/*v*) cosmic calf serum, 1% antibiotic-antimycotic, 1% insulin-transferrin-selenium, and 50 mg/mL gentamycin at 37 °C and 5% CO_2.

2.8. Cell Viability Assay

HAC15 cells (4×10^4 per well) were seeded on 96-well plates for 24 h and then treated with etomoxir (E1905, Sigma-Aldrich, St.Louis, MO, USA). Cell viability was measured using WST-1 assay according to the manufacturer's instructions (Roche Diagnostics GmbH, Mannheim, Germany). Cells without etomoxir treatment were used as a control.

2.9. Statistics

R software (version 4.0.3, Vienna, Austria) and GraphPad Prism 8.0 (GraphPad Software Inc., San Diego, CA, USA) were employed for figures generation and statistical analyses. Differences between the two groups were analyzed through paired *t*-test or paired Wilcoxon test, whereas Kruskal–Wallis test or One-way ANOVA was performed between groups. The statistically significant level was set as $p < 0.05$.

3. Results

3.1. Transcriptome Defined Metabolic Reprogramming towards Fatty Acid β-Oxidation and Glycolysis in APAs

Transcriptome data from GSE60042 were used to analyze the biology of differentially expressed genes in APAs versus paired adjacent adrenal cortex. The top upregulated gene sets were related to oxidative phosphorylation (Figure 1A) consistent with a proteomic analysis of APAs [43].

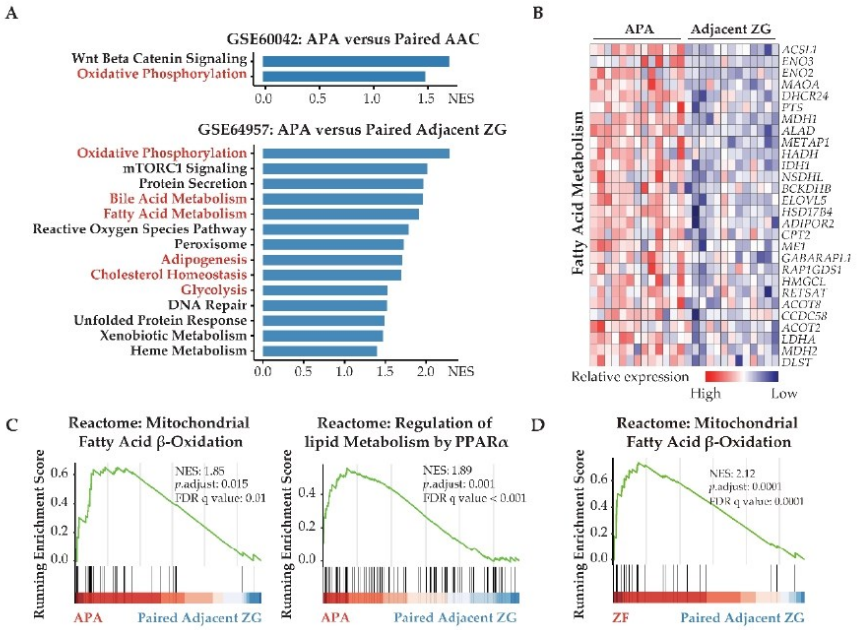

Figure 1. APAs undergo transcriptomic alterations toward increased fatty acid metabolism and glycolysis. (**A**) GSEA showing MSigDB hallmark of upregulated differentially expressed genes in APAs versus AAC (GSE60042) and adjacent ZG (GSE64957). Pathways in red indicate functions related to lipid metabolism and glycolysis. (**B**) Heatmap of the significant upregulated differentially expressed genes with p value < 0.05 for fatty acid metabolism in APAs compared with adjacent ZG. (**C**) GSEA plots showing Reactome pathways of lipid biological processes in APAs versus adjacent ZG. (**D**) GSEA plots showing Reactome pathways of mitochondrial fatty acid β-oxidation in ZF versus paired adjacent ZG. APA, aldosterone-producing adenoma; AAC, adjacent adrenal cortex; ZG, zona glomerulosa; ZF, zona fasciculata; NES, normalized enrichment score; FDR, false discovery rate.

Transcriptome data from GSE64957 were used to evaluate potential metabolic differences between APAs and paired adjacent zona glomerulosa. Alterations in transcriptome signatures related to metabolic synthesis were distinguished, with striking gene set enrichments in APAs of oxidative phosphorylation, fatty acid metabolism, and glycolysis (Figure 1A,B). Reactome gene sets demonstrated that the most significantly upregulated signaling pathways in APAs were mitochondrial fatty acid β-oxidation and peroxisome proliferator-activated receptor-α (PPARα) (Figure 1C). These data suggest that APAs may oxidize fatty acids as an energy source for tumor growth and/or steroidogenesis through PPARα signaling. We explored potential crosstalk between these signaling pathways using Metascape analyses with ClueGo, a Cytoscope plug-in. These network analyses highlighted that most signaling pathways involved aspects of lipid biology at the core of the pathogenesis of APAs. Furthermore, we demonstrated a functional link between lipid biology and ferroptosis. This is relevant because adrenocortical cells have previously been shown to be highly sensitive to cell death by ferroptosis due to the inhibition of glutathione biosynthesis (Figure 2A) [17,44,45]. Of note, the ferroptosis suppressor gene coding for glutamate-cysteine ligase catalytic subunit (GCLC) and the gene coding for stearoyl-CoA desaturase (SCD) are highly expressed in APAs compared with adjacent zona glomerulosa (Figure 2C). In addition, protein–protein interaction network analysis of differentially expressed genes revealed an upregulation of hub genes involved in glycolysis/gluconeogenesis using the Molecular Complex Detection algorithm (Figure 2B). Collectively, our evidence indicates that metabolic reprogramming towards fatty acid β-

oxidation and glycolysis may confer some metabolic advantage to the APA microenvironment that may sustain tumor cell growth and aldosterone overproduction.

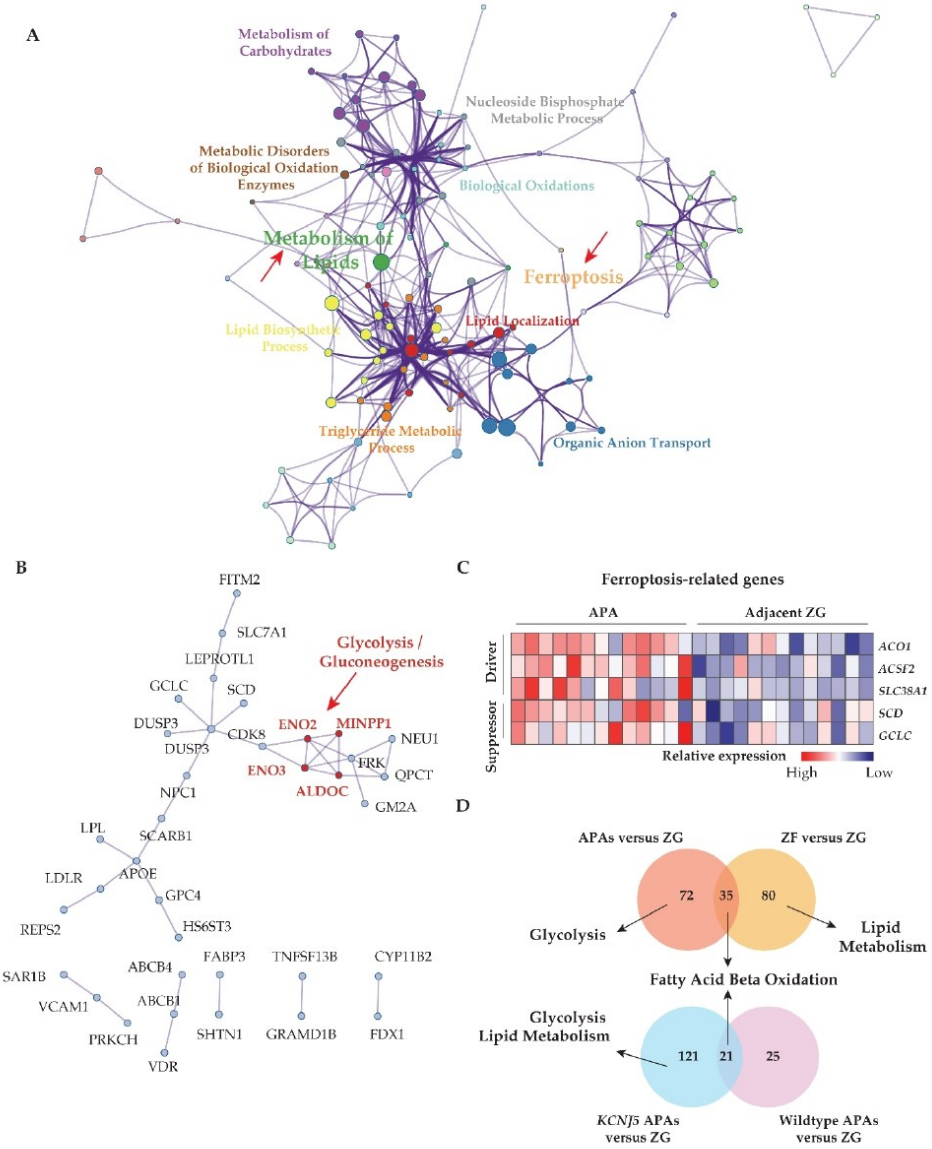

Figure 2. The interaction between lipid metabolism and ferroptosis, and the association of metabolic alterations with adjacent adrenal cortical tissue and APA genotype. (**A**) Metascape functional enrichment analysis of upregulated differentially expressed genes in APAs versus paired adjacent ZG (GSE64957). One node per enriched term, colored by cluster ID. Node size indicates the number of differentially expressed genes involved in the enriched term. (**B**) Protein–protein network using Molecular Complex Detection (MCODE) algorithm. Red fonts represent the core genes of the network involved in the glycolysis/gluconeogenesis pathway. (**C**) Heat map of ferroptosis-related upregulated differentially

expressed genes grouped as driver and suppressor in APAs compared paired adjacent ZG. (**D**) Venn diagrams showing the number of unique and overlapping upregulated differentially expressed genes from APAs and adjacent ZF of those APAs to paired adjacent ZG comparisons, and from *KCNJ5* mutated APAs and APAs without mutations (Wild type) to their adjacent ZG comparisons. Top pathways in which the distinct differentially expressed genes from APAs, adjacent ZF, *KCNJ5*-mutated APA, and APA without mutations (Wild type), respectively compared to paired adjacent ZG, using g:profiler online tool. APA, aldosterone-producing adenoma. AAC, adjacent adrenal cortex; ZG, zona glomerulosa; ZF, zona fasciculata; DEGs, differentially expressed genes; NES, normalized enrichment score; FDR, false discovery rate.

The GSE64957 data set was used to evaluate potential metabolic differences between APAs and paired adjacent zona fasciculata. Fatty acid β-oxidation was observed in adjacent zona fasciculata relative to paired adjacent zona glomerulosa (Figure 1D). We further analyzed the upregulated differentially expressed genes in APAs compared with adjacent zona glomerulosa and in paired zona fasciculata, compared with adjacent zona glomerulosa (Figure 2D). APAs specifically overexpressed genes related to glycolysis/gluconeogenesis, whereas genes that were exclusively upregulated in the paired adjacent zona fasciculata were enriched in pathways related to lipid metabolism.

3.2. KCNJ5 Mutations and Metabolic Reprogramming

APAs with *KCNJ5* mutations show an increased proliferative index compared with other APAs [9]. We investigated if *KCNJ5* mutated APAs display distinct metabolic features. We showed that genes involved in glycolysis and lipid metabolism displayed enhanced transcription in *KCNJ5* mutated APAs relative to Wild type APAs (both normalized to their adjacent zona glomerulosa) (Figure 2D).

3.3. Fatty Acid Oxidation is Required for the Survival of Human Adrenocortical Cells

To further elaborate the functional role of fatty acid oxidation in human adrenal cells, HAC15 cells were treated with etomoxir in culture, an inhibitor of fatty acid oxidation via carnitine palmitoyltransferase-1 inhibition. Etomoxir significantly decreased cell viability of HAC15 cells in a dose-s and time-dependent manner (Figure 3A,B), indicating that fatty acid oxidation may support adrenocortical cell growth.

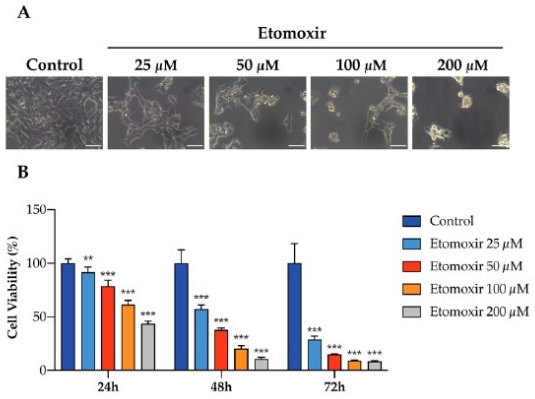

Figure 3. Inhibition of fatty acid oxidation induces cell death in human HAC15 cells. (**A**) Representative images of the effects of etomoxir in HAC15 cells in 6-well plate for 72 h. Scale Bar: 50 μm. (**B**) Cell viability in HAC15 cells treated with increasing concentration of etomoxir (25–200 μM) for 24 h, 48 h, and 72 h. Data are presented as mean ± s.d., One-way ANOVA; ** $p < 0.01$, *** $p < 0.001$.

3.4. Immune Phenotype Alterations in APAs

Dysregulation of tumor cell metabolism is known to contribute to immune evasion within the TME. Therefore, we investigated the effect of metabolic reprogramming of the TME on tumor-infiltrating immune-cell populations in APAs and adjacent adrenal cortical tissue. We used GSEA to screen for downregulated differentially expressed genes in APAs versus paired adjacent adrenal cortex and identified a vast number of immune-related pathways that were relatively increased in adjacent adrenal cortex, including inflammatory response, interferon-gamma response, and IL6 JAK STAT3 signaling (Figure 4A). Further analysis using the ESTIMATE algorithm to predict immune states revealed a statistically significant decrease of the immune and stromal score in APAs compared with paired adjacent adrenal cortex ($p < 0.01$, paired t test, Figure 4C). Collectively, APAs had a higher proportion of tumor cells. To validate these findings, we performed immunohistochemistry analysis of the surface protein CD45, a common marker of immune cells, on 12 formalin-fixed paraffin embedded APA samples with attached adjacent adrenal cortex (Figure 4B). The density and frequency of $CD45^+$ cells per mm^2 were significantly lower in APAs relative to the adjacent adrenal cortex (3.45-fold, $p < 0.001$, paired Wilcoxon test, Figure 4D), which included 6 *KCNJ5*-mutated APAs and 6 APAs without *KCNJ5* mutation. This is consistent with previous studies reporting sparse or no immune-cell infiltration within APAs compared to cortisol-producing adenoma [46]. These findings support the concept of tumor cells within the TME of APAs evading immune surveillance.

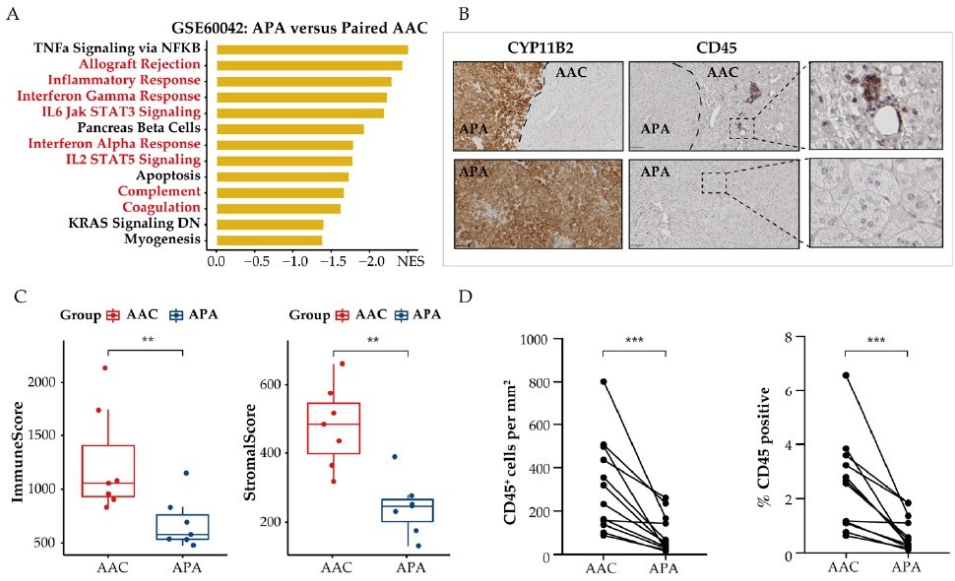

Figure 4. Spatial organization of tumor infiltrating immune cells in APAs versus paired adjacent adrenal cortex (AAC). (**A**) GSEA showing MSigDB hallmark of downregulated differentially expressed genes in APAs versus AAC (GSE60042). Pathways in red indicate functions related to immune response. (**B**) CYP11B2 and CD45 immunohistochemistry staining. The border of APA is defined by the CYP11B2 immunohistochemistry. Scare bar: 100 μm. (**C**) ESTIMATE algorithm showing the distribution of ImmuneScore, StromalScore in APAs versus AAC. ** $p < 0.01$ by paired t test. (**D**) $CD45^+$ immune cell density and positive percentage between APAs and AAC. *** $p < 0.001$ by paired Wilcox test. APA, aldosterone-producing adenoma; AAC, adjacent adrenal cortex; NES, normalized enrichment score.

We used a similar approach to assess tumor-infiltrating immune cells of APAs, paired adjacent zona fasciculata, and adjacent zona glomerulosa (Figure 5A–C). APA had

fewer CD45+ immune cells compared with the adjacent zona glomerulosa and adjacent zona fasciculata, suggesting an immunosuppressive microenvironment at the local site of APA. CD45+ immune cells in the adjacent zona fasciculata showed higher levels compared to those in adjacent zona glomerulosa, indicating that fatty acid β-oxidation may not contribute to the immunosuppressive properties of APA.

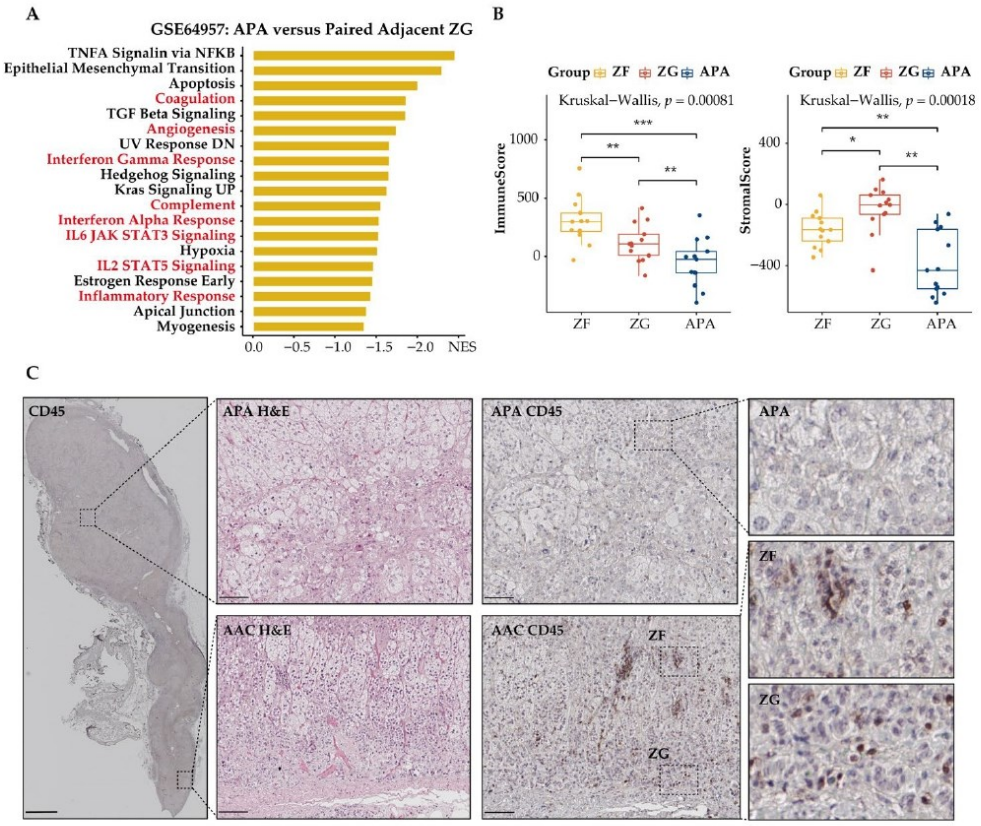

Figure 5. Spatial organization of tumor-infiltrating immune cells in APAs. Tumor-infiltrating immune cells in APAs were determined versus adjacent zona glomerulosa (ZG), and adjacent zona fasciculata (ZF). (**A**) GSEA showing MSigDB hallmark of downregulated differentially expressed genes in APAs versus adjacent ZG (GSE64957). Pathways in red indicate functions related to immune response. (**B**) ESTIMATE algorithm showing the distribution of ImmuneScore, StromalScore among APAs, adjacent ZG, and adjacent ZF. * $p < 0.05$, ** $p < 0.01$, *** $p < 0.001$ by paired Wilcox test. Kruskal–Wallis test was used between groups. (**C**) Immunohistochemistry of H&E and CD45 staining among APA, adjacent ZF, and adjacent ZG. Overview of CD45 image: scale bar 2 mm. Deep zoom images: scare bar 100 µm. APA, aldosterone-producing adenoma; ACC, adjacent adrenal cortex; GSEA, gene set enrichment analysis; NES, normalized enrichment score; ZG, zona glomerulosa; ZF, zona fasciculata.

3.5. Distinct Immune Microenvironment Landscapes in APAs vs. Paired Adjacent Zona Glomerulosa

To further explore differences in the composition of immune cells of APAs and paired adjacent zona glomerulosa, we performed ssGSEA using the MCP-counter algorithm, a method to profile fractions of immune cells by deconvolution of gene expression data, as shown in a heatmap (Figure 6A). Notably, principal component analysis showed

two distinct clusters of tumor-infiltrating immune cells of the TME (APAs vs. paired adjacent zona glomerulosa) (Figure 6B). Further, we observed decreased anti-immune cells (e.g., activated and central memory CD4 T cells, effector memory CD8 T cells, and nature killer cells) and increased pro-immune cells (immature dendritic cells) (Figure 6C–F).

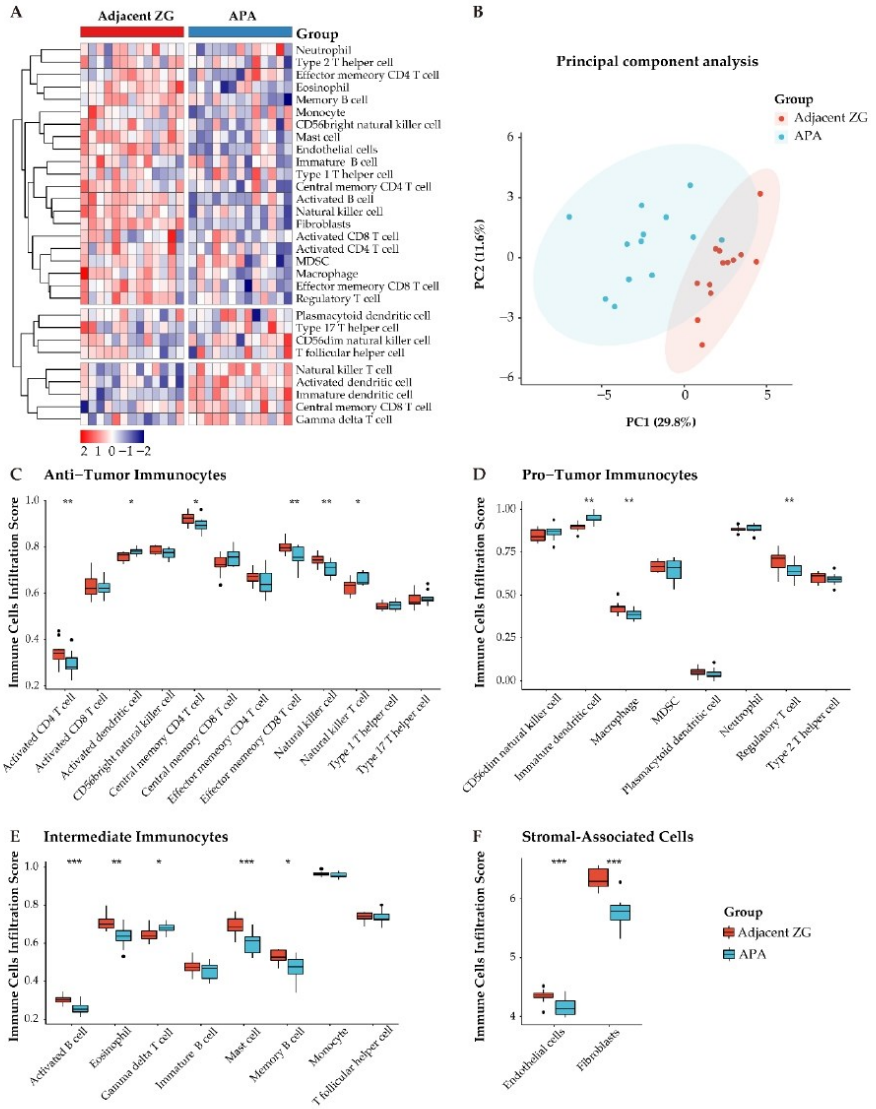

Figure 6. Distinct immune microenvironment landscapes in APA versus paired adjacent zona glomerulosa (ZG). (**A**) Heatmap of 28 tumor infiltration cells between APAs and adjacent ZG (GSE64957). MDSC, myeloid-derived suppressor cells. (**B**) Principal component analysis (PCA) of tumor-infiltrating cells. Two distinct groups were plotted in two-dimensional space: APA and adjacent ZG. PC, principal component. (**C**–**E**) Boxplot of the proportions of tumor microenvironment immune cells in (**A**) using the ssGSEA algorithm. (**F**) Boxplot of the proportions of TME stromal associated cells in (**A**) using MCP-counter algorithm. Box plots: scattered dots, immune score of the two subgroups; middle lines, median

value; bottom and top of the boxes, 25th–75th percentiles. ns, not significant; * $p < 0.05$; ** $p < 0.01$; *** $p < 0.001$ by paired Wilcoxon test. APA, aldosterone-producing adenoma; ZG, zona glomerulosa.

3.6. Functional Characterization of Immune-Related Differentially Expressed Genes in APAs

To classify immune-related genes, we intersected the whole dataset of differentially expressed genes with immune-related genes from ImmPort. A total of 31 differentially expressed immune-related genes were identified; 9 of these 31 were upregulated and the remaining 22 genes were downregulated in APAs versus paired adjacent zona glomerulosa (Figure 7A). GO analysis determined downregulated genes related to the immune response were enriched in the pathways related to "cellular response to oxidative stress" (Figure 7B), suggesting that oxidative stress may elicit an inflammatory response in the adjacent zona glomerulosa.

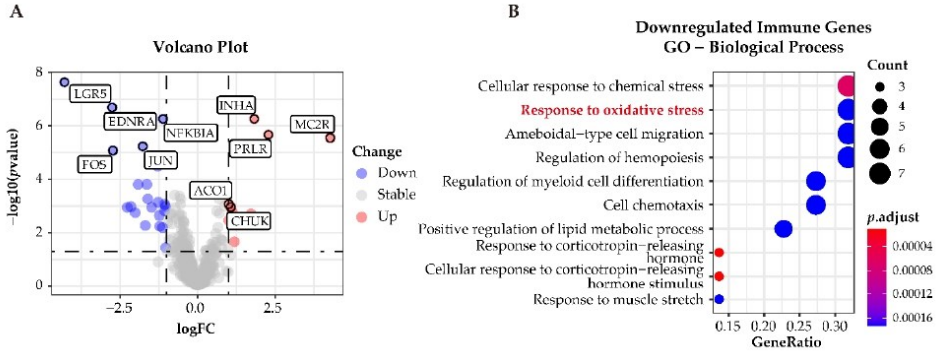

Figure 7. Functional characterization of immune-related differentially expressed genes in APAs versus paired adjacent zona glomerulosa (ZG). (**A**) Volcano Plot showing immune-differentially expressed genes (adjust *p*-value < 0.05 and $|\log_2 FC| > 1$) in APA versus adjacent ZG (GSE64957). Each point represents a gene. Red and Blue dots represent upregulated and downregulated immune-differentially expressed genes, respectively. (**B**) GO analysis of downregulated immune-differentially expressed genes in (**A**). APA, aldosterone-producing adenoma; ZG, zona glomerulosa.

3.7. Enhanced Anti-Oxidative Response Pathways in APAs

Our analyses indicate that adjacent zona glomerulosa are challenged with increased oxidative stress compared to cells of APAs. To investigate the function of ROS within the context of APA cells, we compared differentially expressed genes functionally related to ROS in APAs vs. paired adjacent zona glomerulosa. We identified 22 upregulated ROS genes and 40 downregulated ROS genes. KEGG analysis of the upregulated ROS genes demonstrated upregulation of several metabolic pathways, including cholesterol metabolism, peroxisome proliferator-activated receptor (PPAR) signaling, aldosterone synthesis, and secretion (Figure 8B), suggesting that ROS may be involved in the regulation of metabolism and/or affected by the intermediates of metabolic alterations. In contrast, the most prominently altered processes of downregulated genes related to ROS were the inflammatory response pathways (Figure 8D). Collectively, the link of ROS with metabolism and the inflammatory response may suggest contributory biological mechanisms to the pathogenesis of APAs.

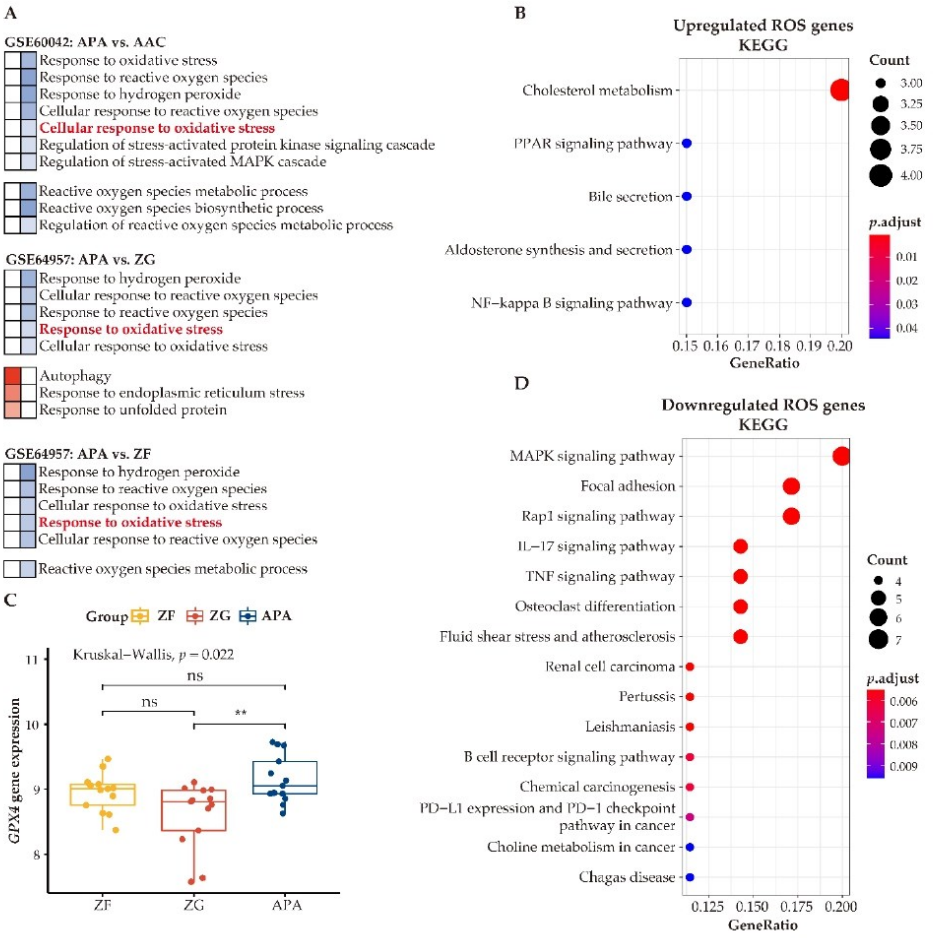

Figure 8. Enhanced antioxidative response pathways in APAs. (**A**) GO analysis of GSEA showing heatmap of ROS-related pathways. Red and blue color indicate upregulated and downregulated pathways ordered by normalized enrichment score in APAs versus AAC, adjacent ZG, and adjacent ZF, respectively. Normalized enrichment score >0 means upregulated pathways (Red), whereas normalized enrichment score <0 means downregulated pathways (Blue). Corresponding pathway enrichments are listed on the side. (**B**,**D**) indicate KEGG pathways of differentially expressed genes involved in ROS in APA versus adjacent ZG. Overexpressed ROS gene categories associated with metabolism pathways, whereas those downregulated ROS genes are associated with immune-response pathways. (**C**) The *GPX4* gene expression between APAs, adjacent ZG, and adjacent ZF. ** $p < 0.01$ by paired Wilcoxon test. Kruskal–Wallis test was used between groups. APA, aldosterone-producing adenoma; AAC, adjacent adrenal cortex; ZG, zona glomerulosa; ZF, zona fasciculata; ROS, reactive oxygen species.

To address how APAs accommodate high ROS levels and ameliorate oxidative stress, we summarized ROS-related pathways between APAs versus paired adjacent adrenal cortex, APAs vs. paired adjacent zona glomerulosa, and APAs versus paired adjacent zona fasciculata. In general, all adjacent tissues showed higher enrichment of genes involved in ROS-related pathways such as "cellular response to oxidative stress" (Figure 8A). Therefore, we postulated that adrenocortical tumor cells may increase antioxidant properties to counteract metabolic stress. Accordingly, we determined upregulation of the

unfolded protein response pathway in APAs (vs. adjacent zona glomerulosa) [47], which is an adaptive mechanism to relieve endoplasmic reticulum stress and restore cellular metabolic function, thereby promoting the survival of tumor cells. In addition, autophagy, a cellular stress-response mechanism [48] that recycles key metabolites under metabolic stress and promotes cellular adaptation to oxidative stress, was also enhanced in APAs. In addition, glutathione peroxidase 4 (GPX4) mRNA levels, a key enzyme for antioxidant defense, were higher in APAs among groups (Figure 8C). Together, these mechanisms ensure an efficient alleviation of oxidative stress that APA cells encounter during excess aldosterone production and abnormal proliferation.

4. Discussion

In this study we used advanced bioinformatics tools to comprehensively evaluate the TME of APAs. We demonstrated that metabolic reprogramming towards fatty acid β-oxidation and glycolysis is a general feature of APAs that may provide a metabolically favorable environment for tumor growth. Furthermore, we showed an immunosuppressive microenvironment in APA and diverse cellular components of the TME (e.g., immune and stromal cells) between APAs and the adjacent zona glomerulosa.

We showed that lipid metabolism is highly associated with APA tumorigenesis. Metabolism reprogramming enables tumor cells to sustain ATP generation for cell growth, division, and survival. Notably, dysregulation of lipid metabolism has been demonstrated as a prominent metabolic alteration in cancers [49]. In particular, increased β-oxidation of stored lipids provides a source of NAPDH and ATP—approximately six times that of oxidation of carbohydrates—through the oxidation of acetyl-CoA by the tricarboxylic acid (TCA) cycle, thereby facilitating tumor progression [50]. Furthermore, NAPDH is critical for two steps in steroidogenesis pathways in the adrenal gland: (1) the rate-limiting step for the conversion of cholesterol to pregnenolone catalyzed by CYP11A1 and (2) the conversion of deoxycorticosterone to aldosterone catalyzed by CYP11B2 [51,52]. Thus, elevated fatty acid β-oxidation in APAs may stimulate aldosterone synthesis by the high metabolic activity of NAPDH generation in mitochondria. In addition, our bioinformatics studies implied that changes in lipid metabolism in APAs are regulated by PPARα. Previous studies reported that transcriptional activation of PPARα regulates β-oxidation in tissues displaying high energy consumption [53,54]. Consistent with our findings, a previous study demonstrated that fenofibrate, a PPARα agonist, increased angiotensin II-independent *CYP11B2* mRNA expression and aldosterone production in human adrenocortical carcinoma H295R cells, whereas a peroxisome proliferator-activated receptor-γ (PPARγ) agonist either had no effect or reduced aldosterone secretion [55]. These data indicate that high activity of fatty acid β-oxidation induced by PPARα signaling may be crucial for excess aldosterone production.

Further to a role for fatty acid β-oxidation in APA pathogenesis, we reported that glycolysis metabolism may also play a key role, especially in *KCNJ5*-mutated APAs. This latter finding is consistent with a mass spectrometry imaging study that identified the activation of glycolysis pathways in APAs as well as in a subgroup of aldosterone-producing micronodules [56] (previously known as aldosterone-producing cell clusters [57]). In contrast, a high-resolution mass spectrometry imaging map of the normal human adrenal gland reported that glycolysis/gluconeogenesis was found to be significantly increased in the medulla [58]. This finding is consistent with the concept that a metabolic switch to glycolysis confers a selective advantage for tumor growth. However, the underlying mechanism of such metabolic phenotypes is unclear. Of potential interest, lactate infusion alone, or in combination with angiotensin II, results in increased aldosterone secretion from rat zona glomerulosa cells [59]. Therefore, the precise relationship between glycolysis and its metabolites and aldosterone production merits further investigation.

Our study showed the low tumor infiltrating $CD45^+$ lymphocyte density in APAs. Such a scenario is in line with previous reports showing sparse immune cell infiltration using hematoxylin-eosin staining in APAs relative to cortisol-producing adenomas [46].

This alteration in the TME may be accounted for by competition for nutrients in the TME, and glycolysis intermediates forming an acidic microenvironment and thereby suppressing immune activation [27,60]. Another potential mechanism is the promotion of immunosurveillance evasion by activated PPAR signaling [61]. PPARα exerts anti-inflammatory activity, for example, and PPARα agonists mediate a variety of effects on the immune response to reverse acute and chronic liver inflammation [54]. Consistently, PPARα-deficient aged mice show a pro-inflammatory phenotype [62]. In addition, the PPARα agonist fenofibrate caused a reduction in blood pressure, especially in salt-sensitive hypertensive subjects [63], suggesting that PPARα may play a role in regulation of renin–angiotensin–aldosterone system activity, and influence aldosterone secretion. This discrepancy may be explained, however, by its dual influence on systemic and local tumor levels. Furthermore, through expression–signature-based approaches, we observed low effector memory CD8 T cell infiltration in APAs, which is in agreement with a previous study that demonstrated decreased viability of effector T cells in a glucose-restricted medium in vitro [64]. These data suggest that metabolic reprogramming towards glycolysis in APA may impose a hypoglycemic environment, restrict glucose uptake by immune cells and therefore hamper their function. In addition, a previous study showed that the distribution of mast cells is more frequently visualized in the adjacent cortex of APAs [11], consistent with the high mast cell infiltration in adjacent zona glomerulosa relative to APAs in our study.

Active steroidogenesis has been implicated in contributing to high ROS production and oxidative stress, triggering cell death [65]. Our analyses demonstrated that the adjacent cortex is challenged with increased oxidative stress compared to APAs, regions of high steroidogenesis. Our finding of enhanced fatty acid β-oxidation in APAs may explain this apparent paradox because it provides NAPDH, which may counteract ROS toxicity from metabolic stress [66]. Furthermore, fatty acid β-oxidation is increased in zona fasciculata relative to paired zona glomerulosa, likely because glucocorticoid production in normal zona fasciculata produces significantly more cellular ROS than from aldosterone synthesis in normal zona glomerulosa due to 40% of "leaky" electrons in the P450c11β (CYP11B1) system [67]. This would require elevated fatty acid β-oxidation for protection of adrenocortical zona fasciculata cells from ROS. In addition, previous work demonstrated that enhanced glycolysis can combat oxidative stress via increasing glutathione metabolism and maintaining redox balance [68], a potential factor contributing to the larger tumor diameter in APAs with *KCNJ5* mutations. Additionally, our data showed an increased antioxidant response via an enhanced unfolding protein response and autophagy [47,48], suggesting that multiple mechanisms participate in the detoxification of ROS and aid adrenocortical tumor cell survival.

It has been reported that adrenocortical cells are sensitive to ferroptosis-triggering agents, such as RSL3, which can inhibit GPX4 activity [17,45]. Indeed, our data showed elevated *GPX4* expression in APAs compared with adjacent zona glomerulosa. Adrenocortical tumor cells must boost their antioxidant capacity to counteract the lipid peroxidation and oxidative stress induced by steroidogenesis to suppress cell death by ferroptosis. Although studies into the molecular mechanisms underlying the adaptation of APA cells to high ROS generation in the local tumor site to circumvent ferroptosis are not well defined, lipid metabolism likely participates, and in particular fatty acid β-oxidation. This hypothesis is partially supported by Kagan et al., who showed that etomoxir, an inhibitor of mitochondrial fatty acid β-oxidation, enhanced RSL3-induced ferroptosis in mouse embryonic fibroblasts [69]. Further, PPARα activator can reduce lipid peroxidation [70]. Considering the known association of fatty acid β-oxidation with PPARα, PPARα activation may feasibly regulate the susceptibility of adrenocortical cells to lipid peroxidation, a key characteristic of ferroptosis, through β-oxidation. Furthermore, we observed increased *SCD* and *GCLC* mRNA expression in APAs. Two key enzymes catalyze monounsaturated fatty acid synthesis and biosynthesis of glutathione, which protect tumor cells against

ferroptosis inducers [71,72]. These exemplify the central hub role of metabolism reprogramming to adapt to metabolic stress.

This study reports a potential role of fatty acid oxidation in supporting adrenocortical cell growth; however, further research is required to delineate the precise mechanisms involved. Our study had several limitations, including the absence of protein-level data corresponding to identified differentially expressed genes related to lipid metabolism with a potential role in APA pathophysiology. In addition, we did not fully characterize the role of oxidative stress (lipid peroxidation) in APA tissues, which warrants further investigation.

5. Conclusions

It is challenging to evaluate the tumorigenic landscape of APAs using experimental methods. As such, it is still unclear how APA tumor adrenocortical cells maintain hypersecretion and cell proliferation despite a nutrient-deprived environment. We address this knowledge gap by shedding light on the energy metabolism and tumor immune microenvironment. Our analyses reveal that metabolic reprogramming involving a switch to fatty acid β-oxidation and glycolysis may stimulate aldosterone production, disturb the TME, mitigate oxidative stress, and support tumor cell survival. Therefore, we highlight metabolic reprogramming as a putative novel mechanism in APA pathophysiology.

Author Contributions: Conceptualization, T.A.W., S.G. and M.R.; data curation, S.G.; formal analysis, S.G. and M.T.; funding acquisition, T.A.W. and M.R.; investigation, S.G.; methodology, T.A.W. and S.G.; project administration, T.A.W.; software, S.G.; supervision, T.A.W.; validation, S.G. and M.T.; writing–original draft, S.G.; writing–review and editing, T.A.W., M.T. and M.R. All authors have read and agreed to the published version of the manuscript.

Funding: This work was financed by the Deutsche Forschungsgemeinschaft (DFG) project number 444776998 to T.A. Williams (WI 5359/2-1) and M. Reincke (RE 752/31-1) and project number 314061271-TRR 205/project B15 to T.A. Williams (within the CRC/Transregio 205/1 "The Adrenal: Central Relay in Health and Disease"). The CRC/Transregio 205/1 also supports the research of M. Reincke. This study was also supported by the European Research Council under the European Union Horizon 2020 research and innovation program (grant agreement No. 694913 to M. Reincke) and the Else Kröner-Fresenius Stiftung in support of the German Conn's Registry-Else-Kröner Hyperaldosteronism Registry (2013_A182, 2015_A171 and 2019_A104 to M. Reincke). Siyuan Gong was supported by the China Scholarship Council (CSC) for supporting her study in LMU Munich.

Institutional Review Board Statement: The study was conducted according to the guidelines of the Declaration of Helsinki, and approved by the Ethics Committee of Ludwig-Maximilians-Universität, München (protocol code 379-10 and 11 January 2012).

Informed Consent Statement: Informed consent was obtained from all subjects involved in the study.

Data Availability Statement: The publicly archived datasets presented in this study can be accessible through GEO series accession number GSE64957 and GSE60042.

Acknowledgments: We thank Isabella-Sabrina Kinker and Petra Rank for their expert technical assistance.

Conflicts of Interest: The authors declare no conflict of interest.

Abbreviation	Definition
PA	Primary aldosteronism
APA	Aldosterone-producing adenoma
AAC	Adjacent adrenal cortex
ZG	Zona glomerulosa
ZF	Zona fasciculata
TME	Tumor microenvironment
ROS	Reactive oxygen species
GO	Gene Ontology

KEGG	Kyoto Encyclopedia of Genes and Genomes
GSEA	Gene set enrichment analysis
MCP-COUNTER	Microenvironment cell populations-counter
ESTIMATE	Estimation of Stromal and Immune cells in Malignant Tumors using Expression data
GCLC	Glutamate-cysteine ligase catalytic subunit
SCD	Stearoyl-CoA desaturase
GPX4	Glutathione peroxidase 4
ATP	Adenosine triphosphate
NADPH	Nicotinamide adenine dinucleotide phosphate
TME	Tumor microenvironment

References

1. Young, W.F. Diagnosis and treatment of primary aldosteronism: Practical clinical perspectives. *J. Intern. Med.* **2019**, *285*, 126–148, doi:10.1111/joim.12831.
2. Rege, J.; Nanba, K.; Blinder, A.R.; Plaska, S.; Udager, A.M.; Vats, P.; Kumar-Sinha, C.; Giordano, T.J.; Rainey, W.E.; Else, T. Identification of Somatic Mutations in CLCN2 in Aldosterone-Producing Adenomas. *J. Endocr. Soc.* **2020**, *4*, bvaa123, doi:10.1210/jendso/bvaa123.
3. Scholl, U.I.; Goh, G.; Stolting, G.; De Oliveira, R.C.; Choi, M.; Overton, J.D.; Fonseca, A.L.; Korah, R.; Starker, L.F.; Kunstman, J.W.; et al. Somatic and germline CACNA1D calcium channel mutations in aldosterone-producing adenomas and primary aldosteronism. *Nat. Genet.* **2013**, *45*, 1050–1054, doi:10.1038/ng.2695.
4. Williams, T.A.; Monticone, S.; Schack, V.R.; Stindl, J.; Burrello, J.; Buffolo, F.; Annaratone, L.; Castellano, I.; Beuschlein, F.; Reincke, M.; et al. Somatic ATP1A1, ATP2B3, and KCNJ5 mutations in aldosterone-producing adenomas. *Hypertension* **2014**, *63*, 188–195, doi:10.1161/HYPERTENSIONAHA.113.01733.
5. Meyer, L.S.; Handgriff, L.; Lim, J.S.; Udager, A.M.; Kinker, I.S.; Ladurner, R.; Wildgruber, M.; Knosel, T.; Bidlingmaier, M.; Rainey, W.E.; et al. Single-Center Prospective Cohort Study on the Histopathology, Genotype, and Postsurgical Outcomes of Patients With Primary Aldosteronism. *Hypertension* **2021**, doi:10.1161/HYPERTENSIONAHA.121.17348.
6. Itcho, K.; Oki, K.; Ohno, H.; Yoneda, M. Update on Genetics of Primary Aldosteronism. *Biomedicines* **2021**, *9*, 409, doi:10.3390/biomedicines9040409.
7. Scholl, U.I.; Nelson-Williams, C.; Yue, P.; Grekin, R.; Wyatt, R.J.; Dillon, M.J.; Couch, R.; Hammer, L.K.; Harley, F.L.; Farhi, A.; et al. Hypertension with or without adrenal hyperplasia due to different inherited mutations in the potassium channel KCNJ5. *Proc. Natl. Acad. Sci. USA* **2012**, *109*, 2533–2538, doi:10.1073/pnas.1121407109.
8. Tamura, A.; Nishimoto, K.; Seki, T.; Matsuzawa, Y.; Saito, J.; Omura, M.; Gomez-Sanchez, C.E.; Makita, K.; Matsui, S.; Moriya, N.; et al. Somatic KCNJ5 mutation occurring early in adrenal development may cause a novel form of juvenile primary aldosteronism. *Mol. Cell. Endocrinol.* **2017**, *441*, 134–139, doi:10.1016/j.mce.2016.07.031.
9. Yang, Y.; Gomez-Sanchez, C.E.; Jaquin, D.; Aristizabal Prada, E.T.; Meyer, L.S.; Knosel, T.; Schneider, H.; Beuschlein, F.; Reincke, M.; Williams, T.A. Primary Aldosteronism: KCNJ5 mutations and Adrenocortical Cell Growth. *Hypertension* **2019**, *74*, 809–816, doi:10.1161/HYPERTENSIONAHA.119.13476.
10. Oki, K.; Gomez-Sanchez, C.E. The landscape of molecular mechanism for aldosterone production in aldosterone-producing adenoma. *Endocr. J.* **2020**, *67*, 989–995, doi:10.1507/endocrj.EJ20-0478.
11. Duparc, C.; Moreau, L.; Dzib, J.F.; Boyer, H.G.; Tetsi Nomigni, M.; Boutelet, I.; Boulkroun, S.; Mukai, K.; Benecke, A.G.; Amar, L.; et al. Mast cell hyperplasia is associated with aldosterone hypersecretion in a subset of aldosterone-producing adenomas. *J. Clin. Endocrinol. Metab.* **2015**, *100*, E550–560, doi:10.1210/jc.2014-3660.
12. Berthon, A.; Drelon, C.; Ragazzon, B.; Boulkroun, S.; Tissier, F.; Amar, L.; Samson-Couterie, B.; Zennaro, M.C.; Plouin, P.F.; Skah, S.; et al. WNT/beta-catenin signalling is activated in aldosterone-producing adenomas and controls aldosterone production. *Hum. Mol. Genet.* **2014**, *23*, 889–905, doi:10.1093/hmg/ddt484.
13. Williams, T.A.; Monticone, S.; Morello, F.; Liew, C.C.; Mengozzi, G.; Pilon, C.; Asioli, S.; Sapino, A.; Veglio, F.; Mulatero, P. Teratocarcinoma-derived growth factor-1 is upregulated in aldosterone-producing adenomas and increases aldosterone secretion and inhibits apoptosis in vitro. *Hypertension* **2010**, *55*, 1468–1475, doi:10.1161/HYPERTENSIONAHA.110.150318.
14. Decmann, A.; Nyiro, G.; Darvasi, O.; Turai, P.; Bancos, I.; Kaur, R.J.; Pezzani, R.; Iacobone, M.; Kraljevic, I.; Kastelan, D.; et al. Circulating miRNA Expression Profiling in Primary Aldosteronism. *Front. Endocrinol.* **2019**, *10*, 739, doi:10.3389/fendo.2019.00739.
15. Tombol, Z.; Turai, P.I.; Decmann, A.; Igaz, P. MicroRNAs and Adrenocortical Tumors: Where do we Stand on Primary Aldosteronism? *Horm. Metab. Res.* **2020**, *52*, 394–403, doi:10.1055/a-1116-2366.
16. Williams, T.A.; Monticone, S.; Crudo, V.; Warth, R.; Veglio, F.; Mulatero, P. Visinin-like 1 is upregulated in aldosterone-producing adenomas with KCNJ5 mutations and protects from calcium-induced apoptosis. *Hypertension* **2012**, *59*, 833–839, doi:10.1161/HYPERTENSIONAHA.111.188532.

17. Yang, Y.; Tetti, M.; Vohra, T.; Adolf, C.; Seissler, J.; Hristov, M.; Belavgeni, A.; Bidlingmaier, M.; Linkermann, A.; Mulatero, P.; et al. BEX1 Is Differentially Expressed in Aldosterone-Producing Adenomas and Protects Human Adrenocortical Cells From Ferroptosis. *Hypertension* **2021**, *77*, 1647–1658, doi:10.1161/HYPERTENSIONAHA.120.16774.
18. Pavlova, N.N.; Thompson, C.B. The Emerging Hallmarks of Cancer Metabolism. *Cell Metab* **2016**, *23*, 27–47, doi:10.1016/j.cmet.2015.12.006.
19. Faubert, B.; Solmonson, A.; DeBerardinis, R.J. Metabolic reprogramming and cancer progression. *Science* **2020**, *368*, eaaw5473, doi:10.1126/science.aaw5473.
20. Ligorio, F.; Pellegrini, I.; Castagnoli, L.; Vingiani, A.; Lobefaro, R.; Zattarin, E.; Santamaria, M.; Pupa, S.M.; Pruneri, G.; de Braud, F.; et al. Targeting lipid metabolism is an emerging strategy to enhance the efficacy of anti-HER2 therapies in HER2-positive breast cancer. *Cancer Lett.* **2021**, *511*, 77–87, doi:10.1016/j.canlet.2021.04.023.
21. Xu, W.; Hu, X.; Anwaier, A.; Wang, J.; Liu, W.; Tian, X.; Zhu, W.; Ma, C.; Wan, F.; Shi, G.; et al. Fatty Acid Synthase Correlates With Prognosis-Related Abdominal Adipose Distribution and Metabolic Disorders of Clear Cell Renal Cell Carcinoma. *Front. Mol. Biosci.* **2020**, *7*, 610229, doi:10.3389/fmolb.2020.610229.
22. Schmidt, D.R.; Patel, R.; Kirsch, D.G.; Lewis, C.A.; Vander Heiden, M.G.; Locasale, J.W. Metabolomics in cancer research and emerging applications in clinical oncology. *CA Cancer J. Clin.* **2021**, doi:10.3322/caac.21670.
23. Reina-Campos, M.; Moscat, J.; Diaz-Meco, M. Metabolism shapes the tumor microenvironment. *Curr. Opin. Cell Biol.* **2017**, *48*, 47–53, doi:10.1016/j.ceb.2017.05.006.
24. Xia, L.; Oyang, L.; Lin, J.; Tan, S.; Han, Y.; Wu, N.; Yi, P.; Tang, L.; Pan, Q.; Rao, S.; et al. The cancer metabolic reprogramming and immune response. *Mol. Cancer* **2021**, *20*, 28, doi:10.1186/s12943-021-01316-8.
25. Ohta, A.; Gorelik, E.; Prasad, S.J.; Ronchese, F.; Lukashev, D.; Wong, M.K.; Huang, X.; Caldwell, S.; Liu, K.; Smith, P.; et al. A2A adenosine receptor protects tumors from antitumor T cells. *Proc. Natl. Acad. Sci. USA* **2006**, *103*, 13132–13137, doi:10.1073/pnas.0605251103.
26. Romero-Garcia, S.; Moreno-Altamirano, M.M.; Prado-Garcia, H.; Sanchez-Garcia, F.J. Lactate Contribution to the Tumor Microenvironment: Mechanisms, Effects on Immune Cells and Therapeutic Relevance. *Front. Immunol.* **2016**, *7*, 52, doi:10.3389/fimmu.2016.00052.
27. Leone, R.D.; Powell, J.D. Metabolism of immune cells in cancer. *Nat. Rev. Cancer* **2020**, *20*, 516–531, doi:10.1038/s41568-020-0273-y.
28. Allison, K.E.; Coomber, B.L.; Bridle, B.W. Metabolic reprogramming in the tumour microenvironment: A hallmark shared by cancer cells and T lymphocytes. *Immunology* **2017**, *152*, 175–184, doi:10.1111/imm.12777.
29. Zhou, J.; Lam, B.; Neogi, S.G.; Yeo, G.S.; Azizan, E.A.; Brown, M.J. Transcriptome Pathway Analysis of Pathological and Physiological Aldosterone-Producing Human Tissues. *Hypertension* **2016**, *68*, 1424–1431, doi:10.1161/HYPERTENSIONAHA.116.08033.
30. Murakami, M.; Yoshimoto, T.; Nakabayashi, K.; Tsuchiya, K.; Minami, I.; Bouchi, R.; Izumiyama, H.; Fujii, Y.; Abe, K.; Tayama, C.; et al. Integration of transcriptome and methylome analysis of aldosterone-producing adenomas. *Eur. J. Endocrinol.* **2015**, *173*, 185–195, doi:10.1530/EJE-15-0148.
31. Mulatero, P.; Monticone, S.; Deinum, J.; Amar, L.; Prejbisz, A.; Zennaro, M.C.; Beuschlein, F.; Rossi, G.P.; Nishikawa, T.; Morganti, A.; et al. Genetics, prevalence, screening and confirmation of primary aldosteronism: A position statement and consensus of the Working Group on Endocrine Hypertension of The European Society of Hypertension. *J. Hypertens.* **2020**, *38*, 1919–1928, doi:10.1097/HJH.0000000000002510.
32. Mulatero, P.; Sechi, L.A.; Williams, T.A.; Lenders, J.W.; Reincke, M.; Satoh, F.; Januszewicz, A.; Naruse, M.; Doumas, M.; Veglio, F.; et al. Subtype diagnosis, treatment, complications and outcomes of primary aldosteronism and future direction of research: a position statement and consensus of the Working Group on Endocrine Hypertension of the European Society of Hypertension. *J. Hypertens.* **2020**, *38*, 1929–1936, doi:10.1097/HJH.0000000000002520.
33. Williams, T.A.; Reincke, M. MANAGEMENT OF ENDOCRINE DISEASE: Diagnosis and management of primary aldosteronism: The Endocrine Society guideline 2016 revisited. *Eur. J. Endocrinol.* **2018**, *179*, R19–R29, doi:10.1530/EJE-17-0990.
34. Zhou, Y.; Zhou, B.; Pache, L.; Chang, M.; Khodabakhshi, A.H.; Tanaseichuk, O.; Benner, C.; Chanda, S.K. Metascape provides a biologist-oriented resource for the analysis of systems-level datasets. *Nat. Commun.* **2019**, *10*, 1523, doi:10.1038/s41467-019-09234-6.
35. Raudvere, U.; Kolberg, L.; Kuzmin, I.; Arak, T.; Adler, P.; Peterson, H.; Vilo, J. g:Profiler: A web server for functional enrichment analysis and conversions of gene lists (2019 update). *Nucleic Acids Res.* **2019**, *47*, W191–W198, doi:10.1093/nar/gkz369.
36. Yoshihara, K.; Shahmoradgoli, M.; Martinez, E.; Vegesna, R.; Kim, H.; Torres-Garcia, W.; Trevino, V.; Shen, H.; Laird, P.W.; Levine, D.A.; et al. Inferring tumour purity and stromal and immune cell admixture from expression data. *Nat. Commun.* **2013**, *4*, 2612, doi:10.1038/ncomms3612.
37. Barbie, D.A.; Tamayo, P.; Boehm, J.S.; Kim, S.Y.; Moody, S.E.; Dunn, I.F.; Schinzel, A.C.; Sandy, P.; Meylan, E.; Scholl, C.; et al. Systematic RNA interference reveals that oncogenic KRAS-driven cancers require TBK1. *Nature* **2009**, *462*, 108–112, doi:10.1038/nature08460.
38. Jia, Q.; Wu, W.; Wang, Y.; Alexander, P.B.; Sun, C.; Gong, Z.; Cheng, J.N.; Sun, H.; Guan, Y.; Xia, X.; et al. Local mutational diversity drives intratumoral immune heterogeneity in non-small cell lung cancer. *Nat. Commun.* **2018**, *9*, 5361, doi:10.1038/s41467-018-07767-w.

39. Charoentong, P.; Finotello, F.; Angelova, M.; Mayer, C.; Efremova, M.; Rieder, D.; Hackl, H.; Trajanoski, Z. Pan-cancer Immunogenomic Analyses Reveal Genotype-Immunophenotype Relationships and Predictors of Response to Checkpoint Blockade. *Cell Rep*. **2017**, *18*, 248–262, doi:10.1016/j.celrep.2016.12.019.
40. Sturm, G.; Finotello, F.; Petitprez, F.; Zhang, J.D.; Baumbach, J.; Fridman, W.H.; List, M.; Aneichyk, T. Comprehensive evaluation of transcriptome-based cell-type quantification methods for immuno-oncology. *Bioinformatics* **2019**, *35*, i436–i445, doi:10.1093/bioinformatics/btz363.
41. Becht, E.; Giraldo, N.A.; Lacroix, L.; Buttard, B.; Elarouci, N.; Petitprez, F.; Selves, J.; Laurent-Puig, P.; Sautes-Fridman, C.; Fridman, W.H.; et al. Estimating the population abundance of tissue-infiltrating immune and stromal cell populations using gene expression. *Genome Biol.* **2016**, *17*, 218, doi:10.1186/s13059-016-1070-5.
42. Zhou, N.; Bao, J. FerrDb: A manually curated resource for regulators and markers of ferroptosis and ferroptosis-disease associations. *Database* **2020**, *2020*, doi:10.1093/database/baaa021.
43. Swierczynska, M.M.; Betz, M.J.; Colombi, M.; Dazert, E.; Jeno, P.; Moes, S.; Pfaff, C.; Glatz, K.; Reincke, M.; Beuschlein, F.; et al. Proteomic Landscape of Aldosterone-Producing Adenoma. *Hypertension* **2019**, *73*, 469–480, doi:10.1161/HYPERTENSIONAHA.118.11733.
44. Belavgeni, A.; Bornstein, S.R.; von Massenhausen, A.; Tonnus, W.; Stumpf, J.; Meyer, C.; Othmar, E.; Latk, M.; Kanczkowski, W.; Kroiss, M.; et al. Exquisite sensitivity of adrenocortical carcinomas to induction of ferroptosis. *Proc. Natl. Acad. Sci. USA* **2019**, *116*, 22269–22274, doi:10.1073/pnas.1912700116.
45. Weigand, I.; Schreiner, J.; Rohrig, F.; Sun, N.; Landwehr, L.S.; Urlaub, H.; Kendl, S.; Kiseljak-Vassiliades, K.; Wierman, M.E.; Angeli, J.P.F.; et al. Active steroid hormone synthesis renders adrenocortical cells highly susceptible to type II ferroptosis induction. *Cell Death Dis*. **2020**, *11*, 192, doi:10.1038/s41419-020-2385-4.
46. Kitawaki, Y.; Nakamura, Y.; Kubota-Nakayama, F.; Yamazaki, Y.; Miki, Y.; Hata, S.; Ise, K.; Kikuchi, K.; Morimoto, R.; Satoh, F.; et al. Tumor microenvironment in functional adrenocortical adenomas: Immune cell infiltration in cortisol-producing adrenocortical adenoma. *Hum. Pathol.* **2018**, *77*, 88–97, doi:10.1016/j.humpath.2018.03.016.
47. Madden, E.; Logue, S.E.; Healy, S.J.; Manie, S.; Samali, A. The role of the unfolded protein response in cancer progression: From oncogenesis to chemoresistance. *Biol. Cell* **2019**, *111*, 1–17, doi:10.1111/boc.201800050.
48. Peker, N.; Gozuacik, D. Autophagy as a Cellular Stress Response Mechanism in the Nervous System. *J. Mol. Biol.* **2020**, *432*, 2560–2588, doi:10.1016/j.jmb.2020.01.017.
49. Snaebjornsson, M.T.; Janaki-Raman, S.; Schulze, A. Greasing the Wheels of the Cancer Machine: The Role of Lipid Metabolism in Cancer. *Cell Metab.* **2020**, *31*, 62–76, doi:10.1016/j.cmet.2019.11.010.
50. Carracedo, A.; Cantley, L.C.; Pandolfi, P.P. Cancer metabolism: Fatty acid oxidation in the limelight. *Nat. Rev. Cancer* **2013**, *13*, 227–232, doi:10.1038/nrc3483.
51. Barrett, P.Q.; Guagliardo, N.A.; Klein, P.M.; Hu, C.; Breault, D.T.; Beenhakker, M.P. Role of voltage-gated calcium channels in the regulation of aldosterone production from zona glomerulosa cells of the adrenal cortex. *J. Physiol.* **2016**, *594*, 5851–5860, doi:10.1113/JP271896.
52. Wiederkehr, A.; Szanda, G.; Akhmedov, D.; Mataki, C.; Heizmann, C.W.; Schoonjans, K.; Pozzan, T.; Spat, A.; Wollheim, C.B. Mitochondrial matrix calcium is an activating signal for hormone secretion. *Cell Metab.* **2011**, *13*, 601–611, doi:10.1016/j.cmet.2011.03.015.
53. Gulick, T.; Cresci, S.; Caira, T.; Moore, D.D.; Kelly, D.P. The peroxisome proliferator-activated receptor regulates mitochondrial fatty acid oxidative enzyme gene expression. *Proc. Natl. Acad. Sci. USA* **1994**, *91*, 11012–11016, doi:10.1073/pnas.91.23.11012.
54. Pawlak, M.; Lefebvre, P.; Staels, B. Molecular mechanism of PPARalpha action and its impact on lipid metabolism, inflammation and fibrosis in non-alcoholic fatty liver disease. *J. Hepatol.* **2015**, *62*, 720–733, doi:10.1016/j.jhep.2014.10.039.
55. Hardege, I.; Long, L.; Al Maskari, R.; Figg, N.; O'Shaughnessy, K.M. Targeted disruption of the Kcnj5 gene in the female mouse lowers aldosterone levels. *Clin. Sci.* **2018**, *132*, 145–156, doi:10.1042/CS20171285.
56. Sun, N.; Meyer, L.S.; Feuchtinger, A.; Kunzke, T.; Knosel, T.; Reincke, M.; Walch, A.; Williams, T.A. Mass Spectrometry Imaging Establishes 2 Distinct Metabolic Phenotypes of Aldosterone-Producing Cell Clusters in Primary Aldosteronism. *Hypertension* **2020**, *75*, 634–644, doi:10.1161/HYPERTENSIONAHA.119.14041.
57. Williams, T.A.; Gomez-Sanchez, C.E.; Rainey, W.E.; Giordano, T.J.; Lam, A.K.; Marker, A.; Mete, O.; Yamazaki, Y.; Zerbini, M.C.N.; Beuschlein, F.; et al. International Histopathology Consensus for Unilateral Primary Aldosteronism. *J. Clin. Endocrinol. Metab.* **2021**, *106*, 42–54, doi:10.1210/clinem/dgaa484.
58. Sun, N.; Wu, Y.; Nanba, K.; Sbiera, S.; Kircher, S.; Kunzke, T.; Aichler, M.; Berezowska, S.; Reibetanz, J.; Rainey, W.E.; et al. High-Resolution Tissue Mass Spectrometry Imaging Reveals a Refined Functional Anatomy of the Human Adult Adrenal Gland. *Endocrinology* **2018**, *159*, 1511–1524, doi:10.1210/en.2018-00064.
59. Lieu, F.K.; Lin, C.Y.; Wang, P.S.; Jian, C.Y.; Yeh, Y.H.; Chen, Y.A.; Wang, K.L.; Lin, Y.C.; Chang, L.L.; Wang, G.J.; et al. Effect of swimming on the production of aldosterone in rats. *PLoS ONE* **2014**, *9*, e87080, doi:10.1371/journal.pone.0087080.
60. Chang, C.H.; Qiu, J.; O'Sullivan, D.; Buck, M.D.; Noguchi, T.; Curtis, J.D.; Chen, Q.; Gindin, M.; Gubin, M.M.; van der Windt, G.J.; et al. Metabolic Competition in the Tumor Microenvironment Is a Driver of Cancer Progression. *Cell* **2015**, *162*, 1229–1241, doi:10.1016/j.cell.2015.08.016.
61. Korpal, M.; Puyang, X.; Jeremy Wu, Z.; Seiler, R.; Furman, C.; Oo, H.Z.; Seiler, M.; Irwin, S.; Subramanian, V.; Julie Joshi, J.; et al. Evasion of immunosurveillance by genomic alterations of PPARgamma/RXRalpha in bladder cancer. *Nat. Commun.* **2017**, *8*, 103, doi:10.1038/s41467-017-00147-w.

62. Poynter, M.E.; Daynes, R.A. Peroxisome proliferator-activated receptor alpha activation modulates cellular redox status, represses nuclear factor-kappaB signaling, and reduces inflammatory cytokine production in aging. *J. Biol. Chem.* **1998**, *273*, 32833–32841, doi:10.1074/jbc.273.49.32833.
63. Gilbert, K.; Nian, H.; Yu, C.; Luther, J.M.; Brown, N.J. Fenofibrate lowers blood pressure in salt-sensitive but not salt-resistant hypertension. *J. Hypertens.* **2013**, *31*, 820–829, doi:10.1097/HJH.0b013e32835e8227.
64. Zhao, E.; Maj, T.; Kryczek, I.; Li, W.; Wu, K.; Zhao, L.; Wei, S.; Crespo, J.; Wan, S.; Vatan, L.; et al. Cancer mediates effector T cell dysfunction by targeting microRNAs and EZH2 via glycolysis restriction. *Nat. Immunol.* **2016**, *17*, 95–103, doi:10.1038/ni.3313.
65. Prasad, R.; Kowalczyk, J.C.; Meimaridou, E.; Storr, H.L.; Metherell, L.A. Oxidative stress and adrenocortical insufficiency. *J. Endocrinol.* **2014**, *221*, R63–73, doi:10.1530/JOE-13-0346.
66. Wu, K.C.; Cui, J.Y.; Klaassen, C.D. Beneficial role of Nrf2 in regulating NADPH generation and consumption. *Toxicol. Sci.* **2011**, *123*, 590–600, doi:10.1093/toxsci/kfr183.
67. Rapoport, R.; Sklan, D.; Hanukoglu, I. Electron leakage from the adrenal cortex mitochondrial P450scc and P450c11 systems: NADPH and steroid dependence. *Arch. Biochem. Biophys.* **1995**, *317*, 412–416, doi:10.1006/abbi.1995.1182.
68. Choi, J.E.; Sebastian, C.; Ferrer, C.M.; Lewis, C.A.; Sade-Feldman, M.; LaSalle, T.; Gonye, A.; Lopez, B.G.C.; Abdelmoula, W.M.; Regan, M.S.; et al. A unique subset of glycolytic tumour-propagating cells drives squamous cell carcinoma. *Nat. Metab.* **2021**, *3*, 182–195, doi:10.1038/s42255-021-00350-6.
69. Kagan, V.E.; Mao, G.; Qu, F.; Angeli, J.P.; Doll, S.; Croix, C.S.; Dar, H.H.; Liu, B.; Tyurin, V.A.; Ritov, V.B.; et al. Oxidized arachidonic and adrenic PEs navigate cells to ferroptosis. *Nat. Chem. Biol.* **2017**, *13*, 81–90, doi:10.1038/nchembio.2238.
70. Martinez, N.; White, V.; Kurtz, M.; Higa, R.; Capobianco, E.; Jawerbaum, A. Activation of the nuclear receptor PPARalpha regulates lipid metabolism in foetal liver from diabetic rats: Implications in diabetes-induced foetal overgrowth. *Diabetes Metab. Res. Rev.* **2011**, *27*, 35–46, doi:10.1002/dmrr.1151.
71. Tesfay, L.; Paul, B.T.; Konstorum, A.; Deng, Z.; Cox, A.O.; Lee, J.; Furdui, C.M.; Hegde, P.; Torti, F.M.; Torti, S.V. Stearoyl-CoA Desaturase 1 Protects Ovarian Cancer Cells from Ferroptotic Cell Death. *Cancer Res.* **2019**, *79*, 5355–5366, doi:10.1158/0008-5472.CAN-19-0369.
72. Gao, M.; Monian, P.; Quadri, N.; Ramasamy, R.; Jiang, X. Glutaminolysis and Transferrin Regulate Ferroptosis. *Mol. Cell* **2015**, *59*, 298–308, doi:10.1016/j.molcel.2015.06.011.

4. Publication II

Hypertension

ORIGINAL ARTICLE

TSPAN12 (Tetraspanin 12) Is a Novel Negative Regulator of Aldosterone Production in Adrenal Physiology and Aldosterone-Producing Adenomas

Siyuan Gong, Martina Tetti, Elisabeth Kemter, Mirko Peitzsch, Paolo Mulatero, Martin Bidlingmaier, Graeme Eisenhofer, Eckhard Wolf, Martin Reincke, Tracy Ann Williams

BACKGROUND: Aldosterone-producing adenomas (APAs) are a major cause of primary aldosteronism, a condition of low-renin hypertension, in which aldosterone overproduction is usually driven by a somatic activating mutation in an ion pump or channel. *TSPAN12* is differentially expressed in different subgroups of APAs suggesting a role in APA pathophysiology. Our objective was to determine the function of TSPAN12 (tetraspanin 12) in adrenal physiology and pathophysiology.

METHODS: APA specimens, pig adrenals under dietary sodium modulation, and a human adrenocortical cell line HAC15 were used for functional characterization of TSPAN12 in vivo and in vitro.

RESULTS: Gene ontology analysis of 21 APA transcriptomes dichotomized according to high versus low *TSPAN12* transcript levels highlighted a function for *TSPAN12* related to the renin-angiotensin system. *TSPAN12* expression levels in a cohort of 30 APAs were inversely correlated with baseline plasma aldosterone concentrations (R=−0.47; P=0.009). In a pig model of renin-angiotensin system activation by dietary salt restriction, *TSPAN12* mRNA levels and TSPAN12 immunostaining were markedly increased in the zona glomerulosa layer of the adrenal cortex. In vitro stimulation of human adrenocortical human adrenocortical cells with 10 nM angiotensin II for 6 hours caused a 1.6-fold±0.13 increase in *TSPAN12* expression, which was ablated by 10 µM nifedipine (P=0.0097) or 30 µM W-7 (P=0.0022). Gene silencing of *TSPAN12* in human adrenocortical cells demonstrated its inverse effect on aldosterone secretion under basal and angiotensin II stimulated conditions.

CONCLUSIONS: Our findings show that TSPAN12 is a negative regulator of aldosterone production and could contribute to aldosterone overproduction in primary aldosteronism. **(*Hypertension*. 2023;80:440–450. DOI: 10.1161/HYPERTENSIONAHA.122.19783.)** • **Supplemental Material**

Key Words: adrenal cortex ■ aldosterone ■ angiotensin II ■ hyperaldosteronism ■ pig model

Primary aldosteronism (PA) is the most common cause of endocrine hypertension and is characterized by inappropriately high plasma aldosterone to renin concentrations.[1] A major subtype of PA is caused by a unilateral aldosterone-producing adenoma (APA), which can be cured by adrenalectomy.[2] Somatic APA mutations in some ion pumps and channels can cause a disturbance in intracellular ion homeostasis resulting in activation of Ca^{2+} signaling, which drives an increase in *CYP11B2* (aldosterone synthase) gene expression and aldosterone production.[3] CYP11B2 immunohistochemistry-guided next generation sequencing has helped identify somatic aldosterone-driver mutations in more than 90% APAs.[4,5]

Correspondence to: Tracy Ann Williams, Medizinische Klinik und Poliklinik IV, Klinikum der Universität München, LMU München, Ziemssenstr. 5, D-80336 München, Germany. Email tracy.williams@med.uni-muenchen.de
Supplemental Material is available at https://www.ahajournals.org/doi/suppl/10.1161/HYPERTENSIONAHA.122.19783.
For Sources of Funding and Disclosures, see page 448.
© 2022 American Heart Association, Inc.
Hypertension is available at www.ahajournals.org/journal/hyp

NOVELTY AND RELEVANCE

What Is New?

Transcriptomics analyses of aldosterone-producing adenomas highlight a link between the renin-angiotensin system and *TSPAN12* gene expression.
TSPAN12 (tetraspanin 12) is highly expressed in pig adrenal zona glomerulosa cells in response to renin-angiotensin system activation by dietary sodium restriction.
Angiotensin II stimulation of human adrenocortical cells promotes *TSPAN12* expression by the Ca^{2+}/calmodulin signaling pathway.
Ablation of *TSPAN12* gene expression enhances angiotensin II stimulated *CYP11B2* (aldosterone synthase) gene expression and aldosterone production.
TSPAN12 expression in aldosterone-producing adenomas is inversely associated with preoperative plasma aldosterone concentrations in the corresponding patients.

What Is Relevant?

TSPAN12 is an endogenous negative regulator of *CYP11B2* gene expression and aldosterone production.
Downregulation of *TSPAN12* in aldosterone-producing adenomas by suppression of the renin-angiotensin system might contribute to pathological aldosterone production.

Clinical/Pathophysiological Implications?

TSPAN12 is a novel target of the renin-angiotensin system under physiological and pathophysiological conditions.

Nonstandard Abbreviations and Acronyms

AngII	angiotensin II
APA	aldosterone-producing adenoma
PA	primary aldosteronism
RAS	renin-angiotensin system
zG	zona glomerulosa

Aldosterone is produced by adrenal zona glomerulosa (zG) cells in response to the physiological stimuli AngII (angiotensin II), circulating potassium, and adrenocorticotropic hormone.[6,7] In healthy individuals, suppression of the circulating renin-angiotensin system (RAS) can lower aldosterone levels in response to high salt or volume expansion.[7] Thus, RAS suppression and elevated plasma aldosterone concentrations should be mutually exclusive under normal physiological conditions. Immunohistochemistry of adult adrenals shows that CYP11B2 expression in the zG layer is mostly suppressed and restricted to aldosterone-producing micronodules that carry aldosterone-driver mutations.[8,9] Several genes have been identified in adrenal zG cells that downregulate *CYP11B2* gene transcription.[10–13] Of these, *NEFM* (Neurofilament medium chain),[11,14] and *LGR5* (leucine-rich repeat containing G protein-coupled receptor 5)[13,14] are differentially expressed in APAs and might function under pathological conditions to modulate aldosterone production.

TSPAN12 belongs to the transmembrane 4 superfamily (or tetraspanin family) and functions in a cell type-specific and disease-specific manner. Loss of endothelial TSPAN12 in the retina impairs vascular morphogenesis,[15] and aberrant TSPAN12 expression in epithelial cells and fibroblasts contributes to cancer progression via FZD4 (frizzled class receptor 4)/LRP5 (low-density-lipoprotein receptor-related protein 5)-mediated β-catenin signaling.[16] Additionally, *Tspan12* transcripts are abundantly expressed in mouse pancreatic α-cells and have been linked to the pathogenesis of diabetes.[17] Recently, we used RNAseq analysis to identify differentially expressed genes in APAs.[18] *TSPAN12* was inversely correlated with APA diameter and was downregulated in APAs with an APA somatic mutation in *KCNJ5* (encoding a G protein-activated inward rectifier potassium channel) compared with APAs with wild-type *KCNJ5*.[18,19] Its function in adrenal physiology and pathology are unknown but might feasibly play a role in steroidogenesis because *TSPAN12* gene expression is a component of the most informative transcriptome signature for adrenal zone-specific steroid production.[20]

Herein, we investigated the role of *TSPAN12* under conditions of RAS activation and suppression using a combined approach of transcriptome analysis of adrenal tumors and of adrenals from a pig model of activated RAS, and functional in vitro studies in human adrenocortical cells.

METHODS

The expanded methods are available in the Supplemental Material. The authors declare that all supporting data are available within the article and Supplemental Material.

Patients

APAs were surgically resected from patients diagnosed with unilateral disease at the Klinikum der Ludwig-Maximilians-Universität München, Munich, Germany, and the Division of Internal Medicine and Hypertension, Turin, Italy.[21–23] Blood

ORIGINAL ARTICLE

pressure, hormonal and biochemical measurements were assessed as described. Diagnosis of PA and differentiation of unilateral from bilateral PA by adrenal venous sampling was performed according to recent recommendations.[1,24,25] The presence of an APA in the resected adrenal was evaluated by CYP11B2 immunohistochemistry.[26,27] APA *KCNJ5* mutations were identified as described previously.[18]

Human Biosamples and Transcriptome Data

RNA-sequencing (RNA-seq) datasets were publicly available from previously published data, either from our group (APAs and pig adrenal zones)[18,28] or from others (comparison of zona glomerulosa adjacent to APA and pheochromocytoma).[14] This study also included a separate cohort of 30 APAs for TaqMan real-time gene expression analysis and the corresponding peripheral blood plasma samples were used for steroid measurements. Adrenal steroid measurements of aldosterone, 18-oxocortisol, and 18-hydroxycortisol in peripheral venous plasma were determined by liquid chromatography-tandem mass spectrometry (LC-MS/MS).[29] All patients gave written informed consent for use of clinical data and biomaterial in accordance with local ethics committees.

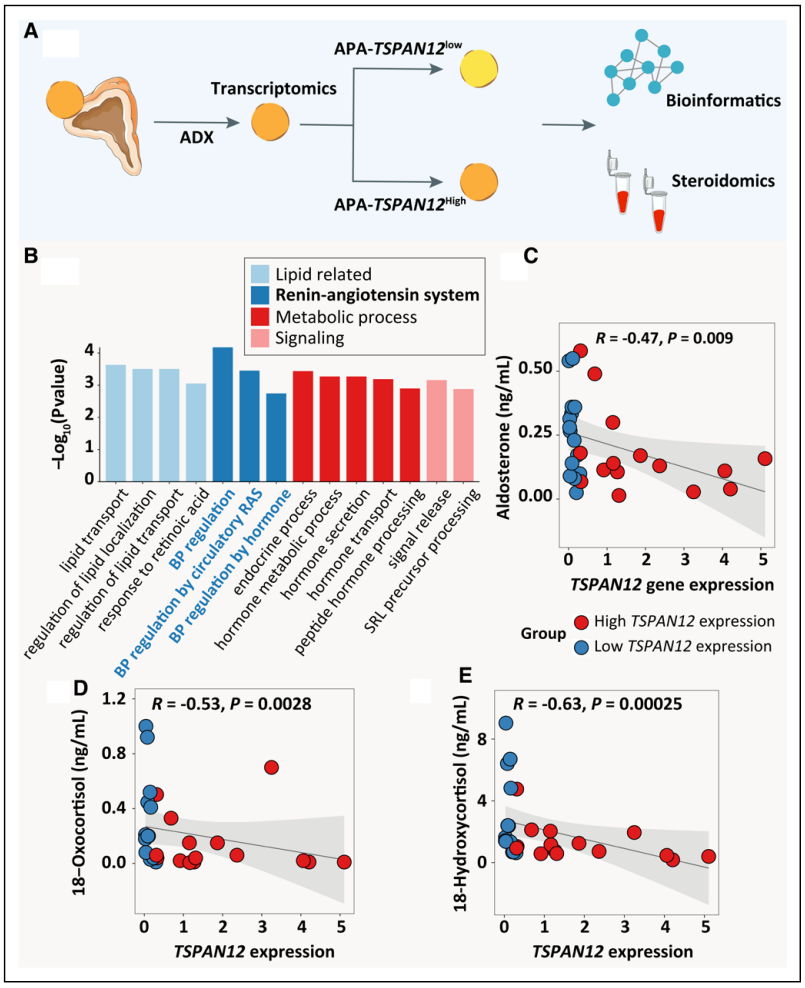

Figure 1. Transcriptomics and steroidomics analyses of patients with aldosterone-producing adenomas (APA).
A, RNAseq analysis of 21 APAs was used to dichotomize APAs into those with high and low *TSPAN12* mRNA levels according to the median value (APA-*TSPAN12*^{high} and APA-*TSPAN12*^{low}). **B**, Bar plots showing Gene Ontology (GO) terms significantly enriched in RNA-seq analysis of APAs in the *TSPAN12*^{high} group (n=10) versus the *TSPAN12*^{low} group (n=11). **C–E**, Scatter plots showing the correlation of *TSPAN12* mRNA levels with plasma aldosterone concentrations, 18-oxocortisol, and 18-hydroxycortisol in a cohort of 30 patients with an APA. *P* and r values were calculated by Spearman correlation. ADX, adrenalectomy; BP, blood pressure; RAS, renin-angiotensin system; and SRL, signaling receptor ligand.

 Hypertension. 2023;80:440–450. DOI: 10.1161/HYPERTENSIONAHA.122.19783

Animal Samples

Adrenal samples from 6-week-old male German Landrace DanBred pigs fed a 14-day diet comprising 0.04% sodium (low-salt group) or 0.7% sodium (high-salt group) were from a previous study.[28]

In Vitro Functional Assays

The HAC15 human adrenocortical cell line[30] was used to investigate the functional role of TSPAN12 in vitro as detailed in the Supplemental Material.

Statistical Analyses and Bioinformatics

GraphPad Prism 9.3.1 was used for all statistical analyses. An unpaired Student *t* test was used for normally distributed data or a Mann-Whitney *U* for non-normally distributed data among 2 groups. For multiple groups, 1- or 2-way ANOVA followed by Tukey post hoc test was performed for normally distributed data or Kruskal-Wallis for non-normally distributed data. Data in time-course experiments were analyzed by repeated measures 2-way ANOVA. Chi-square and Fisher exact tests were performed to compare categorical variables. Correlations were performed using Spearman correlations. $P<0.05$ were considered to indicate significant differences. Differential gene expression analyses were performed using R package DESeq2 (v1.32.0),[31] and R package clusterProfiler (v4.0.5) was used to analyze Gene Ontology.[32]

RESULTS

Clinical Parameters of Patients With APA According to *TSPAN12* Gene Expression Levels

The RNA-seq transcriptome profiles of 21 APAs were dichotomized into those with high or low *TSPAN12* expression levels (*TSPAN12*^{high} versus *TSPAN12*^{low}) according to the median value. Gene Ontology analysis of the *TSPAN12*^{high} versus *TSPAN12*^{low} groups demonstrated that *TSPAN12* gene expression was closely related to the activity of the RAS and in particular blood pressure regulation by the circulatory RAS and by hormones (Figure 1A and 1B).

TSPAN12 gene expression levels were also determined in a separate sample set of 30 APAs, which were likewise dichotomized into *TSPAN12*^{high} and *TSPAN12*^{low} groups according to the median *TSPAN12* expression level in this sample set. Patients in the *TSPAN12*^{high} group displayed higher systolic blood pressure (BP) compared with the *TSPAN12*^{low} group

Table 1. Clinical Parameters of Patients With an APA Stratified by *TSPAN12* Gene Expression Levels

Variables	Total cohort (n=30)	*TSPAN12* gene expression		*P* Value
		High (n=15)	Low (n=15)	
Age at surgery, y (n=30)	46.30±10.55	48.27±11.42	44.33±9.57	0.316
Sex (ref. women; n=30)	17 (56.7%)	7 (46.7%)	10 (66.7%)	0.461
BMI, kg/m² (n=30)	27.76 (22.88–30.33)	29.00 (24.90–30.98)	25.60 (22.20–28.82)	0.101
Systolic BP, mmHg (n=30)	150.00 (140.75–163.00)	160.00 (148.85–182.15)	145.00 (136.50–151.50)	0.011
Diastolic BP, mmHg (n=30)	94.15 (86.75–104.28)	105.70 (95.00–110.00)	90.00 (85.50–94.15)	0.012
Duration HTN, mo (n=30)	77.50 (41.25–112.50)	91.00 (59.00–131.50)	67.00 (18.50–101.00)	0.245
Anti-HTN meds (DDD; n=30)	4.00 (3.00–5.62)	5.00 (3.00–6.00)	3.50(1.25–4.88)	0.080
PAC, pmol/L (n=30)	792.00 (575.60–1301.42)	643.60 (448.00–1004.20)	1090.20 (606.10–1451.35)	0.272
DRC, mU/L (n=15)	3.30 (2.00–9.20)	3.10 (2.00–7.35)	4.50 (1.95–10.25)	0.728
ARR_DRC (n=15)	180.50 (62.15–324.20)	180.50 (79.25–254.50)	191.10 (47.78–358.72)	1
PRA, pmol/L per min (n=15)	2.56 (2.56–3.84)	3.20 (2.56–5.44)	2.56 (1.92–3.20)	0.206
ARR_PRA (n=15)	418.30 (242.70–708.15)	253.55 (116.95–411.75)	609.00 (488.20–829.50)	0.049
Lowest serum K^+, mmol/L (n=30)	2.98±0.57	3.03±0.54	2.94±0.62	0.687
Nodule diameter, mm (n=30)	15.00 (12.25–17.75)	13.00 (10.50–15.50)	17.00 (14.00–24.50)	0.021
TSPAN12 expression	0.30 (0.09–1.24)	1.27 (0.80–2.81)	0.09 (0.04–0.16)	<0.001
Genotype				0.027
KCNJ5 mutation	17 (56.7%)	5 (33.3%)	12 (80.0%)	
KCNJ5 wild type	13 (43.3%)	10 (66.7%)	3 (20.0%)	

Baseline variables were stratified as APA-*TSPAN12*^{high} (>median *TSPAN12* gene expression level) and APA-*TSPAN12*^{low} (≤median). *TSPAN12* relative expression for each sample was calculated using the $2^{-\Delta\Delta Ct}$ formula. Quantitative normally distributed variables are shown as means±SD and nonnormally distributed variables are reported as medians (IQR). Categorical variables are shown as absolute numbers and percentage. *P* Value were calculated using χ^2 and Fisher exact tests or *t* tests or Mann-Whitney *U* test as appropriate. *P* Value of <0.05 were considered significant. The DDD is the assumed average maintenance dose per day for a drug used for its main indication in adults (https://www.who.int/tools/atc-ddd-toolkit/about-ddd). The 30 APAs used for this analysis were from patients diagnosed at 2 different centres (Munich and Turin) using different methods for the measurement of renin levels (DRC or PRA). APA indicates aldosterone-producing adenoma; ARR, aldosterone-to-renin ratio; BMI, body mass index; BP, blood pressure; DDD, defined daily dose; DRC, direct renin concentration; HTN, hypertension; K^+, potassium ions; *KCNJ5*, gene encoding potassium inwardly rectifying channel subfamily J member 5; meds, medications; N, number; PAC, plasma aldosterone concentration; and PRA, plasma renin activity.

ORIGINAL ARTICLE

(160 versus 145 mmHg; P=0.011), and higher diastolic BP (105.7 versus 90 mmHg; P=0.012; Table 1). A higher proportion of APAs with a *KCNJ5* mutation were identified in the *TSPAN12*^{low} group than in the *TSPAN12*^{high} group (80.0% in *TSPAN12*^{low} versus 33.3% in *TSPAN12*^{high} APAs; P=0.027). Lower APA *TSPAN12* gene expression was associated with higher peripheral plasma concentrations of aldosterone (R=−0.47; P=0.009; Figure 1C), and the hybrid steroids 18-oxocortisol (R=−0.53; P=0.0028; Figure 1D), and 18-hydroxycortisol (R=−0.63; P=0.00025; Figure 1E) measured by LC-MS/MS.

TSPAN12 Gene Expression in zG Cells Adjacent to an APA or Pheochromocytoma

Because Gene Ontology analysis highlighted a link between *TSPAN12* and the RAS, we assessed *TSPAN12* gene expression levels in zG cells adjacent to an APA (a form of low renin hypertension) and adjacent to a pheochromocytoma (a form of high renin hypertension) using publicly available transcriptome data (GSE64957).[14] *TSPAN12* expression levels in zG cells adjacent to APA (n=13) were 3.93-fold lower than in zG cells adjacent to pheochromocytoma (n=7; P<0.001; Figure S1A). Indeed, the absence of TSPAN12 immunostaining was observed in zona glomerulosa adjacent to an APA (Figure S2) indicating the downregulation of TSPAN12 under conditions of a suppressed RAS. In addition, *TSPAN12* gene expression in APAs with a *KCNJ5* mutation (n=17) was downregulated compared with APAs without a *KCNJ5* mutation (n=13; P<0.05; Figure S1B; Table 1) and markedly lower intensity of TSPAN12 immunostaining was detected in *KCNJ5* mutated relative to *KCNJ5* wild-type APAs (Figure 2).

TSPAN12 Expression in Pig Adrenals in Response to RAS Activation

To explore the physiological response of *TSPAN12* to RAS activation, we evaluated *TSPAN12* gene expression and TSPAN12 immunostaining in adrenal glands from pigs after RAS activation by a 14-day low-salt diet compared with a high-salt diet.[28] RNA-seq analysis of the dissected zG layer demonstrated notably increased *TSPAN12* gene expression in pigs following the low salt diet (P<0.001; Figure 3A). In addition, immunohistochemistry established higher TSPAN12 expression localized to the zG of pig adrenals on the low versus high sodium diet (Figure 3B).

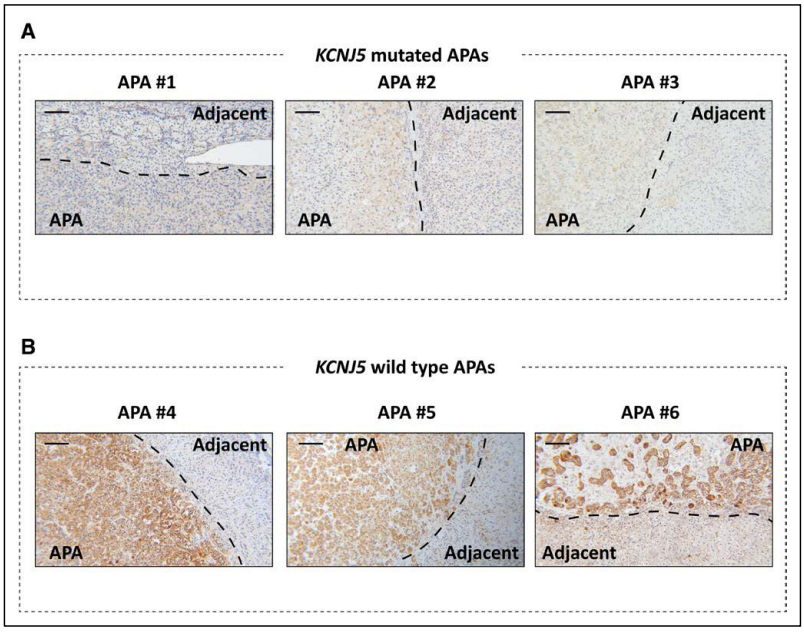

Figure 2. TSPAN12 (tetraspanin 12) immunohistochemistry of aldosterone-producing adenomas (APAs) with or without a KCNJ5 mutation.
Immunohistochemical staining of TSPAN12 in APAs with a *KCNJ5* mutation (**A**) or in APAs without a *KCNJ5* mutation (**B**). APA from patient 4 and patient 5 carry *CACNA1D* mutations. The APA from patient 6 carries an *ATP1A1* mutation. Pictures are representative of 10 adrenals per group. Scale bars=200 µm. *KCNJ5*, gene encoding G-protein-coupled inwardly rectifying potassium channel; *CACNA1D*, gene encoding Cav1.3 Ca^{2+} channel; *ATP1A1*, gene encoding Na^+/K^+ ATPase 1.

 Hypertension. 2023;80:440–450. DOI: 10.1161/HYPERTENSIONAHA.122.19783

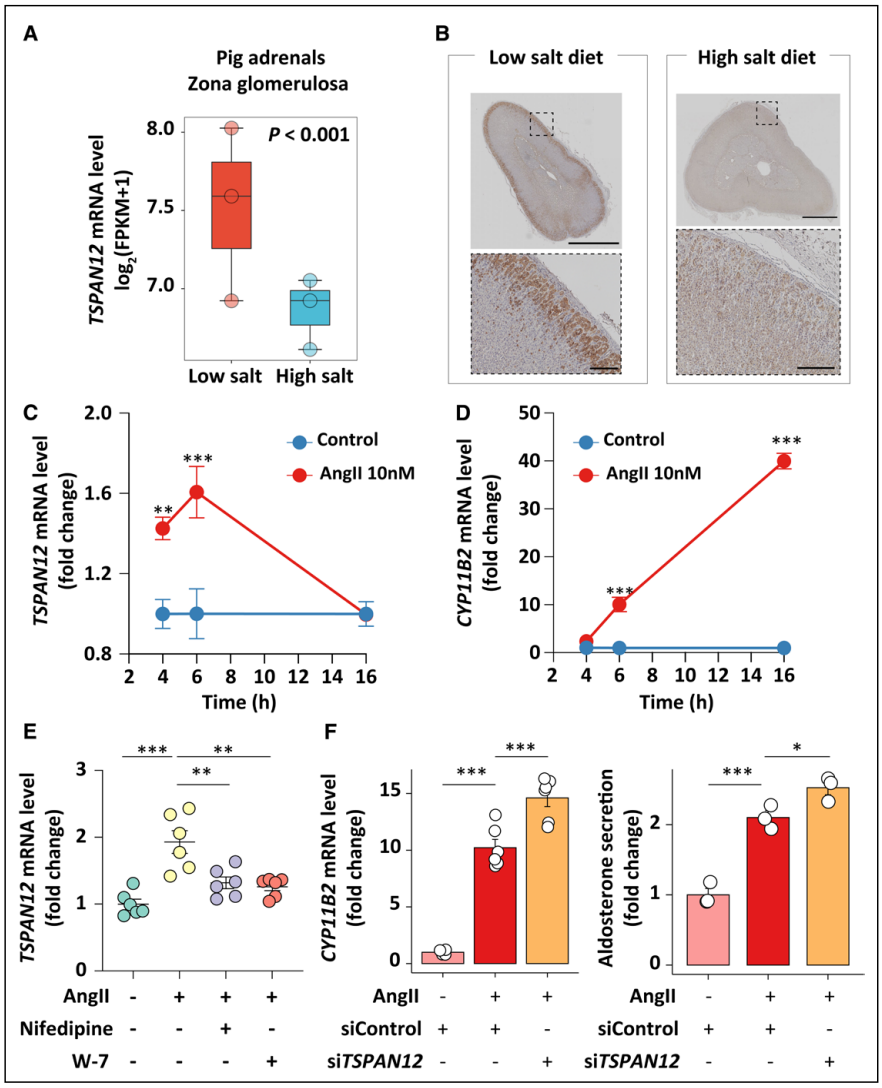

Figure 3. Effect of renin angiotensin system activation and Ang II (angiotensin II) on TSPAN12 (tetraspanin 12) in pig adrenals and in human adrenocortical cells.

A, *TSPAN12* gene expression levels using FPKM normalization were assessed in the zG of pig adrenals on low versus high sodium diet from RNA-seq data (n=3 per group). Data are represented as box-and-whisker plots with minimum to maximum values. **B**, Representative immunohistochemistry staining of TSPAN12 in adrenal sections from pigs on low versus high sodium diet. Scale bar, 2 mm (whole images) and 200 µm (magnifications). **C** and **D**, Time course of *TSPAN12* (**C**) and *CYP11B2* (**D**) mRNA levels in HAC15 cells treated with 10 nM AngII (n=8 independent experiments per group). Data represent mean±SEM. Statistical significance was determined by repeated measures 2-way ANOVA. **E**, Levels of *TSPAN12* mRNA in HAC15 cells treated for 6 hours with vehicle (dimethyl sulfoxide [DMSO]) or AngII (10 nmol/L) in the presence or absence of the calcium channel blocker nifedipine (10 µmol/L) or calmodulin antagonist W-7 hydrochloride (30 µmol/L; 6 independent experiments per group). **F**, Levels of *CYP11B2* mRNA or aldosterone production in HAC15 cells transfected with control siRNA (siControl) or *TSPAN12*-specific siRNA (si*TSPAN12*) treated with or without AngII (10 nmol/L) for 6 hours (n=6 independent experiments per group) or 24 hours (right, n=3 independent experiments per group). Data represent mean±SEM. Statistical significance was calculated by 1-way ANOVA and Tukey post hoc test. $^{**}P<0.01$, $^{***}P<0.001$. Scale bars (**B**, upper)=2 µm; scale bar (**B**, lower)=200 µm. FPKM indicates fragments per kilo base of transcript per million mapped fragments; HAC15 cells, human adrenocortical cell line; IHC, immunohistochemistry; and zG, zona glomerulosa.

ORIGINAL ARTICLE

In Vitro Functional Analysis of *TSPAN12* Expressed in Human Adrenocortical Cells

CYP11B2 gene expression was quantified in HAC15 cells after overexpression or silencing of *TSPAN12* (Figure 4A and 4C). *TSPAN12* overexpression displayed a 33% reduction in *CYP11B2* gene expression (P=0.0036; Figure 4B). Silencing *TSPAN12* resulted in a 30% increase in *CYP11B2* expression (P<0.0001; Figure 4D) and a 41% increase in aldosterone production (P<0.05; Figure 4E). Angiotensin II (10 nM) stimulation of HAC15 cells led to a transient 1.43-fold increase in *TSPAN12* expression at 4h compared with basal levels (P=0.0004) and as expected, an increase in *CYP11B2* gene expression over the 16-hour time course (Figure 3C and 3D). The stimulatory effect of AngII on aldosterone biosynthesis in zG cells is mediated by the calcium signaling pathway. To investigate if calcium signaling mediates the effect of AngII on *TSPAN12* gene expression, HAC15 cells were treated with 10 nM AngII for 6 hours in the presence and absence of either 10 µM of the calcium channel blocker nifedipine or 30 µM of the calmodulin antagonist W-7 (N-[6-aminohexyl]-5-chloro-1-naphthalenesulfonamide hydrochloride). Both calcium pathway inhibitors ablated the AngII-induced increase in *TSPAN12* expression levels (P=0.0097 and P=0.0022; Figure 3E).

TSPAN12 gene silencing in HAC15 cells caused an amplification of *CYP11B2* mRNA levels and aldosterone secretion in response to AngII compared with AngII-stimulated HAC15 cells transfected with a control siRNA (14.6-fold increase in *CYP11B2* mRNA with *TSPAN12* gene silencing versus 10.2-fold increase in AngII-stimulated control cells, P=0.0004; 2.5-fold increase in aldosterone secretion with *TSPAN12* gene silencing versus 2.1-fold increase in AngII-stimulated control cells; P<0.05; Figure 3F).

We investigated the effect of *TSPAN12* on HAC15 cell death and proliferation. Cell viability and flow cytometry analyses demonstrated the absence of an effect of *TSPAN12* gene silencing or overexpression on HAC15 cell proliferation (Figure S3A and S3B), staurosporine-induced apoptosis (Figure S3C and S3D) or RSL3-induced cell death by ferroptosis (Figure S3E and S3F) under the conditions tested.[18]

DISCUSSION

TSPAN12 has a widely studied role in endothelial cells in the promotion of vascular morphogenesis and

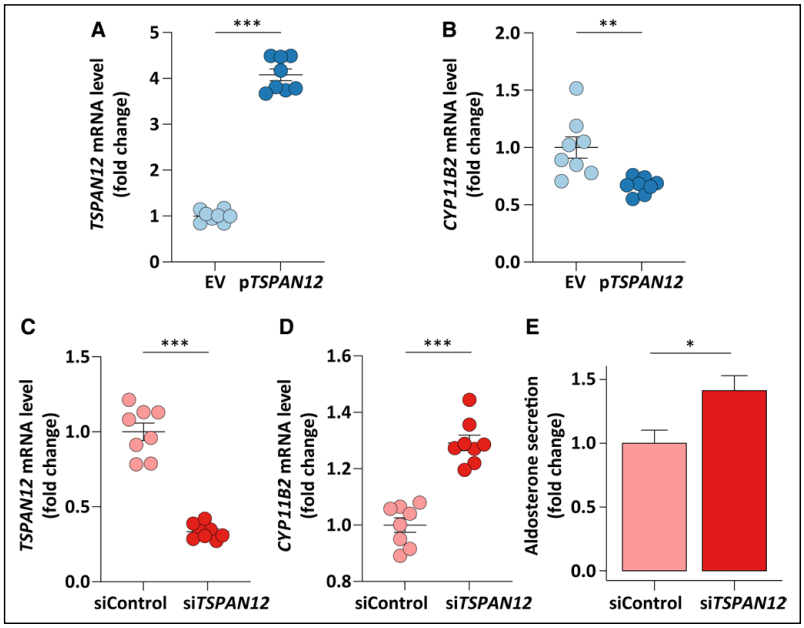

Figure 4. Effect of TSPAN12 (tetraspanin 12) gene expression on CYP11B2 gene expression and aldosterone production in human adrenocortical cells.
Real-time PCR gene expression assays of *TSPAN12* (**A**) and *CYP11B2* (**B**) in HAC15 cells transfected with empty vector (EV) or pcDNA3.1-*TSPAN12* (p*TSPAN12*; 8 independent experiments per group). Real-time PCR analysis of *TSPAN12* (**C**) and *CYP11B2* (**D**) gene expression in human adrenocortical cell line (HAC15) cells transfected with non-targeting siRNA (siControl) or *TSPAN12*-specific siRNA (si*TSPAN12*). *TSPAN12* silencing in HAC15 cells caused increased aldosterone production compared with controls. Cell medium was collected 48 hours after transfection for aldosterone measurements (n=23) and aldosterone levels were normalized relative to total protein in cell lysates (**E**). Data are presented as mean of 8 independent experiments ±SEM. *P<0.05, **P<0.01, ***P<0.001 by a 2-sided unpaired Student t test.

 Hypertension. 2023;80:440–450. DOI: 10.1161/HYPERTENSIONAHA.122.19783

barrier formation (blood-brain barrier and blood-retina barrier).[15,33–35] Endothelial cell-specific inactivation of *TSPAN12* results in abnormal angiogenesis and barrier dysfunction.[15] The role of TSPAN12 in the adrenal gland is unknown but a potential role in APA pathophysiology is suggested by the inverse correlation of *TSPAN12* gene expression with APA nodule diameter[18] and the downregulation of *TSPAN12* expression in APAs carrying a *KCNJ5* mutation (compared with APAs without this variant).[19]

In this study, we combined transcriptome data from both human adrenal tissue samples and a pig translational model of human adrenal steroidogenesis, with functional in vitro studies in adrenocortical cells to identify TSPAN12 as a negative regulator of basal *CYP11B2* gene expression with a functional role linked to the RAS. *CYP11B2* expression was upregulated by *TSPAN12* gene silencing and downregulated by *TSPAN12* overexpression under basal conditions in human adrenocortical HAC15 cells. *TSPAN12* expression was upregulated in response to AngII stimulation by Ca^{2+}/calmodulin signaling in HAC15 cells and in response to RAS activation in vivo. Conversely, under pathological conditions of RAS suppression, *TSPAN12* expression was downregulated in zG cells adjacent to an APA compared with zG cells adjacent to a pheochromocytoma thereby demonstrating differential expression of *TSPAN12* under conditions of low versus high renin hypertension.

A study of 677 individuals without primary aldosteronism demonstrated a progressive decline of plasma renin activity with increasing age associated with age-related autonomous aldosteronism.[9] The same study also demonstrated the change of CYP11B2 expression in the zG layer with age from a continuous to a discontinuous pattern and the accumulation of aldosterone-producing micronodules[8,9] such that most zG cells in the adult human adrenal do not express CYP11B2.[26,36] Zhou et al[10] identified 7 highly upregulated genes (> 10-fold) from a transcriptome analysis of zG versus zona fasciculata. Of these, 4 were negative regulators of aldosterone production (*LGR5*, *ANO4*, *NEFM*, *DACH1*),[10–13] and 2 were positive regulators (*NR4A2* and *VSNL1*).[37,38] These findings, together with the data of the present study, highlight genes that potentially function in the suppression of aldosterone production.

Like our findings with *TSPAN12*, a low sodium diet and AngII infusion induced *RGS2* (regulator of G protein signaling 2) and *RGS4* (regulator of G protein signaling 4) gene expression through the calcium/calmodulin-dependent kinase pathway in human adrenocortical cells.[39,40] Overexpression of *RGS2* or *RGS4* resulted in decreased AngII-induced aldosterone secretion, supporting the hypothesis that counterregulatory mechanisms function in the maintenance of appropriate levels of aldosterone production in vivo.[41]

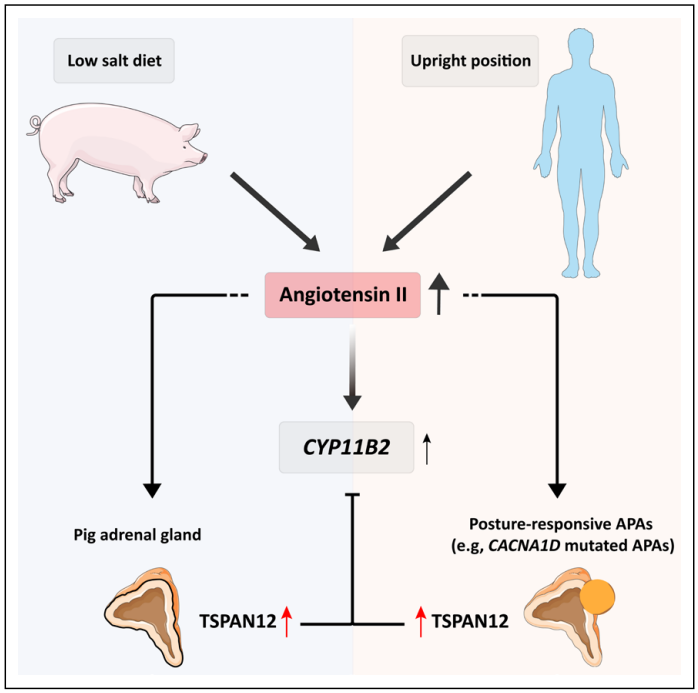

Figure 5. TSPAN12 (tetraspanin 12) is regulated by the renin-angiotensin-system (RAS) under physiological and pathophysiological conditions. *TSPAN12* gene expression is upregulated by increased RAS activity and may form part of a counterregulatory response to elevated aldosterone production by inhibition of *CYP11B2* expression. Figure produced using https://smart.servier.com/. APA indicates aldosterone-producing adenomas.

ORIGINAL ARTICLE

We observed a positive association between TSPAN12 gene expression and blood pressure in our cohort instead of an expected negative correlation. This apparent paradox can be explained by the multiple factors that influence blood pressure such as glomerular filtration rate, distal tubular sodium delivery, arterial compliance, and the duration and amplitude of aldosterone excess.[42,43] Our transcriptome data from APAs with high versus low *TSPAN12* gene expression indicate that *TSPAN12* function is linked with RAS activity under pathological conditions. In PA, aldosterone production is autonomous of the RAS. However, most PA patients, ≈40% of patients with an APA and most patients with bilateral PA, display increased aldosterone production in response to RAS activation by upright posture (posture-responsive APAs).[7,44,45] The majority of posture-responsive APAs do not have a *KCNJ5* mutation and comprise a relatively high proportion of compact eosinophilic cells (zG-like cells).[46,47] In contrast, posture-unresponsive APAs show a slight preponderance of *KCNJ5* mutations and are predominantly composed of clear zona fasciculata-like cells.[47–51] Patients with posture-unresponsive APAs display higher plasma concentrations of the hybrid steroids 18-oxocortisol and 18-hydroxycortisol, which are reported as a feature of APAs with a *KCNJ5* mutation.[52–54] Therefore, the link between the RAS and *TSPAN12* function underscored by the transcriptomics analyses is conceivably related to the posture-responsive APA phenotype (Figure 5).

Perspectives

TSPAN12 gene expression is upregulated by increased RAS activity and may comprise a counterregulatory response to elevated aldosterone through downregulation of *CYP11B2* expression. Further studies are required to elucidate the mechanism by which TSPAN12 exerts its negative regulatory effects on *CYP11B2* gene expression and adrenal aldosterone production. In addition, the potential role of chronic RAS suppression in APA pathophysiology and *TSPAN12* function in posture-responsive and posture-unresponsive APAs remains to be elucidated.

ARTICLE INFORMATION

Received June 9, 2022; accepted November 20, 2022.

Affiliations

Medizinische Klinik und Poliklinik IV, Klinikum der Universität München, LMU München, Germany (S.G., M.T., M.B., M.R., T.A.W.). Division of Internal Medicine and Hypertension, Department of Medical Sciences, University of Turin, Italy (M.T., P.M., T.A.W.). Chair for Molecular Animal Breeding and Biotechnology, Gene Center and Department of Veterinary Sciences, Ludwig-Maximilians-Universität München, Munich, Germany (E.K., E.W.). Institute of Clinical Chemistry and Laboratory Medicine, University Hospital and Faculty of Medicine Carl Gustav Carus, Technische Universität Dresden, Germany (M.P., G.E.). Department of Medicine III, University Hospital Carl Gustav Carus, Technische Universität Dresden, Germany (G.E.).

Acknowledgments

We are grateful for the excellent technical assistance of Isabella Sabrina-Kinker at the LMU, Munich.

Sources of Funding

This work was financed by the European Research Council (ERC) under the European Union's Horizon 2020 research and innovation programme (grant agreement no. 694913 to M Reincke) and the Deutsche Forschungsgemeinschaft (DFG) project number 444776998 to TA Williams (WI 5359/2-1) and M Reincke (RE 752/31-1) and project number 314061271-TRR 205 "The Adrenal: Central Relay in Health and Disease" to M Bidlingmaier, G Eisenhofer, E Kemter, M Peitzsch, M Reincke, and TA Williams, E Wolf. The Else Kröner-Fresenius Stiftung (2012_A103, 2015_A228, and 2019_A104; Else-Kröner Hyperaldosteronismus- German Conn Registry) also support the work of M Reincke.

Disclosures

None.

REFERENCES

1. Reincke M, Bancos I, Mulatero P, Scholl UI, Stowasser M, Williams TA. Diagnosis and treatment of primary aldosteronism. *Lancet Diabetes Endocrinol.* 2021;9:876–892. doi: 10.1016/S2213-8587(21)00210-2
2. Williams TA, Lenders JWM, Mulatero P, Burrello J, Rottenkolber M, Adolf C, Satoh F, Amar L, Quinkler M, Deinum J, et al; Primary Aldosteronism Surgery Outcome (PASO) investigators. Outcomes after adrenalectomy for unilateral primary aldosteronism: an international consensus on outcome measures and analysis of remission rates in an international cohort. *Lancet Diabetes Endocrinol.* 2017;5:689–699. doi: 10.1016/S2213-8587(17)30135-3
3. Scholl UI. Genetics of primary aldosteronism. *Hypertension.* 2022;79:887–897. doi: 10.1161/HYPERTENSIONAHA.121.16498
4. Nanba K, Rainey WE. GENETICS IN ENDOCRINOLOGY: impact of race and sex on genetic causes of aldosterone-producing adenomas. *Eur J Endocrinol.* 2021;185:R1–R11. doi: 10.1530/EJE-21-0031
5. De Sousa K, Boulkroun S, Baron S, Nanba K, Wack M, Rainey WE, Rocha A, Giscos-Douriez I, Meatchi T, Amar L, et al. Genetic, cellular, and molecular heterogeneity in adrenals with aldosterone-producing adenoma. *Hypertension.* 2020;75:1034–1044. doi: 10.1161/HYPERTENSIONAHA.119.14177
6. Hattangady NG, Olala LO, Bollag WB, Rainey WE. Acute and chronic regulation of aldosterone production. *Mol Cell Endocrinol.* 2012;350:151–162. doi: 10.1016/j.mce.2011.07.034
7. Stowasser M, Gordon RD. Primary aldosteronism: changing definitions and new concepts of physiology and pathophysiology both inside and outside the kidney. *Physiol Rev.* 2016;96:1327–1384. doi: 10.1152/physrev.00026.2015
8. Nishimoto K, Tomlins SA, Kuick R, Cani AK, Giordano TJ, Hovelson DH, Liu CJ, Sanjanwala AR, Edwards MA, Gomez-Sanchez CE, et al. Aldosterone-stimulating somatic gene mutations are common in normal adrenal glands. *Proc Natl Acad Sci USA.* 2015;112:E4591–E4599. doi: 10.1073/pnas.1505529112
9. Nanba K, Vaidya A, Williams GH, Zheng I, Else T, Rainey WE. Age-related autonomous aldosteronism. *Circulation.* 2017;136:347–355. doi: 10.1161/CIRCULATIONAHA.117.028201
10. Zhou J, Shaikh LH, Neogi SG, McFarlane I, Zhao W, Figg N, Brighton CA, Maniero C, Teo AE, Azizan EA, et al. DACH1, a zona glomerulosa selective gene in the human adrenal, activates transforming growth factor-beta signaling and suppresses aldosterone secretion. *Hypertension.* 2015;65:1103–1110. doi: 10.1161/HYP.0000000000000025
11. Maniero C, Garg S, Zhao W, Johnson TI, Zhou J, Gurnell M, Brown MJ. NEFM (neurofilament medium) polypeptide, a marker for zona glomerulosa cells in human adrenal, inhibits D1R (dopamine D1 receptor)-mediated secretion of aldosterone. *Hypertension.* 2017;70:357–364. doi: 10.1161/HYPERTENSIONAHA.117.09231
12. Maniero C, Scudieri P, Haris Shaikh L, Zhao W, Gurnell M, Galietta LJV, Brown MJ. ANO4 (anoctamin 4) is a novel marker of zona glomerulosa that regulates stimulated aldosterone secretion. *Hypertension.* 2019;74:1152–1159. doi: 10.1161/HYPERTENSIONAHA.119.13287
13. Shaikh LH, Zhou J, Teo AE, Garg S, Neogi SG, Figg N, Yeo GS, Yu H, Maguire JJ, Zhao W, et al. LGR5 activates noncanonical Wnt signaling and inhibits aldosterone production in the human adrenal. *J Clin Endocrinol Metab.* 2015;100:E836–E844. doi: 10.1210/jc.2015-1734
14. Zhou J, Lam B, Neogi SG, Yeo GS, Azizan EA, Brown MJ. Transcriptome pathway analysis of pathological and physiological aldosterone-producing

human tissues. *Hypertension.* 2016;68:1424–1431. doi: 10.1161/HYPERTENSIONAHA.116.08033
15. Zhang C, Lai MB, Pedler MG, Johnson V, Adams RH, Petrash JM, Chen Z, Junge HJ. Endothelial cell-specific inactivation of TSPAN12 (tetraspanin 12) reveals pathological consequences of barrier defects in an otherwise intact vasculature. *Arterioscler Thromb Vasc Biol.* 2018;38:2691–2705. doi: 10.1161/ATVBAHA.118.311689
16. Otomo R, Otsubo C, Matsushima-Hibiya Y, Miyazaki M, Tashiro F, Ichikawa H, Kohno T, Ochiya T, Yokota J, Nakagama H, et al. TSPAN12 is a critical factor for cancer-fibroblast cell contact-mediated cancer invasion. *Proc Natl Acad Sci USA.* 2014;111:18691–18696. doi: 10.1073/pnas.1412062112
17. Yin Q, Ni Q, Wang Y, Zhang H, Li W, Nie A, Wang S, Gu Y, Wang Q, Ning G. Raptor determines beta-cell identity and plasticity independent of hyperglycemia in mice. *Nat Commun.* 2020;11:2538. doi: 10.1038/s41467-020-15935-0
18. Yang Y, Tetti M, Vohra T, Adolf C, Seissler J, Hristov M, Belavgeni A, Bidlingmaier M, Linkermann A, Mulatero P, et al. BEX1 is differentially expressed in aldosterone-producing adenomas and protects human adrenocortical cells from ferroptosis. *Hypertension.* 2021;77:1647–1658. doi: 10.1161/HYPERTENSIONAHA.120.16774
19. Monticone S, Hattangady NG, Nishimoto K, Mantero F, Rubin B, Cicala MV, Pezzani R, Auchus RJ, Ghayee HK, Shibata H, et al. Effect of KCNJ5 mutations on gene expression in aldosterone-producing adenomas and adrenocortical cells. *J Clin Endocrinol Metab.* 2012;97:E1567–E1572. doi: 10.1210/jc.2011-3132
20. Baker JE, Plaska SW, Qin Z, Liu CJ, Rege J, Rainey WE, Udager AM. Targeted RNA sequencing of adrenal zones using immunohistochemistry-guided capture of formalin-fixed paraffin-embedded tissue. *Mol Cell Endocrinol.* 2021;530:111296. doi: 10.1016/j.mce.2021.111296
21. Williams B, Mancia G, Spiering W, Agabiti Rosei E, Azizi M, Burnier M, Clement DL, Coca A, de Simone G, Dominiczak A, et al; ESC Scientific Document Group. 2018 ESC/ESH Guidelines for the management of arterial hypertension. *Eur Heart J.* 2018;39:3021–3104. doi: 10.1093/eurheartj/ehy339
22. Riester A, Fischer E, Degenhart C, Reiser MF, Bidlingmaier M, Beuschlein F, Reincke M, Quinkler M. Age below 40 or a recently proposed clinical prediction score cannot bypass adrenal venous sampling in primary aldosteronism. *J Clin Endocrinol Metab.* 2014;99:E1035–E1039. doi: 10.1210/jc.2013-3789
23. Mulatero P, Bertello C, Sukor N, Gordon R, Rossato D, Daunt N, Leggett D, Mengozzi G, Veglio F, Stowasser M. Impact of different diagnostic criteria during adrenal vein sampling on reproducibility of subtype diagnosis in patients with primary aldosteronism. *Hypertension.* 2010;55:667–673. doi: 10.1161/HYPERTENSIONAHA.109.146613
24. Mulatero P, Monticone S, Deinum J, Amar L, Prejbisz A, Zennaro MC, Beuschlein F, Rossi GP, Nishikawa T, Morganti A, et al. Genetics, prevalence, screening and confirmation of primary aldosteronism: a position statement and consensus of the working group on endocrine hypertension of the european society of hypertension. *J Hypertens.* 2020;38:1919–1928. doi: 10.1097/HJH.0000000000002510
25. Mulatero P, Sechi LA, Williams TA, Lenders JWM, Reincke M, Satoh F, Januszewicz A, Naruse M, Doumas M, Veglio F, et al. Subtype diagnosis, treatment, complications and outcomes of primary aldosteronism and future direction of research: a position statement and consensus of the Working Group on Endocrine Hypertension of the European Society of Hypertension. *J Hypertens.* 2020;38:1929–1936. doi: 10.1097/HJH.0000000000002520
26. Gomez-Sanchez CE, Qi X, Velarde-Miranda C, Plonczynski MW, Parker CR, Rainey W, Satoh F, Maekawa T, Nakamura Y, Sasano H, et al. Development of monoclonal antibodies against human CYP11B1 and CYP11B2. *Mol Cell Endocrinol.* 2014;383:111–117. doi: 10.1016/j.mce.2013.11.022
27. Williams TA, Gomez-Sanchez CE, Rainey WE, Giordano TJ, Lam AK, Marker A, Mete O, Yamazaki Y, Zerbini MCN, Beuschlein F, et al. International histopathology consensus for unilateral primary aldosteronism. *J Clin Endocrinol Metab.* 2021;106:42–54. doi: 10.1210/clinem/dgaa484
28. Vohra T, Kemter E, Sun N, Dobenecker B, Hinrichs A, Burrello J, Gomez-Sanchez EP, Gomez-Sanchez CE, Wang J, Kinker IS, et al. Effect of dietary sodium modulation on pig adrenal steroidogenesis and transcriptome profiles. *Hypertension.* 2020;76:1769–1777. doi: 10.1161/HYPERTENSIONAHA.120.15998
29. Peitzsch M, Dekkers T, Haase M, Sweep FC, Quack I, Antoch G, Siegert G, Lenders JW, Deinum J, Willenberg HS, et al. An LC-MS/MS method for steroid profiling during adrenal venous sampling for investigation of primary aldosteronism. *J Steroid Biochem Mol Biol.* 2015;145:75–84. doi: 10.1016/j.jsbmb.2014.10.006
30. Parmar J, Key RE, Rainey WE. Development of an adrenocorticotropin-responsive human adrenocortical carcinoma cell line. *J Clin Endocrinol Metab.* 2008;93:4542–4546. doi: 10.1210/jc.2008-0903
31. Love MI, Huber W, Anders S. Moderated estimation of fold change and dispersion for RNA-seq data with DESeq2. *Genome Biol.* 2014;15:550. doi: 10.1186/s13059-014-0550-8
32. Wu T, Hu E, Xu S, Chen M, Guo P, Dai Z, Feng T, Zhou L, Tang W, Zhan L, et al. clusterProfiler 4.0: A universal enrichment tool for interpreting omics data. *Innovation (N Y).* 2021;2:100141. doi: 10.1016/j.xinn.2021.100141
33. Bucher F, Zhang D, Aguilar E, Sakimoto S, Diaz-Aguilar S, Rosenfeld M, Zha Z, Zhang H, Friedlander M, Yea K. Antibody-mediated inhibition of Tspan12 ameliorates vasoproliferative retinopathy through suppression of β-catenin signaling. *Circulation.* 2017;136:180–195. doi: 10.1161/CIRCULATIONAHA.116.025604
34. Junge HJ, Yang S, Burton JB, Paes K, Shu X, French DM, Costa M, Rice DS, Ye W. TSPAN12 regulates retinal vascular development by promoting Norrin- but not Wnt-induced FZD4/beta-catenin signaling. *Cell.* 2009;139:299–311. doi: 10.1016/j.cell.2009.07.048
35. Shoda T, Wen T, Caldwell JM, Ben-Baruch Morgenstern N, Osswald GA, Rochman M, Mack LE, Felton JM, Abonia JP, Arva NC, et al; Consortium of Eosinophilic Gastrointestinal Disease Researchers (CEGIR) Investigators Group. Loss of endothelial TSPAN12 promotes fibrostenotic eosinophilic esophagitis via endothelial cell-fibroblast crosstalk. *Gastroenterology.* 2022;162:439–453. doi: 10.1053/j.gastro.2021.10.016
36. Gomez-Sanchez CE, Gomez-Sanchez EP, Nishimoto K. Immunohistochemistry of the human adrenal CYP11B2 in normal individuals and in patients with primary aldosteronism. *Horm Metab Res.* 2020;52:421–426. doi: 10.1055/a-1139-2079
37. Bassett MH, Suzuki T, Sasano H, White PC, Rainey WE. The orphan nuclear receptors NURR1 and NGFIB regulate adrenal aldosterone production. *Mol Endocrinol.* 2004;18:279–290. doi: 10.1210/me.2003-0005
38. Williams TA, Monticone S, Crudo V, Warth R, Veglio F, Mulatero P. Visinin-like 1 is upregulated in aldosterone-producing adenomas with KCNJ5 mutations and protects from calcium-induced apoptosis. *Hypertension.* 2012;59:833–839. doi: 10.1161/HYPERTENSIONAHA.111.188532
39. Romero DG, Plonczynski MW, Gomez-Sanchez EP, Yanes LL, Gomez-Sanchez CE. RGS2 is regulated by angiotensin II and functions as a negative feedback of aldosterone production in H295R human adrenocortical cells. *Endocrinology.* 2006;147:3889–3897. doi: 10.1210/en.2005-1532
40. Romero DG, Zhou MY, Yanes LL, Plonczynski MW, Washington TR, Gomez-Sanchez CE, Gomez-Sanchez EP. Regulators of G-protein signaling 4 in adrenal gland: localization, regulation, and role in aldosterone secretion. *J Endocrinol.* 2007;194:429–440. doi: 10.1677/JOE-07-0153
41. Aptel HB, Johnson EI, Vallotton MB, Rossier MF, Capponi AM. Demonstration of an angiotensin II-induced negative feedback effect on aldosterone synthesis in isolated rat adrenal zona glomerulosa cells. *Mol Cell Endocrinol.* 1996;119:105–111. doi: 10.1016/0303-7207(96)03805-1
42. Safar ME, Asmar R, Benetos A, Blacher J, Boutouyrie P, Lacolley P, Laurent S, London G, Pannier B, Protogerou A, et al; French Study Group on Arterial Stiffness. Interaction between hypertension and arterial stiffness. *Hypertension.* 2018;72:796–805. doi: 10.1161/HYPERTENSIONAHA.118.11212
43. Vaidya A, Mulatero P, Baudrand R, Adler GK. The expanding spectrum of primary aldosteronism: implications for diagnosis, pathogenesis, and treatment. *Endocr Rev.* 2018;39:1057–1088. doi: 10.1210/er.2018-00139
44. Ahmed AH, Cowley D, Wolley M, Gordon RD, Xu S, Taylor PJ, Stowasser M. Seated saline suppression testing for the diagnosis of primary aldosteronism: a preliminary study. *J Clin Endocrinol Metab.* 2014;99:2745–2753. doi: 10.1210/jc.2014-1153
45. Wisgerhof M, Carpenter PC, Brown RD. Increased adrenal sensitivity to angiotensin II in idiopathic hyperaldosteronism. *J Clin Endocrinol Metab.* 1978;47:938–943. doi: 10.1210/jcem-47-5-938
46. Tunny TJ, Gordon RD, Klemm SA, Cohn D. Histological and biochemical distinctiveness of atypical aldosterone-producing adenomas responsive to upright posture and angiotensin. *Clin Endocrinol (Oxf).* 1991;34:363–369. doi: 10.1111/j.1365-2265.1991.tb00306.x
47. Guo Z, Nanba K, Udager A, McWhinney BC, Ungerer JPJ, Wolley M, Thuzar M, Gordon RD, Rainey WE, Stowasser M. Biochemical, histopathological, and genetic characterization of posture-responsive and unresponsive APAs. *J Clin Endocrinol Metab.* 2020;105:e3224–e3235. doi: 10.1210/clinem/dgaa367
48. Azizan EA, Murthy M, Stowasser M, Gordon R, Kowalski B, Xu S, Brown MJ, O'Shaughnessy KM. Somatic mutations affecting the selectivity filter of KCNJ5 are frequent in 2 large unselected collections

of adrenal aldosteronomas. *Hypertension.* 2012;59:587–591. doi: 10.1161/HYPERTENSIONAHA.111.186239
49. Azizan EA, Lam BY, Newhouse SJ, Zhou J, Kuc RE, Clarke J, Happerfield L, Marker A, Hoffman GJ, Brown MJ. Microarray, qPCR, and KCNJ5 sequencing of aldosterone-producing adenomas reveal differences in genotype and phenotype between zona glomerulosa- and zona fasciculata-like tumors. *J Clin Endocrinol Metab.* 2012;97:E819–E829. doi: 10.1210/jc.2011-2965
50. Monticone S, Castellano I, Versace K, Lucatello B, Veglio F, Gomez-Sanchez CE, Williams TA, Mulatero P. Immunohistochemical, genetic and clinical characterization of sporadic aldosterone-producing adenomas. *Mol Cell Endocrinol.* 2015;411:146–154. doi: 10.1016/j.mce.2015.04.022
51. Dekkers T, ter Meer M, Lenders JW, Hermus AR, Schultze Kool L, Langenhuijsen JF, Nishimoto K, Ogishima T, Mukai K, Azizan EA, et al. Adrenal nodularity and somatic mutations in primary aldosteronism: one node is the culprit?. *J Clin Endocrinol Metab.* 2014;99:E1341–E1351. doi: 10.1210/jc.2013-4255
52. Williams TA, Peitzsch M, Dietz AS, Dekkers T, Bidlingmaier M, Riester A, Treitl M, Rhayem Y, Beuschlein F, Lenders JW, et al. Genotype-specific steroid profiles associated with aldosterone-producing adenomas. *Hypertension.* 2016;67:139–145. doi: 10.1161/HYPERTENSIONAHA.115.06186
53. Tezuka Y, Yamazaki Y, Kitada M, Morimoto R, Kudo M, Seiji K, Takase K, Kawasaki Y, Mitsuzuka K, Ito A, et al. 18-Oxocortisol synthesis in aldosterone-producing adrenocortical adenoma and significance of KCNJ5 mutation status. *Hypertension.* 2019;73:1283–1290. doi: 10.1161/HYPERTENSIONAHA.118.12064
54. Turcu AF, Wannachalee T, Tsodikov A, Nanba AT, Ren J, Shields JJ, O'Day PJ, Giacherio D, Rainey WE, Auchus RJ. Comprehensive analysis of steroid biomarkers for guiding primary aldosteronism subtyping. *Hypertension.* 2020;75:183–192. doi: 10.1161/HYPERTENSIONAHA.119.13866

Online-only supplement

TSPAN12 is a novel negative regulator of aldosterone production in adrenal physiology and aldosterone-producing adenomas

Siyuan Gong[1], Martina Tetti[1,2], Elisabeth Kemter[3], Mirko Peitzsch[4], Paolo Mulatero[2], Martin Bidlingmaier[1], Graeme Eisenhofer[4,5], Eckhard Wolf[3], Martin Reincke[1], Tracy Ann Williams[1,2]

[1]Medizinische Klinik und Poliklinik IV, Klinikum der Universität München, LMU München, München, Germany (**S Gong, M Tetti, M Bidlingmaier, M Reincke, TA Williams**)

[2]Division of Internal Medicine and Hypertension, Department of Medical Sciences, University of Turin, Turin, Italy (**M Tetti, P Mulatero, TA Williams**)

[3]Chair for Molecular Animal Breeding and Biotechnology, Gene Center and Department of Veterinary Sciences, Ludwig-Maximilians-Universität München, Munich, Germany (**E Kemter, E Wolf**)

[4]Institute of Clinical Chemistry and Laboratory Medicine, University Hospital and Faculty of Medicine Carl Gustav Carus, Technische Universität Dresden, Dresden, Germany (**M Peitzsch, G Eisenhofer**)

[5]Department of Medicine III, University Hospital Carl Gustav Carus, Technische Universität Dresden, Dresden, Germany (**G Eisenhofer**)

***Corresponding author*:**
Tracy Ann Williams PhD, Medizinische Klinik und Poliklinik IV, Klinikum der Universität München, LMU München, Ziemssenstr. 5, D-80336 München, Germany
Tel: +49 89 4400 52137; Fax: +49 89 4400 54428;
Email: Tracy.Williams@med.uni-muenchen.de

Expanded Materials and Methods

Clinical measurements

Baseline blood pressure (BP) was measured at the first visit under treatment using a mercury sphygmomanometer. BP measurements were initiated after the patients was seated in a quiet room for 3 to 5 minutes. Seated blood pressure measurements were evaluated at least twice, at a 1-to-2-minute interval and the average BP was calculated.[1]

Hormonal measurements were performed following withdrawal of interfering medications and correction of hypokalemia with potassium supplementation. Plasma aldosterone, cortisol, and direct renin concentrations or plasma renin activity were measured according to local protocols.[2,3]

Immunohistochemistry

Formalin-fixed paraffin-embedded adrenals from 6-week-old male German Landrace DanBred pigs fed a 14-day 0.04% sodium diet (low salt group) or 0.7% sodium (high salt group) were from a previous study.[4] Pig and APA adrenal sections were cut (3 µm thick) and used for TSPAN12 immunohistochemistry with an anti-TSPAN12 primary antibody diluted 1:100 (LSBio)[5] and KCNJ5 immunohistochemistry with the KCNJ5 monoclonal antibody (clone No. 36-33-5, dilution 1:2000).[6] Negative controls were performed on APA and pig adrenal sections by replacing the primary antibody with equivalent dilutions and concentrations of rabbit immunoglobulin (Ig)G fractions (X0903; Dako). TSPAN12 staining in the human placental tissues were used as positive controls (Figure S4).

***In vitro* functional assays**

Human adrenal carcinoma cell line HAC15 cells[7] were cultured at 37°C in 5% CO_2 in DMEM/F12 (1:1) medium supplemented with 10% Cosmic Calf serum, 1x insulin-transferrin-selenium, 1% antibiotic-antimycotic, and 0.01% Gentamicin. Prior to cell treatments, cells were incubated overnight in starvation medium (DMEM/F12 medium containing 0.1% Cosmic Calf serum). Cells were treated with combinations of 10 nM angiotensin II (AngII), 10 µM nifedipine; 30 µM W-7 hydrochloride as indicated. Cells were pre-incubated with inhibitors for 1 hour before AngII stimulation as appropriate.

Silencer Select small interfering RNA (siRNA) for *TSPAN12* (Thermofisher Scientific) and pcDNA3.1+/C-(k)DYK-*TSPAN12* was from GenScript. For gene silencing experiments, HAC15 cells ($1x10^6$) were transfected with 1 µL of a 100 µmol/L solution of silencer select *TSPAN12* siRNA. For TSPAN12 overexpression experiments, HAC15 cells ($3x10^6$) were transfected with 3 µg pcDNA3.1-*TSPAN12* using the Amaxa Cell Line Nucleofector Kit R and the Nucleofector™ 2b (program X-005) (Lonza) according to manufacturers´ instructions. Samples were collected for RT-qPCR analysis at 48h post-transfection. Total RNA was extracted using a Maxwell 16 device and reverse transcription was performed with GoScript™ reverse transcriptase mix, oligo (dT) (Promega) according to the manufacturer's protocol. qPCR reactions were performed on the QuantStudio 5 Real-Time PCR instrument (Applied Biosystems) using TaqMan gene expression assays. *GAPDH* was used for normalization. The following TaqMan probes were used: *TSPAN12*, Hs01113125_m1; *CYP11B2*,

Hs01597732_m1; *GAPDH*, Hs02786624_g1. $2^{-\Delta\Delta Ct}$ relative quantification method was used for calculating gene expression levels.

Aldosterone and protein assays

Transfected HAC15 cells were seeded on 24-well plates. After 24 hours, cells were washed with DPBS, serum deprived overnight and then incubated for another 48 h in starvation medium or 24h in starvation medium with 10 nM AngII. Following this, supernatant and cells were harvested for aldosterone measurements and protein quantification of cell lysates, respectively. Aldosterone was measured in cell culture supernatants using the Aldosterone Parameter Assay Kit (KGE016, R&D systems) following the manufacturer's instructions. Protein concentration was determined using Pierce™ BCA Protein Assay Kit (Thermofisher Scientific). Aldosterone levels per well were normalized to protein concentrations.

Cell proliferation and viability assay

For cell proliferation experiments, HAC15 cells (4×10^4 cells/well) were plated in 96-well plates and incubated for 72 hours. For apoptosis experiments, transfected HAC15 cells (2.5×10^4 cells/well) were plated in 96-well plates. After 24 hours, cells were treated with 1 µmol/L staurosporine (STS, inducer of apoptosis) for 24 hours. Cell proliferation and cell apoptosis were determined with a water-soluble tetrazolium salt-1 (WST-1) assay (Roche). After incubation with WST-1 at 37°C for 3 hours, absorbance at 450 nm and 690 nm were determined on a FLUOstar Omega plate reader (BMG LABTECH).

Flow Cytometry

For cell death experiments, transfected HAC15 cells were seeded into 6-well plates ($1x10^6$ cells/well) and incubated for 24 hours, followed by a further 24 hours in starvation medium. Cells were then treated for 24 hours with either vehicle alone (0.03% DMSO) or an inducer of ferroptosis (1 µmol/L and 1.5 µmol/L RSL3 ([1S,3R]-RSL3).[8] Viable and floating dead cells were collected and stained with propidium iodide (PI) (eBioscience, catalog no. 00-6990-50). At least 10,000 cells were acquired per sample. Data analysis was conducted using the FlowJo Software (v.10.4).

References

1) Williams B, Mancia G, Spiering W, Agabiti Rosei E, Azizi M, Burnier M, Clement DL, Coca A, de Simone G, Dominiczak A, et al. 2018 ESC/ESH Guidelines for the management of arterial hypertension. *Eur Heart J*. 2018;39:3021-3104. doi: 10.1093/eurheartj/ehy339

2) Riester A, Fischer E, Degenhart C, Reiser MF, Bidlingmaier M, Beuschlein F, Reincke M, Quinkler M. Age below 40 or a recently proposed clinical prediction score cannot bypass adrenal venous sampling in primary aldosteronism. *J Clin Endocrinol Metab*. 2014;99:E1035-1039. doi: 10.1210/jc.2013-3789

3) Mulatero P, Bertello C, Sukor N, Gordon R, Rossato D, Daunt N, Leggett D, Mengozzi G, Veglio F, Stowasser M. Impact of different diagnostic criteria during adrenal vein sampling on reproducibility of subtype diagnosis in patients with primary aldosteronism. *Hypertension*. 2010;55:667-673. doi: 10.1161/HYPERTENSIONAHA.109.146613

4) Vohra T, Kemter E, Sun N, Dobenecker B, Hinrichs A, Burrello J, Gomez-Sanchez EP, Gomez-Sanchez CE, Wang J, Kinker IS, et al. Effect of dietary sodium modulation on pig adrenal steroidogenesis and transcriptome profiles. *Hypertension*. 2020;76:1769-1777. doi: 10.1161/HYPERTENSIONAHA.120.15998

5) Bucher F, Zhang D, Aguilar E, Sakimoto S, Diaz-Aguilar S, Rosenfeld M, Zha Z, Zhang H, Friedlander M, Yea K. Antibody-mediated inhibition of Tspan12 ameliorates vasoproliferative retinopathy through suppression of β-catenin signaling. *Circulation*. 2017;136:180-195. doi: 10.1161/CIRCULATIONAHA.116.025604

6) Yang Y, Gomez-Sanchez CE, Jaquin D, Aristizabal Prada ET, Meyer LS, Knosel T, Schneider H, Beuschlein F, Reincke M, Williams TA. Primary aldosteronism: *KCNJ5* mutations and adrenocortical cell growth. *Hypertension*. 2019;74:809-816. doi: 10.1161/HYPERTENSIONAHA.119.13476

7) Parmar J, Key RE, Rainey WE. Development of an adrenocorticotropin-responsive human adrenocortical carcinoma cell line. *J Clin Endocrinol Metab*. 2008;93:4542-4546. doi: 10.1210/jc.2008-0903

8) Yang Y, Tetti M, Vohra T, Adolf C, Seissler J, Hristov M, Belavgeni A, Bidlingmaier M, Linkermann A, Mulatero P, et al. BEX1 is differentially expressed in aldosterone-producing adenomas and protects human adrenocortical cells from ferroptosis. *Hypertension*. 2021;77:1647-1658. doi: 10.1161/HYPERTENSIONAHA.120.16774

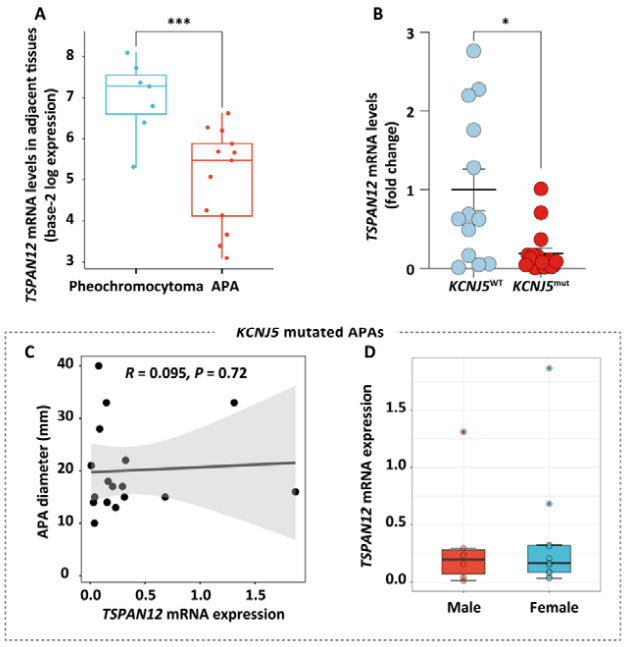

Figure S1. Differential expression of *TSPAN12* in adrenal tissues.
(A) *TSPAN12* gene expression is downregulated in the zG adjacent to APAs (n=13) compared with zG adjacent to pheochromocytomas (n=7) (transcriptome data from GSE64957). **(B)** real-time PCR analysis of *TSPAN12* gene expression in APA without a *KCNJ5* mutation (*KCNJ5*^{WT}, n=13) and with a *KCNJ5* mutation (*KCNJ5*^{mut}, n=17). **(C),** There was no correlation between APA diameter and *TSPAN12* expression in *KCNJ5* mutated APAs (n=17). *P* and r values were calculated by Spearman correlation. **(D),** *TSPAN12* expression was independent of sex within groups of *KCNJ5* mutated APAs. Data represent mean ± SEM. Statistical significance was calculated using a Mann-Whitney test. **P* < 0.05, ****P* < 0.001. APA, aldosterone-producing adenoma; zG, zona glomerulosa.

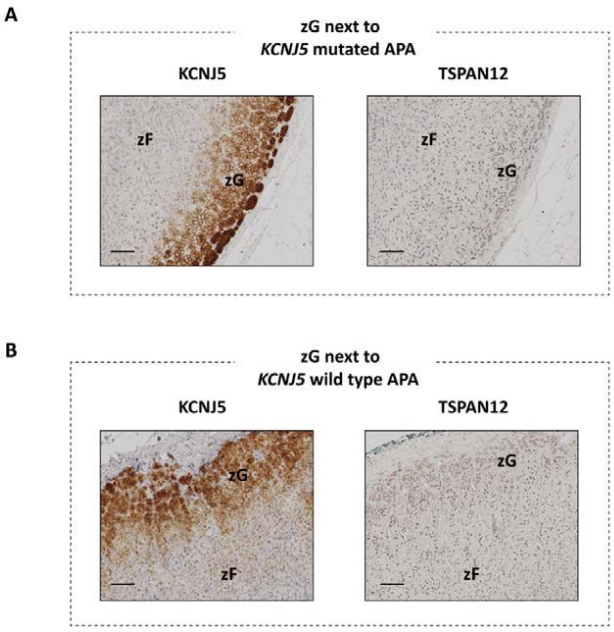

Figure S2. TSPAN12 immunohistochemistry of adrenal zona glomerulosa adjacent to APA.
TSPAN12 immunostaining was absent in the zona glomerulosa (zG) adjacent to APA. Representative immunohistochemistry of KCNJ5 (as a zG marker) and TSPAN12 in zG adjacent to a *KCNJ5* mutated APA **(Panel A)** or adjacent to a *KCNJ5* wild type APA **(Panel B)**. The negative and positive controls for TSPAN12 immunohistochemistry are shown in Figure S4. Scale bars = 100 μm. APA, aldosterone-producing adenoma; zG, zona glomerulosa; zF, zona fasciculata.

5

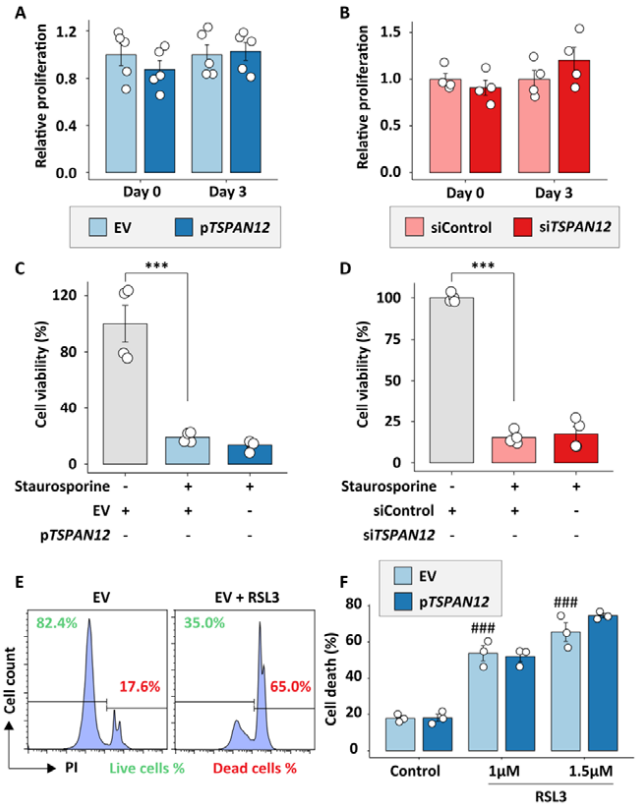

Figure S3. *TSPAN12* has no effect on cell proliferation, and adrenocortical cell death.
A-B, Analysis of cell viability by WST-1 assay in HAC15 cells with *TSPAN12* overexpression **(A)** or in HAC15 cells with *TSPAN12* siRNA knockdown **(B)** compared with control cells transfected with empty vector (EV) or a control siRNA, as appropriate. Data are normalized to negative control. Statistical significance was calculated by unpaired Student's *t*-test. **C-D**, Cell viability of HAC15 cells with *TSPAN12* overexpression **(C)** or in HAC15 cells with *TSPAN12* siRNA knockdown **(D)** compared with control cells transfected with empty vector (EV) or a control siRNA after 24 h treatment with vehicle (0.02% DMSO) or 1 µmol/L STS (staurosporine, inducer of apoptosis). Cell viability was measured using WST-1 assay and STS-treated HAC15 cells were used as positive control for the experiment. Statistical significance was calculated by one-way ANOVA with Tukey's multiple comparisons test. **E**, Representative flow cytometry plots of PI^- (live cells in green) or PI^+ (dead cells in red) HAC15 EV cells untreated (left) or treated (right) with 1.5 µmol/L ferroptosis inducer RSL3 ([1S, 3R]-RSL3) for 24 h. RSL3-treated HAC15 cells serve as positive control for flow cytometry experiments. **F**, Flow cytometry analysis of cell death in *TSPAN12*-overexpressing HAC15 cells compared to negative control (EV) after treatment with vehicle (0.03% DMSO), 1 µmol/L RSL3 and 1.5 µmol/L RSL3 for 24h. Statistical significances were calculated by two-way ANOVA with Tukey's multiple comparisons test. ***$P < 0.001$. $^{###}$ difference ($P<0.001$) from HAC15 EV cells treated with vehicle. Data are presented as mean ± SEM.

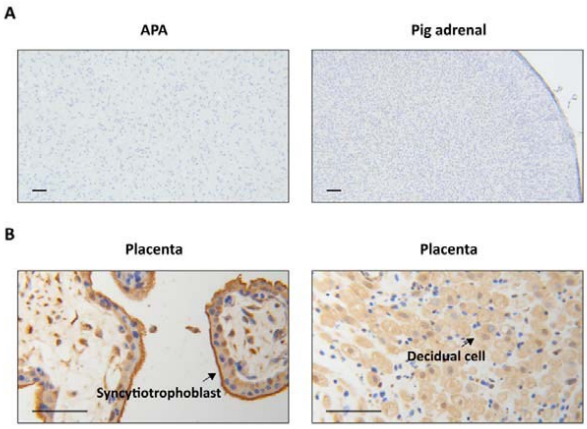

Figure S4. TSPAN12 antibody validation for immunohistochemistry.
A, IHC (immunohistochemistry) analysis of paraffin-embedded APA (left) and pig adrenal (right) sections, using negative control rabbit immunoglobulin (Ig)G fractions (X0903, Dako). **B**, TSPAN12 IHC of paraffin-embedded human placenta sections, used as positive controls. Strong TSPAN12 immunostaining was evident in syncytiotrophoblasts and decidual cells. Scale bars = 100 μm. APA, aldosterone-producing adenoma

5. Publication III

Hypertension

ORIGINAL ARTICLE

Primary Aldosteronism: Spatial Multiomics Mapping of Genotype-Dependent Heterogeneity and Tumor Expansion of Aldosterone-Producing Adenomas

Siyuan Gong, Na Sun,* Lucie S. Meyer,* Martina Tetti, Christina Koupourtidou, Stefan Krebs, Giacomo Masserdotti, Helmut Blum, William E. Rainey, Martin Reincke, Axel Walch, Tracy Ann Williams

BACKGROUND: Primary aldosteronism is frequently caused by an adrenocortical aldosterone-producing adenoma (APA) carrying a somatic mutation that drives aldosterone overproduction. APAs with a mutation in *KCNJ5* (APA-*KCNJ5*^{MUT}) are characterized by heterogeneous CYP11B2 (aldosterone synthase) expression, a particular cellular composition and larger tumor diameter than those with wild-type *KCNJ5* (APA-*KCNJ5*^{WT}). We exploited these differences to decipher the roles of transcriptome and metabolome reprogramming in tumor pathogenesis.

METHODS: Consecutive adrenal cryosections (7 APAs and 7 paired adjacent adrenal cortex) were analyzed by spatial transcriptomics (10x Genomics platform) and metabolomics (in situ matrix-assisted laser desorption/ionization mass spectrometry imaging) co-integrated with CYP11B2 immunohistochemistry.

RESULTS: We identified intratumoral transcriptional heterogeneity that delineated functionally distinct biological pathways. Common transcriptomic signatures were established across all APA specimens which encompassed 2 distinct transcriptional profiles in CYP11B2-immunopositive regions (*CYP11B2*-type 1 or 2). The *CYP11B2*-type 1 signature was characterized by zona glomerulosa gene markers and was detected in both APA-*KCNJ5*^{MUT} and APA-*KCNJ5*^{WT}. The *CYP11B2*-type 2 signature displayed markers of the zona fasciculata or reticularis and predominated in APA-*KCNJ5*^{MUT}. Metabolites that promote oxidative stress and cell death accumulated in APA-*KCNJ5*^{WT}. In contrast, antioxidant metabolites were abundant in APA-*KCNJ5*^{MUT}. Finally, APA-like cell subpopulations—negative for CYP11B2 gene expression—were identified in adrenocortical tissue adjacent to APAs suggesting the existence of tumor precursor states.

CONCLUSIONS: Our findings provide insight into intra- and intertumoral transcriptional heterogeneity and support a role for prooxidant versus antioxidant systems in APA pathogenesis highlighting genotype-dependent capacities for tumor expansion.
***(Hypertension.* 2023;80:1555–1567. DOI: 10.1161/HYPERTENSIONAHA.123.20921.)** • **Supplement Material**.

Key Words: adrenal glands ■ hyperaldosteronism ■ oxidative stress ■ spatial metabolomics ■ spatial transcriptomics

Aldosterone-producing adenomas (APAs) are a major subtype of primary aldosteronism in which a single somatic mutation drives the constitutive upregulation of *CYP11B2* gene transcription (encoding aldosterone synthase) and aldosterone biosynthesis in adrenal zona glomerulosa (zG) cells.[1] These mutations include variants in the GIRK4 K^+ channel[2] (encoded by *KCNJ5*), the calcium channels CaV1.3[3,4] and CaV3.2[5] (*CACNA1D* and *CACNA1H*, respectively) and the ClC-2 chloride channel[6] (*CLCN2*), as well as in subunits of the ion pumps Na^+/K^+-ATPase[4,7] (*ATP1A1*), and the plasma membrane Ca^{2+} transporting ATPase[7] (*ATP2B3*). In most reports, APA mutations in *KCNJ5* predominate over mutations in other genes.[8,9]

Correspondence to: Tracy Ann Williams, Medizinische Klinik und Poliklinik IV, Klinikum der Universität München, LMU München, Ziemssenstr. 5, D-80336 München, Germany. Email tracy.williams@med.uni-muenchen.de
*N. Sun and L.S. Meyer are co-second authors and contributed equally.
Supplemental Material is available at https://www.ahajournals.org/doi/suppl/10.1161/HYPERTENSIONAHA.123.20921.
For Sources of Funding and Disclosures, see page 1565.
© 2023 American Heart Association, Inc.
Hypertension is available at www.ahajournals.org/journal/hyp

ORIGINAL ARTICLE

Novelty and Relevance

What Is New?

We integrated spatial transcriptomics and spatial metabolomics profiles with CYP11B2 immunohistochemistry of surgically removed adrenals from patients operated for an aldosterone-producing adenoma (APA).

What Is Relevant?

Despite high intertumoral transcriptional heterogeneity, 2 specific transcriptional signatures common to all APAs were identified that characterize compact eosinophilic cells or lipid-rich clear cells.

Antioxidant metabolites are enriched in APAs with a *KCNJ5* mutation and prooxidant metabolites are enriched in APAs without a *KCNJ5* mutation.

Novel APA-like molecular subpopulations without *CYP11B2* expression are identified in the adrenal cortex that suggest the existence of tumor precursor states.

Clinical/Pathophysiological Implications

Our findings advance the understanding of the transcriptional context of inter- and intratumoral APA heterogeneity and provide novel insight into the genotype-dependent tumor expansion capabilities of APAs.

Nonstandard Abbreviations and Acronyms

APA	aldosterone-producing adenoma
PUFA	polyunsaturated fatty acid
zG	zona glomerulosa
zF	zona fasciculata

Cells with the potential to produce aldosterone in adrenal tissues can be localized using specific antibodies to CYP11B2 in immunohistochemistry of adrenal sections,[10–12] which has provided new insight into APA pathogenesis from a histological perspective.[11,13,14] *KCNJ5*-mutated APAs (APA-*KCNJ5*^{MUT}) display distinct phenotypes from other APA (APA-*KCNJ5*^{WT}). These differences include the intratumoral heterogeneous CYP11B2 expression that is frequently observed in the tumor areas of APA-*KCNJ5*^{MUT} by immunostaining.[15,16] Moreover, APA-*KCNJ5*^{MUT} display a predominance of lipid-rich clear cells (zona fasciculata [zF]-like cells with CYP11B1 [11β-hydroxylase] and CYP17A1 [17β-hydroxylase/17,20-lyase] expression) rather than the prevailing small compact eosinophilic cell phenotype (zG-like cells with CYP11B2 expression) in APA-*KCNJ5*^{WT}.[17] Further, APA-*KCNJ5*^{MUT} are generally larger than APA-*KCNJ5*^{WT},[9,18] suggesting divergent mechanisms of tumorigenesis.[19] However, transcriptional networks that determine the APA-*KCNJ5*^{MUT} phenotype remain to be elucidated.

Spatial transcriptomics is a powerful approach to dissect the transcriptional diversity of complex biological systems within the morphological context.[20,21] In addition, spatial metabolomics using matrix-assisted laser desorption/ionization mass spectrometry imaging of paraffin-embedded tissue sections has been used to investigate adrenal gland physiology[22] and pathophysiology[23,24] and has shown distinct metabolome patterns of APA-*KCNJ5*^{MUT} compared with APA-*CACNA1D*^{MUT}.[23] However, the use of paraffin-embedded tissue can result in the decreased detection of functionally relevant lipid species, which are lost during the tissue embedding process.[25,26]

Herein, we combined spatial transcriptomics and MSI-based spatial metabolomic profiling of adrenal tissue cryosections to define the role of transcriptomic and metabolomic reprogramming in APA pathophysiology. We hypothesized that the elucidation of biological processes which differentiate APA-*KCNJ5*^{MUT} and APA-*KCNJ5*^{WT} can identify causal molecular and cellular mechanisms of APA histological heterogeneity and tumor growth.

METHODS

Data Availability

The expanded methods are available in the Supplemental Material. The authors declare that all supporting data are available within the article and Supplemental Material or are available upon reasonable request. Details of patients, diagnosis of primary aldosteronism,[11,27–30] adrenal tissue samples and histology,[10] sample processing,[24,31–33] genotyping,[34,35] methods for spatial transcriptomics, and spatial metabolomics,[36–39] and bioinformatics are provided in the Supplemental Material.

Ethical Statement

The study was performed in accordance with local ethics committee guidelines and was approved by the institutional review board at the Ludwig Maximilian University of Munich (ref. 379-10). All patients provided written informed consent.

RESULTS

Intratumoral Transcriptional Heterogeneity of APAs

To delineate and compare APA intratumoral transcriptional heterogeneity stratified by genotype, we

 Hypertension. 2023;80:1555–1567. DOI: 10.1161/HYPERTENSIONAHA.123.20921

conducted spatial transcriptomics (Visium, 10X genomics) of adrenal cryosections from APA-*KCNJ5*^{MUT} (n=4) and APA-*KCNJ5*^{WT} (n=3; Figure 1; Table S1). First, we deconvolved APA-*KCNJ5*^{MUT} samples using a non-negative matrix factorization approach to quantify factors that were preferentially co-expressed by subsets of spots representing transcriptionally distinct regions within each sample specimen (Figure S1), as exemplified by non-negative matrix factorization of the APA section from Patient 1 (Figure 2A). Of the 3 tumor-related transcriptome signatures (factors 1, 3, and 4), factors 1 and 3 exhibited high *CYP11B2* expression and defined structures with aldosterone hypersecretion. Gene ontology analysis revealed a functional difference between factors 1 and 3, with enrichment of cell death-related pathways in factor 1 (Figure 2B) and of pathways associated with metabolic processes in factor 3 (Figure 2C). The tumor region annotated by factor 4 was negative for *CYP11B2* expression and associated with tissue remodeling, defined by the expression of genes of the extracellular matrix (*IGFBP7*, *MGP*), angiogenesis and cell population proliferation (Figure 2D). Factors 2 and 5 were transcriptional signatures associated with nontumor regions of the adjacent adrenal tissue (Figure S2).

CYP11B2 heterogeneity characterized by a lower proportion of cells with CYP11B2-positive immunostaining is often seen in APA-*KCNJ5*^{MUT}.[15,16] To identify molecular profiles, which distinguish diverse *CYP11B2* expression levels in APA-*KCNJ5*^{MUT}, tumor spatial transcriptomic spots were annotated into 2 clusters after subdivision into high and low *CYP11B2* expression (Figure S3A). Gene and pathway enrichment analysis predicted by PROGENy showed that high *CYP11B2* expressing transcriptome populations displayed upregulated steroidogenesis-related genes- like *PCP4, FDX1, MC2R*- and steroidogenesis-related pathways- like VEGF signaling, p53 signaling, and androgen signaling (Figure S3B through S3D). In the CYP11B2-expressing regions of Patients 4 and 6, a single APA-*KCNJ5*^{WT} tumor-related transcriptome signature was identified. In contrast, 3 distinct transcriptome signatures were annotated in the *CYP11B2*-expressing tumor regions of Patient 2 (factors 2, 3, and 4; Figures S4 and S5). Together, these data validate the previously reported tumor cell heterogeneity in APAs[16] and illustrate the intratumoral diversity of transcriptional programs.

Spatial Profiling of APA Reveals 2 Distinct Transcriptional Profiles in CYP11B2-Immunopositive Adrenal Regions

Hierarchical cluster analysis identified common transcriptional signatures (or factors) across all 7 APAs and highlighted 2 distinct transcriptional signatures in CYP11B2-expressing regions (referred to here as *CYP11B2*-type 1 and *CYP11B2*-type 2; Figure 3A). The *CYP11B2*-type 1 and *CYP11B2*-type 2 signatures each comprised genes, which were markers of different cell types of the adrenal cortex (from the zG, zF, and zona reticularis [zR]; Table S2). Thus, the *CYP11B2*-type 1 region primarily encompassed genes expressed in the zG, such as *KCNJ5* and *VSNL1*, and showed functional enrichment of hallmark gene sets- from Molecular Signatures Database (MSigDB) hallmark-associated with cell stress (defined by the TP53 pathway, reactive oxygen species pathway and apoptosis). The *CYP11B2*-type 2 region expressed the zF and zR genes *CYP17A1*, *CYP11B1,* and *SULT2A1*, and showed enrichment of pathways related to mTORC1 and hypoxia-associated signals (Figure 3B). *CYP11B2*-type 1 was dominant in APA-*KCNJ5*^{WT}, consistent with their predominance of compact eosinophilic cells with *CYP11B2* and *KCNJ5* expression (zG-like cells).[7,9] *CYP11B2*-type 2 was dominant in APA-*KCNJ5*^{MUT} coherent with their higher proportion of lipid-rich clear cells with *CYP11B1* and *CYP17A1* expression (zF-like cells)[7,9] (Figure 3C).

Spatial metabolomics was used to further characterize genotype-related heterogeneity. We used in situ MALDI-MS imaging of all adrenal specimens (7 APAs and their paired adjacent cortex) to quantify and visualize metabolites and identify the enriched metabolomic profiles in tumor regions. We identified 207 discriminative masses: 162 enriched in APA-*KCNJ5*^{WT} and 45 abundant in APA-*KCNJ5*^{MUT}. APA-*KCNJ5*^{WT} were characterized by metabolomic signatures related to linoleic acid metabolism and the biosynthesis of polyunsaturated fatty acids (PUFAs; for example, adrenic acid and docosapentaenoic acid) and an abundance of phosphatidylethanolamine (PE; 40:4), PE (38:4), and PE (40:6) (Figure 3D and 3E; Table S3). In contrast, APA-*KCNJ5*^{MUT} exhibited abundant metabolites of glutamine and glutamate metabolism. The accumulation of ferroptosis-promoting PUFAs and PE in APA-*KCNJ5*^{WT} support a role for activated cell death mechanisms to restrict tumor cell expansion.[40,41] In contrast, elevated pools of glutamine and glutamate in APA-*KCNJ5*^{MUT} reflect the presence of active metabolic signals favorable for tumor survival and growth.[42,43]

Spatial Profiling of APA and Adjacent Adrenal Tissue Uncovers Mechanisms Underlying Genotype-Related Differences in Tumor Size

We investigated the transcriptomic and metabolomic divergence of APA from paired adjacent adrenal tissue. For this, 14 cryosections were processed for spatial multiomics profiling comprising the 7 APAs described above, plus a section of adrenocortical tissue adjacent to each APA. The basic structure of APA and adjacent adrenal was captured by non-negative matrix factorization,[44] which identified 3 transcriptomic structural

ORIGINAL ARTICLE

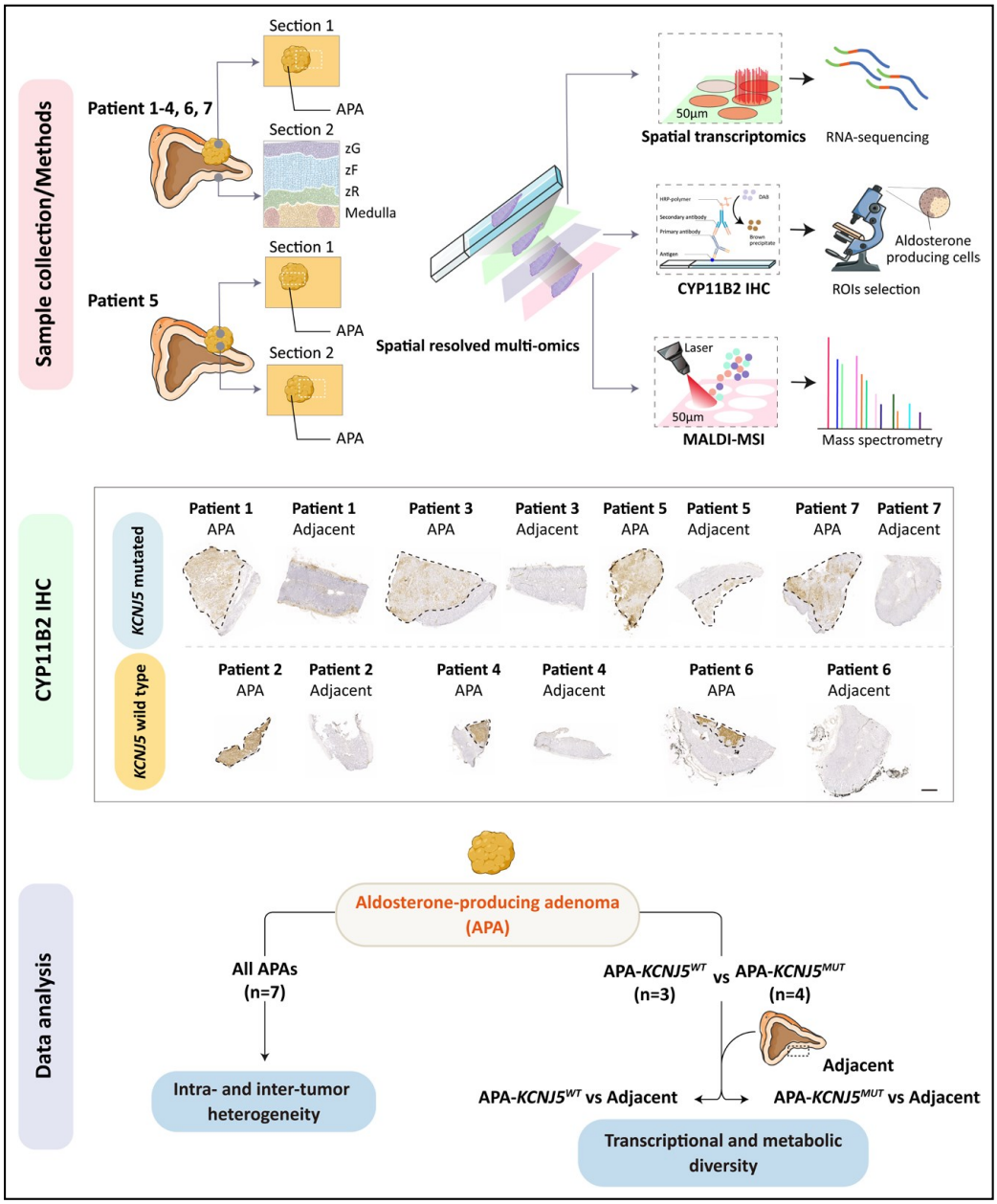

Figure 1. Adrenal tissue sections for spatial multiomics profiling.
Illustration of adrenal samples used for spatial datasets. For patients 1–4 and 6–7, an adrenal section with an aldosterone-producing adenoma (APA; section 1) and a separate section of adjacent adrenal tissue (section 2 showing adrenal zones: zona glomerulosa [zG]; zona fasciculate [zF]; zona reticularis [zR]) was used. For patient 5, section 1 comprised APA tissue only, section 2 encompassed adjacent adrenal and an APA region. Tumor regions are outlined with a black dashed line. An overview of analytical approaches used is also shown (**Upper**). Successive cryosections were processed for spatial transcriptomic (10x Genomics Visium platform), CYP11B2 immunohistochemistry (IHC) to identify regions of interest (ROIs; **Middle**; ROIs indicated by dashed lines, scale bar, 1 mm), and matrix-assisted laser desorption/ionization mass spectrometry imaging (MALDI-MSI). An overview of the data analysis strategy is also shown (**Bottom**). IHC indicates immunohistochemistry. Illustration used SMART servier medical art (https://smart.servier.com/).

 Hypertension. 2023;80:1555–1567. DOI: 10.1161/HYPERTENSIONAHA.123.20921

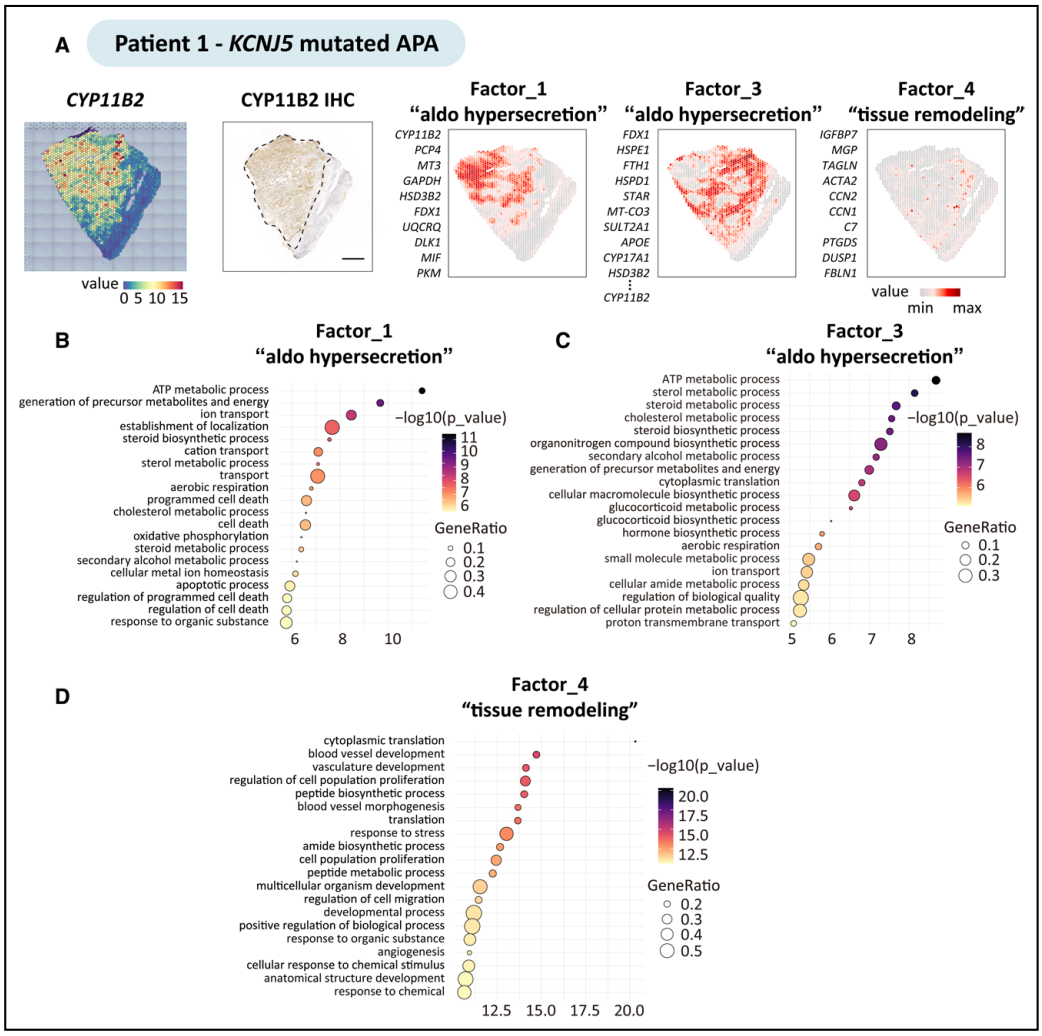

Figure 2. Intratumoral transcriptional heterogeneity of an aldosterone-producing adenoma (APA) with a *KCNJ5* mutation. Non-negative matrix factorization expression-based analysis identified the top genes defining factors (transcriptionally distinct regions) in adrenal sections with an APA. The figure shows the analysis of patient 1 carrying a *KCNJ5* mutation; the same approach was used for the analysis of patients 2 to 7. **A**, Spatial CYP11B2 expression and spatial distribution of tumor-related factors, color-codes indicate gene expression levels. Factors 1, 3, and 4 are tumor-related factors: factor 1 and factor 3 comprised gene sets preferentially co-expressed in subsets of CYP11B2 expressing tumor regions. *CYP11B2*, *PCP4*, *MT3*, *GAPDH*, and *HSD3B2* were the top genes defining factor 1; *FDX1*, *HSPE1*, *FTH1*, *HSPD1*, and *STAR*, as well as *CYP11B2* defined factor 3; conversely factor 4 defined tumor regions without *CYP11B2* gene expression with enrichment of angiogenesis and cell proliferation. Scale bar, 1 mm. **B–D**, Geno Ontology analysis showing enriched biological processes associated with factors related to aldosterone hypersecretion (factor 1 and factor 3) and tissue remodeling (factor 4).

landscapes classified as adjacent zF and zR, adrenal medulla, and a mixture of APA and adjacent zG demonstrating that different morphological regions can have the same basic structure with shared transcriptional programs (APA-*KCNJ5*^{MUT}, Figure S6; Figure 4A; APA-*KCNJ5*^{WT}, Figure S7; Figure 4B). Multiple biological processes of metabolism and steroid biosynthesis were identified in APA-*KCNJ5*^{MUT} whereas abundant cell death pathways with anti-tumoral metabolic signatures were highlighted in APA-*KCNJ5*^{WT} (Figure 4C and 4D). These observations were further supported by spatial metabolomic profiling which identified the enrichment of

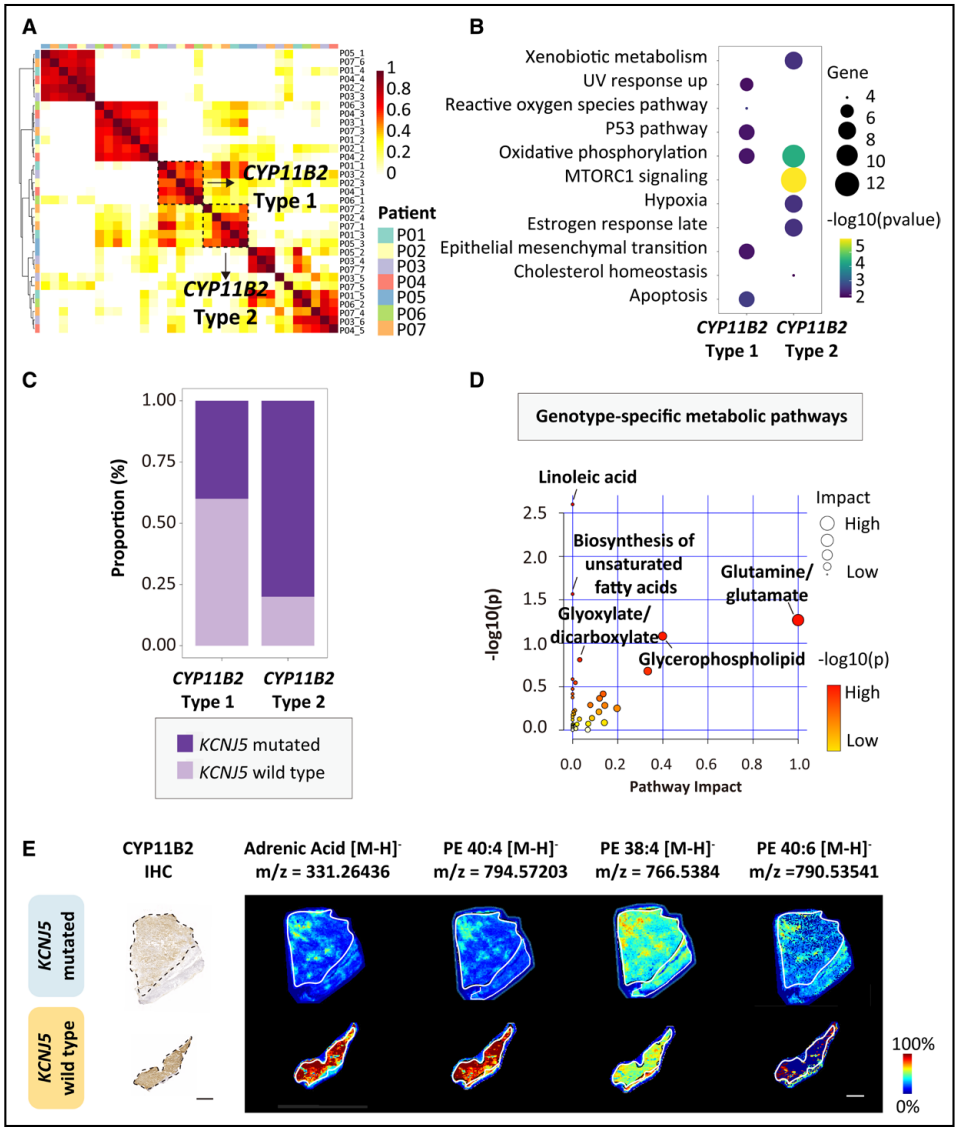

Figure 3. Co-integrated spatial transcriptomics and metabolomics of aldosterone-producing adenomas (APAs).
A, Spatial-weighted correlation analysis and Ward.D2 hierarchical clustering of 7 APA (P01-P07) identified 2 distinct signatures with *CYP11B2* expression (*CYP11B2*-type 1 and *CYP11B2*-type 2). **B**, HALLMARK gene set enrichment of *CYP11B2*-type 1 and *CYP11B2*-type 2. **C**, Distribution of *KCNJ5* mutated (APA-*KCNJ5*^{MUT}) and wild-type APA (APA-*KCNJ5*^{WT}) according to *CYP11B2*-type 1 and *CYP11B2*-type 2 transcriptomic signatures. **D**, MetaboAnalyst 5.0 pathway enrichment analysis of discriminative metabolites in APA-*KCNJ5*^{MUT} vs APA-*KCNJ5*^{WT}. Annotated pathways selected by unadjusted $P<0.05$ (hypergeometric test). Circles indicate pathway impact (horizontal axis, topology analyses; vertical axis, enrichment). **E**, CYP11B2 immunohistochemistry and matrix-assisted laser desorption/ionization mass spectrometry imaging (MALDI-MSI) showing spatial distribution of proferroptotic metabolites in 2 APAs with or without a *KCNJ5* mutation. Scale bars, 1 mm. MTORC1 indicates mammalian target of rapamycin complex 1; and UV, ultraviolet.

glucose metabolism in APA-*KCNJ5*^{MUT} versus adjacent adrenal cortex demonstrating active pathways for protection from steroidogenesis-mediated oxidative stress, including the oxidative arm of the pentose phosphate pathway and pentose glucuronate interconversions (Figure 4E; Figure S8; Table S4).

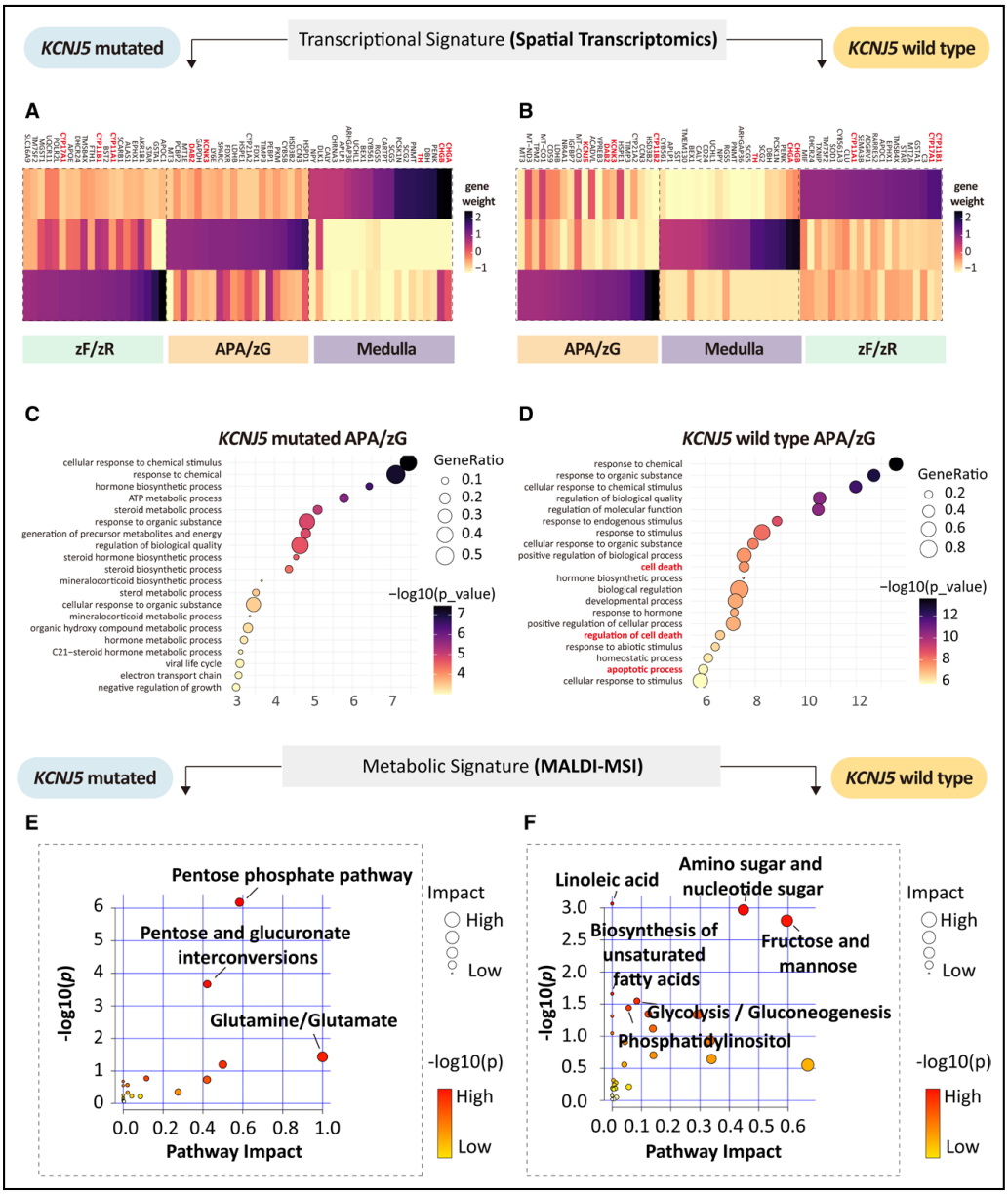

Figure 4. Spatial transcriptomics and metabolomics of aldosterone-producing adenomas (APAs) and adjacent adrenal tissue. **A** and **B**, Heatmap of top genes contributing to each factor (transcriptionally distinct region) of APA-*KCNJ5*^{MUT} and APA-*KCNJ5*^{WT}. Genes indicated in red represent zonation markers of the zona glomerulosa (zG; *CYP11B2*, *DAB2*, and *KCNJ5*); markers of the zona fasciculata (zF) or zona reticularis (zR; *CYP11B1* and *CYP17A1*); and of the adrenal medulla (*CHGB*, *CHGA*, and *TH*). **C** and **D,** Gene ontology analysis (biological process) of tumor-related factors (factor 2 in APA-*KCNJ5*^{MUT}, Figure S6; factor 3 in APA-*KCNJ5*^{WT}, Figure S7). **E** and **F**, Pathway enrichment analysis of upregulated metabolites in APA-*KCNJ5*^{MUT} (left) or APA-*KCNJ5*^{WT} (right) vs adjacent adrenal (unadjusted $P<0.05$, hypergeometric test). MALDI-MSI indicates matrix-assisted laser desorption/ionization mass spectrometry imaging.

Analysis of APA-*KCNJ5*^{WT} versus the adjacent adrenal cortex identified enrichment of omega-3 (eg, alpha-linolenic acid and docosahexaenoic acid) and omega-6 (eg, docosapentaenoic acid and gamma-linolenic acid) PUFAs (Figures 4F and 5; Table S5) whereas metabolites of glutathione metabolism were preferentially localized in APA-*KCNJ5*^{MUT} (Figure S9). Therefore, the enrichment of PUFAs in APA-*KCNJ5*^{WT} and glutathione in APA-*KCNJ5*^{MUT} highlight prooxidant versus antioxidant responses indicating genotype-related diverse capacities for tumor expansion.

APA-Like Subpopulations in the Adjacent Adrenal Cortex

Tissue-covered transcriptomics spots in APA and adjacent cortex stratified by APA genotype were integrated and corrected for batch effects. TSNE (t-distributed stochastic neighbor embedding) identified 6 unique transcriptome subpopulations in adrenals (APA + adjacent cortex) from patients with APA-*KCNJ5*^{MUT} and 7 unique subpopulations in adrenals from patients with APA-*KCNJ5*^{WT} (Figure 6). Subpopulations were annotated based on CYP11B2 immunostaining (Figure 1), expression of marker genes (Figures S10 and S11; Table S6), and gene ontology analyses. The adrenals with APA-*KCNJ5*^{MUT} comprised 2 clearly distinct tumor clusters, termed clusters APA-like 1 and APA-like 2. APA-like 1 displayed *CYP11B2* gene expression whereas APA-like 2 did not (Figure S10). Both APA-like clusters were also located in the adjacent cortex to APA-*KCNJ5*^{MUT} (Figure 6A, 6C, and 6E). Adrenals with APA-*KCNJ5*^{WT} exhibited a single tumor cluster- termed APA-like 3—which expressed the *CYP11B2* gene (Figure S10) and was in the tumor region and the adjacent cortex (Figure 6B, 6D, and 6F). Notably, although the signature of APA-like subpopulations 1 and 3 comprised the *CYP11B2* gene transcript, *CYP11B2* gene expression was present only within tumor regions and not in the corresponding subpopulations in the adjacent adrenal cortex. Comparisons of tumor samples versus the adjacent cortex of patients with a different APA genotype, for example, tumor specimens from APA-*KCNJ5*^{MUT} compared with the adjacent cortex of APA-*KCNJ5*^{WT} and vice versa, consistently identified APA-like 1, 2, and 3 subpopulations (Figure S12). However, the APA-like 1 subpopulation in the tumor regions of APA-*KCNJ5*^{MUT} was undetectable in the adrenal cortical tissue adjacent to APA-*KCNJ5*^{WT} (Figure S12E).

DISCUSSION

The biological mechanisms driving the predominant APA-*KCNJ5*^{MUT} phenotype of larger tumor diameter, particular cell composition and heterogeneous CYP11B2 immunostaining, are unknown.[4,9,15,16,18,19] To address this knowledge gap, this study had 3 main goals: (1) to characterize the intra- and inter-tumor transcriptional heterogeneity of APAs; (2) to delineate the transcriptional and metabolomic mechanisms through which *KCNJ5* mutation status contributes to tumor expansion; (3) to spatially distinguish preAPA-like cells in the adrenal cortex adjacent to APAs.

The histological heterogeneity of CYP11B2 immunostaining in APA-*KCNJ5*^{MUT} has been previously reported.[15,16] In this context, tumor regions with varying levels of CYP11B2 expression in APA-*KCNJ5*^{MUT} share identical somatic *KCNJ5* variants with similar variant allele frequencies,[15,45] indicating that transcriptional diversity between tumor regions with different CYP11B2 expression levels should occur in a spatial context. Here, we establish APA heterogeneity at the transcriptional level through the unbiased analysis of the transcriptome landscape. Our findings suggest that heterogenous CYP11B2 expression may be caused by differential regulation of specific signaling pathways because biological pathways related to the stimulation of aldosterone production, such as VEGF,[46] p53,[47] and androgen[48] pathways, are dominant in tumor regions of APA-*KCNJ5*^{MUT} with higher *CYP11B2* expression.

Defining the functional significance of clear versus compact eosinophilic cells in APAs using spatial transcriptomics is of particular interest because it has been challenging to define the transcriptional programs of these different cell subpopulations, in part because APAs comprise a mixture of the 2 cell types.[4] Our bioinformatics analyses identified 2 distinct APA transcriptional signatures associated with CYP11B2 expressing regions, referred to here as *CYP11B2*-type 1 and *CYP11B2*-type 2, across genotype groups. The distribution of these signatures matched that of the previously described APA morphology (small compact versus clear cells) with diverse relative proportions of these cell types according to *KCNJ5* mutation status and tumor diameter.[15,17,49] In the spatial context of our study, the *CYP11B2*-type 1 transcriptome signature was enriched in compact eosinophilic cells and was characterized by increased cell stress-associated signaling activity, suggesting that microenvironmental stress conditions may restrict their capacity for cell proliferation. Conversely, the *CYP11B2*-type 2 transcriptome signature, which predominated in APA-*KCNJ5*^{MUT}—which have a higher proportion of lipid-rich clear cells—exhibited enhanced mTORC1 and hypoxia-associated signaling activity, consistent with the promotion of metabolic adaptations for proliferation under hypoxic conditions.[50,51]

We resolve enriched cell stress transcriptional signals and accumulated PUFAs and proferroptotic arachidonoyl-PE species in APA-*KCNJ5*^{WT} relative to their adjacent cortex and to APA-*KCNJ5*^{MUT}. Prior studies have demonstrated that an abundance of PUFAs and proferroptotic arachidonoyl-PE species can activate

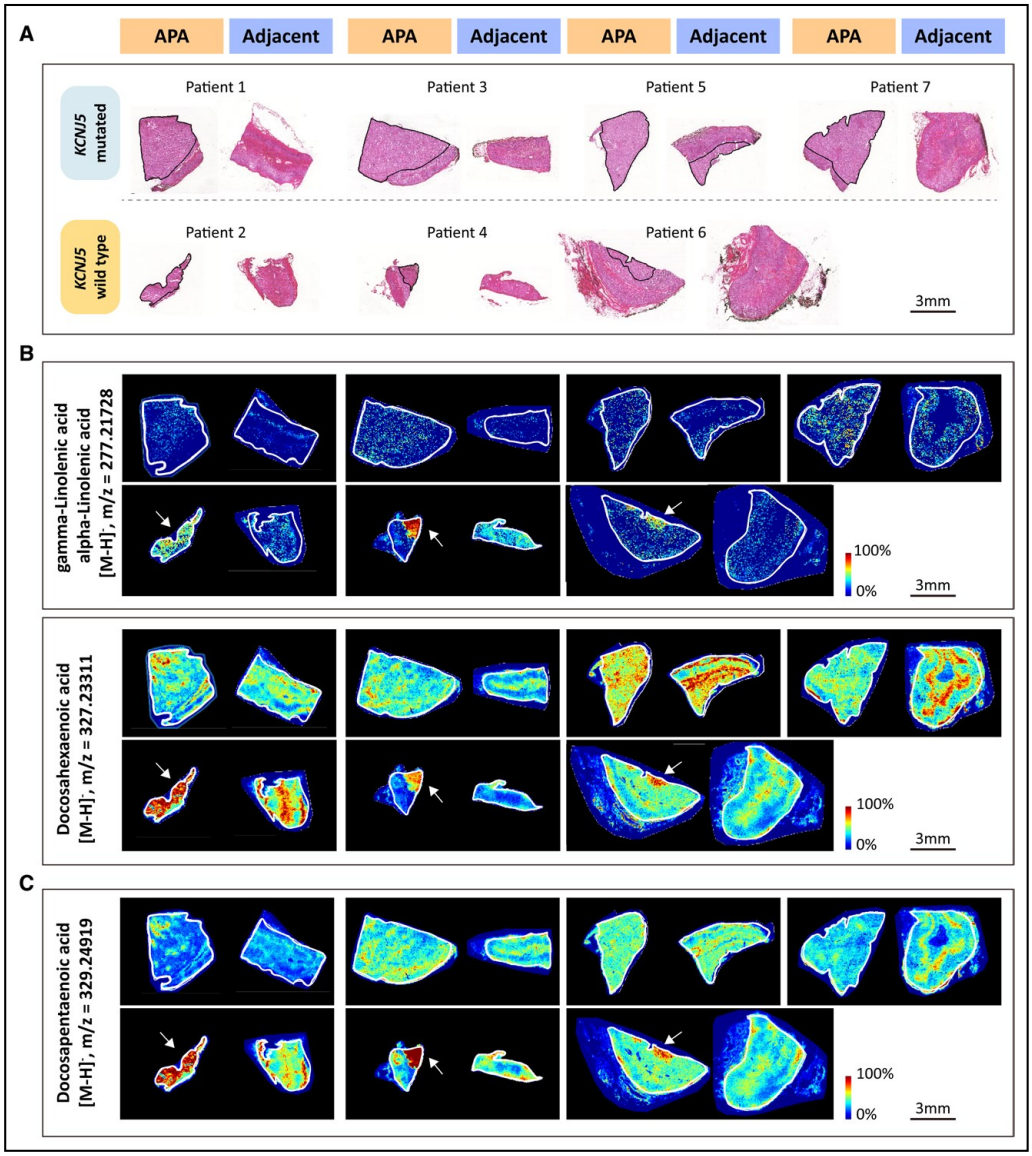

Figure 5. Matrix-assisted laser desorption/ionization mass spectrometry imaging (MALDI-MSI) identification of upregulated omega-3 and omega-6 polyunsaturated fatty acids in *KCNJ5* mutated aldosterone-producing adenoma (APA) compared with adjacent adrenal cortex.

A, Corresponding hematoxylin and eosin (H&E)-stained tissues of *KCNJ5* mutated APA (**Upper**) or *KCNJ5* wild-type APA (**Lower**) and adjacent adrenal gland used for MALDI-MSI. Outlined regions in black indicate APA tumor areas with positive CYP11B2 immunostaining. **B** and **C**, Representative images showing spatial distribution of omega-3 polyunsaturated fatty acids (**B**) and omega-6 polyunsaturated fatty acids (**C**). Outlined regions in white represent the borders of the tissue section.

cell death pathways such as ferroptosis in various diseases.[40,41,52,53] In contrast, enriched metabolites of the oxidative pentose phosphate pathway and of glutathione metabolism in APA-*KCNJ5*^{MUT} highlight active antioxidant defense mechanisms to eliminate stress overload signals and maintain tissue homeostasis.[54–56] Therefore,

ORIGINAL ARTICLE

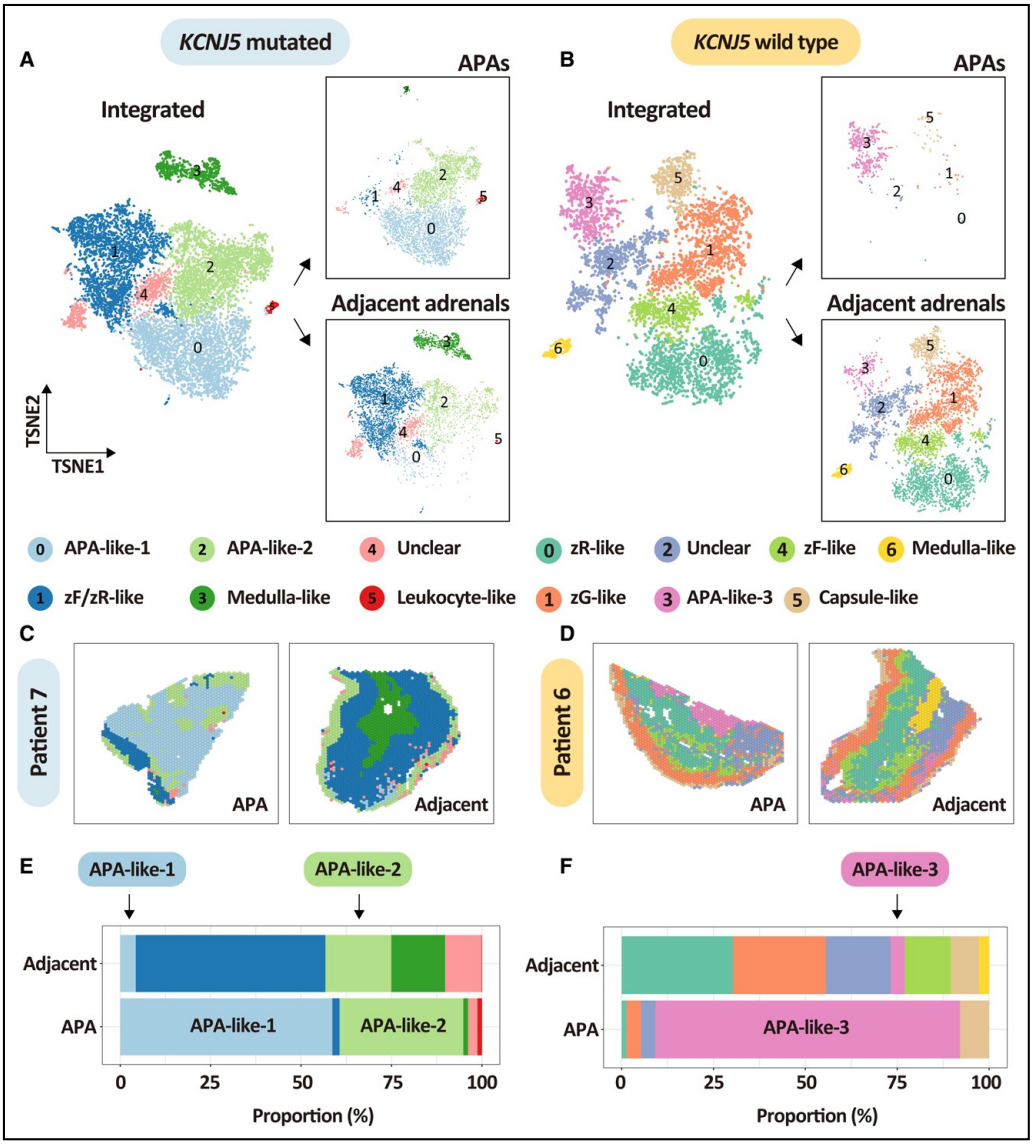

Figure 6. Spatial transcriptomics establishes aldosterone-producing adenoma (APA)-like subpopulations in the adjacent adrenal cortex.

A and **B**, t-distributed stochastic neighbor embedding representations of the integrated spatial transcriptomes of APAs and adjacent adrenal tissues stratified by APA-*KCNJ5* mutation status and tissue type. Show integrated spatial transcriptomic spots from APAs and adjacent adrenal tissues (left image of **A** and **B**) as well as separated into APAs (boxed image, top right of **A** and **B**) and adjacent adrenal tissues (boxed image, bottom right of **A** and **B**). Colors represent transcriptome subpopulations as indicated. **A**, APA-*KCNJ5*^{MUT} (n=4) and their adjacent adrenal cortex (n=4). **B**, APA-*KCNJ5*^{WT} (n=3) and their adjacent adrenal cortex (n=3). **C** and **D**, Representative spatial transcriptomics sections showing the distribution of spots in APAs and adjacent adrenals from patient 7 with a *KCNJ5* mutation (male) and patient 6 without a *KCNJ5* mutation (female). **E** and **F**, Stacked plots showing the proportion of each transcriptome cluster in APAs and adjacent adrenals. Left and right indicate adrenal tissues from patients with a *KCNJ5* mutation (represented in light blue, left,) or without a *KCNJ5* mutation (represented in light yellow, right). All APA-like signatures (APA-like 1, 2, and 3) are common to tumor areas and adjacent tissue and may represent precursor APA subpopulations. TSNE indicates t-distributed stochastic neighbor embedding.

 Hypertension. 2023;80:1555–1567. DOI: 10.1161/HYPERTENSIONAHA.123.20921

taken together, these data can help explain the restricted growth of APA-*KCNJ5*^{WT} tumors and the sustained growth of APA-*KCNJ5*^{MUT} and help account for the genotype-related differences in APA tumor size.

Our data report previously unappreciated APA-like molecular regions in the adrenal cortex adjacent to APAs. We identified 2 APA-like transcriptome subpopulations common to APA-*KCNJ5*^{MUT} and their paired adjacent cortex (APA-like 1 and APA-like 2), and a single APA-like subpopulation in the tumor and adjacent cortex of APA-*KCNJ5*^{WT} (APA-like 3). Spatial transcriptomics spots of these APA-like subpopulations in APA and their adjacent cortex were clustered according to their similar gene expression profiles. *CYP11B2* transcripts were absent from the APA-like 2 subpopulation in APA-*KCNJ5*^{MUT}, which is consistent with the heterogeneous CYP11B2 immunostaining observed in these tumors.[15] In contrast, *CYP11B2* transcripts were part of the APA-like 1 and APA-like 3 signatures; however, the corresponding subpopulations expressed the *CYP11B2* gene only in tumor regions and not in the adjacent cortex. Thus, APA-like 1 and APA-like 3 are distinct from aldosterone-producing micronodules[11] and might represent distinct precursor APA-like states. In addition, the APA-like-1 subpopulation identified in APA-*KCNJ5*^{MUT} and the adjacent cortex was apparently absent from the adjacent cortex to APA-*KCNJ5*^{WT} thus indicating that this signature could be a unique feature of adrenals harboring a APA-*KCNJ5*^{MUT}. However, because tumors may influence their surrounding microenvironment, we cannot rule-out the possibility that the APA-like 1 signature in the adjacent cortex to APA-*KCNJ5*^{MUT} resulted from modulatory effects on the tumor microenvironment by the APA itself. Further investigation of larger cohorts is needed to confirm our findings and assess the potential influence of gender in the context of *KCNJ5* mutations.

In conclusion, we demonstrate intratumoral transcriptional heterogeneity of APA-*KCNJ5*^{MUT} and the transcriptome signatures of the component compact eosinophilic cells and lipid-rich clear cells. We propose that APA tumor cells require metabolic adaptations to oxidative stress signals to survive and proliferate and we provide evidence to support the existence of novel molecular zones in the adrenal cortex, which might represent tumor precursor states.

PERSPECTIVES

Conventional techniques that apply bulk or single cell RNA sequencing cannot effectively dissect the tissue organization of gene expression levels. In contrast, spatially resolved transcriptomics profiling (spatial RNA sequencing) combined with state-of-the-art bioinformatics platforms can quantifiably assess gene expression at the cellular level within the context of tissue morphology. We applied this approach to surgically removed adrenal glands from patients operated for an APA. We established transcriptomics signatures, which define the distinct cell compositions of APAs and the molecular and cellular diversity of these tumors according to *KCNJ5* mutation status. Further, the integration of spatial transcriptomics and metabolomics datasets demonstrated that the cellular response to oxidative stress might direct genotype-related APA size differences. In the adrenocortical tissue adjacent to APAs, APA-like transcriptomic signatures were uncovered without aldosterone synthase transcription thereby suggesting the existence of novel tumor precursor cells before the acquisition of autonomous aldosterone production. Overall, we establish how spatial omics technologies can provide a blueprint for understanding the spatial architecture and genotype-specific tumorigenesis of APAs.

ARTICLE INFORMATION

Received January 10, 2023; accepted April 10, 2023.

Affiliations

Medizinische Klinik und Poliklinik IV, Klinikum der Universität München, Ludwig-Maximilians-Universität (LMU) München, Germany (S.G., L.S.M., M.T., M.R., T.A.W.). Institute of Stem Cell Research, Helmholtz Center Munich, Neuherberg, Germany (G.M.); Department for Cell Biology and Anatomy, Biomedical Center, LMU, Planegg-Martinsried, Germany (C.K.). Graduate School Systemic Neurosciences, LMU, Planegg-Martinsried, Germany (C.K.). Physiological Genomics, Biomedical Center (BMC), LMU, Planegg-Martinsried, Germany (G.M.). Laboratory for Functional Genome Analysis, Gene Center, LMU Munich, Germany (S.K., H.B.). Department of Molecular and Integrative Physiology, University of Michigan, Ann Arbor, MI (W.E.R.). Division of Metabolism, Endocrine, and Diabetes, Department of Internal Medicine, University of Michigan, Ann Arbor, MI (W.E.R.). Research Unit Analytical Pathology, German Research Center for Environmental Health, Helmholtz Zentrum München, Germany (N.S., A.W.).

Acknowledgments

The authors thank Isabella Sabrina-Kinker (LMU Munich, Germany) for assistance with cryosectioning and immunohistochemistry and Manuel Schulze (TU Dresden, Germany) for advice with the high-performance computing system platform used for data analysis.

Sources of Funding

This work was financed by the European Research Council (ERC) under the European Union's Horizon 2020 research and innovation program (grant agreement no. 694913 to M. Reincke) and the Deutsche Forschungsgemeinschaft (DFG) project number 444776998 to T.A. Williams (WI 5359/2-1) and M. Reincke (RE 752/31-1) and project number 314061271-TRR 205 "The Adrenal: Central Relay in Health and Disease" to M. Reincke, A. Walch, and T.A. Williams. The Else Kröner-Fresenius Stiftung (2012_A103, 2015_A228, and 2019_A104; Else-Kröner Hyperaldosteronismus-German Conn Registry) also supports the work of M. Reincke. W.E. Rainey is supported by the National Institutes of Health/National Institute of Diabetes and Digestive and Kidney Diseases (R01DK043140). S. Gong is supported by a fellowship from the China Scholarship Council.

Disclosures

None.

REFERENCES

1. Williams TA, Reincke M. Pathophysiology and histopathology of primary aldosteronism. *Trends Endocrinol Metab*. 2022;33:36–49. doi: 10.1016/j.tem.2021.10.002
2. Choi M, Scholl UI, Yue P, Bjorklund P, Zhao B, Nelson-Williams C, Ji W, Cho Y, Patel A, Men CJ, et al. K+ channel mutations in adrenal aldosterone-producing adenomas and hereditary hypertension. *Science*. 2011;331:768–772. doi: 10.1126/science.1198785

ORIGINAL ARTICLE

3. Scholl UI, Goh G, Stolting G, de Oliveira RC, Choi M, Overton JD, Fonseca AL, Korah R, Starker LF, Kunstman JW, et al. Somatic and germline CACNA1D calcium channel mutations in aldosterone-producing adenomas and primary aldosteronism. *Nat Genet*. 2013;45:1050–1054. doi: 10.1038/ng.2695
4. Azizan EA, Poulsen H, Tuluc P, Zhou J, Clausen MV, Lieb A, Maniero C, Garg S, Bochukova EG, Zhao W, et al. Somatic mutations in ATP1A1 and CACNA1D underlie a common subtype of adrenal hypertension. *Nat Genet*. 2013;45:1055–1060. doi: 10.1038/ng.2716
5. Nanba K, Blinder AR, Rege J, Hattangady NG, Else T, Liu CJ, Tomlins SA, Vats P, Kumar-Sinha C, Giordano TJ, et al. Somatic CACNA1H mutation as a cause of aldosterone-producing adenoma. *Hypertension*. 2020;75:645–649. doi: 10.1161/HYPERTENSIONAHA.119.14349
6. Dutta RK, Arnesen T, Heie A, Walz M, Alesina P, Soderkvist P, Gimm O. A somatic mutation in CLCN2 identified in a sporadic aldosterone-producing adenoma. *Eur J Endocrinol*. 2019;181:K37–K41. doi: 10.1530/EJE-19-0377
7. Beuschlein F, Boulkroun S, Osswald A, Wieland T, Nielsen HN, Lichtenauer UD, Penton D, Schack VR, Amar L, Fischer E, et al. Somatic mutations in ATP1A1 and ATP2B3 lead to aldosterone-producing adenomas and secondary hypertension. *Nat Genet*. 2013;45:440–4, 444e1. doi: 10.1038/ng.2550
8. Williams TA, Monticone S, Mulatero P. KCNJ5 mutations are the most frequent genetic alteration in primary aldosteronism. *Hypertension*. 2015;65:507–509. doi: 10.1161/HYPERTENSIONAHA.114.04636
9. Lenzini L, Rossitto G, Maiolino G, Letizia C, Funder JW, Rossi GP. A meta-analysis of somatic KCNJ5 K(+) channel mutations in 1636 patients with an aldosterone-producing adenoma. *J Clin Endocrinol Metab*. 2015;100:E1089–E1095. doi: 10.1210/jc.2015-2149
10. Gomez-Sanchez CE, Qi X, Velarde-Miranda C, Plonczynski MW, Parker CR, Rainey W, Satoh F, Maekawa T, Nakamura Y, Sasano H, et al. Development of monoclonal antibodies against human CYP11B1 and CYP11B2. *Mol Cell Endocrinol*. 2014;383:111–117. doi: 10.1016/j.mce.2013.11.022
11. Williams TA, Gomez-Sanchez CE, Rainey WE, Giordano TJ, Lam AK, Marker A, Mete O, Yamazaki Y, Zerbini MCN, Beuschlein F, et al. International histopathology consensus for unilateral primary aldosteronism. *J Clin Endocrinol Metab*. 2021;106:42–54. doi: 10.1210/clinem/dgaa484
12. Mete O, Erickson LA, Juhlin CC, de Krijger RR, Sasano H, Volante M, Papotti MG. Overview of the 2022 WHO classification of adrenal cortical tumors. *Endocr Pathol*. 2022;33:155–196. doi: 10.1007/s12022-022-09710-8
13. Meyer LS, Handgriff L, Lim JS, Udager AM, Kinker IS, Ladurner R, Wildgruber M, Knosel T, Bidlingmaier M, Rainey WE, et al. Single-center prospective cohort study on the histopathology, genotype, and postsurgical outcomes of patients with primary aldosteronism. *Hypertension*. 2021;78:738–746. doi: 10.1161/HYPERTENSIONAHA.121.17348
14. Wu VC, Peng KY, Kuo YP, Liu H, Tan BC, Lin YH, Lai TS, Chen YM, Chueh JS; TAIPAI. Subtypes of histopathologically classical aldosterone-producing adenomas yield various transcriptomic signaling and outcomes. *Hypertension*. 2021;78:1791–1800. doi: 10.1161/HYPERTENSIONAHA.121.18006
15. De Sousa K, Boulkroun S, Baron S, Nanba K, Wack M, Rainey WE, Rocha A, Giscos-Douriez I, Meatchi T, Amar L, et al. Genetic, cellular, and molecular heterogeneity in adrenals with aldosterone-producing adenoma. *Hypertension*. 2020;75:1034–1044. doi: 10.1161/HYPERTENSIONAHA.119.14177
16. Yamazaki Y, Omata K, Tezuka Y, Ono Y, Morimoto R, Adachi Y, Ise K, Nakamura Y, Gomez-Sanchez CE, Shibahara Y, et al. Tumor cell subtypes based on the intracellular hormonal activity in KCNJ5-mutated aldosterone-producing adenoma. *Hypertension*. 2018;72:632–640. doi: 10.1161/HYPERTENSIONAHA.118.10907
17. Ono Y, Yamazaki Y, Omata K, Else T, Tomlins SA, Rhayem Y, Williams TA, Reincke M, Carling T, Monticone S, et al. Histological characterization of aldosterone-producing adrenocortical adenomas with different somatic mutations. *J Clin Endocrinol Metab*. 2020;105:e282–e289. doi: 10.1210/clinem/dgz235
18. Zheng FF, Zhu LM, Nie AF, Li XY, Lin JR, Zhang K, Chen J, Zhou WL, Shen ZJ, Zhu YC, et al. Clinical characteristics of somatic mutations in Chinese patients with aldosterone-producing adenoma. *Hypertension*. 2015;65:622–628. doi: 10.1161/HYPERTENSIONAHA.114.03346
19. Yang Y, Gomez-Sanchez CE, Jaquin D, Aristizabal Prada ET, Meyer LS, Knosel T, Schneider H, Beuschlein F, Reincke M, Williams TA. Primary aldosteronism: KCNJ5 mutations and adrenocortical cell growth. *Hypertension*. 2019;74:809–816. doi: 10.1161/HYPERTENSIONAHA.119.13476
20. Marx V. Method of the Year: spatially resolved transcriptomics. *Nat Methods*. 2021;18:9–14. doi: 10.1038/s41592-020-01033-y
21. Rao A, Barkley D, Franca GS, Yanai I. Exploring tissue architecture using spatial transcriptomics. *Nature*. 2021;596:211–220. doi: 10.1038/s41586-021-03634-9
22. Sun N, Wu Y, Nanba K, Sbiera S, Kircher S, Kunzke T, Aichler M, Berezowska S, Reibetanz J, Rainey WE, et al. High-resolution tissue mass spectrometry imaging reveals a refined functional anatomy of the human adult adrenal gland. *Endocrinology*. 2018;159:1511–1524. doi: 10.1210/en.2018-00064
23. Murakami M, Rhayem Y, Kunzke T, Sun N, Feuchtinger A, Ludwig P, Strom TM, Gomez-Sanchez C, Knosel T, Kirchner T, et al. In situ metabolomics of aldosterone-producing adenomas. *JCI Insight*. 2019;4:e130356. doi: 10.1172/jci.insight.130356
24. Sun N, Meyer LS, Feuchtinger A, Kunzke T, Knosel T, Reincke M, Walch A, Williams TA. Mass spectrometry imaging establishes 2 distinct metabolic phenotypes of aldosterone-producing cell clusters in primary aldosteronism. *Hypertension*. 2020;75:634–644. doi: 10.1161/HYPERTENSIONAHA.119.14041
25. Buck A, Ly A, Balluff B, Sun N, Gorzolka K, Feuchtinger A, Janssen KP, Kuppen PJ, van de Velde CJ, Weirich G, et al. High-resolution MALDI-FT-ICR MS imaging for the analysis of metabolites from formalin-fixed, paraffin-embedded clinical tissue samples. *J Pathol*. 2015;237:123–132. doi: 10.1002/path.4560
26. Butler LM, Perone Y, Dehairs J, Lupien LE, de Laat V, Talebi A, Loda M, Kinlaw WB, Swinnen JV. Lipids and cancer: emerging roles in pathogenesis, diagnosis and therapeutic intervention. *Adv Drug Deliv Rev*. 2020;159:245–293. doi: 10.1016/j.addr.2020.07.013
27. Funder JW, Carey RM, Mantero F, Murad MH, Reincke M, Shibata H, Stowasser M, Young WF Jr. The management of primary aldosteronism: case detection, diagnosis, and treatment: an endocrine society clinical practice guideline. *J Clin Endocrinol Metab*. 2016;101:1889–1916. doi: 10.1210/jc.2015-4061
28. Williams TA, Reincke M. Management of endocrine disease: diagnosis and management of primary aldosteronism: the Endocrine Society guideline 2016 revisited. *Eur J Endocrinol*. 2018;179:R19–R29. doi: 10.1530/EJE-17-0990
29. Mulatero P, Monticone S, Deinum J, Amar L, Prejbisz A, Zennaro MC, Beuschlein F, Rossi GP, Nishikawa T, Morganti A, et al. Genetics, prevalence, screening and confirmation of primary aldosteronism: a position statement and consensus of the Working Group on Endocrine Hypertension of The European Society of Hypertension. *J Hypertens*. 2020;38:1919–1928. doi: 10.1097/HJH.0000000000002510
30. Williams TA, Lenders JWM, Mulatero P, Burrello J, Rottenkolber M, Adolf C, Satoh F, Amar L, Quinkler M, Deinum J, et al; Primary Aldosteronism Surgery Outcome (PASO) investigators. Outcomes after adrenalectomy for unilateral primary aldosteronism: an international consensus on outcome measures and analysis of remission rates in an international cohort. *Lancet Diabetes Endocrinol*. 2017;5:689–699. doi: 10.1016/S2213-8587(17)30135-3
31. Girardot C, Scholtalbers J, Sauer S, Su SY, Furlong EE. Je, a versatile suite to handle multiplexed NGS libraries with unique molecular identifiers. *BMC Bioinf*. 2016;17:419. doi: 10.1186/s12859-016-1284-2
32. Parigi SM, Larsson L, Das S, Ramirez Flores RO, Frede A, Tripathi KP, Diaz OE, Selin K, Morales RA, Luo X, et al. The spatial transcriptomic landscape of the healing mouse intestine following damage. *Nat Commun*. 2022;13:828. doi: 10.1038/s41467-022-28497-0
33. Andersson A, Larsson L, Stenbeck L, Salmen F, Ehinger A, Wu SZ, Al-Eryani G, Roden D, Swarbrick A, Borg A, et al. Spatial deconvolution of HER2-positive breast cancer delineates tumor-associated cell type interactions. *Nat Commun*. 2021;12:6012. doi: 10.1038/s41467-021-26271-2
34. Nanba K, Omata K, Else T, Beck PCC, Nanba AT, Turcu AF, Miller BS, Giordano TJ, Tomlins SA, Rainey WE. Targeted molecular characterization of aldosterone-producing adenomas in White Americans. *J Clin Endocrinol Metab*. 2018;103:3869–3876. doi: 10.1210/jc.2018-01004
35. Nanba K, Rainey WE, Udager AM. Approaches to gene mutation analysis using formalin-fixed paraffin-embedded adrenal tumor tissue from patients with primary aldosteronism. *Front Endocrinol (Lausanne)*. 2021;12:683588. doi: 10.3389/fendo.2021.683588
36. Chen YP, Yin JH, Li WF, Li HJ, Chen DP, Zhang CJ, Lv JW, Wang YQ, Li XM, Li JY, et al. Single-cell transcriptomics reveals regulators underlying immune cell diversity and immune subtypes associated with prognosis in nasopharyngeal carcinoma. *Cell Res*. 2020;30:1024–1042. doi: 10.1038/s41422-020-0374-x
37. Hanzelmann S, Castelo R, Guinney J. GSVA: gene set variation analysis for microarray and RNA-seq data. *BMC Bioinf*. 2013;14:7. doi: 10.1186/1471-2105-14-7
38. Korsunsky I, Millard N, Fan J, Slowikowski K, Zhang F, Wei K, Baglaenko Y, Brenner M, Loh PR, Raychaudhuri S. Fast, sensitive and accurate integration of single-cell data with Harmony. *Nat Methods*. 2019;16:1289–1296. doi: 10.1038/s41592-019-0619-0

39. Zappia L, Oshlack A. Clustering trees: a visualization for evaluating clusterings at multiple resolutions. *GigaScience*. 2018;7:giy083. doi: 10.1093/gigascience/giy083
40. Yang WS, Kim KJ, Gaschler MM, Patel M, Shchepinov MS, Stockwell BR. Peroxidation of polyunsaturated fatty acids by lipoxygenases drives ferroptosis. *Proc Natl Acad Sci U S A*. 2016;113:E4966–E4975. doi: 10.1073/pnas.1603244113
41. Dierge E, Debock E, Guilbaud C, Corbet C, Mignolet E, Mignard L, Bastien E, Dessy C, Larondelle Y, Feron O. Peroxidation of n-3 and n-6 polyunsaturated fatty acids in the acidic tumor environment leads to ferroptosis-mediated anticancer effects. *Cell Metab*. 2021;33:1701–1715.e5. doi: 10.1016/j.cmet.2021.05.016
42. Altman BJ, Stine ZE, Dang CV. From Krebs to clinic: glutamine metabolism to cancer therapy. *Nat Rev Cancer*. 2016;16:619–634. doi: 10.1038/nrc.2016.71
43. Yoo HC, Yu YC, Sung Y, Han JM. Glutamine reliance in cell metabolism. *Exp Mol Med*. 2020;52:1496–1516. doi: 10.1038/s12276-020-00504-8
44. Lin X, Boutros PC. Optimization and expansion of non-negative matrix factorization. *BMC Bioinf*. 2020;21:7. doi: 10.1186/s12859-019-3312-5
45. Lerario AM, Nanba K, Blinder AR, Suematsu S, Omura M, Nishikawa T, Giordano TJ, Rainey WE, Else T. Genetics of aldosterone-producing adenomas with pathogenic KCNJ5 variants. *Endocr Relat Cancer*. 2019;26:463–470. doi: 10.1530/ERC-18-0364
46. Gennari-Moser C, Khankin EV, Escher G, Burkhard F, Frey BM, Karumanchi SA, Frey FJ, Mohaupt MG. Vascular endothelial growth factor-A and aldosterone: relevance to normal pregnancy and preeclampsia. *Hypertension*. 2013;61:1111–1117. doi: 10.1161/HYPERTENSIONAHA.111.00575
47. Cherian-Shaw M, Das R, Vandevoort CA, Chaffin CL. Regulation of steroidogenesis by p53 in macaque granulosa cells and H295R human adrenocortical cells. *Endocrinology*. 2004;145:5734–5744. doi: 10.1210/en.2004-0253
48. Yanes LL, Romero DG. Dihydrotestosterone stimulates aldosterone secretion by H295R human adrenocortical cells. *Mol Cell Endocrinol*. 2009;303:50–56. doi: 10.1016/j.mce.2008.12.020
49. Monticone S, Castellano I, Versace K, Lucatello B, Veglio F, Gomez-Sanchez CE, Williams TA, Mulatero P. Immunohistochemical, genetic and clinical characterization of sporadic aldosterone-producing adenomas. *Mol Cell Endocrinol*. 2015;411:146–154. doi: 10.1016/j.mce.2015.04.022
50. Tsai PY, Lee MS, Jadhav U, Naqvi I, Madha S, Adler A, Mistry M, Naumenko S, Lewis CA, Hitchcock DS, et al. Adaptation of pancreatic cancer cells to nutrient deprivation is reversible and requires glutamine synthetase stabilization by mTORC1. *Proc Natl Acad Sci U S A*. 2021;118:e2003014118. doi: 10.1073/pnas.2003014118
51. Saxton RA, Sabatini DM. mTOR signaling in growth, metabolism, and disease. *Cell*. 2017;168:960–976. doi: 10.1016/j.cell.2017.02.004
52. Das UN. Saturated fatty acids, MUFAs and PUFAs regulate ferroptosis. *Cell Chem Biol*. 2019;26:309–311. doi: 10.1016/j.chembiol.2019.03.001
53. Liu J, Xu M, Zhao Y, Ao C, Wu Y, Chen Z, Wang B, Bai X, Li M, Hu W. n-3 polyunsaturated fatty acids abrogate mTORC1/2 signaling and inhibit adrenocortical carcinoma growth in vitro and in vivo. *Oncol Rep*. 2016;35:3514–3522. doi: 10.3892/or.2016.4720
54. Kuehne A, Emmert H, Soehle J, Winnefeld M, Fischer F, Wenck H, Gallinat S, Terstegen L, Lucius R, Hildebrand J, et al. Acute activation of oxidative pentose phosphate pathway as first-line response to oxidative stress in human skin cells. *Mol Cell*. 2015;59:359–371. doi: 10.1016/j.molcel.2015.06.017
55. Bansal A, Simon MC. Glutathione metabolism in cancer progression and treatment resistance. *J Cell Biol*. 2018;217:2291–2298. doi: 10.1083/jcb.201804161
56. Patra KC, Hay N. The pentose phosphate pathway and cancer. *Trends Biochem Sci*. 2014;39:347–354. doi: 10.1016/j.tibs.2014.06.005

Online-only supplement

Primary aldosteronism: spatial multi-omics mapping of genotype-dependent heterogeneity and tumor expansion of aldosterone-producing adenomas

Siyuan Gong, Na Sun[†], Lucie S Meyer[†], Martina Tetti, Christina Koupourtidou, Stefan Krebs, Giacomo Masserdotti, Helmut Blum, William E. Rainey, Martin Reincke, Axel Walch, Tracy Ann Williams*

[†]Na Sun and Lucie S Meyer are co-second authors and contributed equally to this work.

***Affiliations*:** Medizinische Klinik und Poliklinik IV, Klinikum der Universität München, LMU München, München, Germany (S Gong, LS Meyer, M Tetti, M Reincke, TA Williams); Institute of Stem Cell Research, Helmholtz Center Munich, Neuherberg, Germany (G Masserdotti); Department for Cell Biology and Anatomy, Biomedical Center, Ludwig-Maximilians-Universität (LMU), Planegg-Martinsried, Germany (C Koupourtidou); Graduate School Systemic Neurosciences, Ludwig-Maximilians-Universität (LMU), Planegg-Martinsried, Germany (C Koupourtidou); Physiological Genomics, Biomedical Center (BMC), Ludwig-Maximilians-Universität (LMU), Planegg-Martinsried, Germany (G Masserdotti); Laboratory for Functional Genome Analysis, Gene Center, LMU Munich, 81377 Munich, Germany (S Krebs, H Blum); Department of Molecular and Integrative Physiology, University of Michigan, Ann Arbor, Michigan, USA (WE Rainey); Division of Metabolism, Endocrine, and Diabetes, Department of Internal Medicine, University of Michigan, Ann Arbor, Michigan, USA (WE Rainey); Research Unit Analytical Pathology, German Research Center for Environmental Health, Helmholtz Zentrum München, Germany (N Sun, A Walch).

****Corresponding author***: Tracy Ann Williams PhD, Medizinische Klinik und Poliklinik IV, Klinikum der Universität München, LMU München, Ziemssenstr. 5, D-80336 München, Germany.
Tel: +49 89 4400 52137; Fax: +49 89 4400 54428; Email: Tracy.Williams@med.uni-muenchen.de

Table of contents

Supplementary Methods
Patients … page 2
DNA sequencing … page 2
Tissue sample preparation and quality control … page 2
Spatial sample preparation and sequencing … page 2
MALDI-mass spectrometry imaging … page 2
Immunohistochemistry … page 3
Pre-processing of spatial transcriptomics data … page 3
Deconvolution of spatial transcriptomics data … page 3
Identification of distinct spatially transcriptomic regions across APA … page 3
Estimate of functional information of signatures … page 3
Dimensionality reduction of APA and adjacent adrenal cortex … page 3
Deconvolution of APA and adjacent adrenal cortex … page 4
Manual region selection of heterogeneous *CYP11B2* expression spots … page 4
Differential expression analyses … page 4
Estimate of functional information of high and low CYP11B2 … page 4
Bioinformatics and statistical analysis of MALDI–MSI data … page 4

Supplementary References … page 4-5

Supplementary Tables
Table S1. Clinical parameters of surgically treated patients for and aldosterone-producing adenoma … page 6
Table S2. Top 100 genes detected in *CYP11B2*-type 1 and *CYP11B2*-type 2 … page 7
Table S3. Discriminative pathways distinguish APA-*KCNJ5*^{WT} and APA-*KCNJ5*^{MUT} … page 8
Table S4. Discriminative pathways distinguish APA-*KCNJ5*^{MUT} and adjacent adrenal cortex … page 9
Table S5. Discriminative pathways distinguish APA-*KCNJ5*^{WT} and adjacent adrenal cortex … page 10
Table S6. Differentially expressed steroidogenesis enzyme genes between subpopulations … page 11

Supplementary Figures
Figure S1. Identification of transcriptionally distinct regions by stability and error using consensus non-negative matrix factorization.… page 12
Figure S2. Non-negative matrix factorization reveals distinct molecular patterns in the adjacent adrenal gland of APA with a *KCNJ5* mutation … page 13
Figure S3. Heterogeneity of *CYP11B2* gene expression in *KCNJ5* mutated APAs … page 14
Figure S4. Intra-tumoral transcriptional heterogeneity of APAs without a *KCNJ5* mutation … page 15
Figure S5. Non-negative matrix factorization reveals distinct molecular patterns in the in the adjacent adrenal gland of APAs without a *KCNJ5* mutation … page 16
Figure S6. Non-negative matrix factorization to identify the spatial distribution of transcriptionally distinct regions in APAs with a *KCNJ5* mutation and their adjacent cortex … page 17
Figure S7. Non-negative matrix factorization to identify the spatial distribution of transcriptionally distinct regions in APAs without a *KCNJ5* mutation and their adjacent cortex … page 18
Figure S8. MALDI-MSI identification of upregulated oxidative pentose phosphate pathway metabolites in *KCNJ5* mutated APAs compared with adjacent adrenal cortex.… page 19
Figure S9. MALDI-MSI identification of upregulated glutathione metabolism metabolites in *KCNJ5* mutated APAs compared with adjacent adrenal cortex … page 20
Figure S10. Identification of transcriptomic subpopulations … page 21
Figure S11. Expression of steroidogenic enzyme genes in adrenal cell types … page 22
Figure S12. The validation of APA-like subpopulations through comparisons of non-matching tumor-adjacent cortex pairs … page 23-24

Expanded Materials and Methods

Patients. Surgically removed adrenals from 7 patients diagnosed with unilateral primary aldosteronism (PA) and with a histopathological classification of an aldosterone-producing adenoma (APA)[1] were used for this study. Patients were diagnosed with unilateral PA according to the Endocrine Society Clinical Practice Guideline[2] implemented into local standard operational procedures.[3] Briefly, the plasma aldosterone-to-direct renin concentration ratio was used for screening and the diagnosis of PA was confirmed by intravenous saline load testing.[2,4] Subtype differentiation of unilateral from bilateral aldosterone hypersecretion was performed by adrenal venous sampling.[3] The correct diagnosis of unilateral PA with aldosterone hypersecretion lateralized to one adrenal gland was confirmed by postsurgical complete biochemical success.[5]

DNA sequencing. CYP11B2-guided Sanger sequencing of formalin-fixed paraffin-embedded (FFPE) resected adrenals was used for mutation analysis.[6] Accordingly, genomic DNA was extracted from APA, and, for confirmation of the somatic origin of identified mutations, DNA was also extracted from the adjacent cortex or peripheral blood leukocytes before DNA Sanger sequencing of *KCNJ5*.[6] When a *KCNJ5* mutation was not detected by Sanger sequencing, extracted DNA was further analyzed for PA-driver mutations using NGS panels.[7]

Tissue sample preparation and quality control. After resection, fresh tumor and paired adjacent adrenal tissue were snap-frozen in liquid nitrogen and stored at −80 °C. Frozen tissues were embedded in optimal cutting temperature compound (Tissue-Tek). For RNA quality control, RNA integrity number (RIN) analysis was determined (2100 Bioanalyzer, Agilent). Samples with a RIN>7 were used for spatial transcriptomics analyses. Consecutive sections of each sample were cut for spatial gene expression slides, CYP11B2 immunohistochemistry and MALDI slides.

Spatial transcriptomics sample preparation and sequencing. Tissue cryosections (10 µm thick) were mounted onto capture areas (6.5 × 6.5 mm) of a pre-chilled Visium tissue optimization slide (Visium, 10x Genomics, PN-1000193) and the optimal tissue permeabilization time was established as 18 min (10x Genomics, CG000238 Rev D). Cryosections (10 µm thick) mounted on capture areas (6.5 × 6.5 mm) of spatial gene expression slides (Visium, 10x Genomics, PN-1000187) were used for hematoxylin and eosin (H&E) staining and bright field imaging (Zeiss Axio Imager M2 microscope) before tissue permeabilization and cDNA library preparation (10X Genomics, CG000239 Rev D). Libraries were sequenced on the Illumina NextSeq1000 platform. The number of bases sequenced were Read 1, 28 cycles; i5 and i7 indexes, 10 cycles; Read 2, 90 cycles.

MALDI-mass spectrometry imaging. Samples were processed for spatial metabolomics analyses by high-mass-resolution in situ MALDI-MSI (matrix assisted laser desorption/ionization-mass spectrometry imaging) as described previously.[8] Cryosections (12 µm thick) were mounted onto indium-tin-oxide-coated glass slides. The matrix solution consisted of 10 mg/mL 9-aminoacridine hydrochloride monohydrate (9-AA) (Sigma-Aldrich, Germany) in water/methanol 30:70 (v/v). A SunCollect automatic sprayer (Sunchrom, Friedrichsdorf, Germany) was used for matrix application. MALDI-MSI measurements were conducted on a Bruker Solarix 7T FT-ICR-MS (Bruker Daltonik, Bremen, Germany) in negative ion mode using 100 laser shots at a frequency of 1,000 Hz. The MALDI-MSI data were acquired over a mass range of *m/z* 75–1,000 with 50 µm lateral resolution. Following MALDI imaging, tissue sections were H&E stained and scanned (AxioScan.Z1 digital slide scanner with a 20x objective, Zeiss, Jena, Germany). The mass spectra underwent root mean square normalization and processed using SCiLS Lab v. 2022 (Bruker Daltonics, Germany).

Immunohistochemistry. Frozen tissues (10 µm thick) were fixed with 70% ethanol for 2 min, washed 3 times with Tris-buffered saline, 0.1% Tween-20 detergent (TBST), before blocking with human antiserum for 1h at room temperature. Sections were incubated with a mouse CYP11B2 monoclonal antibody (1:200, clone 41-17B,[9] a kind gift from Celso E. Gomez-Sanchez, University of Mississippi Medical Center, Jackson, MS) at 4°C overnight, followed by 3 washes with TBST. Endogenous peroxidase activity was blocked with peroxidase suppressor (Thermo Scientific) and immunopositive regions were detected using the Dako REAL EnVision Detection System Peroxidase/DAB Rabbit/Mouse kit (Agilent).

Pre-processing of spatial transcriptomics data. Demultiplexed FASTQs were obtained using je-suite.[10] Gene expression matrices were generated with the Space Ranger pipeline (10x Genomics) with the "-reorient-images" option enabled and human genome reference 2020-A (GRCh38 and Ensembl 98) alignment. STUtility built on top of the Seurat R package was used for subsequent analyses.[11,12] A Seurat object was constructed using the InputFromTable function filtered with the criteria of a total count <100 detected across all spots, gene expressed <5 spots, and spots with a total UMI count <200. Count matrices were further matched for gene types (protein coding genes, TR_V_gene, TR_D_gene, TR_J_gene, TR_C_gene, IG_LV_gene, IG_V_gene, IG_J_gene, IG_C_gene, IG_D_gene).

Deconvolution of spatial transcriptomics data. Each tumor section was scaled and normalized using SCTransform (STUtility) with the top 2,000 most variable genes included. Non-negative matrix factorization (NMF) was performed, and the spatial transcriptomics dataset was deconvoluted for identified factors using RunNMF implemented in STUtility. The number of factors per section was determined by stability and error using consensus NMF with 2000 over-dispersed genes used for the factorization steps (cNMF v1.4 python package; patients 1-7, k = 5, 4, 6, 5, 3, 3, 7) (**Figure S9**). Top contributing genes were selected based on the feature loading matrix and enriched for biological processes using gprofiler2R (organism = "hsapiens", sources = "GO:BP"). The significance of enrichment was defined with the hypergeometric test followed by correction for multiple testing.

Identification of distinct spatial transcriptomics regions across APA. To capture shared spatial transcriptomic regions across all 7 APA, a total of 33 factors identified on all APA were computed by hierarchical clustering, using one minus the Pearson correlation coefficient over all gene scores as a distance metric. Two clusters of signatures were identified in manually identified CYP11B2 expressing regions (*CYP11B2*-type 1 and *CYP11B2*-type 2). The top 100 genes with the highest loading for each signature were calculated as described previously.[13] Briefly, the top 50 genes of each factor were combined and average loadings for each gene were computed. Total loadings for repetitive genes were summarized, original loadings for exclusive genes were retained, and loadings of each gene were divided by the number of metagenes within the signature.

Estimate of functional information of signatures. For the two main signatures (*CYP11B2*-type 1 and *CYP11B2*-type 2), an enrichment analysis was performed on the signature´s top 100 most contributing genes using the enricher function against the 50 hallmark gene sets ($P<0.05$).[14]

Dimensionality reduction of APA and adjacent adrenal cortex. To integrate APA and adjacent adrenal tissue, filtered feature-barcode matrices for each sample were merged and converted into a Seurat object using SCTransform (STUtility) with the same filter criteria as above. Integrated Seurat objects were normalized with SCTransform (parameters: variable.features n = 2,000). To reduce dimensionality, principal component analysis was used with RunPCA and 30 dimensions. PCA correction was performed with harmony package[15] using as covariates the section source. A shared nearest neighbor (SNN) graph was created with FindNeighbors (dims = 1:30), followed by FindClusters to cluster spatial spots with a

Louvain algorithm. Clustering was visualized in a 2D embedding, t-distributed stochastic neighbor embedding (TSNE) was created with RunTSNE using the first 30 principal components. A resolution (0.2) was selected in all groups using the Clustree package.[16]

Deconvolution of APA and adjacent adrenal cortex. To explore spatial organization of APA and adjacent adrenal, NMF was applied to the integrated Seurat object (RunNMF function with nfactors = 3) on the SCTransform normalized data omitting ribosomal protein coding genes. Top contributing genes were selected based on the feature loading matrix and enriched for biological processes using gprofiler2R.

Manual region selection of heterogeneous *CYP11B2* expression spots within *KCNJ5* mutated APA. In a tumor structure with a *KCNJ5* mutation, annotation of spatial transcriptomic (ST) spots was performed using Loupe Browser 6. Briefly, the standardised $\log_{10}$-transformed *CYP11B2* expression in tumour regions was calculated on each tumour slide. High *CYP11B2* expressing tumor ST spots were assigned with an expression level above the median and the low *CYP11B2* expressing tumor ST spots were assigned with an expression level below the median. Non-tumor ST spots were annotated as Non-tumor ST spots. *CYP11B2* annotations were exported into Seurat to calculate differentially expressed genes (with the FindAllMarkers function) and pathway enrichment activities.

Differential expression analyses. Differential expression analyses for high *CYP11B2* expressing and low *CYP11B2* expressing clusters were performed using the FindAllMarkers function with Wilcoxon tests. Differentially expressed genes (DGEs) were filtered with an absolute value average log2FC > 0.25 and a false discovery rate (FDR)-adjusted P < 0.05.

Estimate of functional information of high and low *CYP11B2* expressing tumour ST spots. For each ST spot, we estimated signalling pathway activities with PROGENy using the top 1,000 genes of each transcriptional footprint. Input expression matrices were normalised using the SCTransform function.

Bioinformatics and statistical analyses of MALDI–MSI data. Tumor regions were annotated as regions of interest (ROIs) based on CYP11B2 immunostaining. Receiver operating characteristic (ROC) analysis as implemented in SCiLS Lab v. 2022 was performed to find masses which discriminated APA from adjacent adrenal tissue and APA-$KCNJ5^{WT}$ from APA-$KCNJ5^{MUT}$. Discriminative masses with an AUC>0.75 were annotated by accurate mass matching in Human Metabolome Database (http://www.hmdb.ca/; ion mode: negative; adduct type: [M−H], [M−H2O−H], [M+Na−2H], [M+Cl], and [M+K−2H]; mass accuracy, ≤4 ppm) and Lipid Maps (https://www.lipidmaps.org/; negative mode: [M−H]- and [M+Cl]-; Mass Tolerance: +/- 0.005 m/z). Pathway analysis was performed with MetaboAnalyst 5.0 (http://www.metaboanalyst.ca) and Kyoto Encyclopedia of Genes and Genomes database (http://www.genome.jp/kegg/).

References

1. Williams TA, Gomez-Sanchez CE, Rainey WE, Giordano TJ, Lam AK, Marker A, Mete O, Yamazaki Y, Zerbini MCN, Beuschlein F, et al. International Histopathology Consensus for Unilateral Primary Aldosteronism. *J Clin Endocrinol Metab*. 2021;106:42-54. doi: 10.1210/clinem/dgaa484
2. Funder JW, Carey RM, Mantero F, Murad MH, Reincke M, Shibata H, Stowasser M, Young WF, Jr. The Management of Primary Aldosteronism: Case Detection, Diagnosis, and Treatment: An Endocrine Society Clinical Practice Guideline. *J Clin Endocrinol Metab*. 2016;101:1889-1916. doi: 10.1210/jc.2015-4061

3. Williams TA, Reincke M. MANAGEMENT OF ENDOCRINE DISEASE: Diagnosis and management of primary aldosteronism: the Endocrine Society guideline 2016 revisited. *Eur J Endocrinol*. 2018;179:R19-R29. doi: 10.1530/EJE-17-0990
4. Mulatero P, Monticone S, Deinum J, Amar L, Prejbisz A, Zennaro MC, Beuschlein F, Rossi GP, Nishikawa T, Morganti A, et al. Genetics, prevalence, screening and confirmation of primary aldosteronism: a position statement and consensus of the Working Group on Endocrine Hypertension of The European Society of Hypertension. *J Hypertens*. 2020;38:1919-1928. doi: 10.1097/HJH.0000000000002510
5. Williams TA, Lenders JWM, Mulatero P, Burrello J, Rottenkolber M, Adolf C, Satoh F, Amar L, Quinkler M, Deinum J, et al. Outcomes after adrenalectomy for unilateral primary aldosteronism: an international consensus on outcome measures and analysis of remission rates in an international cohort. *Lancet Diabetes Endocrinol*. 2017;5:689-699. doi: 10.1016/S2213-8587(17)30135-3
6. Nanba K, Omata K, Else T, Beck PCC, Nanba AT, Turcu AF, Miller BS, Giordano TJ, Tomlins SA, Rainey WE. Targeted Molecular Characterization of Aldosterone-Producing Adenomas in White Americans. *J Clin Endocrinol Metab*. 2018;103:3869-3876. doi: 10.1210/jc.2018-01004
7. Nanba K, Rainey WE, Udager AM. Approaches to Gene Mutation Analysis Using Formalin-Fixed Paraffin-Embedded Adrenal Tumor Tissue From Patients With Primary Aldosteronism. *Front Endocrinol (Lausanne)*. 2021;12:683588. doi: 10.3389/fendo.2021.683588
8. Sun N, Meyer LS, Feuchtinger A, Kunzke T, Knosel T, Reincke M, Walch A, Williams TA. Mass Spectrometry Imaging Establishes 2 Distinct Metabolic Phenotypes of Aldosterone-Producing Cell Clusters in Primary Aldosteronism. *Hypertension*. 2020;75:634-644. doi: 10.1161/HYPERTENSIONAHA.119.14041
9. Gomez-Sanchez CE, Qi X, Velarde-Miranda C, Plonczynski MW, Parker CR, Rainey W, Satoh F, Maekawa T, Nakamura Y, Sasano H, et al. Development of monoclonal antibodies against human CYP11B1 and CYP11B2. *Mol Cell Endocrinol*. 2014;383:111-117. doi: 10.1016/j.mce.2013.11.022
10. Girardot C, Scholtalbers J, Sauer S, Su SY, Furlong EE. Je, a versatile suite to handle multiplexed NGS libraries with unique molecular identifiers. *BMC Bioinformatics*. 2016;17:419. doi: 10.1186/s12859-016-1284-2
11. Parigi SM, Larsson L, Das S, Ramirez Flores RO, Frede A, Tripathi KP, Diaz OE, Selin K, Morales RA, Luo X, et al. The spatial transcriptomic landscape of the healing mouse intestine following damage. *Nat Commun*. 2022;13:828. doi: 10.1038/s41467-022-28497-0
12. Andersson A, Larsson L, Stenbeck L, Salmen F, Ehinger A, Wu SZ, Al-Eryani G, Roden D, Swarbrick A, Borg A, et al. Spatial deconvolution of HER2-positive breast cancer delineates tumor-associated cell type interactions. *Nat Commun*. 2021;12:6012. doi: 10.1038/s41467-021-26271-2
13. Chen YP, Yin JH, Li WF, Li HJ, Chen DP, Zhang CJ, Lv JW, Wang YQ, Li XM, Li JY, et al. Single-cell transcriptomics reveals regulators underlying immune cell diversity and immune subtypes associated with prognosis in nasopharyngeal carcinoma. *Cell Res*. 2020;30:1024-1042. doi: 10.1038/s41422-020-0374-x
14. Hanzelmann S, Castelo R, Guinney J. GSVA: gene set variation analysis for microarray and RNA-seq data. *BMC Bioinformatics*. 2013;14:7. doi: 10.1186/1471-2105-14-7
15. Korsunsky I, Millard N, Fan J, Slowikowski K, Zhang F, Wei K, Baglaenko Y, Brenner M, Loh PR, Raychaudhuri S. Fast, sensitive and accurate integration of single-cell data with Harmony. *Nat Methods*. 2019;16:1289-1296. doi: 10.1038/s41592-019-0619-0
16. Zappia L, Oshlack A. Clustering trees: a visualization for evaluating clusterings at multiple resolutions. *Gigascience*. 2018;7. doi: 10.1093/gigascience/giy083

5

Table S1. Clinical parameters of surgically treated patients for an aldosterone-producing adenoma.

Parameter	Patient						
	1	**2**	**3**	**4**	**5**	**6**	**7**
Age at surgery (yrs)	35	42	45	56	33	40	43
Sex	Female	Male	Female	Male	Female	Female	Male
BMI (kg/m^2)	21.5	26.4	20.8	25.3	22.9	26.1	26.6
Systolic BP (mmHg)	144	129	173	161	174	142	166
Diastolic BP (mmHg)	96	81	111	81	128	90	103
Anti-HTN meds (DDD)	0.00	0.50	4.00	2.00	0.33	4.00	2.50
Lowest K^+ (mmol/L)	3.4	3.7	3.3	3.3	2.7	2.9	3.3
PAC (pg/mL)	108	129	351	198	357	300	262
DRC (mU/L)	2.0	3.0	2.0	2.0	3.1	12.0	3.5
ARR	54	43	176	99	115	25	75
Largest nodule (mm)	14	7	15	7	19	13	17
*G*enotype	KCNJ5-L168R	NMD	KCNJ5-L168R	CACNA1D-L403R	KCNJ5-L168R	NMD	KCNJ5-G151R

Baseline variables of the 7 patients operated for an APA are shown. The defined daily dose (DDD) is the assumed average maintenance dose per day for a drug used for its main indication in adults (https://www.who.int/tools/atc-ddd-toolkit/about-ddd). APA, aldosterone-producing adenoma; ARR, aldosterone-to-renin ratio; BMI, body mass index; BP, blood pressure; DDD, defined daily dose; PAC, plasma aldosterone concentration; DRC, direct renin concentration; HTN, hypertension; K^+, potassium ions; KCNJ5, gene encoding potassium inwardly rectifying channel subfamily J member 5; meds, medications; PRA, plasma renin activity; NMD, no mutations detected in *KCNJ5, ATP1A1, ATP2B3, CACNA1D*.

Table S2. **Top 100 genes detected in *CYP11B2*-type 1 and *CYP11B2*-type 2.** Genes are sorted from the highest to the lowest significance.

CYP11B2-type 1		CYP11B2-type 2	
Genes 1-50	Genes 51-100	Genes 1-50	Genes 51-100
CYP11B2	LMOD1	FDX1	PAPSS2
HSD3B2	VAT1L	STAR	SLC37A2
PCP4	ATP1B1	CYP11B2	SOAT1
MT3	A2M	HSPE1	HSD3B2
VPREB3	STAR	MT2A	SLC23A2
CYP21A2	VDR	MT3	MT1E
TIMP3	CHCHD10	CYP21A2	RHBDD2
QPCT	PEG10	CYP17A1	FTH1
CCN3	ATP6V1G1	CYP11B1	FTL
KCNJ5	CD81	DHCR24	TUBB
LY6E	DLK1	PPP2R1A	NPTX2
GAPDH	KCNQ1	CYP11A1	LDHB
SMS	ATP1A1	SCARB1	PRKAR2B
FTL	MERTK	SULT2A1	PDK4
FDX1	GPRC5C	GAPDH	MC2R
NPTX2	LSR	CTSA	CTNNB1
COL15A1	ELP1	PCP4	HLA.B
NR4A1	SLC37A2	HIF1A	SQSTM1
PDK4	MC2R	MGST1	B2M
MGP	CPB1	ADGRV1	CBR1
UGCG	EEF1A2	ELP1	TPP1
KCNK3	TSPAN12	CXCR4	PPIF
TSPAN7	SLC6A6	MTCH1	COX17
HOPX	TOMM34	CD55	CCN3
CXCR4	SEC61G	HSPD1	ATP6V1E1
COX20	SELENOW	QPCT	ENO1
VSNL1	MT.ND4L	SH3BP5	RPL26
IGFBP2	MGST1	CD9	RPS27L
WNT4	DNAJC12	ATP6V1G1	BZW1
TPM2	IFITM10	TIMP3	CEBPB
HSPE1	MT.ND2	RPL17	SPARC
LDHB	COX17	TUBB4A	CLU
LSP1	CLRN1	TNFRSF14	CYCS
IGFBP7	CTSA	HSP90B1	KCNK3
ATP2A3	TUBB4A	LY6E	MOB4
MOB4	TBC1D4	COX7B	TOB1
CADM1	CLU	DNAJC12	AKR1B1
RPS27L	TIMP1	PEG10	MDH1
COMMD6	ERN1	TCEAL9	MT.CO3
RAN	TLN1	SLC6A6	TUBB4B
TPP1	PSME2	APOE	SDCBP
SELENOM	NR5A1	CST3	FAM210B
FDXR	RPL26	PKM	CDK2AP2
CTNNB1	CTSB	MCFD2	SLC47A1
ASAH1	PDE2A	ABCB1	MT.CO1
HSPB7	SOD2	FDXR	RDX
SQSTM1	VCAM1	ATP6V0B	PGAM1
CBR1	BEX1	TM7SF2	RPS12
MDH1	RPS12	LDHA	SSR3
MT.ND5	AEBP1	SEC61G	TPM2

Table S3. Discriminative pathways distinguish APA-*KCNJ5*^{WT} and APA-*KCNJ5*^{MUT}

Pathways	-LOG10(p)	Impact
Linoleic acid metabolism	3.916	0
Biosynthesis of unsaturated fatty acids	3.8513	0
Glycerophospholipid metabolism	2.8884	0.39907
Glyoxylate and dicarboxylate metabolism	2.2126	0.03175
D-Glutamine and D-glutamate metabolism	2.1061	1
alpha-Linolenic acid metabolism	1.4358	0.33333
Butanoate metabolism	1.3197	0
Glycerolipid metabolism	1.2682	0.01246
Tryptophan metabolism	1.1446	0.07848
Ether lipid metabolism	1.0943	0
Citrate cycle (TCA cycle)	1.0943	0.13536
Primary bile acid biosynthesis	1.0261	0.00977
Pentose phosphate pathway	1.0223	0.11955
Glycolysis / Gluconeogenesis	0.89954	0.14277
Alanine, aspartate and glutamate metabolism	0.84663	0.19712
Glycine, serine and threonine metabolism	0.73301	0.0058
Arginine and proline metabolism	0.63993	0.086

Table shows pathway enrichment analysis for metabolites identified by MALDI-MSI.

Table S4. Discriminative pathways distinguish APA-*KCNJ5*^{MUT} and adjacent adrenal cortex

Pathways	-LOG10(p)	Impact
Pentose phosphate pathway	6.1792	0.5836
Pentose and glucuronate interconversions	3.6621	0.42186
D-Glutamine and D-glutamate metabolism	1.4327	1
Ascorbate and aldarate metabolism	1.1919	0.5
Arginine biosynthesis	0.76917	0.11675
Alanine, aspartate and glutamate metabolism	0.73024	0.42068
Histidine metabolism	0.6782	0
Pantothenate and CoA biosynthesis	0.5676	0.02143
Glutathione metabolism	0.34877	0.27562
Purine metabolism	0.33342	0.02277
Amino sugar and nucleotide sugar metabolism	0.22226	0.04254
Arginine and proline metabolism	0.21166	0.086
Aminoacyl-tRNA biosynthesis	0.13074	0

Table shows pathway enrichment analysis for metabolites identified by MALDI-MSI

Table S5. Discriminative pathways distinguish APA-*KCNJ5*^{WT} and adjacent adrenal cortex, related to Figure 4F

Pathways	-LOG10(p)	Impact
Linoleic acid metabolism	3.064	0
Amino sugar and nucleotide sugar metabolism	2.9687	0.44731
Fructose and mannose metabolism	2.7998	0.59558
Biosynthesis of unsaturated fatty acids	1.6622	0
Glycolysis / Gluconeogenesis	1.5506	0.08444
Phosphatidylinositol signaling system	1.4439	0.05631
Inositol phosphate metabolism	1.347	0.12365
Starch and sucrose metabolism	1.3388	0.29163
Valine, leucine and isoleucine biosynthesis	1.3148	0
Pentose phosphate pathway	1.1193	0.13892
alpha-Linolenic acid metabolism	0.93353	0.33333
Galactose metabolism	0.91036	0.04375
Pentose and glucuronate interconversions	0.70338	0.14062
Glycerophospholipid metabolism	0.6461	0.33882
Valine, leucine and isoleucine degradation	0.5589	0.04154
N-Glycan biosynthesis	0.24475	0.00676
Primary bile acid biosynthesis	0.19857	0.00977
Aminoacyl-tRNA biosynthesis	0.18278	0

Table shows pathway enrichment analysis for metabolites identified by MALDI-MSI.

10

Table S6. Differentially expressed steroidogenesis enzyme genes between subpopulations.

	APA-like-1 versus APA-like-2 in patients with *KCNJ5* mutation			APA-like-3 versus other subpopulations in patients without *KCNJ5* mutation		
	avg_log$_2$FC	**p-value**	**Adjusted p-value**	**avg_log2FC**	**p-value**	**Adjusted p-value**
CYP11B2	1.711878629	0	0	3.498849164	1.8047E-252	2.44E-248
CYP17A1	0.583643006	1.66E-106	2.24E-102	-1.354281505	1.5088E-211	2.0389E-207
CYP11B1	0.311975826	5.23E-32	7.07E-28	-1.328623301	1.6772E-204	2.2664E-200

avg_log$_2$FC, log fold-change of the average expression between the groups. Positive values indicate higher expression in the former group. The data refer to subpopulations annotated in Figure 6 (main manuscript).

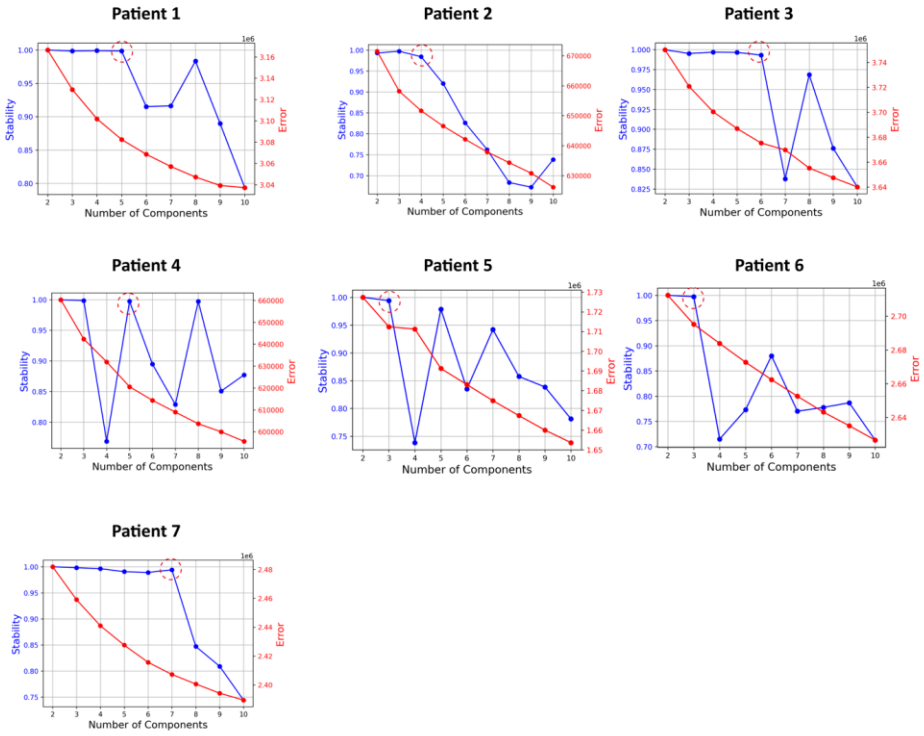

Figure S1. Identification of transcriptionally distinct regions by stability and error using consensus non-negative matrix factorization.
Consensus non-negative matrix factorisation (cNNMF) was used to quantify the optimal number of factors preferentially co-expressed by subsets of spatial transcriptomics spots representing transcriptionally distinct regions within each of the 7 adrenal sections with an APA. Factor number determination for each patient is based on the largest value that is reasonably stable and/or a local maximum in stability and a balance between stability and error, as shown by the dashed circles. By the stability of the solution (as captured by the silhouette score; in blue, left axis) and the Frobenius reconstruction error (in red, right axis) using consensus non-negative matrix factorisation, patients 1 to 7 displayed 5, 4, 6, 5, 3, 3, 7 transcriptionally distinct regions in the adrenal sections.

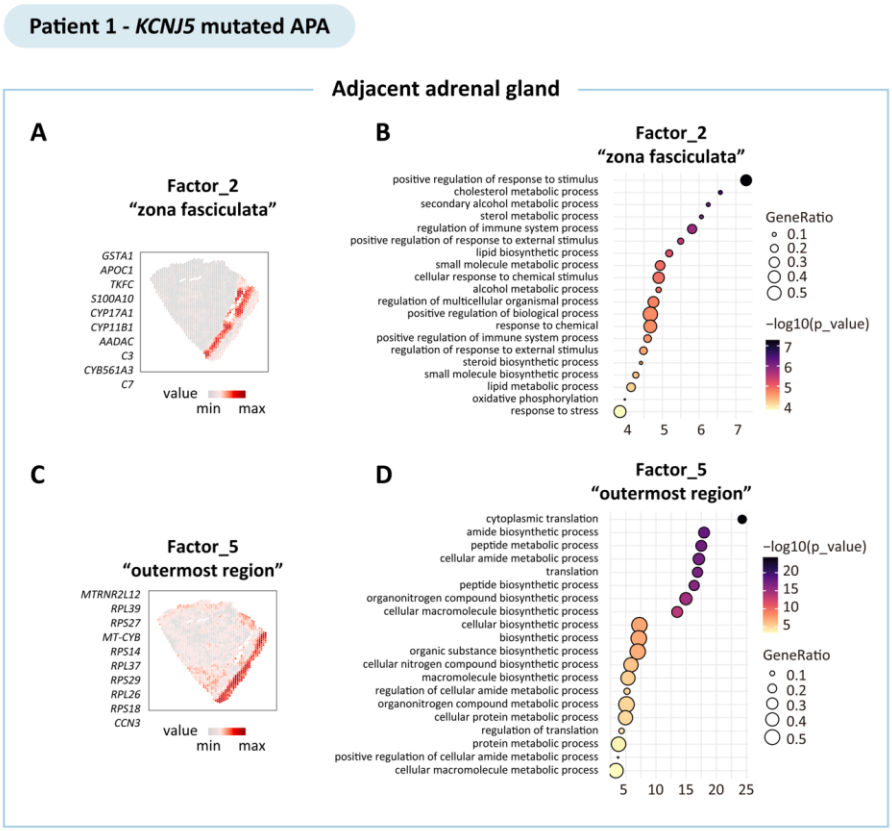

Figure S2. Non-negative matrix factorization reveals distinct molecular patterns in the adjacent adrenal gland of APA with a *KCNJ5* mutation

A and **C**, Spatial distribution of the nontumor-related factors and top 10 genes annotated in the diverse factors. Color-codes indicate gene expression levels. Factor 2 was characterized by zonation markers of zona fasciculata (e.g., *CYP17A1* and *CYP11B1*), whereas factor 5 histologically defined structures that resembled outermost region of the adrenal gland adjacent to an APA. **B** and **D**, Geno Ontology analysis showing enriched biological processes associated with factors related to "zona fasciculata" (factor 2, **Panel A**) and "outermost region" (factor 5, **Panel C**).

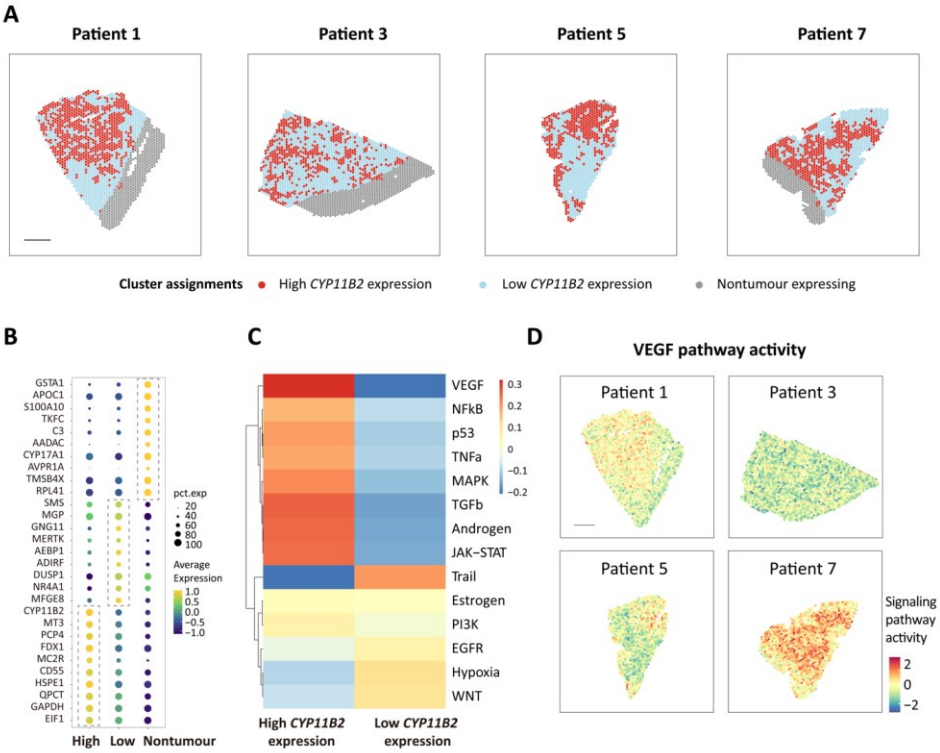

Figure S3 Heterogeneity of *CYP11B2* gene expression in *KCNJ5* mutated APAs.

A, *CYP11B2* expression levels in spatial transcriptomic spots of *KCNJ5* mutated APA. Spatial spots with high or low *CYP11B2* expression within the tumor area are indicated in red or blue, respectively, and spots from non-tumor regions are shown in grey. Scale bar, 1mm. **B**, bubble mapping of significantly differentially expressed genes associated with each of the 3 clusters of high or low *CYP11B2* expression or non-tumor area. Bubble size indicates the percentage of cluster spots expressing the corresponding gene and the color code indicates the average gene expression. **C**, heatmap showing the correlation *CYP11B2* expression levels and PROGENy pathway activity scores. Colour code indicates the corresponding signaling pathway activity. D, an example of the spatial distribution of the VEGF pathway in adrenal tissues that shows relative VEGF pathway activation in spatial spots with high *CYP11B2* expression.

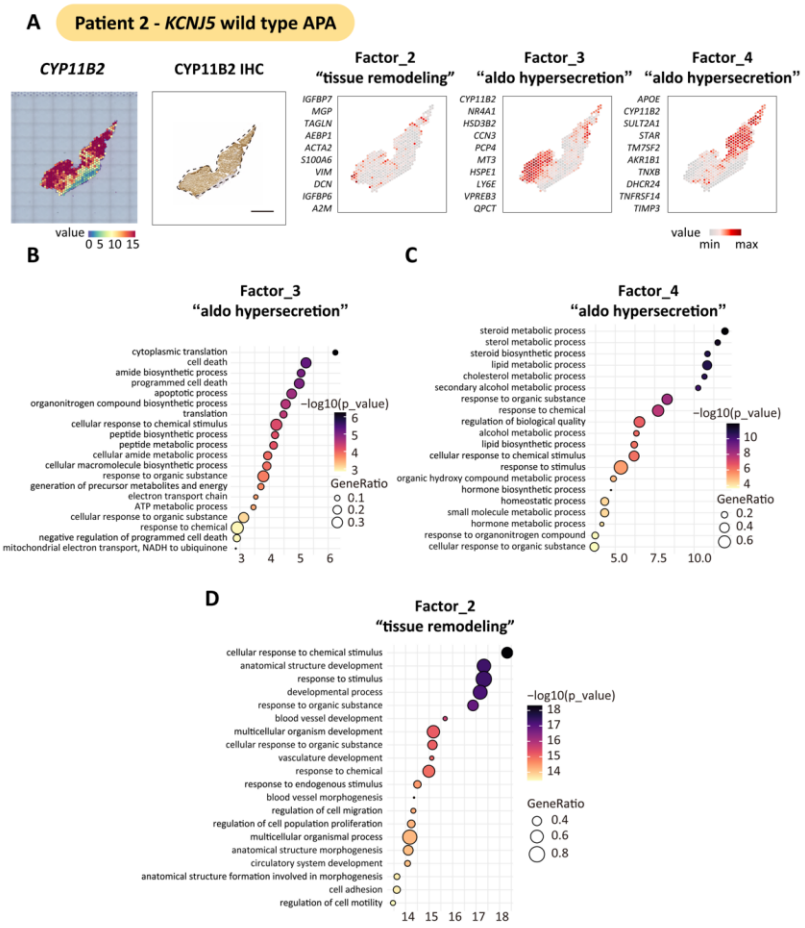

Figure S4 Intra-tumoral transcriptional heterogeneity of APAs without a *KCNJ5* mutation.
NNMF expression-based analysis identified the top genes which define factors (transcriptionally distinct regions) in adrenal sections with an APA. The figure shows the analysis of patient 2 without a *KCNJ5* mutation. **A**, Spatial CYP11B2 and spatial distribution of the tumor-related factors, color-codes indicate gene expression levels. **Factors 2, 3 and 4,** are tumor-related factors: factor 3 and factor 4 comprise gene sets preferentially co-expressed in subsets of *CYP11B2* expressing tumor regions. *CYP11B2*, *NR4A1*, *HSD3B2*, *CCN3*, and *PCP4* were the top genes defining factor 3; *APOE*, *CYP11B2*, *SULT2A1*, *STAR*, and *TM7SF2* defined factor 4; conversely factor 2 defined tumor regions without CYP11B2 expression and was associated with tissue remodeling. Scale bar, 1 mm. **B-D**, Geno Ontology analysis showing enriched biological processes associated with factors related to "aldosterone hypersecretion" (factor 3 and factor 4) and "tissue remodeling" (factor 2).

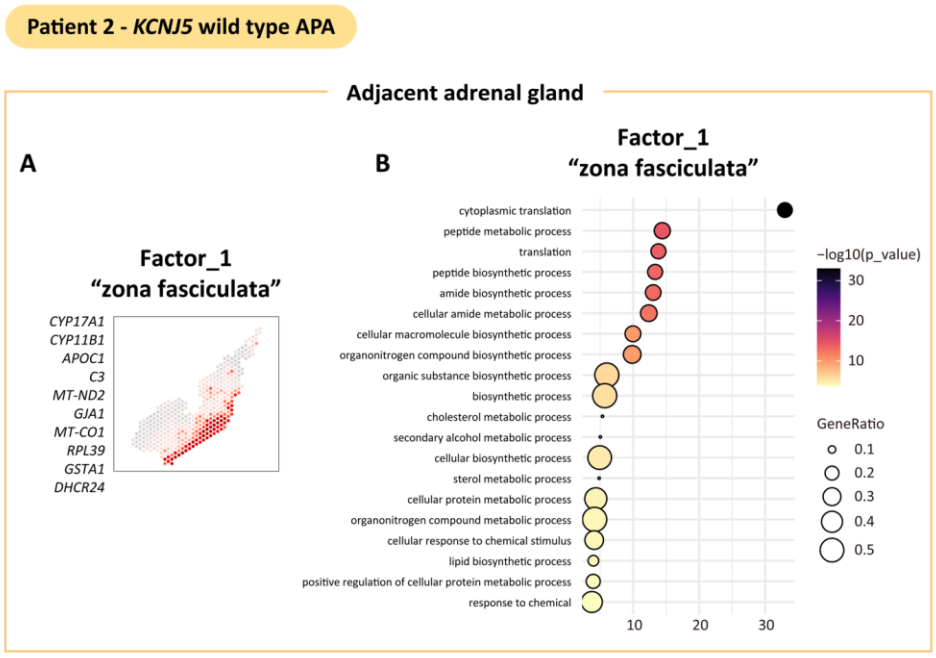

Figure S5. Non-negative matrix factorization reveals distinct molecular patterns in the adjacent adrenal gland of APAs without a *KCNJ5* mutation

A, Spatial distribution of the nontumor-related factor 1 and the associated top 10 annotated genes. Color-codes indicate gene expression levels. Factor 1 was characterized by zonation markers of the zona fasciculata (e.g., *CYP17A1* and *CYP11B1*). **B**, Geno Ontology analysis showing enriched biological processes associated with factor 1 related to "zona fasciculata" (factor 1, **Panel A**).

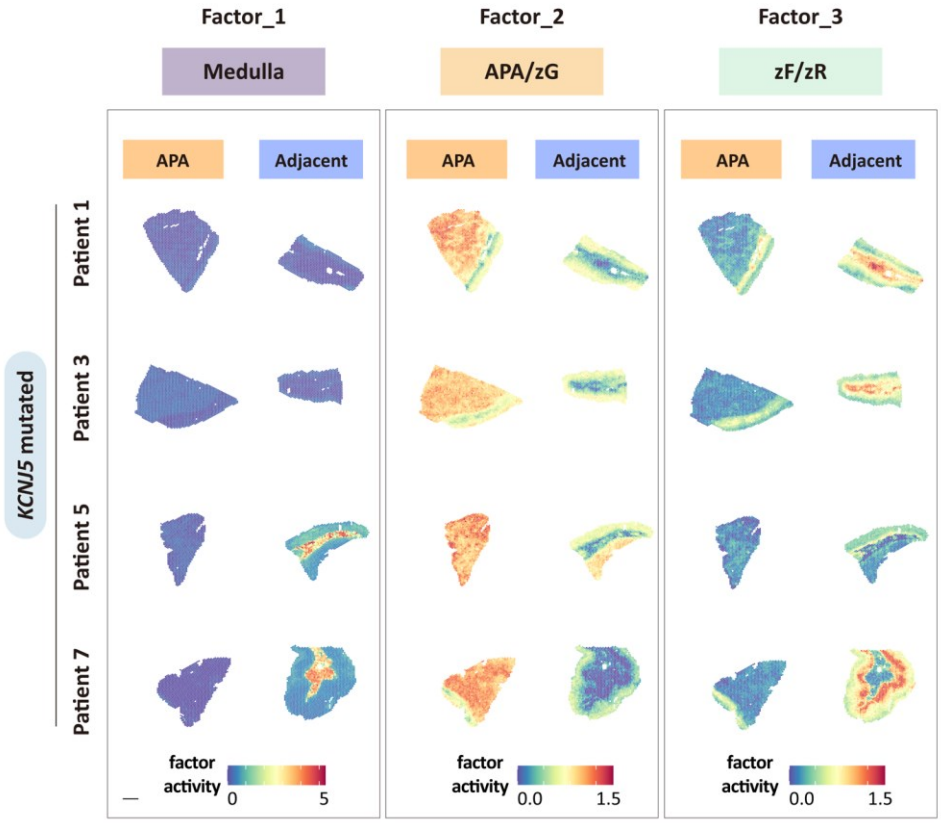

Figure S6. Non-negative matrix factorization to identify the spatial distribution of transcriptionally distinct regions in APAs with *KCNJ5* mutation and their adjacent cortex.
Spatial distribution of the 3 factors (transcriptionally distinct regions, factors 1-3) which distinguish zona fasciculata and zona reticularis, medulla, and a mixture of APA and zona glomerulosa in APA with a *KCNJ5* mutation. The color score assigned to spatial transcriptomics spots is based on the expression level of the genes which define each factor. Scale bar, 1mm.

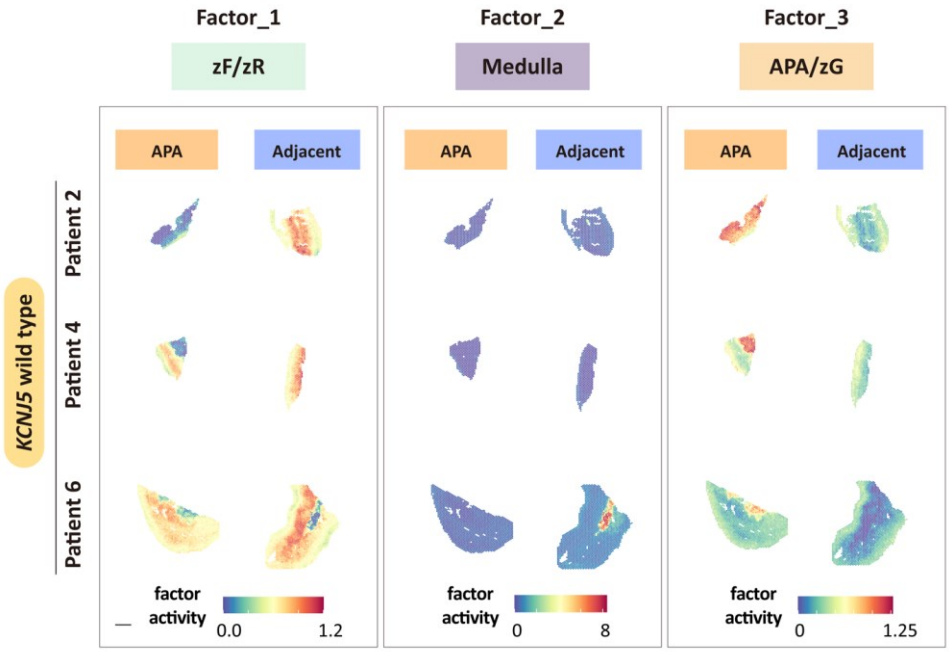

Figure S7. Non-negative matrix factorization to identify the spatial distribution of transcriptionally distinct regions in APAs without *KCNJ5* mutation and their adjacent cortex.
Spatial distribution of the 3 factors (transcriptionally distinct regions, factors 1-3) which distinguish zona fasciculata and zona reticularis, medulla, and a mixture of APA and zona glomerulosa in APA without a *KCNJ5* mutation. The color score assigned to spatial transcriptomics spots is based on the expression level of the genes which define each factor. Scale bar, 1mm.

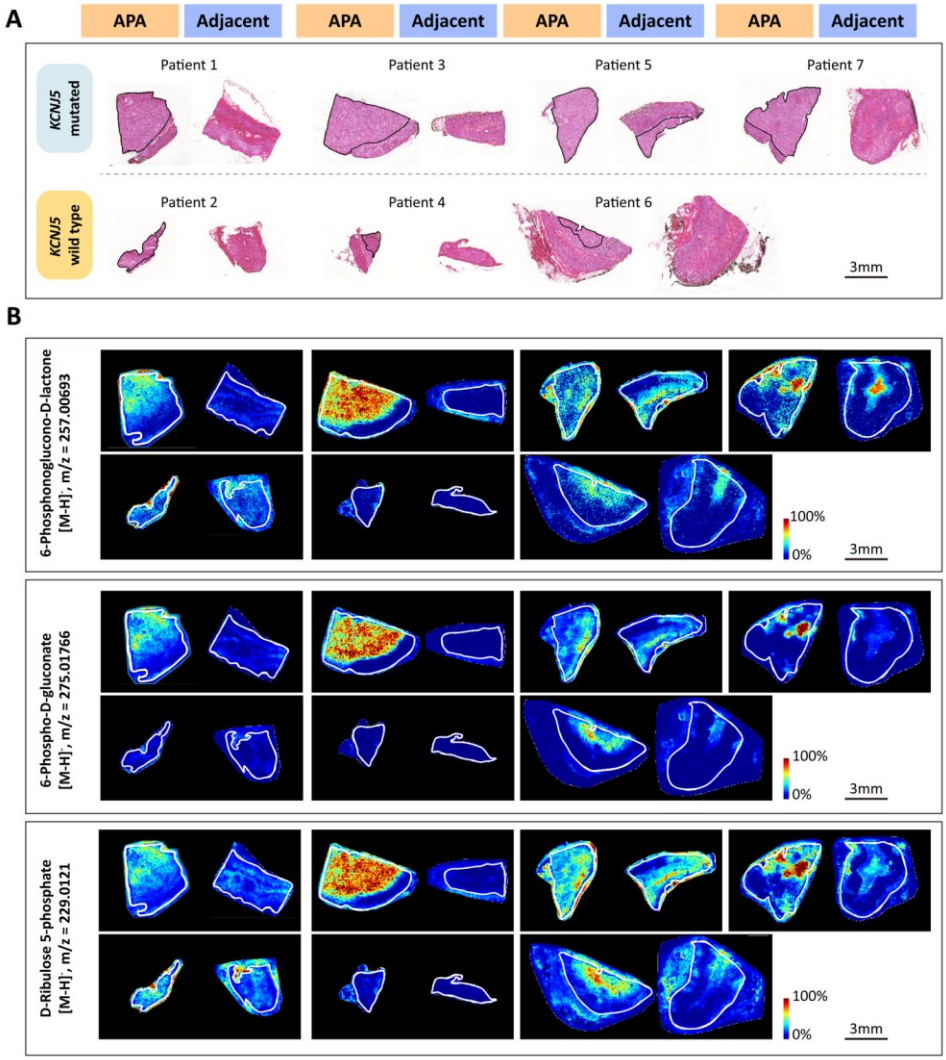

Figure S8. MALDI-MSI identification of upregulated oxidative pentose phosphate pathway metabolites in *KCNJ5* mutated APA compared with adjacent adrenal cortex.
A, Corresponding H&E-stained tissues of *KCNJ5* mutated (Upper) or *KCNJ5* wild type APA (Lower) and paired adjacent cortex for MALDI imaging. Outlined regions in black indicate APA tumor areas with positive CYP11B2 immunostaining. **B**, representative images of the spatial distribution of oxidative pentose phosphate pathway metabolites. Outlined regions in white indicate the borders of the tissue section.

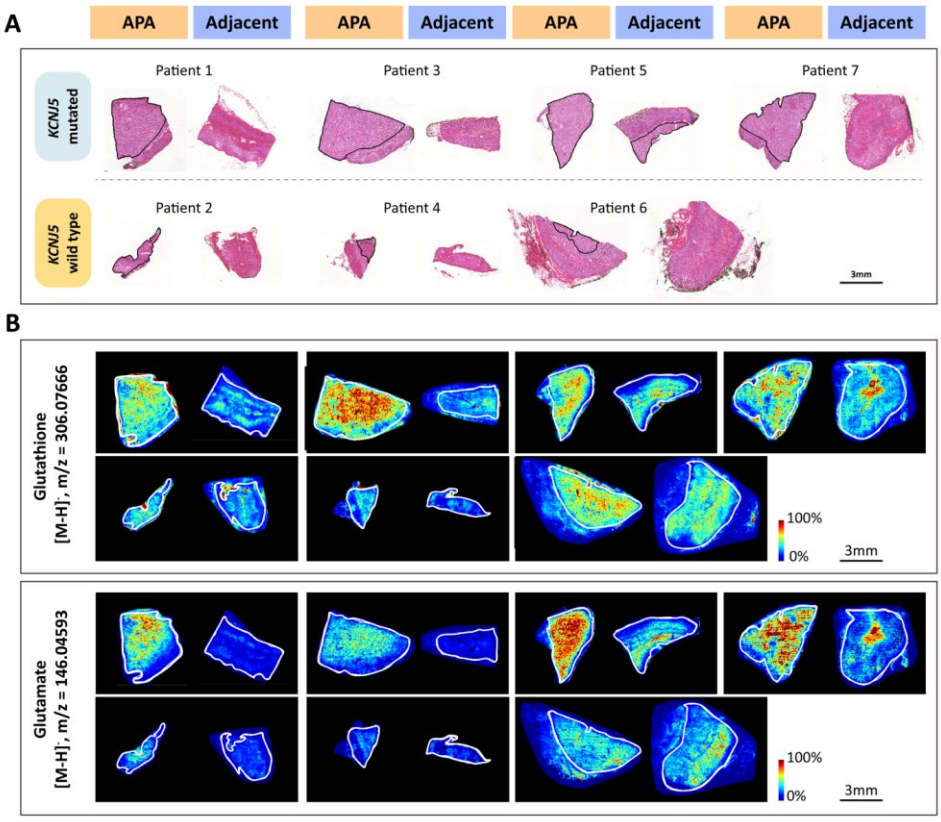

Figure S9. MALDI-MSI identification of upregulated glutathione metabolism metabolites in *KCNJ5* mutated APA compared with adjacent adrenal cortex.
A, corresponding H&E-stained tissues of *KCNJ5* mutated APA (Upper) or *KCNJ5* wild type APA (Lower) and adjacent adrenal gland for MALDI MSI. Outlined regions in black indicate APA tumor areas with positive CYP11B2 immunostaining. **B**, representative images showing spatial distribution of glutathione metabolism metabolites (glutathione and glutamate). Outlined regions in white indicate the borders of the tissue section.

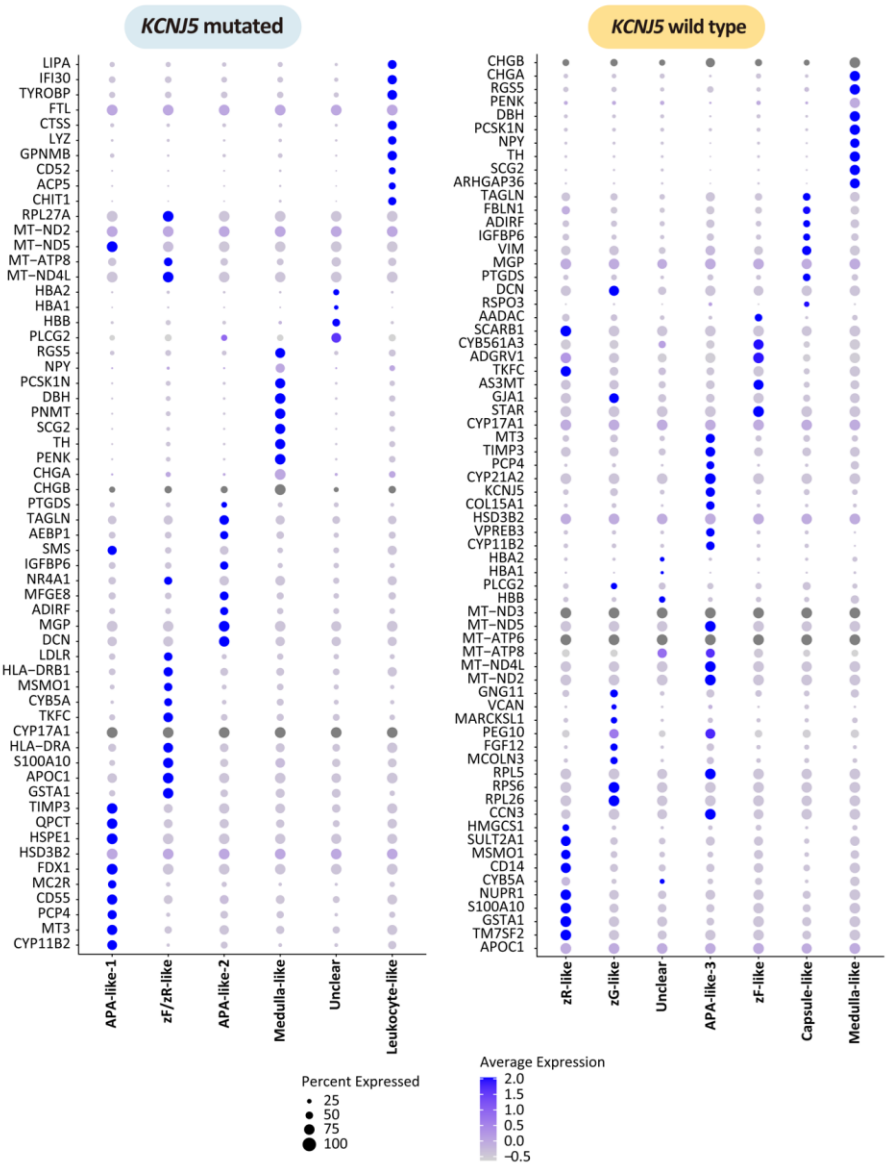

Figure S10. Identification of transcriptomic subpopulations
Bubble plot showing the top 10 differentially expressed genes within each transcriptomic cluster shown in Figure 6 (main manuscript) stratified by APA genotype.

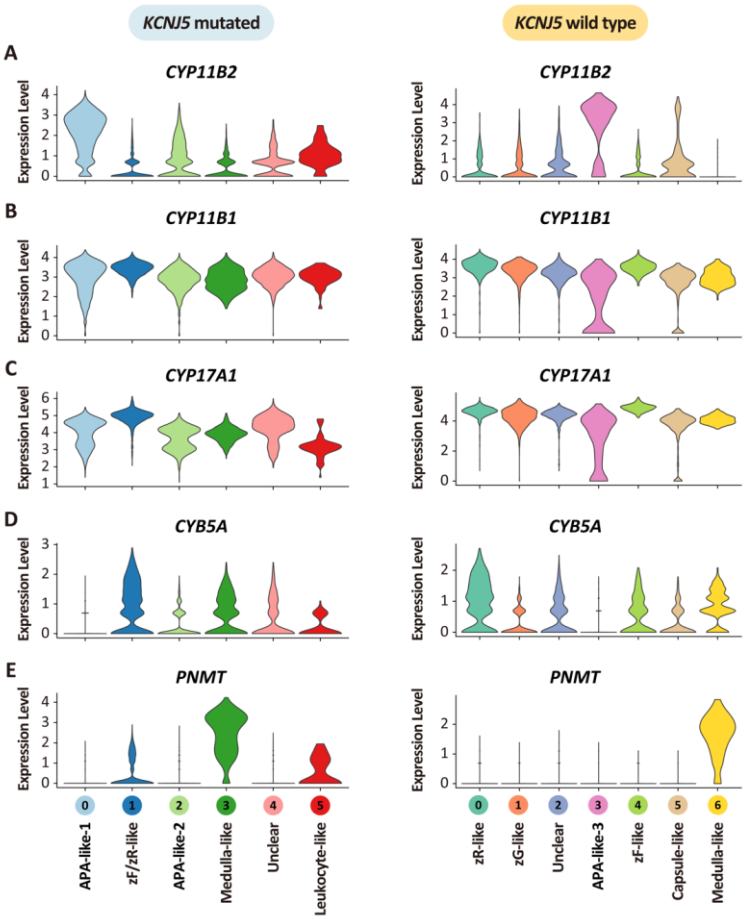

Figure S11. **Expression of steroidogenic enzyme genes in adrenal cell types.**
Violin plots showing the expression of genes encoding steroidogenic enzyme known to be expressed in a cell-type specific manner. **A**, *CYP11B2* gene was selectively enriched in APA-like clusters (APA-like-1 in patients with APA-*KCNJ5*^{MUT} (Left); APA-like-3 in patients with APA-*KCNJ5*^{WT} (Right)). **B-D**, *CYP11B1*, *CYP17A1*, and *CYB5A* genes were enriched in regions with a high abundance of zona fasciculata and zona reticularis cells (zF/zR-like cluster in patients with APA-*KCNJ5*^{MUT} (Left); zR-like and zF-like clusters in patients with APA-*KCNJ5*^{WT} (Right)). **E**, PNMT gene was enriched in medulla-like clusters in patients with APA-*KCNJ5*^{MUT} and patients with APA-*KCNJ5*^{WT}, respectively. Left and right panels indicate adrenal tissues from patients with a *KCNJ5* mutation (Left) or without a *KCNJ5* mutation (Right)). The fill color of the violin plots indicates the subpopulations identified in Figure 6 (main text). APA, aldosterone-producing adenoma; zG, zona glomerulosa; zF, zona fasciculata; zR, zona reticularis.

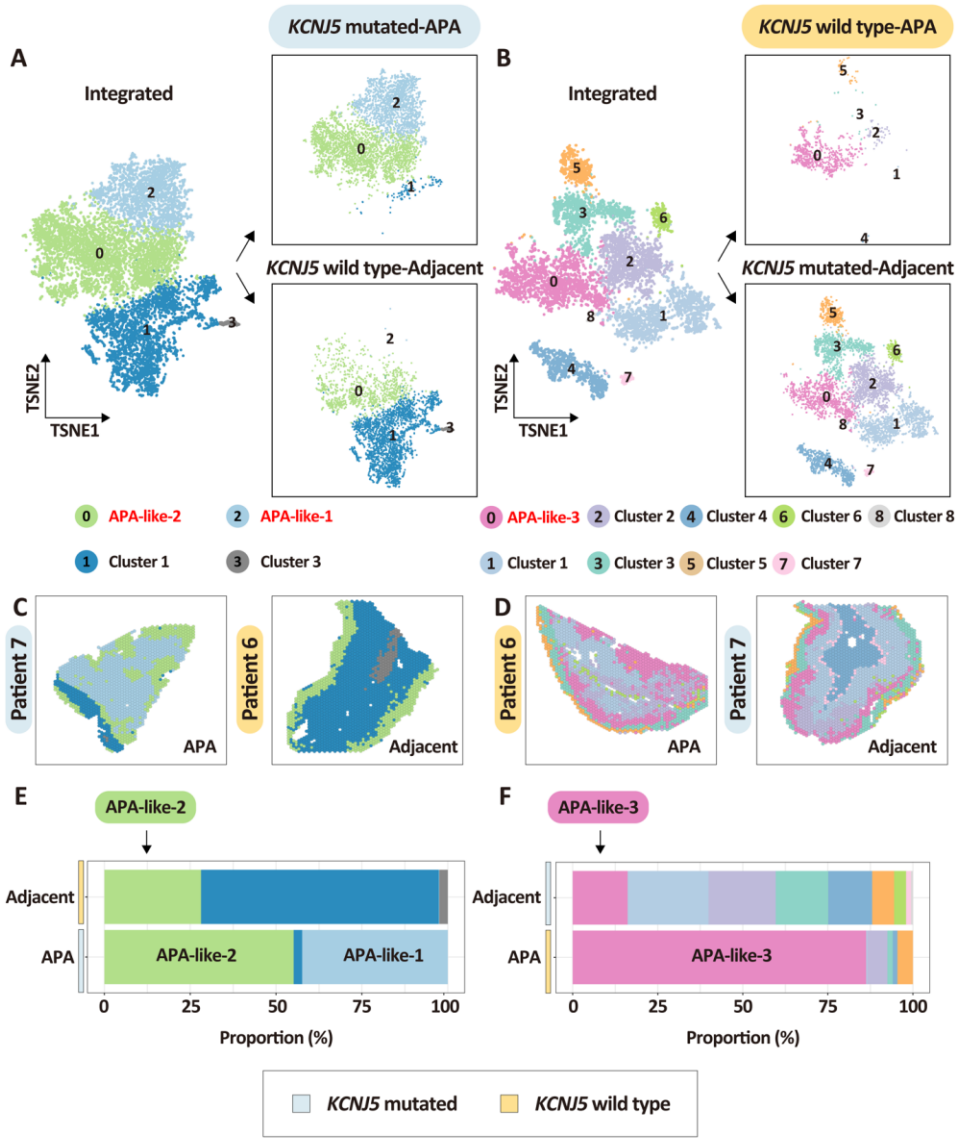

Figure S12. The validation of APA-like subpopulations through comparisons of non-matching tumor-adjacent cortex pairs.

We excluded potential excessive interpretation of the algorithm used by integrative analysis of *KCNJ5*-mutated APAs compared with the adjacent adrenal cortex of APAs without a *KCNJ5* mutation (**A**, **C**, and **E**) and of APAs without a *KCNJ5* mutation compared with the adjacent adrenal cortex of APAs with a *KCNJ5* mutation (**B**, **D**, and **F**). **A-B**, t-distributed stochastic neighbor embedding representations of the integrated spatial transcriptomes of APAs and adjacent adrenal tissues stratified by APA-*KCNJ5* mutation status and tissue type. **A** and **B** show integrated spatial transcriptomic spots from APAs and adjacent adrenal tissues (left image of **A** and **B**) as well as separated into APAs (boxed image, top right of **A** and **B**) and adjacent tissues (boxed image, bottom right of **A** and **B**). Colors represent transcriptome subpopulations as indicated. APA-like clusters are marked in red writing. **A**, APA-$KCNJ5^{MUT}$ (n= 4) and adjacent adrenal cortex of APA-$KCNJ5^{WT}$ (n = 3). **B**, APA-$KCNJ5^{WT}$ (n = 3) and adjacent adrenals of APA-$KCNJ5^{MUT}$ (n = 4). **C-D**, Representative spatial transcriptomics sections showing the distribution of spots in APAs and adjacent adrenals from patient 7 with a *KCNJ5* mutation (male) and patient 6 without a *KCNJ5* mutation (female). **E-F**, stacked plots showing the proportion of each transcriptome cluster in APAs and non-matching adjacent adrenals. **E**, APAs-$KCNJ5^{MUT}$ and adjacent adrenals of APAs-$KCNJ5^{WT}$. **F**, APAs-$KCNJ5^{WT}$ and adjacent adrenals of APAs-$KCNJ5^{MUT}$.

Note that in panel **C**, the APA-like-1 and APA-like-2 subpopulations in APA-$KCNJ5^{MUT}$ of patient 7 (cluster 2 and cluster 0) *versus* the adjacent cortex to the APA-$KCNJ5^{WT}$ of patient 6 displayed a similar spatial distribution as compared to its own corresponding paired adjacent cortex shown in **Figure 6C** (main manuscript). Likewise, in panel **D**, the APA-like 3 subpopulation in APA-$KCNJ5^{WT}$ of patient 6 (cluster 0) *versus* the adjacent cortex to the APA-$KCNJ5^{MUT}$of patient 7 displayed a similar spatial distribution as compared to its own corresponding paired adjacent cortex shown in **Figure 6D** (main manuscript). Also note that subpopulations APA-like 2 and APA-like 3 are common to tumor areas and the adjacent tissue in this analysis of non-matched APAs and adjacent cortex to an APA of different genotype and in the analysis of APA and paired adjacent cortex from the same patient in **Figure 6E and F** (main manuscript). In contrast, APA-like 1 is present only in the tumor tissue of APA-$KCNJ5^{MUT}$ but is undetectable in the adjacent adrenal cortex to APA-$KCNJ5^{WT}$ (**E**) but present in its paired adjacent cortex **Figure 6E** (main manuscript).

6. References

1. Arnold, J. Ein Beitrag zur feineren Struktur und dem Chemismus der Nebennieren. *Virchow Arch Patholog Anatomie Physiol Klin Med* **35**, 64–107 (1866).
2. Miller, E.H. A transitory zone in the adrenal cortex which shows age and sex relationships. *American Journal of Anatomy* **40**, 251-293 (1927).
3. Miller, W.L. & Auchus, R.J. The molecular biology, biochemistry, and physiology of human steroidogenesis and its disorders. *Endocr Rev* **32**, 81-151 (2011).
4. Guagliardo, N.A., Yao, J., Hu, C. & Barrett, P.Q. Minireview: aldosterone biosynthesis: electrically gated for our protection. *Endocrinology* **153**, 3579-86 (2012).
5. Seccia, T.M., Caroccia, B., Gomez-Sanchez, E.P., Gomez-Sanchez, C.E. & Rossi, G.P. The Biology of Normal Zona Glomerulosa and Aldosterone-Producing Adenoma: Pathological Implications. *Endocr Rev* **39**, 1029-1056 (2018).
6. Kojima, I., Shibata, H. & Ogata, E. Phorbol ester inhibits angiotensin-induced activation of phospholipase C in adrenal glomerulosa cells. Its implication in the sustained action of angiotensin. *Biochem J* **237**, 253-8 (1986).
7. Spat, A. & Hunyady, L. Control of aldosterone secretion: a model for convergence in cellular signaling pathways. *Physiol Rev* **84**, 489-539 (2004).
8. Olala, L.O., Choudhary, V., Johnson, M.H. & Bollag, W.B. Angiotensin II-induced protein kinase D activates the ATF/CREB family of transcription factors and promotes StAR mRNA expression. *Endocrinology* **155**, 2524-33 (2014).
9. Heitzmann, D. *et al.* Invalidation of TASK1 potassium channels disrupts adrenal gland zonation and mineralocorticoid homeostasis. *EMBO J* **27**, 179-87 (2008).
10. Lenzini, L. *et al.* Lower expression of the TWIK-related acid-sensitive K+ channel 2 (TASK-2) gene is a hallmark of aldosterone-producing adenoma causing human primary aldosteronism. *J Clin Endocrinol Metab* **99**, E674-82 (2014).
11. Yao, J. *et al.* Functional TASK-3-Like Channels in Mitochondria of Aldosterone-Producing Zona Glomerulosa Cells. *Hypertension* **70**, 347-356 (2017).

12. Enyeart, J.A., Danthi, S.J. & Enyeart, J.J. TREK-1 K+ channels couple angiotensin II receptors to membrane depolarization and aldosterone secretion in bovine adrenal glomerulosa cells. *Am J Physiol Endocrinol Metab* **287**, E1154-65 (2004).
13. Oki, K., Plonczynski, M.W., Lam, M.L., Gomez-Sanchez, E.P. & Gomez-Sanchez, C.E. The potassium channel, Kir3.4 participates in angiotensin II-stimulated aldosterone production by a human adrenocortical cell line. *Endocrinology* **153**, 4328-35 (2012).
14. St-Jean, M., Bourdeau, I., Martin, M. & Lacroix, A. Aldosterone is Aberrantly Regulated by Various Stimuli in a High Proportion of Patients with Primary Aldosteronism. *J Clin Endocrinol Metab* **106**, e45-e60 (2021).
15. Zwermann, O., Suttmann, Y., Bidlingmaier, M., Beuschlein, F. & Reincke, M. Screening for membrane hormone receptor expression in primary aldosteronism. *Eur J Endocrinol* **160**, 443-51 (2009).
16. Monticone, S. *et al.* Prevalence and Clinical Manifestations of Primary Aldosteronism Encountered in Primary Care Practice. *J Am Coll Cardiol* **69**, 1811-1820 (2017).
17. Hannemann, A. & Wallaschofski, H. Prevalence of primary aldosteronism in patient's cohorts and in population-based studies--a review of the current literature. *Horm Metab Res* **44**, 157-62 (2012).
18. Brown, J.M. *et al.* The Unrecognized Prevalence of Primary Aldosteronism: A Cross-sectional Study. *Ann Intern Med* **173**, 10-20 (2020).
19. Calhoun, D.A. Hyperaldosteronism as a common cause of resistant hypertension. *Annu Rev Med* **64**, 233-47 (2013).
20. Reincke, M. *et al.* Diagnosis and treatment of primary aldosteronism. *Lancet Diabetes Endocrinol* **9**, 876-892 (2021).
21. Funder, J.W. *et al.* The Management of Primary Aldosteronism: Case Detection, Diagnosis, and Treatment: An Endocrine Society Clinical Practice Guideline. *J Clin Endocrinol Metab* **101**, 1889-916 (2016).
22. Williams, T.A. *et al.* International Histopathology Consensus for Unilateral Primary Aldosteronism. *J Clin Endocrinol Metab* **106**, 42-54 (2021).

23. Gomez-Sanchez, C.E. *et al.* Development of monoclonal antibodies against human CYP11B1 and CYP11B2. *Mol Cell Endocrinol* **383**, 111-7 (2014).
24. Yamazaki, Y. *et al.* Histopathological Classification of Cross-Sectional Image-Negative Hyperaldosteronism. *J Clin Endocrinol Metab* **102**, 1182-1192 (2017).
25. Meyer, L.S. *et al.* Immunohistopathology and Steroid Profiles Associated With Biochemical Outcomes After Adrenalectomy for Unilateral Primary Aldosteronism. *Hypertension* **72**, 650-657 (2018).
26. De Sousa, K. *et al.* Genetic, Cellular, and Molecular Heterogeneity in Adrenals With Aldosterone-Producing Adenoma. *Hypertension* **75**, 1034-1044 (2020).
27. Nishimoto, K. *et al.* Aldosterone-stimulating somatic gene mutations are common in normal adrenal glands. *Proc Natl Acad Sci U S A* **112**, E4591-9 (2015).
28. Nanba, K. *et al.* Age-Related Autonomous Aldosteronism. *Circulation* **136**, 347-355 (2017).
29. Nishimoto, K. *et al.* Immunohistochemistry of aldosterone synthase leads the way to the pathogenesis of primary aldosteronism. *Mol Cell Endocrinol* **441**, 124-133 (2017).
30. Sun, N. *et al.* Mass Spectrometry Imaging Establishes 2 Distinct Metabolic Phenotypes of Aldosterone-Producing Cell Clusters in Primary Aldosteronism. *Hypertension* **75**, 634-644 (2020).
31. Omata, K. *et al.* Cellular and Genetic Causes of Idiopathic Hyperaldosteronism. *Hypertension* **72**, 874-880 (2018).
32. Meyer, L.S. *et al.* Single-Center Prospective Cohort Study on the Histopathology, Genotype, and Postsurgical Outcomes of Patients With Primary Aldosteronism. *Hypertension* **78**, 738-746 (2021).
33. Lifton, R.P. *et al.* A chimaeric 11 beta-hydroxylase/aldosterone synthase gene causes glucocorticoid-remediable aldosteronism and human hypertension. *Nature* **355**, 262-5 (1992).
34. Stowasser, M. *et al.* Familial hyperaldosteronism type II: five families with a new variety of primary aldosteronism. *Clin Exp Pharmacol Physiol* **19**, 319-22 (1992).

35. Geller, D.S. *et al.* A novel form of human mendelian hypertension featuring nonglucocorticoid-remediable aldosteronism. *J Clin Endocrinol Metab* **93**, 3117-23 (2008).
36. Scholl, U.I. *et al.* Recurrent gain of function mutation in calcium channel CACNA1H causes early-onset hypertension with primary aldosteronism. *Elife* **4**, e06315 (2015).
37. Scholl, U.I. *et al.* Somatic and germline CACNA1D calcium channel mutations in aldosterone-producing adenomas and primary aldosteronism. *Nat Genet* **45**, 1050-4 (2013).
38. Nanba, K. *et al.* Targeted Molecular Characterization of Aldosterone-Producing Adenomas in White Americans. *J Clin Endocrinol Metab* **103**, 3869-3876 (2018).
39. Nanba, K. *et al.* Genetic Characteristics of Aldosterone-Producing Adenomas in Blacks. *Hypertension* **73**, 885-892 (2019).
40. Nanba, K. *et al.* Prevalence of Somatic Mutations in Aldosterone-Producing Adenomas in Japanese Patients. *J Clin Endocrinol Metab* **105**, e4066-73 (2020).
41. Choi, M. *et al.* K+ channel mutations in adrenal aldosterone-producing adenomas and hereditary hypertension. *Science* **331**, 768-72 (2011).
42. Fernandes-Rosa, F.L. *et al.* Genetic spectrum and clinical correlates of somatic mutations in aldosterone-producing adenoma. *Hypertension* **64**, 354-61 (2014).
43. Lenzini, L. *et al.* A Meta-Analysis of Somatic KCNJ5 K(+) Channel Mutations In 1636 Patients With an Aldosterone-Producing Adenoma. *J Clin Endocrinol Metab* **100**, E1089-95 (2015).
44. Ono, Y. *et al.* Histological Characterization of Aldosterone-producing Adrenocortical Adenomas with Different Somatic Mutations. *J Clin Endocrinol Metab* **105**, e282-9 (2020).
45. Azizan, E.A. *et al.* Microarray, qPCR, and KCNJ5 sequencing of aldosterone-producing adenomas reveal differences in genotype and phenotype between zona glomerulosa- and zona fasciculata-like tumors. *J Clin Endocrinol Metab* **97**, E819-29 (2012).

46. Satoh, F. *et al.* Measurement of peripheral plasma 18-oxocortisol can discriminate unilateral adenoma from bilateral diseases in patients with primary aldosteronism. *Hypertension* **65**, 1096-102 (2015).
47. Guo, Z. *et al.* Biochemical, Histopathological, and Genetic Characterization of Posture-Responsive and Unresponsive APAs. *J Clin Endocrinol Metab* **105**, e3224-35 (2020).
48. Tezuka, Y. *et al.* 18-Oxocortisol Synthesis in Aldosterone-Producing Adrenocortical Adenoma and Significance of KCNJ5 Mutation Status. *Hypertension* **73**, 1283-1290 (2019).
49. Williams, T.A. *et al.* Genotype-Specific Steroid Profiles Associated With Aldosterone-Producing Adenomas. *Hypertension* **67**, 139-45 (2016).
50. Beuschlein, F. *et al.* Somatic mutations in ATP1A1 and ATP2B3 lead to aldosterone-producing adenomas and secondary hypertension. *Nat Genet* **45**, 440-4, 444e1-2 (2013).
51. Scholl, U.I. *et al.* Novel somatic mutations in primary hyperaldosteronism are related to the clinical, radiological and pathological phenotype. *Clin Endocrinol (Oxf)* **83**, 779-89 (2015).
52. Akerstrom, T. *et al.* Activating mutations in CTNNB1 in aldosterone producing adenomas. *Sci Rep* **6**, 19546 (2016).
53. Nishimoto, K. *et al.* Adrenocortical zonation in humans under normal and pathological conditions. *J Clin Endocrinol Metab* **95**, 2296-305 (2010).
54. Boulkroun, S. *et al.* Adrenal cortex remodeling and functional zona glomerulosa hyperplasia in primary aldosteronism. *Hypertension* **56**, 885-92 (2010).
55. Nishimoto, K. *et al.* Case Report: Nodule Development From Subcapsular Aldosterone-Producing Cell Clusters Causes Hyperaldosteronism. *J Clin Endocrinol Metab* **101**, 6-9 (2016).
56. Scholl, U.I. *et al.* Hypertension with or without adrenal hyperplasia due to different inherited mutations in the potassium channel KCNJ5. *Proc Natl Acad Sci U S A* **109**, 2533-8 (2012).
57. Yang, Y. *et al.* Primary Aldosteronism: KCNJ5 Mutations and Adrenocortical Cell Growth. *Hypertension* **74**, 809-816 (2019).

58. Zheng, F.F. *et al.* Clinical characteristics of somatic mutations in Chinese patients with aldosterone-producing adenoma. *Hypertension* **65**, 622-8 (2015).

59. Tamura, A. *et al.* Somatic KCNJ5 mutation occurring early in adrenal development may cause a novel form of juvenile primary aldosteronism. *Mol Cell Endocrinol* **441**, 134-139 (2017).

60. Maria, A.G. *et al.* Mosaicism for KCNJ5 Causing Early-Onset Primary Aldosteronism due to Bilateral Adrenocortical Hyperplasia. *Am J Hypertens* **33**, 124-130 (2020).

61. Vouillarmet, J. *et al.* Aldosterone-Producing Adenoma With a Somatic KCNJ5 Mutation Revealing APC-Dependent Familial Adenomatous Polyposis. *J Clin Endocrinol Metab* **101**, 3874-3878 (2016).

62. Taguchi, R. *et al.* Expression and mutations of KCNJ5 mRNA in Japanese patients with aldosterone-producing adenomas. *J Clin Endocrinol Metab* **97**, 1311-9 (2012).

63. Cheng, C.J. *et al.* Novel KCNJ5 mutations in sporadic aldosterone-producing adenoma reduce Kir3.4 membrane abundance. *J Clin Endocrinol Metab* **100**, E155-63 (2015).

64. Ganguly, A., Melada, G.A., Luetscher, J.A. & Dowdy, A.J. Control of plasma aldosterone in primary aldosteronism: distinction between adenoma and hyperplasia. *J Clin Endocrinol Metab* **37**, 765-75 (1973).

65. Schambelan, M., Brust, N.L., Chang, B.C., Slater, K.L. & Biglieri, E.G. Circadian rhythm and effect of posture on plasma aldosterone concentration in primary aldosteronism. *J Clin Endocrinol Metab* **43**, 115-31 (1976).

66. Biglieri, E.G. Effect of posture on the plasma concentrations of aldosterone in hypertension and primary hyperaldosteronism. *Nephron* **23**, 112-5 (1979).

67. Irony, I., Kater, C.E., Biglieri, E.G. & Shackleton, C.H. Correctable subsets of primary aldosteronism. Primary adrenal hyperplasia and renin responsive adenoma. *Am J Hypertens* **3**, 576-82 (1990).

68. Fontes, R.G., Kater, C.E., Biglieri, E.G. & Irony, I. Reassessment of the predictive value of the postural stimulation test in primary aldosteronism. *Am J Hypertens* **4**, 786-91 (1991).

69. Hamlet, S.M., Gordon, R.D., Gomez-Sanchez, C.E., Tunny, T.J. & Klemm, S.A. Adrenal transitional zone steroids, 18-oxo and 18-hydroxycortisol, useful in the diagnosis of

primary aldosteronism, are ACTH-dependent. *Clin Exp Pharmacol Physiol* **15**, 317-22 (1988).

70. Tunny, T.J., Gordon, R.D., Klemm, S.A. & Cohn, D. Histological and biochemical distinctiveness of atypical aldosterone-producing adenomas responsive to upright posture and angiotensin. *Clin Endocrinol (Oxf)* **34**, 363-9 (1991).
71. Tunny, T.J., Klemm, S.A., Stowasser, M. & Gordon, R.D. Angiotensin-responsive aldosterone-producing adenomas: postoperative disappearance of aldosterone response to angiotensin. *Clin Exp Pharmacol Physiol* **20**, 306-9 (1993).
72. Gordon, R.D., Stowasser, M., Klemm, S.A. & Tunny, T.J. Primary aldosteronism--some genetic, morphological, and biochemical aspects of subtypes. *Steroids* **60**, 35-41 (1995).
73. Stowasser, M., Bachmann, A.W., Tunny, T.J. & Gordon, R.D. Production of 18-oxo-cortisol in subtypes of primary aldosteronism. *Clin Exp Pharmacol Physiol* **23**, 591-3 (1996).
74. Azizan, E.A. *et al.* Somatic mutations affecting the selectivity filter of KCNJ5 are frequent in 2 large unselected collections of adrenal aldosteronomas. *Hypertension* **59**, 587-91 (2012).
75. Murakami, M. *et al.* In situ metabolomics of aldosterone-producing adenomas. *JCI Insight* **4**(2019).
76. Schwartz, L., Supuran, C.T. & Alfarouk, K.O. The Warburg Effect and the Hallmarks of Cancer. *Anticancer Agents Med Chem* **17**, 164-170 (2017).
77. Jiang, P., Du, W. & Wu, M. Regulation of the pentose phosphate pathway in cancer. *Protein Cell* **5**, 592-602 (2014).
78. Berthon, A. *et al.* WNT/beta-catenin signalling is activated in aldosterone-producing adenomas and controls aldosterone production. *Hum Mol Genet* **23**, 889-905 (2014).
79. Bassett, M.H., Suzuki, T., Sasano, H., White, P.C. & Rainey, W.E. The orphan nuclear receptors NURR1 and NGFIB regulate adrenal aldosterone production. *Mol Endocrinol* **18**, 279-90 (2004).
80. Bassett, M.H. *et al.* Expression profiles for steroidogenic enzymes in adrenocortical disease. *J Clin Endocrinol Metab* **90**, 5446-55 (2005).

81. Zhou, J. *et al.* Transcriptome Pathway Analysis of Pathological and Physiological Aldosterone-Producing Human Tissues. *Hypertension* **68**, 1424-1431 (2016).

82. Reincke, M. *et al.* DAX-1 expression in human adrenocortical neoplasms: implications for steroidogenesis. *J Clin Endocrinol Metab* **83**, 2597-600 (1998).

83. Hu, D. *et al.* Elementary studies on elevated steroidogenic factor-1 expression in aldosterone-producing adenoma. *Urol Oncol* **30**, 457-62 (2012).

84. El Zein, R.M. *et al.* Retinoic acid receptor alpha as a novel contributor to adrenal cortex structure and function through interactions with Wnt and Vegfa signalling. *Sci Rep* **9**, 14677 (2019).

85. Assie, G. *et al.* Steroidogenesis in aldosterone-producing adenoma revisited by transcriptome analysis. *J Clin Endocrinol Metab* **90**, 6638-49 (2005).

86. Xing, Y. *et al.* Aldosterone production in human adrenocortical cells is stimulated by high-density lipoprotein 2 (HDL2) through increased expression of aldosterone synthase (CYP11B2). *Endocrinology* **152**, 751-63 (2011).

87. Azizan, E.A. *et al.* Somatic mutations in ATP1A1 and CACNA1D underlie a common subtype of adrenal hypertension. *Nat Genet* **45**, 1055-60 (2013).

88. Maniero, C. *et al.* ANO4 (Anoctamin 4) Is a Novel Marker of Zona Glomerulosa That Regulates Stimulated Aldosterone Secretion. *Hypertension* **74**, 1152-1159 (2019).

89. Daniil, G. *et al.* CACNA1H Mutations Are Associated With Different Forms of Primary Aldosteronism. *EBioMedicine* **13**, 225-236 (2016).

90. Lenzini, L. *et al.* Heterogeneity of aldosterone-producing adenomas revealed by a whole transcriptome analysis. *Hypertension* **50**, 1106-13 (2007).

91. Condon, J.C., Pezzi, V., Drummond, B.M., Yin, S. & Rainey, W.E. Calmodulin-dependent kinase I regulates adrenal cell expression of aldosterone synthase. *Endocrinology* **143**, 3651-7 (2002).

92. Kobuke, K. *et al.* Calneuron 1 Increased Ca(2+) in the Endoplasmic Reticulum and Aldosterone Production in Aldosterone-Producing Adenoma. *Hypertension* **71**, 125-133 (2018).

93. Itcho, K. *et al.* Endoplasmic Reticulum Chaperone Calmegin Is Upregulated in Aldosterone-Producing Adenoma and Associates With Aldosterone Production. *Hypertension* **75**, 492-499 (2020).

94. Wang, T. *et al.* Gene expression profiles in aldosterone-producing adenomas and adjacent adrenal glands. *Eur J Endocrinol* **164**, 613-9 (2011).

95. Felizola, S.J. *et al.* PCP4: a regulator of aldosterone synthesis in human adrenocortical tissues. *J Mol Endocrinol* **52**, 159-67 (2014).

96. Williams, T.A. *et al.* Visinin-like 1 is upregulated in aldosterone-producing adenomas with KCNJ5 mutations and protects from calcium-induced apoptosis. *Hypertension* **59**, 833-9 (2012).

97. Plaska, S.W. *et al.* Targeted RNAseq of Formalin-Fixed Paraffin-Embedded Tissue to Differentiate Among Benign and Malignant Adrenal Cortical Tumors. *Horm Metab Res* **52**, 607-613 (2020).

98. Li, X. *et al.* GSTA1 Expression Is Correlated With Aldosterone Level in KCNJ5-Mutated Adrenal Aldosterone-Producing Adenoma. *J Clin Endocrinol Metab* **103**, 813-823 (2018).

99. Saner-Amigh, K. *et al.* Elevated expression of luteinizing hormone receptor in aldosterone-producing adenomas. *J Clin Endocrinol Metab* **91**, 1136-42 (2006).

100. Zhou, J. *et al.* Somatic mutations of GNA11 and GNAQ in CTNNB1-mutant aldosterone-producing adenomas presenting in puberty, pregnancy or menopause. *Nat Genet* **53**, 1360-1372 (2021).

101. Ye, P., Mariniello, B., Mantero, F., Shibata, H. & Rainey, W.E. G-protein-coupled receptors in aldosterone-producing adenomas: a potential cause of hyperaldosteronism. *J Endocrinol* **195**, 39-48 (2007).

102. Nakamura, Y. *et al.* Aberrant gonadotropin-releasing hormone receptor (GnRHR) expression and its regulation of CYP11B2 expression and aldosterone production in adrenal aldosterone-producing adenoma (APA). *Mol Cell Endocrinol* **384**, 102-8 (2014).

103. Lefebvre, H. *et al.* Characterization of serotonin(4) receptors in adrenocortical aldosterone-producing adenomas: in vivo and in vitro studies. *J Clin Endocrinol Metab* **87**, 1211-6 (2002).

104. Lefebvre, H. *et al.* Effect of the serotonin 5-HT4 receptor agonist cisapride on aldosterone secretion in corticotropic insufficiency and primary hyperaldosteronism. *Neuroendocrinology* **66**, 229-33 (1997).

105. Itcho, K. *et al.* Aberrant G protein-receptor expression is associated with DNA methylation in aldosterone-producing adenoma. *Mol Cell Endocrinol* **461**, 100-104 (2018).

106. Lim, J.S., Plaska, S.W., Rege, J., Rainey, W.E. & Turcu, A.F. Aldosterone-Regulating Receptors and Aldosterone-Driver Somatic Mutations. *Front Endocrinol (Lausanne)* **12**, 644382 (2021).

107. Kem, D.C. *et al.* Autoimmune mechanisms activating the angiotensin AT1 receptor in 'primary' aldosteronism. *J Clin Endocrinol Metab* **99**, 1790-7 (2014).

108. Felizola, S.J.A. *et al.* Glutamate receptors and the regulation of steroidogenesis in the human adrenal gland: the metabotropic pathway. *Mol Cell Endocrinol* **382**, 170-177 (2014).

109. Inoue, K. *et al.* Aldosterone Suppression by Dexamethasone in Patients With KCNJ5-Mutated Aldosterone-Producing Adenoma. *J Clin Endocrinol Metab* **103**, 3477-3485 (2018).

110. Caroccia, B. *et al.* GPER-1 and estrogen receptor-beta ligands modulate aldosterone synthesis. *Endocrinology* **155**, 4296-304 (2014).

111. Swierczynska, M.M. *et al.* Proteomic Landscape of Aldosterone-Producing Adenoma. *Hypertension* **73**, 469-480 (2019).

112. Nakamura, Y. *et al.* Human adrenal cells that express both 3beta-hydroxysteroid dehydrogenase type 2 (HSD3B2) and cytochrome b5 (CYB5A) contribute to adrenal androstenedione production. *J Steroid Biochem Mol Biol* **123**, 122-6 (2011).

113. Chu, C. *et al.* Transcriptome analysis of primary aldosteronism in adrenal glands and controls. *Int J Clin Exp Pathol* **10**, 10009-10018 (2017).

114. Maniero, C. *et al.* NEFM (Neurofilament Medium) Polypeptide, a Marker for Zona Glomerulosa Cells in Human Adrenal, Inhibits D1R (Dopamine D1 Receptor)-Mediated Secretion of Aldosterone. *Hypertension* **70**, 357-364 (2017).

115. Teo, A.E. *et al.* Physiological and Pathological Roles in Human Adrenal of the Glomeruli-Defining Matrix Protein NPNT (Nephronectin). *Hypertension* **69**, 1207-1216 (2017).

116. Jimenez, P., Saner, K., Mayhew, B. & Rainey, W.E. GATA-6 is expressed in the human adrenal and regulates transcription of genes required for adrenal androgen biosynthesis. *Endocrinology* **144**, 4285-8 (2003).

117. Zhou, J. *et al.* DACH1, a zona glomerulosa selective gene in the human adrenal, activates transforming growth factor-beta signaling and suppresses aldosterone secretion. *Hypertension* **65**, 1103-10 (2015).

118. Yang, Y. *et al.* BEX1 Is Differentially Expressed in Aldosterone-Producing Adenomas and Protects Human Adrenocortical Cells From Ferroptosis. *Hypertension* **77**, 1647-1658 (2021).

119. Cerquetti, L. *et al.* C-MYC modulation induces responsiveness to paclitaxel in adrenocortical cancer cell lines. *Int J Oncol* **46**, 2231-40 (2015).

120. Hoeflich, A. *et al.* Overexpression of insulin-like growth factor-binding protein-2 results in increased tumorigenic potential in Y-1 adrenocortical tumor cells. *Cancer Res* **60**, 834-8 (2000).

121. Doghman, M. *et al.* Nephroblastoma overexpressed/cysteine-rich protein 61/connective tissue growth factor/nephroblastoma overexpressed gene-3 (NOV/CCN3), a selective adrenocortical cell proapoptotic factor, is down-regulated in childhood adrenocortical tumors. *J Clin Endocrinol Metab* **92**, 3253-60 (2007).

122. Williams, T.A. *et al.* Teratocarcinoma-derived growth factor-1 is upregulated in aldosterone-producing adenomas and increases aldosterone secretion and inhibits apoptosis in vitro. *Hypertension* **55**, 1468-75 (2010).

123. Monticone, S. *et al.* Effect of KCNJ5 mutations on gene expression in aldosterone-producing adenomas and adrenocortical cells. *J Clin Endocrinol Metab* **97**, E1567-72 (2012).

124. Zhang, C. *et al.* Endothelial Cell-Specific Inactivation of TSPAN12 (Tetraspanin 12) Reveals Pathological Consequences of Barrier Defects in an Otherwise Intact Vasculature. *Arterioscler Thromb Vasc Biol* **38**, 2691-2705 (2018).

125. Yin, Q. *et al.* Raptor determines beta-cell identity and plasticity independent of hyperglycemia in mice. *Nat Commun* **11**, 2538 (2020).
126. Otomo, R. *et al.* TSPAN12 is a critical factor for cancer-fibroblast cell contact-mediated cancer invasion. *Proc Natl Acad Sci U S A* **111**, 18691-6 (2014).
127. Baker, J.E. *et al.* Targeted RNA sequencing of adrenal zones using immunohistochemistry-guided capture of formalin-fixed paraffin-embedded tissue. *Mol Cell Endocrinol* **530**, 111296 (2021).
128. Eisenhofer, G. *et al.* Use of Steroid Profiling Combined With Machine Learning for Identification and Subtype Classification in Primary Aldosteronism. *JAMA Netw Open* **3**, e2016209 (2020).
129. Yamazaki, Y. *et al.* Tumor Cell Subtypes Based on the Intracellular Hormonal Activity in KCNJ5-Mutated Aldosterone-Producing Adenoma. *Hypertension* **72**, 632-640 (2018).
130. Stahl, P.L. *et al.* Visualization and analysis of gene expression in tissue sections by spatial transcriptomics. *Science* **353**, 78-82 (2016).
131. Wu, S.Z. *et al.* A single-cell and spatially resolved atlas of human breast cancers. *Nat Genet* **53**, 1334-1347 (2021).
132. Andersson, A. *et al.* Spatial deconvolution of HER2-positive breast cancer delineates tumor-associated cell type interactions. *Nat Commun* **12**, 6012 (2021).
133. Wu, R. *et al.* Comprehensive analysis of spatial architecture in primary liver cancer. *Sci Adv* **7**, eabg3750 (2021).
134. Pavlova, N.N. & Thompson, C.B. The Emerging Hallmarks of Cancer Metabolism. *Cell Metab* **23**, 27-47 (2016).
135. Faubert, B., Solmonson, A. & DeBerardinis, R.J. Metabolic reprogramming and cancer progression. *Science* **368**(2020).
136. Ligorio, F. *et al.* Targeting lipid metabolism is an emerging strategy to enhance the efficacy of anti-HER2 therapies in HER2-positive breast cancer. *Cancer Lett* **511**, 77-87 (2021).

137. Xu, W. *et al.* Fatty Acid Synthase Correlates With Prognosis-Related Abdominal Adipose Distribution and Metabolic Disorders of Clear Cell Renal Cell Carcinoma. *Front Mol Biosci* **7**, 610229 (2020).
138. Schmidt, D.R. *et al.* Metabolomics in cancer research and emerging applications in clinical oncology. *CA Cancer J Clin* **71**, 333-358 (2021).
139. Feng, J. *et al.* Metabolic profiling reveals distinct metabolic alterations in different subtypes of pituitary adenomas and confers therapeutic targets. *J Transl Med* **17**, 291 (2019).
140. Ohta, A. *et al.* A2A adenosine receptor protects tumors from antitumor T cells. *Proc Natl Acad Sci U S A* **103**, 13132-7 (2006).
141. Romero-Garcia, S., Moreno-Altamirano, M.M., Prado-Garcia, H. & Sanchez-Garcia, F.J. Lactate Contribution to the Tumor Microenvironment: Mechanisms, Effects on Immune Cells and Therapeutic Relevance. *Front Immunol* **7**, 52 (2016).
142. Leone, R.D. & Powell, J.D. Metabolism of immune cells in cancer. *Nat Rev Cancer* **20**, 516-531 (2020).
143. Mulatero, P. *et al.* Genetics, prevalence, screening and confirmation of primary aldosteronism: a position statement and consensus of the Working Group on Endocrine Hypertension of The European Society of Hypertension. *J Hypertens* **38**, 1919-1928 (2020).
144. Yozamp, N. *et al.* Intraindividual Variability of Aldosterone Concentrations in Primary Aldosteronism: Implications for Case Detection. *Hypertension* **77**, 891-899 (2021).
145. Leung, A.A. *et al.* Performance of Confirmatory Tests for Diagnosing Primary Aldosteronism: a Systematic Review and Meta-Analysis. *Hypertension* **79**, 1835-1844 (2022).
146. Rossi, G.P. *et al.* Long-term control of arterial hypertension and regression of left ventricular hypertrophy with treatment of primary aldosteronism. *Hypertension* **62**, 62-9 (2013).
147. Rossi, G.P. *et al.* Adrenalectomy Lowers Incident Atrial Fibrillation in Primary Aldosteronism Patients at Long Term. *Hypertension* **71**, 585-591 (2018).

148. Hundemer, G.L., Curhan, G.C., Yozamp, N., Wang, M. & Vaidya, A. Renal Outcomes in Medically and Surgically Treated Primary Aldosteronism. *Hypertension* **72**, 658-666 (2018).

149. Ahmed, A.H., Gordon, R.D., Sukor, N., Pimenta, E. & Stowasser, M. Quality of life in patients with bilateral primary aldosteronism before and during treatment with spironolactone and/or amiloride, including a comparison with our previously published results in those with unilateral disease treated surgically. *J Clin Endocrinol Metab* **96**, 2904-11 (2011).

150. Williams, T.A. *et al.* Outcomes after adrenalectomy for unilateral primary aldosteronism: an international consensus on outcome measures and analysis of remission rates in an international cohort. *Lancet Diabetes Endocrinol* **5**, 689-699 (2017).

151. Biglieri, E.G., Schambelan, M., Slaton, P.E. & Stockigt, J.R. The intercurrent hypertension of primary aldosteronism. *Circ Res* **27**, 195-202 (1970).

152. Groth, H. *et al.* Adrenalectomy in primary aldosteronism: a long-term follow-up study. *Cardiology* **72 Suppl 1**, 107-16 (1985).

153. Sukor, N., Gordon, R.D., Ku, Y.K., Jones, M. & Stowasser, M. Role of unilateral adrenalectomy in bilateral primary aldosteronism: a 22-year single center experience. *J Clin Endocrinol Metab* **94**, 2437-45 (2009).

154. Gong, S., Tetti, M., Reincke, M. & Williams, T.A. Primary Aldosteronism: Metabolic Reprogramming and the Pathogenesis of Aldosterone-Producing Adenomas. *Cancers (Basel)* **13**(2021).

155. Prasad, R., Kowalczyk, J.C., Meimaridou, E., Storr, H.L. & Metherell, L.A. Oxidative stress and adrenocortical insufficiency. *J Endocrinol* **221**, R63-73 (2014).

156. Gong, S. *et al.* TSPAN12 (Tetraspanin 12) Is a Novel Negative Regulator of Aldosterone Production in Adrenal Physiology and Aldosterone-Producing Adenomas. *Hypertension* **80**, 440-450 (2023).

7. Acknowledgement

I would like to express my sincerest gratitude to my beloved supervisor, **Dr. Tracy Ann Williams**, for the love, care, and support she has shown me throughout my PhD studies. Her exceptional expertise and insightful guidance have shaped my understanding of the subject matter of primary aldosteronism, providing me with a clear direction for my research. Her availability to answer my queries, provide feedback on my work, and offer words of encouragement when I needed it most was truly invaluable. Her ability to communicate complex ideas in a way that was easy for me to understand was truly remarkable. Furthermore, I cherish the trust and confidence she placed in me throughout my studies, and her unwavering belief in my abilities has been a constant source of inspiration for me to strive for excellence and reach my full potential. Her exquisite and profound academic attainments, combined with her rigorous and solid style of governance, have deeply influenced my work and life in ways that I could never have imagined. Without her guidance and support, I would not have been able to achieve the accomplishments and progress that I have made thus far. I am honored to have had such a remarkable supervisor and mentor, and I am thankful for the impact she has had on my life.

I am deeply grateful to my supervisor **Prof. Dr. med. Martin Reincke** for his support, guidance, and mentorship. He not only provided the much-needed financial support that made this research possible, but also shared his extensive experience and expertise in the field, which helped me achieve my goals. His insights and guidance were instrumental in shaping the direction of my research and contributed significantly to its overall quality. In addition to his financial and advisory contributions, he was always available and willing to provide assistance whenever I encountered obstacles or challenges in my work. His dedication to my project and his commitment to my success was truly inspiring, and I feel incredibly fortunate to have had him as my supervisor.

I am also grateful to my third supervisor **Prof. Dr. Paolo Mulatero**. His unwavering support, wise counsel, and warm heart have sustained me through the highs and lows of this research journey. He is a kind and generous mentor who has always made time for me, and I feel extremely lucky to have had the opportunity to work with him.

My heart overflows with gratitude to the incredible team at AG Williams and Medizinische Klinik und Poliklinik IV (LMU Klinikum), without whom this work would not have come to fruition. I am truly blessed to have had the opportunity to work in such an exceptional environment, and it is undoubtedly due in large part to the leadership of Prof. Dr. med. Martin Reincke and Dr. Tracy Ann Williams, as well as the tireless efforts of each staff member. I am indebted to every single member of staff who has helped me along the way, including Dr. Lucie Sophie Meyer, Dr. Yuhong Yang, Dr. Martina Tetti, Dr. Twinkle Vohra, Dr. Dunja Reiss, Isabella-Sabrina Kinker, Petra Rank, Carolin Ellerbrock, Youssra Mohammed Ahmed, and Beate Heuser. Their guidance and support have been invaluable in helping me navigate the complexities of my research. I am also grateful for the exceptional assistance of Sanas Mir-Bashiri, Yingxian Pang, and Zhuolun Sun, whose contributions have been essential to the success of this work. To AG Williams and Medizinische Klinik und Poliklinik IV, I offer my most profound thanks. Your support, guidance, and encouragement have been an essential part of this journey, and I feel truly blessed to have had the privilege of working with such an exceptional group of individuals. I would like to extend my heartfelt appreciation to the lovely Dr. Martina Tetti and Dr. Lucie Sophie Meyer, with whom I had the privilege of working. Their incredible attitude towards work and dedication to excellence was truly inspiring. I learned so much from them, including valuable skills in multitasking and task organization. They were always there to offer me their support whenever I needed it. I am incredibly grateful for their guidance and encouragement, which have undoubtedly helped me achieve success in my work.

To all the patients who graciously gave their consent to participate in this research, my deepest thanks. Your generosity in allowing us to study and learn from you has been a priceless gift, and without your cooperation, this work would not have been possible. I am awed by your willingness to help and by your trust in us, and your contribution to advancing knowledge in this field is immeasurable.

I would like to extend my sincere thanks and appreciation to the China Scholarship Council (CSC), whose generous support has made my PhD studies in Germany a reality.

The journey to earning a doctorate is a long and challenging one, and I would like to acknowledge the support of those who have been with me from the very beginning: my parents and friends.

My heart is filled with gratitude for my dear parents, who have devoted countless hours to my education and imparted to me their boundless love and wisdom. Through their unwavering support and encouragement, they have instilled in me a deep passion for learning and a relentless commitment to excellence. I am forever grateful for the immeasurable gifts of guidance and strength that my parents have bestowed upon me. They have taught me to believe in myself and to persevere through adversity, inspiring me to pursue my dreams with unwavering determination.

As I look back on my doctoral journey, my heart swells with gratitude and admiration for my dearest Zhi Ma, whose steadfast love and support have been the anchor that has kept me steady through it all. Without his constant encouragement, dedication, and patience, I would not have been able to achieve this milestone. Having him by my side has been a great source of stability and comfort. I feel incredibly fortunate to have met him during my studies in Germany. As partners and best friends, we exchange ideas and share knowledge, and our connection has only grown stronger as we navigate the complexities of academic pursuit. With him by my side, I know that we have a brighter future ahead of us.